Cancer Genetics & Stem Cell Group

Cancer Biology Unit

Division of Cancer & Stem Cells

School of Medicine

University of Nottingham

Mechanisms and roles of FLYWCH1 in Colorectal Cancer

By

Emenike .K. Onyido, B.Sc., M.Sc.

Thesis submitted to the University of Nottingham
for the degree of Doctor of Philosophy

January 31st, 2017

Declaration

Except where acknowledged in the text, I declare that this thesis report is my own work and prepared by me under the supervision of Dr. Abdolrahman S. Nateri and Dr. Roya Babaei-Jadidi in Cancer Genetics & Stem Cell Group. This report have not been submitted neither has it been used in any university here in the United Kingdom.

Also, part of Chapter 1 was taken from my review article published in Molecular Cancer Journal (see publication list, page vi).

Name: Emenike .K. Onyido

Student ID: 4198350

Date: 31/01/2017

Abstract

Human colorectal cancer (CRC) is the fourth most common cause of cancer-related death in the UK and worldwide. Defects in conserved signalling pathways play key roles in the development of almost all cancers and, in CRCs, over 80% of tumours show hyper-activation of the canonical Wnt signalling pathway. This pathway, through the transcriptional activity of β-catenin (and its binding partner, TCF4), maintains the stem cell compartment of colon and intestinal-crypts as well as cancer-initiating cells. Whilst the role of β-catenin/TCF4 in the development of both normal and neoplastic colon/intestinal tissues is well documented, the molecular basis of these functionally distinct nuclear-transcriptional programs is still under investigation, hence the functional elucidation of nuclear cofactors that interact with nuclear β-catenin contribute to further unravel the mechanisms involved in the β-catenin-mediated nuclear transcription. In addition to LEF/TCFs, interaction of β-catenin with a plethora of other transcriptional co-activators and/or co-repressors remains vital for gene regulation.

To this end, our lab have been dedicated to identifying β-catenin/TCF4 interacting partner proteins (CIPs) capable of fine-tuning the Wnt-level in CRC cells. Among other CIPs, my proposed project was focused on FLYWCH1, a totally novel protein with a FLYWCH/Zn-finger DNA-binding domain, called "FLYWCH". Previous data in our lab demonstrated that FLYWCH1 preferentially binds the nuclear/ un-phosphorylated-β-catenin whilst β-catenin is still bound to TCF4 (Muhammed et al., submitted). Muhammed et al., found that FLYWCH1 is able to modulate transcription of many β-catenin target genes

including the stem cell marker (Lgr5) and genes that are associated with migration and invasion of CRC cells. They also showed that *FLYWCH*1 mRNA expression is restricted to a subpopulation of tumour cells in both human CRCs and Apc^{Min} model mouse for intestinal cancer via *in-situ* hybridization (ISH). However, prior to these almost nothing was known about the FLYWCH1.

In my research project it was proposed, to build on these advances in FLYWCH1, Wnt and CRC, and to undertake a cell & molecular research program on the role of the FLYWCH1-transcription regulator in potential suppression of colon cancer via direct regulation of microRNAs. However, commercially available FLYWCH1-antibodies worked endogenously only for immunocytochemistry/immunofluorescent (IF), but not for immunohisto-chemistry (IHC) and Western blotting analysis.

Here we provide evidences via FLYWCH1 overexpression and shRNA knockdown in cultured fibroblast (TIG119) and CRC cell lines that FLYWCH1 possess tumour suppressor functions mainly by;

i) Inhibition of cell migration via modulating actin cytoskeleton re-modelling and stress fibre formation and by targeting E-cadherin suppressor ZEB1.
ii) Inhibiting cancer stemness *in-vitro* (colonosphere assays), by modulating the Wnt/β-catenin signalling pathway and possibly in a GSK-3β dependent manner.
iii) The localization of FLYWCH1 speckled nuclear with splicing factor SC-35 foci, a potential mechanism involved in regulation of miRNA expression.

iv) Positively regulating the expression of let-7 miRNA expression via modulating the LIN28A and LIN28B subcellular distribution.

We also showed that FLYWCH1 expression is correlated positively with let-7 miRNA expression in primary colorectal cancer samples and matched metastases from patients. While we are currently striving for obtaining substantial knowledge about FLYWCH1 function *in-vivo* and mechanistic insight into the regulatory circuitry of FLYWCH1/miRNAs, collectively, our data suggest that FLYWCH1 possesses tumour suppressor activity and may exert its influence on cancer cells homeostasis through miRNA regulation.

Acknowledgement

Firstly, I would like to give my deepest thanks to God almighty for giving me the strength to enable me complete my PhD programme.

Secondly, I would like to show deepest gratitude to my excellent supervisor, Dr. Abdolrahman S. Nateri for his support throughout the duration of my research. His availability, guidance and supervision was extremely helpful in ensuring my understanding of the project especially at the initial stages.

I would also like to thank my second supervisor, Dr. Roya Babaei-Jadidi for making out time to assist me in the technical aspect of my research and also in situations where my supervisor was not available due to other obligations. My warm appreciation also goes out to my friends, colleagues and wonderful lab mates for contributing to the conducive atmosphere of the Cancer Genetics and Stem Cells Laboratory and for all the wonderful experience we have had over the last four years.

Finally, I would like to show my deepest appreciation and love to my family most especially my parents for providing their utmost love and moral, emotional support all through the duration of my program.

Publication List

Accepted & Published

- **Emenike K. Onyido**, Eloise Sweeney & Abdolrahman Shams Nateri. (2016). Wnt signalling pathways and microRNAs network in carcinogenesis: Experimental and bioinformatics approaches. *Molecular Cancer* 15:56. Pg 1 – 17. DOI: 10.1186/s12943-016-0541-3.

(In Submission, * currently under peer review)

- * Belal A. Muhammad, Roya Babaei-Jadidi, **Emenike K. Onyido**, Anas Saadeddin, Bradley Spencer, Mohammed Ilyas, Axel Behrens and Abdolrahman Shams Nateri. FLYWCH1, a novel suppressor of nuclear β-catenin regulates cell migration & morphology. *Nature Oncogene.*

- **Emenike K. Onyido**, Roya Babaei-Jadidi, Belal Muhammad, Victoria James, & Abdolrahman Shams Nateri. β-catenin interacting protein, FLYWCH1 protein positively regulates let-7 activity in cancer cells. *Nucleic Acid Research.*

List of Figures

Figure 1-1: The multiple stages of CRC progression. Overview of CRC development via mucosa-adenoma-carcinoma transformation.. 4

Figure 1-2: Representation of Canonical Wnt/β-catenin pathway.. 11

Figure 1-3: Aberrant activation Wnt/β-catenin signalling in carcinogenesis.. . 15

Figure 1-4: Structural organization and transcriptional regulation of canonical Wnt regulators. 18

Figure 1-5: Schematic of Non-Canonical Wnt pathway..... 21

Figure 1-6: Wnt/β-catenin signalling regulation in Intestinal Stem Cells (ISCs).. 23

Figure 1-7: Importance of Wnt signalling in the regulation of stem cells. 25

Figure 1-8: C_2H_2 zinc finger motif. 27

Figure 1-9: Characterization of FLYWCH motifs within human FLYWCH1 protein. 34

Figure 1-10: FLYWCH1 amino acid sequence alignment in human and mouse. 36

Figure 1-11: Biogenesis of miRNA. 41

Figure 2-1: Layout of the Neubauer haemocytometer slide grid..... 66

Figure 2-2: Plasmid DNA isolation using Genopure midiprep kit. 74

Figure 2-3: DNA Ladders (HypperLadder ™ Bioline). Different DNA ladders used for gel electrophoresis depending on agarose percentage. 76

Figure 2-4: Total RNA extraction using TRIzol®. 79

Figure 2-5: cDNA synthesis. 81

Figure 2-6: Conversion of mature miRNAs into cDNA following manufacturer' recommendations.. 88

Figure 2-7: Protein markers used for SDS-PAGE analysis.. 93

Figure 2-8: Schematic representation of the principles of ECIS. 107

Figure 3-1: Nuclear localization of FLYWCH1 foci in normal and CRC cells.. 121

Figure 3-2: Expression and localization patterns of GFP in stable cell lines generated for FLYWCH1^{shRNA} and GFP expression.. 125

Figure 3-3: Downregulation of *FLYWCH1* expression in stable FLYWCH1^{shRNA}.. 128

Figure 3-4: Validation of FLYWCH1 in FLYWCH1^{shRNA} TIG119 cells.. 130

Figure 3-5: Knockdown of FLYWCH1 triggers formation of ventral stress fibres.. 133

Figure 3-6: FLYWCH1 triggers morphological changes in CRC SW480 cells… 138

Figure 3-7: FLYWCH1 triggers actin re-arrangements in SW480 cells. 140

Figure 3-8: Knockdown of FLYWCH1 expression promotes filopodia formation..... 143

Figure 3-9: FLYWCH1 influences cell attachment and spreading. 146

Figure 3-10: FLYWCH1 reduces wound-closure capacity of CRC cells..... 146

Figure 3-11: Influence of FLYWCH1 on cell cycle progression in normal & CRC cells.. 151

Figure 3-12: FLYWCH1 positively regulates E-cadherin..... 154

Figure 3-13: FLYWCH1 negatively regulates ZEB1 in SW480 cells.. 156

Figure 3-14: qRT-PCR analysis of FLYWCH1, EPHA4 and ZEB1 mRNA expression 157

Figure 3-15: Stress fibres..... 160

Figure 3-16: Possible mechanism illustrating FLYWCH1-mediated involvement in cell migration and attachment..... 166

Figure 4-1: Phosphorylation and inactivation of GSK-3β by FLYWCH1 overexpression.. 173

Figure 4-2: FLYWCH1 increased membrane bound phosphorylated β-catenin. 177

Figure 4-3: FLYWCH1 overexpression confers GSK-3β inhibitor resistance in SW480 CRC cell lines. 181

Figure 4-4: FLYWCH1-mediated morphology changes occur in a GSK-3β independent manner.. 183

Figure 4-5: Loss of FLYWCH1 caused morphological changes in SW480-derived colonospheres.. 186

Figure 4-6: Knockdown of FLYWCH1 expression increases β-catenin expression patterns in colonospheres..... 189

Figure 4-7: Knockdown of FLYWCH1 expression increases ZEB1 expression patterns. 192

Figure 4-8: FLYWCH1 knockdown reduces BMP4 expression.. 195

Figure 4-9: Knockdown of FLYWCH1 elevates CD44 expression. 198

Figure 4-10: Knockdown of FLYWCH1 expression reduces expression of differentiation marker, MUC2. 201

Figure 4-11: Proposed model illustrating the involvement of FLYWCH1 in the regulation of Wnt/β-catenin signalling in cancer state. 206

Figure 4-12: Opposing roles of FLYWCH1 on Wnt/β-catenin signalling. 210

Figure 5-1: FLYWCH1 co-localizes with nuclear splicing factor 'SC35' but not with Fibrillarin.. 217

Figure 5-2: FLYWCH1 may not be involved in DNA damage..... 220

Figure 5-3: FLYWCH1 is not involved in RNA splicing activity.. 225

Figure 5-4: FLYWCH1 is not involved in RNA splicing activity. 227

Figure 5-5: Preliminary analysis of FLYWCH1 on miRNA gene expression profile in TIG119 cells..... 228

Figure 5-6: Preliminary analysis suggest influence of FLYWCH1 on miRNA gene expression profile. 231

Figure 5-7: FLYWCH1 positively regulates miRNA tumour suppressor expression. 235

Figure 5-8: Influence of ectopic FLYWCH1 expression on let-7 gene expression profile..... 237

Figure 5-9: Influence of FLYWCH1 knockdown on let-7 gene expression profile..... 238

Figure 5-10: FLYWCH1 may alter the expression of LIN28A in TIG119 cells. 240

Figure 5-11: FLYWCH1 does not alter the expression of LIN28B in TIG119 cells.. 241

Figure 5-12: Quantitative analysis ofLIN28A and LIN28B in TIG119 cells.. 242

Figure 5-13: FLYWCH1 alters the expression of LIN28A in SW480 cells.. 244

Figure 5-14: FLYWCH1 alters the expression of LIN28B in SW480 cells... 245

Figure 5-15: Quantitative analysis of LIN28A and LIN28B in SW480 cells. 246

Figure 5-16: FLYWCH1 may bind directly to let-7 3'UTR target.. 248

Figure 5-17: FLYWCH1 shows positive correlation with let-7 in repressing HMGA-2. 252

Figure 5-18: Ectopic expression of β-catenin have no effect on let-7/luciferase reporter activity. 253

Figure 5-19: Influence of FLYWCH1 on let-7 gene expression profile in normal vs primary tumour vs metastasis samples.. 255

Figure 5-20: Proposed FLYWCH1-mediated regulation of let-7. 263

Figure 6-1: FLYWCH1 modulates transcriptional activity of canonical Wnt pathway (TCF4/β-catenin) to regulate ZEB1 expression. 275

Figure 6-2: FLYWCH1-mediated regulation of let-7. 280

List of Tables

Table 1-1: Structural classification of zinc fingers. 30

Table 1-2 : FLYWCH1 homology vs other mammals.. 35

Table 1-3: Alterations of miRNAs/Wnt/β-catenin signalling in cancer 47

Table 2-1: Non-commercial buffers and solutions used in this study. 54

Table 2-2: Comprehensive list of primary antibodies used for Western blotting and Immunofluorescent analysis. “NA” means not applicable. 58

Table 2-3: Comprehensive list of secondary antibodies used for Western blotting and Immunofluorescent analysis. 60

Table 2-4: Primers Used in this study..... 62

Table 2-5: Restriction enzymes used for plasmid validation..... 75

Table 2-6: Cycling parameters to perform standard polymerase chain reaction. 78

Table 2-7: Amplification parameters used for the quantative real time polymerase chain reaction (qRT-PCR)..... 83

Table 2-8: Cycling parameters for the real-time polymerase chain reaction for profiling of mature miRNA expression. 88

Table 2-9: Preparation of Tris-glycine staking gel for SDS-PAGE. 91

Table 2-10: Preparation of Tris-glycine resolving gel for SDS-PAGE. 91

Table 2-11: Fractionation kit contents 95

Table 5-1: FLYWCH1-mediated up-down regulation of miRNAs. 231

Table 5-2: List of internal controls 233

Abbreviations

APC = Adenomatous Polyposis Coli

BMP = Bone Morphogenic Protein

BSA = Bovine Serum Albumin

β-TRCP = beta-Transducin Repeat-Containing Protein

CBC = Crypt Base Columnar

CBX = Chromobox Homolog

C_2H_2 = Cystein2-Histidine2

CK 1 = Casein Kinase 1

CRC = Colorectal Cancer

CSCs = Cancer Stem Cells

DDR = DNA Damage Repair

Dkk = Dickkopf Family

DMSO = Dimethyl Sulfoxide

DNA = Deoxyribonucleic acid

dH2O = distilled Water

dsRNA = double stranded RNA

dCBP = drosophila CREB-Binding Protein

dGFZF = drosophila GST-Containing FLYWCH Zinc Finger Protein

DSB = Double Stranded Breaks

Dvl = Dishevelled

EDTA = Ethylenediaminetetraacetic acid

EMT = Epithelial Mesenchymal Transition

eGFP = Enhanced Green Fluorescent Protein

FAP = Familial Adenomatous Polyposis

Fz = Frizzled

GFP =Green Fluorescent Protein

GSK-3β = Glycogen Synthase Kinase 3 beta

GST = Glutathione SH-Transferase

HDAC = Histone Deacetylases

HMG = High Mobility Group

HNPCC = Hereditary Non-Polyposis Colon Cancer

HSC70 = Heat Shock Cognate Protein 70kDa

HSP90 = Heat Shock Protein 90

ICAT = Inhibitor of β-catenin and TCF4

ISC = Intestinal Stem Cell

JNK = Jun N-terminal Kinase

Kb = Kilo base

KDa = Kilo Dalton

KLF6 = Kruppel-like factor 6

LB = Luria Broth

LEF = Lymphoid Enhancer Factors

Lgr5 = Leucine-rich Repeat-containing G-protein Coupled Receptor

LRC = Label-retaining Cells

LRP = Lipoprotein Receptor-related Protein

MCS = Multiple Cloning Site

MET = Mesenchymal Epithelial Transition

MSI = Microsatellite Instability

MSS = Microsatellite Stability

PBS = Phosphate Buffered Saline

PCR = Polymerase Chain Reaction

PEI = Polyethyenimine

PFA = Paraformaldehyde

PI3K = Phosphoinositide-3-kinase

Porc = Porcupine

PVDF = Polyvinylidene difluoride

PYG = Pygopus

RISC = RNA induced silencing complex

RNA = Ribonucleic acid

Rpm = Round per minutes

ROS = Reactive Oxygen Species

RT = Room Temperature

SDS-PAGE = Sodium Dodecyl Sulphate-Polyacrylamide Gel Electrophoresis

SFRPs = Secreted frizzled-related proteins

SNP = Single Nucleotide Polymorphism

Sox9 = SRY-box containing gene 9

SR = Serine/arginine-rich

TAE = Tris-acetate-EDTA

TBS-T = Tris buffer saline-Tween-20

TCF = T-cell Factor

TGFβR2 = Transforming Growth Factor beta Receptor 2

TRBP = dsRNA binding protein

UTR = Un-translated Region

WIF = Wnt Inhibitory Factor

WT = Wild Type

ZFPs = Zinc Finger Proteins

Table of Contents

DECLARATION ..... **i**

ABSTRACT ..... **ii**

ACKNOWLEDGEMENT ..... **v**

PUBLICATION LIST ..... **vi**

LIST OF FIGURES ..... **vii**

LIST OF TABLES ..... **xi**

ABBREVIATION ..... **xii**

TABLE OF CONTENTS ..... **xv**

1 CHAPTER 1 ..... **1**

1.1 A Brief Introduction to Human Colorectal Cancer (CRC) 2

1.1.1 The Multistep Nature of CRC Development 3

1.2 The Wnt/β-catenin Signalling Pathway 5

1.2.1 Wnt as a ligand 5

1.2.2 Wnt Biogenesis 6

1.2.2.1 Intracellular and extracellular modifications of Wnt ligand 6

1.2.3 Canonical WNT Signalling Pathway 8

1.2.4 Deregulation of Wnt Signalling activity via Genetic Mutations 12

1.2.5 Regulation of β-catenin/TCF complex assembly 15

1.2.6 Non canonical Wnt signalling pathway 19

1.3 Influence of the Canonical Wnt Signalling Pathway in the Maintenance of Normal Intestinal Architecture 22

1.3.1 Role of Wnt signalling in Intestinal Crypts Cell Migration & Positioning 22

1.4 Zinc Finger Family of Proteins 26

1.5 FLYWCH Zinc Finger Protein 31

1.5.1 Discovery & Description 31
1.5.2 Bioinformatics of human FLYWCH1 motif 33
1.5.3 Functions & Properties 37
1.6 A Brief Overview of microRNA 38
1.6.1 MicroRNA Biogenesis 39
1.6.2 MiRNA-mediated Regulation of Wnt/β-catenin signalling 41
1.7 MiRNA Dysregulation in Cancer 43
1.7.1 Alterations of miRNAs/ β-catenin signalling in cancer 45
1.8 Rational and objectives of this study 48
1.8.1 Rational 48
1.8.2 Aims & Objectives 50

2 CHAPTER 2 52
2.1 Materials 53
2.1.1 Reagents and buffers 53
2.1.2 Cell lines 56
2.1.3 Human Tissue Specimen 57
2.1.4 Plasmid Constructs 57
2.1.5 Antibodies 58
2.1.6 Oligonucleotides 61
2.2 Methods 63
2.2.1 General Tissue Culture Techniques 63
2.2.1.1 Human cell culture conditions 63
2.2.1.2 Cell Counting 64
2.2.1.2.1 Viability 65
2.2.1.3 Colonospheres Formation 66
2.2.1.4 Transient transfection 67
2.2.1.5 RNAi Transfection 68

2.2.1.6 Generation of stable cell lines (Puromycin selection) 68
2.2.1.6.1 Single cell cloning via serial dilution..... 70
2.2.1.7 Freezing and thawing cells..... 70
2.3 DNA preparation..... 71
2.3.1 DNA transformation and amplification..... 71
2.3.2 DNA plasmid isolation & purification using midi prep kits..... 72
2.3.3 DNA quantification and storage..... 74
2.3.4 Restriction enzyme digestion..... 74
2.3.5 DNA Agarose gel electrophoresis..... 75
2.3.6 Standard polymerase chain reaction (PCR)..... 77
2.4 Ribonucleic acid (RNA) isolation and reverse transcription..... 78
2.4.1 RNA Isolation..... 78
2.4.2 RNA gel electrophoresis..... 80
2.4.3 Reverse transcription and complementary Deoxyribo-nucleic acid (cDNA) synthesis..... 80
2.4.4 Quantitative real time polymerase chain reaction (qRT-PCR)... 81
2.4.4.1 Primer design..... 81
2.4.4.2 Reaction Preparation..... 82
2.4.4.3 Data Analysis..... 83
2.4.5 miRNA PCR Arrays..... 84
2.4.5.1 Pathway-focused miScript miRNA PCR array for mature miRNA expression profiling..... 84
2.4.5.2 Heat map Generation..... 85
2.4.5.3 Validation of Pathway-Focused miScript miRNA PCR Array…..... 86
2.5 Protein lysate preparation and analysis..... 89
2.5.1 Protein extraction and purification..... 89
2.5.2 Protein Quantification..... 89
2.5.3 Western blotting (WB) analysis..... 90
2.5.3.1 Sample preparation and SDS-PAGE electrophoresis..... 90

2.5.3.2 Immunoblotting..... 94
2.6 Sub-cellular Fractionation..... 95
2.6.1 Cytoplasmic Extraction..... 96
2.6.2 Nuclear Extraction..... 96
2.7 RNA Immunoprecipitation (RIP)..... 97
2.7.1 Nuclei Isolation & Nuclear pellet lysis..... 97
2.7.2 Agarose Beads..... 97
2.7.3 Formation of bead-antibody complex..... 98
2.7.4 Immunoprecipitation..... 98
2.7.5 Isolation and purification of RNA bound to immunoprecipitated RBP……99
2.7.6 PCR Analysis of RIP..... 100
2.8 Protein Immunoprecipitation..... 100
2.9 Functional analysis..... 101
2.9.1 *In-vitro* scratch assay..... 101
2.9.2 Luciferase Reporter assay..... 102
2.9.3 Cell cycle analysis..... 104
2.9.4 Electric Cell-substrate Impedance Sensing (ECIS) for Cell Attachment Quantification..... 105
2.9.4.1 Array Stabilization..... 105
2.9.4.2 Inoculation of Cells..... 106
2.9.5 Cytotoxicity & Viability Assay..... 107
2.9.6 Immunofluorescent (IF) analysis..... 108
2.9.6.1 Cell Preparation..... 108
2.9.6.2 Fixation & Permeabilisation..... 109
2.9.6.3 Blocking Buffer..... 109
2.9.6.4 Staining with Primary and Secondary antibodies..... 109
2.9.6.5 Immunofluorescence Staining of Colonospheres..... 110
2.10 Phalloidin staining..... 111

2.11 Patient sample Analysis 112

2.12 Statistical analysis 113

2.12.1 Quantitative Image Analysis of Colonospheres 113

3 CHAPTER 3 116

3.1 Brief Introduction 117

3.2 Results 118

3.2.1 Endogenous nuclear localization of FLYWCH1 in human cell lines 118

3.2.2 Generation of cells stably expressing GFP for gain-of-function and piLenti-FLYWCH1^{shRNA} for loss-of-function studies of FLYWCH1 121

3.2.3 Validation of cells stably expressing piLenti-FLYWCH1^{shRNA} 125

3.2.4 Ectopic FLYWCH1 expression mediates change in morphology of CRC cells as well as formation of actin stress fibres in TIG119 cells. 130

3.2.4.1 Knock-down of FLYWCH1 expression triggers filopodia formation in CRC SW480 cells 140

3.2.5 FLYWCH1 influences the cell spreading & attachment properties 143

3.2.6 Knock-down of FLYWCH1 increases wound healing capacity 147

3.2.7 FLYWCH1 has varying cell cycle effect in CRC cell lines 146

3.2.8 FLYWCH1 modulate cell morphology by targeting E-cadherin antagonist ZEB1 152

3.3 Discussion 158

4 CHAPTER 4 167

4.1 Brief Introduction 168

4.2. Results 170

4.2.1 FLYWCH1 inhibits the serine 9 phosphorylation of GSK-3β that results in the induction of phosphorylated β-catenin 170

4.2.2 FLYWCH1 overexpression reduces sensitivity of SW480 CRC cells to GSK-3β drug inhibitor..... 178

4.2.3 FLYWCH1-mediated cell morphology alteration is independent of its effect on GSK-3β activity 181

4.2.4 FLYWCH1 knock-down enhances the colonosphere formation efficiency..... 184

4.2.4.1 Evaluation of loss of FLYWCH1 effect on self-renewal and differentiation activities in colonospheres. 187

4.3 Discussion 202

5 CHAPTER 5 213

5.1 Brief Introduction..... 214

5.2 Results..... 215

5.2.1 The FLYWCH1 nuclear speckles co-localizes with nuclear splicing factor “SC35” and partially with heterochromatin marker, HP1α…… 215

5.2.2 Evaluation of FLYWCH1/SC-35 complex in pre-mRNA splicing activity…..... 221

5.2.2.1 FLYWCH1 with no changes in splicing activity..... 222

5.2.3 FLYWCH1 modulates the expression of cancer-associated miRNAs in TIG119 and CRC cell lines..... 227

5.2.4 FLYWCH1-mediated control of let-7 miRNA may reduce cytoplasmic localization of LIN28B in cultured CRC cell lines. 239

5.2.4.1 FLYWCH1 may regulate the expression of genes targeted by let-7 miRNA 247

5.2.4.2 FLYWCH1 shows a positive correlation with let-7 in negatively regulating HMGA-2..... 249

5.2.5 Gene Expression Profiling for FLYWCH1 in Correlation with Let-7 in Colon cancer tissues..... 253

5.3 Discussion 256

6 CHAPTER 6 264

6.1 Overview 265

6.2 FLYWCH1 mediates the anti-migratory effects of CRC cells via alterations in cell-cell adhesion 267

6.3 Molecular mechanism underlying role of FLYWCH1 in Wnt/β-catenin signalling pathway 272

6.4 FLYWCH1 and let7 miRNA expression in CRCs 276

6.5 Experimental Limitations 281

6.6 Concluding Remarks & future directions 283

REFERENCES 287

APPENDIX 299

Appendix 1: pEGFP-C2 plasmid vector 320

Appendix 2: pEGFP-FLYWCH1 WT plasmid vector 320

Appendix 3: pEGFP-FLYWCH1-ΔC350 plasmid vector. 321

Appendix 4: pLVX-Puro plasmid vector 321

Appendix 5: pLVX-EGFP plasmid vector. 322

Appendix 6: pLVX-EGFP-FLYWCH1 WT plasmid vector .. 322

Appendix 7: piLenti-shRNA-FLYWCH1-GFP plasmid map 323

Appendix 8: Intron-less (Luc) plasmid construct 324

Appendix 9: Intron-less (Luc) plasmid construct 324

Appendix 10: LIN28A expression pattern in HCT116 cell lines 325

Appendix 11: LIN28B expression pattern in HCT116 cell lines 326

1 CHAPTER 1

General Introduction

1.1 A Brief Introduction to Human Colorectal Cancer (CRC)

Colorectal cancer is a common cause of mortality and morbidity, (Kamiyama et al., 2014; van Zijp et al., 2008) that mostly manifests sporadically either as a result of dietary, environmental, life-style or hereditary factors. According to Cancer Research UK (2013), it is currently the fourth most prevalent form of cancer and accounts for about 12% of all new cases in the UK (Read more at http://www.cancerresearchuk.org/health-professional/cancer-statistics/statistics-by-cancer-type/bowel-cancer#DrkZ28S8DXG3jUsc.99). It is also the fourth cause of cancer-related death worldwide (Stewart and Wild, 2014). According to the CRUK, an estimate of 41,600 people were diagnosed with colorectal cancer in 2011 in the UK alone, an equivalent of more than 110 people every day while approximately 16,200 people died of colorectal cancer in 2012 in the UK, equivalent of more than 44 people every day. Additionally, approximately 12% of CRC accounts for cancer cases in UK with around 41,300 cases reported in 2014 (CRUK, Bowel cancer report 2014). Furthermore, according to World Health Organization: International Agency for Research on Cancer (GLOBOCAN, 2012), around 694,000 people worldwide were estimated to have died from colorectal cancer in 2012 (http://globocan.iarc.fr/Pages/fact_sheets_cancer.aspx?cancer=colorectal), although mortality rates vary across the world.

Similar to other forms of cancer, factors that can elevate the risks of colorectal cancer can be caused either by extrinsic factors such as smoking, uncontrolled intake of alcohol, and consumption of diets composed of a high fat content or

intrinsic factors triggered by gender, diabetes mellitus, stomach ulcer or inflammatory bowel disease.

1.1.1 The Multistep Nature of CRC Development

A series of Histo-pathological alterations drives CRC development in an adenoma-carcinoma multistep sequence. This follows a temporal pattern in which genetic mutations and epigenetic events occurring in different genes initiate multiple pathways for CRC progression and malignant tumour development (Fearon, 2011; Pancione et al., 2012). The initiation of the disease is stimulated by the formation of multiple adenomatous polyps resulting to the histological dysregulation in the innermost lining of the mucosa, small intestine. These polyps (usually benign) grow through the sequence of mucosa-adenoma-carcinoma transformation due to the sequential acquisition of mutations in tumour suppressor genes and/or oncogenes responsible for the regulation of critical signalling pathways such as Wnt/β-catenin pathway (Figure 1-1). These mutations lead to gradual progression of the benign adenomatous polyps into carcinoma. Additionally, mutations to DNA stability genes arises resulting in an impaired DNA repair system which contributes to the progression of CRC development (Boyle and Langman, 2000; Grady and Carethers, 2008). These alterations cause gradual changes in tumour cell physiology, which ultimately lead to aberrant biological activities identified as hallmarks of cancer such as uncontrolled cell proliferation, resistance of cell death, insensitivity to antigrowth signals, angiogenesis.

The transition from normal mucosa to polyps and cancer occurs during the period of 10-15 years during which oncogene mutation and dysregulation of intracellular signalling pathway influence the diverse stages of tumour progression (Lao and Grady, 2011). The genes which appear to be most frequently mutated in CRC include *APC* (Adenomatous polyposis coli), *KRAS* (Kristen rat sarcoma viral oncogene), *TP53* (Tumour protein p53) *SMAD4* (Network, 2012; Smith et al., 2002) and FBXW7 which is mutated by 10-17% of colorectal cancer cases (Cai et al., 2014) (Figure 1-1). A major consequence of accumulation of mutation of these genes is the de-regulation and disruption of their respective signalling pathways involved in apoptosis, proliferation, cell survival and differentiation.

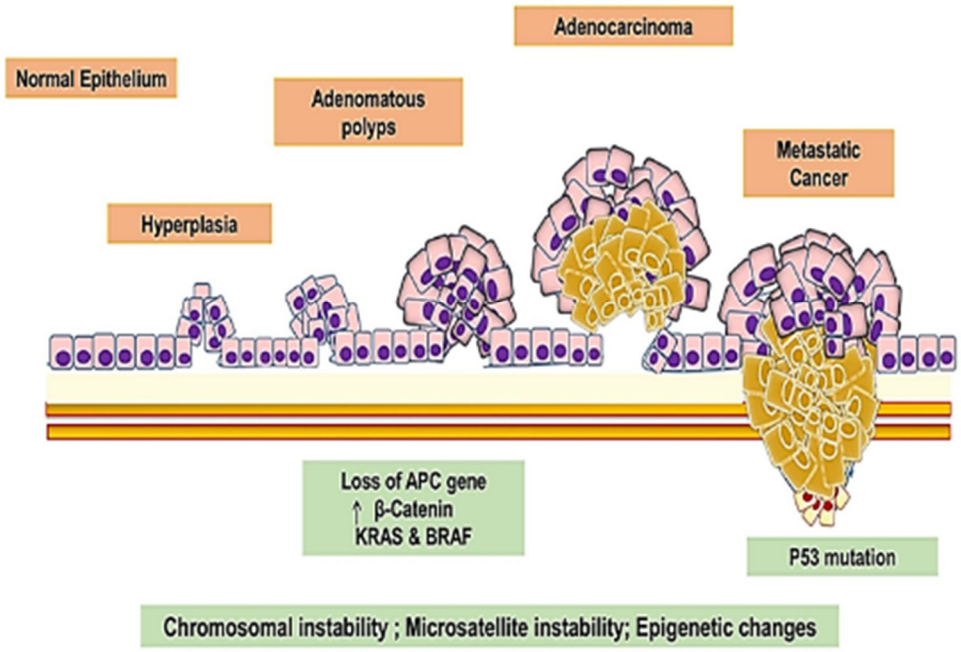


Figure 1-1: The multiple stages of CRC progression. Overview of CRC development via mucosa-adenoma-carcinoma transformation. The initial step towards colorectal tumorigenesis involves mutation of *APC* gene, which results to aberrant Wnt signalling pathway characterized with accumulation of nuclear

β-catenin. Subsequently, formation of small and large adenomas occurs due to mutations of the proto-oncogene KRAS and BRAF. Finally, mutations in TP53, Smad4, FBXW7, PTEN and loss of heterozygosity at chromosome 18q occurs late in the adenoma–carcinoma sequence. Chromosomal instability often increases with tumour progression. Taken from (Subramaniam et al., 2016).

1.2 The Wnt/β-catenin Signalling Pathway

The importance of Wnt/β-catenin signalling activity levels in maintenance of CRC cells provides a potential new therapeutic target in order to improve the prognosis of CRC patients. Interestingly, it has become evident that, apart from CRC, other types of malignancies are also dependent on de-regulation of Wnt/β-catenin signalling activity (Jang et al., 2015; Stewart, 2014). Therefore, the therapeutic benefit of drugs successfully targeting the Wnt signalling pathway is also evident for not only colorectal cancer but also various cancer types.

1.2.1 Wnt as a ligand

The Wnt pathway is a highly conserved signalling pathway that controls numerous steps during animal development and tissue homeostasis. Wnt proteins comprise a highly conserved and diverse family of genes found in humans, mice, Xenopus, Zebrafish and Drosophila (Clevers and Nusse, 2012). The Wnt ligand is composed of conserved 22 cysteine residues as well as other features such as possession of a secretion signal sequence and a high level of glycosylation sites (Mikels and Nusse, 2006). The Wnt gene (originally identified as Int-1) was discovered over 30 years ago as a gene activated via the

mouse mammary tumour virus pro-viral DNA integrated into virally induced breast tumours (Yang et al., 2016). The Wnt family, which consists of 19 members in mammals, is crucial for embryonic development, tissue homeostasis as well as homeostasis of the intestinal epithelium (Reya and Clevers, 2005). Proteins encoded by this family of genes are defined as small secreted glycoproteins of about 40 kDa that share high (27% to 83%) amino acid sequence identity, including a conserved pattern of 23 or 24 cysteine residues, a signal sequence for secretion, and many glycosylation sites.

1.2.2 Wnt Biogenesis

In the human intestine, myofibroblasts located beneath the base of the crypts are responsible for the secretion of Wnt ligands (Salazar et al., 2009). These Wnt ligands are subject to both intracellular and extracellular factors/modification. These fine adjustments are essential for the maturation process of Wnt molecules that facilitates secretion, trafficking, spreading and signalling activities of Wnt proteins.

1.2.2.1 Intracellular and extracellular modifications of Wnt ligand

Intracellular modification of Wnt includes post-translational enhancement via lipid and glycosylation modifications carried out in the endoplasmic reticulum by Porcupine (Porc) (MacDonald et al., 2009), and lipid modification accomplished via palmitoylation (Reya and Clevers, 2005). Palmitoylation (the

attachment of fatty acid molecules) of Wnt proteins is also essential for N-linked glycosylation, which serves to attach proteins to the endoplasmic reticulum. Lipid modification is extremely important due to the increase in hydrophobicity of Wnt ligands, which aids in the transportation to its target membrane receptor. On the other hand, extracellular signalling molecules that act as either antagonists or agonists of Wnt ligand characterize the extracellular modulation. A notable secreted protein that antagonizes the Wnt/β-catenin signalling pathway is Dkk1 (Dickkopf family) that belongs to the group of low-density lipoprotein receptor-related protein 5/6 (LRP5/6) ligands. Dkk1 exerts its influence via high affinity interaction with LRP6 through transmembrane kremen; thereby triggering endocytosis which completely removes cell membrane bound LRP6 and in effect prevents cellular response to Wnt (Coombs et al., 2010) as well as inhibition of receptor complex formed by LRP5/6, frizzled and the Wnt ligand (Rao and Kühl, 2010).

Molecules that function as agonists of the Wnt cascade include the ligand Norrin and R-spondin (Rspo) proteins. Rspo has been shown to positively regulate the canonical Wnt pathway by directly exhibiting synergy with frizzled-8 and LRP5/6 (MacDonald et al., 2009). Rspo also competes with Dkk1 for the binding site of transmembrane kremen (Rao and Kühl, 2010). Another extracellular protein, Norrin (that is associated with LRP5 receptors), up-regulates Wnt/β-catenin signal via induction of Fzd4 gene that encodes frizzled-4 receptor protein. Biochemical evidence from mouse specimen shows that Tspanl-2, a Norrin-specific co-receptor is capable of positively mediating the Wnt/β-catenin pathway (Clevers and Nusse, 2012).

Following intra/extracellular modifications, Wnt molecules function as extracellular ligands to activate the Wnt signalling pathway through direct interaction with Fz and LRP-5/6 cell surface receptors. Consequently, the intracellular transduction of Wnt-signals initiates the canonical (β-catenin dependent) or non-canonical (β-catenin independent) pathways.

1.2.3 Canonical WNT Signalling Pathway

The canonical Wnt-signalling cascade refers to the transduction of series of signals mediated via the interaction of specific Wnt ligands with their target receptor resulting in the accumulation of β-catenin (Figure 1-2). Accumulation of β-catenin plays a crucial role as the central transducer in the activation of downstream factors (MacDonald et al., 2009). The cytoplasmic stability of β-catenin is usually maintained at a minimal level by the destruction complex composed of a scaffold combination of tumour suppressor protein APC, Axin2, casein kinase1 (CK1) and glycogen synthase kinase 3 (GSK-3) (Miller et al., 1999). Aberrant Wnt/β-catenin signalling is a common hallmark of malignant CRC cells hence, mutations in any of the components of the destruction complex can potentially result to cytosolic β-catenin accumulation and subsequent activation of Wnt target genes that drive proliferation (Anastas and Moon, 2013; Reya and Clevers, 2005).

In the absence of Wnt ligand interaction (*OFF-state*) (Figure 1-2), the membrane receptor complex is inactivated, thereby preventing the clustering of a trimeric complex composed of Wnt ligand/Fzd/LRP receptors and eventually results to

β-catenin ubiquitination and degradation (Anastas and Moon, 2013). Although the Wnt/Fzd/LRP complex model is widely accepted, the precise mechanism of formation is yet to be fully understood. β-catenin levels are regulated by a phosphorylation event that is mediated by GSK3α/β-isoforms, which targets β-catenin for ubiquitination and proteasomal degradation (Metcalfe and Bienz, 2011). However, phosphorylation of GSK3β at tyrosine 216 or GSK3α at tyrosine 279 has been established to be required for GSK3 full kinase activity (Gao et al., 2014b). This phosphorylation occurs simultaneously at specific sites, with Serine 45 (Ser45) N-terminus of β-catenin phosphorylated by CK1 while phosphorylation at Threonine 41 (Thr41), Ser33 and Ser37 sites is carried out by GSK-3β (MacDonald et al., 2009; Rao and Kühl, 2010). Interestingly, studies have shown that Wnt signalling is un-affected in double knock-in mice in which the $Gsk3\alpha^{ser21}$ and $Gsk3\beta^{ser9}$ phosphorylation sites have been mutated to alanine, further demonstrating that inhibition of GSK-3 may occur by a mechanism other than Ser21/9 phosphorylation (Valvezan and Klein, 2012). Nevertheless, the consequence of these series of phosphorylation activities results in the recruitment of APC to the destruction complex.

The APC protein forms a complex with other components of the destruction complex and mediates the degradation of cytoplasmic β-catenin. APC serves a very important role in the destruction complex due to its tumour suppressor properties (Aoki and Taketo, 2007; Miller et al., 1999), as numerous scientific evidences show mutations in the *APC* gene are not only responsible for familial adenomatous polyposis (FAP), but also plays a significant rate-limiting role in the initial stages of majority of sporadic colorectal cancers via formation of the

destruction complex (Aoki and Taketo, 2007; Fodde, 2002). Subsequently, the phosphorylated regions of β-catenin are exposed to the F-box/WD repeat protein which is a component of E3 ubiquitin ligase complex β-transducin repeat-containing protein (β-TRcP) which mediates the ubiquitination and the proteasomal degradation of β-catenin (Clevers and Nusse, 2012). Once β-catenin is degraded Wnt target genes fails to be transcribed. This process keeps the cytoplasmic β-catenin level low thereby preventing the translocation of β-catenin into the nucleus.

Conversely, the *ON-state* (Figure 1-2) of canonical Wnt-signalling is activated by the binding of Wnt ligands, (secreted mainly by myofibroblasts beneath the base of the crypts in the small intestine), to Frizzled and LRP 5/6 co-receptors at the cell surface (Clevers, 2006; Wantae et al., 2013). Additionally, studies show that cancer associated fibroblasts (CAF) are associated with the canonical Wnt-signalling pathway (Augsten, 2014), with stromal fibroblasts also implicated in the secretion of pro-tumorigenic factors that promote skin squamous cell carcinomas through activation of the Wnt/β-catenin signalling pathway (Sobel et al., 2015). Formation of this receptor complex triggers the activation of Dsh/Dvl, a cytoplasmic scaffolding protein crucial for Wnt-induced LRP6 phosphorylation (Bilić et al., 2007; Zeng et al., 2008), which proceeds to inhibit GSK-3β enzyme activity, triggering a complex series of events that prevents the phosphorylation and subsequent degradation of β-catenin resulting to its consequent stabilization and accumulation in the cytoplasm. Accumulated cytoplasmic β-catenin then translocate to the nucleus, where it displaces Groucho (a co-repressor transcriptional factor) due to its stronger affinity to

engage TCF/LEF transcription factors (Angers and Moon, 2009; Nusse, 2012) to activate transcription of target Wnt genes such as c-*myc*, *c-jun*, *Axin2*, *Eph*B/*ephrin*-B and *Cyclin*D1 (these genes are also activated in canonical Wnt-driven carcinogenesis). These target genes all play crucial roles in the regulation of a plethora of cellular processes including but not restricted to cell proliferation, cell division, stem cell maintenance as well as regulation of various stages of embryogenesis (Ten Berge et al., 2011), hence a major consequence of dysregulation of β-catenin could result to maintenance of cancer phenotype (Wantae et al., 2013). Interestingly, the progression of tumours to invasive cancers and metastatic disease may also involve the switch from canonical to non-canonical Wnt-signalling (Bordonaro et al., 2011)..

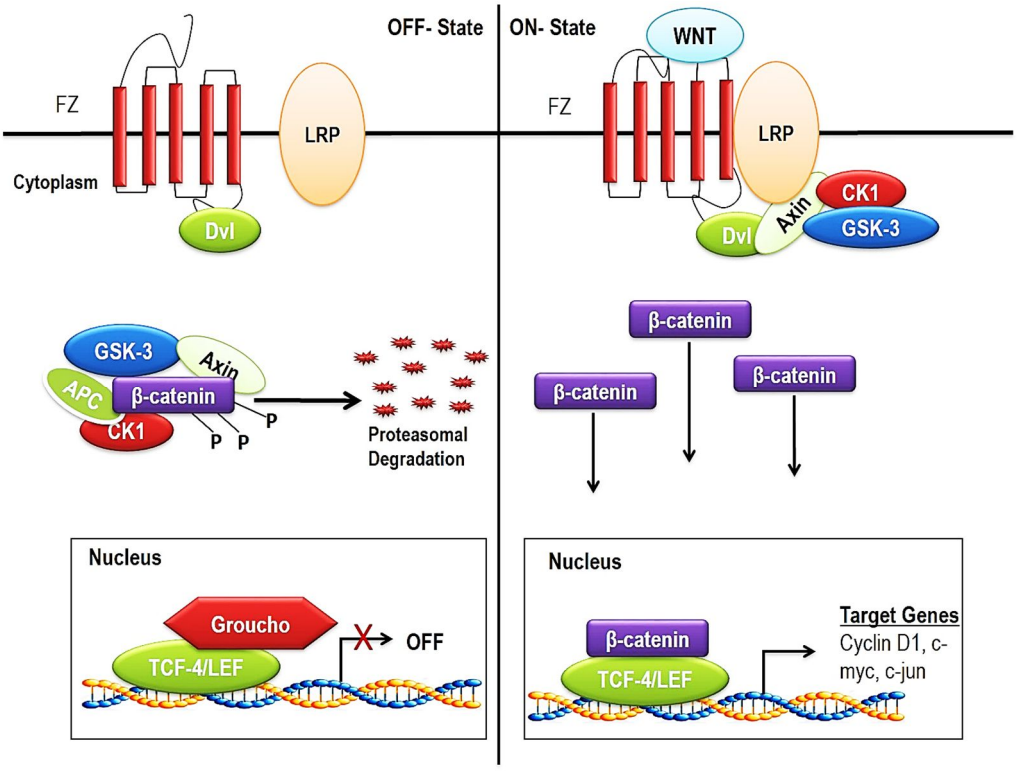


Figure 1-2: Representation of Canonical Wnt/β-catenin pathway. OFF-STATE: The destruction complex regulates β-catenin in the absence of Wnt

ligands. GSK-3 and CK1 facilitates the phosphorylation of β-catenin at specific serine and threonine sites rendering it a target for proteosomal degradation by β-TRCP. Because of this degradation, β-catenin is prevented from translocating into the nucleus prompting Groucho (co-repressor) to be bound to TCF thereby repressing gene transcription. **ON STATE:** Once binding of Wnt ligand to Fzd and LRP5/6 co-receptors occurs, Dvl-fzd complex is formed resulting to the phosphorylation of LRP5/6 by GSK-3 and triggering the recruitment of Axin2 from the destruction complex. The disassembly of the complex promotes stabilization and accumulation of cytoplasmic β-catenin, which eventually translocates to the nucleus where Groucho is dislodged and TCF is converted into a transcription factor ensuring the transcription of many genes including *c-myc*, *Ascl2*, *cyclin D1*, which are essential stem cell regulators as well as mediators of proliferation and differentiation. Taken from (Onyido et al., 2016).

1.2.4 Deregulation of Wnt Signalling activity via Genetic Mutations

Generally, cancerous genetic mutations on any gene that participates in the Wnt/β-catenin signalling cascade inappropriately reactivate the pathway, leading to abnormal ON-state activity. In effect, the activity of Wnt signalling in the cell is no longer governed by the presence of Wnt ligands. Therefore, Wnt signalling may be switched into the ON-state even in the absence of Wnt ligand–receptor interaction, leading to the characteristic sequence of ON-state activity: disassembly of the destruction complex, accumulation of nuclear β-catenin and activation of Wnt-induced gene transcription (Figure 1-3).

Disruption of Wnt/β-catenin signalling via genetic mutations includes mutations in genes encoding component proteins of the signalling cascade. For instance, mutations in the genes for β-catenin (*CTNNB1*), APC, and Axin1 have been identified in various neoplasms (MacDonald et al., 2009). Mutations in *CTNNB1*

have been implicated in colon cancer, gastric cancer, medulloblastoma, melanoma, ovarian cancer, pancreatic cancer, and prostate cancer (Abdelmaksoud-Damak et al., 2015; Lee et al., 2015). Mutations in *APC* gene have frequently been identified in colon cancer as well, while mutations in *AXIN1*, the gene for Axin1, have been identified in hepatocellular carcinoma (Satoh et al., 2000) and medulloblastoma (Silva et al., 2013). Thus, there is considerable evidence for abnormalities in the Wnt signalling pathway in tumorigenesis.

A major consequence of mutations in APC, Axin, GSK-3 and β-catenin genes is the increased nuclear β-catenin levels, which is already a proven prerequisite for intestinal tumorigenesis. Consequently, mutant APC protein becomes unable to form a proper destruction complex with GSK-3, which inevitably impairs the phosphorylation of β-catenin on specific sites. Similarly, mutations resulting to amino acid substitutions in the phosphorylated residues of β-catenin may hinder phosphorylation and recognition by the E3 ligase ubiquitin system thereby prompting the cytoplasmic stabilization and nuclear translocation of β-catenin (Samowitz et al., 2007). Interestingly, GSK-3α mutation has been identified as a cause for the disruption of Wnt/β-catenin signalling pathway as studies demonstrate that both deletion of APC or GSK3 α and β using mouse models ($AhCreER^{+}$ $APC^{fl/fl}$, $AhCreER^{+}$ $Catnb^{exon3fl/exon3fl}$ and $AhCreER^{+}$ $GSK3\alpha^{fl/fl}$ $\beta^{fl/fl}$) lead to immediate nuclear β-catenin accumulation and subsequent transcription of Wnt target gene expression (Radulescu et al., 2013). This acute Wnt signalling activation perturbs differentiation within the adult stomach resulting to a rapid tumour formation**.** Additionally, mutation in β-catenin gene *CTNNB1* can ultimately instigate a gain of function mutation, which activates β-catenin,

increasing its transcriptional activity and enabling the protein to evade phosphorylation and subsequent degradation (Lüchtenborg et al., 2005; Morikawa et al., 2011). Activation of GSK-3β and GSK-3α is regulated by site-specific phosphorylation of tyrosine 216 and tyrosine 279 sites respectively. Amino acid substitution of these tyrosine phosphorylation sites would permanently inactivate GSK-3 thereby hindering the phosphorylation and ubiquitination of β-catenin and, consequently, the cytoplasmic level of β-catenin increases. In the nucleus, β-catenin is tightly regulated via several regulatory co-factors. This compact regulation of both cytoplasmic and nuclear β-catenin is aimed to transcriptionally modulate Wnt-target genes.

Mutations on these regulatory factors could further facilitate transcription of Wnt target genes required for tumour development. Mutations also occur in Frizzled genes resulting to loss of the functional Wnt-receptor interaction responsible for the initiation of the Wnt signalling cascade while mutation of the Secreted frizzled-related proteins (SFRPs) through epigenetic silencing of the gene that encodes it could activate Wnt signalling through the receptor FRZ. This would potentially inactivate the destruction complex, allowing β-catenin accumulation in the cytoplasm and subsequent translocation to the nucleus

These genetic mutations ultimately inappropriately instigate or hinder the initiation of both canonical and non-canonical signalling cascade, thus compromising the integrity of the intestinal epithelium particularly the crypt base region (Ueno et al., 2008; You et al., 2007).

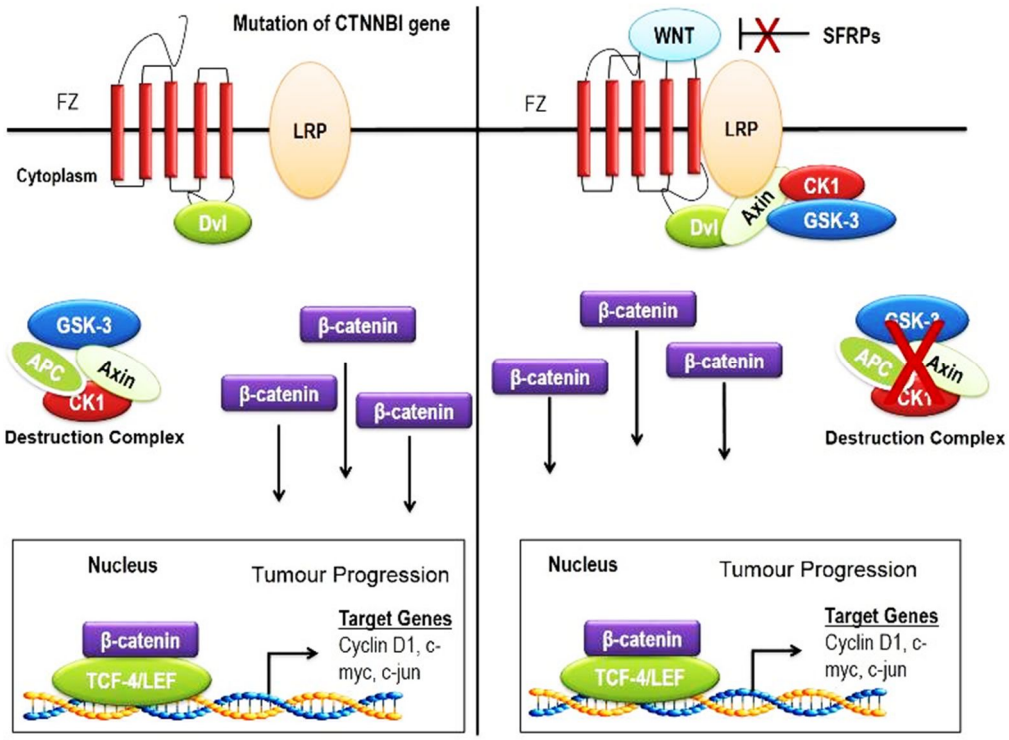


Figure 1-3: Aberrant activation Wnt/β-catenin signalling in carcinogenesis. Mutation of β-catenin gene (*CTNNBI*) as well as the mutation of components of the destruction complex can result in aberrant Wnt signalling thereby facilitating tumour progression. Loss of SFRPs via epigenetic silencing disrupts the destruction complex thereby allowing cytoplasmic and nuclear β-catenin accumulation. Subsequent activation of transcription genes such as *cyclin D1*, *c-myc*, *c-jun* promotes cell proliferation and survival rather than differentiation which eventually facilitates tumour progression.

1.2.5 Regulation of β-catenin/TCF complex assembly

Numerous scientific documentations have shown that Wnt signalling through the formation of β-catenin/TCF complex has been established as the most accepted prerequisite for Wnt target gene activation (Barker and Clevers, 2006; Van der Flier et al., 2007). However, strong evidence has accumulated over the past few years identifying a large number of proteins that interact with nuclear β-catenin

to either promote or antagonize its transcriptional activity resulting in transcriptional activation or repression of Wnt-target genes respectively. This mechanism through which the maintenance of the balance between activation and repression of Wnt signalling pathway is executed is crucial in normal embryonic developmental processes such as limb morphogenesis, limb bud initiation and limb skeletal development (Church and Francis-West, 2002; Geetha-Loganathan et al., 2008). For instance, a major consequence of an imbalance could result to congenital limb deficiency.

Certain co-activators interact with β-catenin in the nucleus to facilitate its transcriptional activity toward activation of Wnt-target genes (Figure 1-4). This occurs by either enhancing promoter binding to facilitate the chromatin remodelling at the promoter site of Wnt-target genes such as p300/CBP and Brg-1 (Barker et al., 2001; Hecht et al., 2000), while others promotes nuclear localization of β-catenin such as pygopus (Townsley et al., 2004). While the central Arm-repeats of β-catenin associate with TCF, and the amino-terminal Arm-repeat binds to BCL9, most of the co-activator complexes interact with the β-catenin carboxyl terminal portion, creating an interplay between β-catenin and the transcriptional apparatus and the chromatin. Activation of the Wnt/β-catenin signalling pathway eventually results to elevated expression of genes that control different biological processes relevant to the maintenance of cell integrity and normal developmental function such as c-myc, cyclin D1, c-jun, fra-1, EphB/ephrin-B, Twist, and many more (Herbst et al., 2014).

The Groucho/TLE family protein of repressors is a major repressor of the β-catenin/TCF complex via direct interaction with TCF/LEF transcription factors.

Generally, Groucho/TLE proteins are transcriptional co-repressors and have been implicated in interacting with histone deacetylases, enzymes that maintain chromatin in a transcriptionally inactive state (Daniels and Weis, 2005). It is proposed that the recruitment of histone deacetlyases to the TCF/LEF promoter region may counteract CBP/p300 and Brg-1 activities, and thereby enhance repression of Wnt signalling. The repressor activity of Groucho/TLE proteins is however disrupted following the translocation of β-catenin into the nucleus upon Wnt activation. Some co-repressors tend to regulate the Wnt/β-catenin signalling pathway via mechanisms other than binding directly to the TCF/LEF complex. For instance, the N-terminus of Sox9 containing the HMG domain promotes β-catenin degradation via nuclear phosphorylation, whereas the C-terminal transactivation domain inhibits the transcriptional activity of β-catenin (Topol et al., 2009). The activity of Sox9 shows phosphorylation of β-catenin also occurs in the nucleus. Further studies have also shown that β-catenin phosphorylation and degradation can occur in the nucleus rather than solely in the cytoplasm (Xue et al., 2015).

Furthermore, Chibby, a nuclear antagonist was shown to inhibit Wnt signalling via direct interaction with β-catenin in the nucleus thus blocking its association with TCF/LEF transcription factors (Takemaru et al., 2003) and interfering with the abundance of β-catenin localization arm through its efficient nuclear/cytoplasmic shuttling (Li et al., 2010).

Generally, these findings indicate that under normal circumstances β-catenin co-repressors function as regulators of the β-catenin/TCF complex, thus ensuring that adequate threshold of β-catenin is maintained prior to interaction with TCFs

(Figure 1-4). Apart from cytoplasmic β-catenin regulation via the destruction complex, the regulatory importance of interactions between nuclear co-activators and co-repressors with the β-catenin/TCF complex determines the final downstream effects in both normal and cancer development. Therefore, it is expected that identification of novel protein-protein interaction with the nuclear β-catenin could have crucial impact in normal versus tumour development.

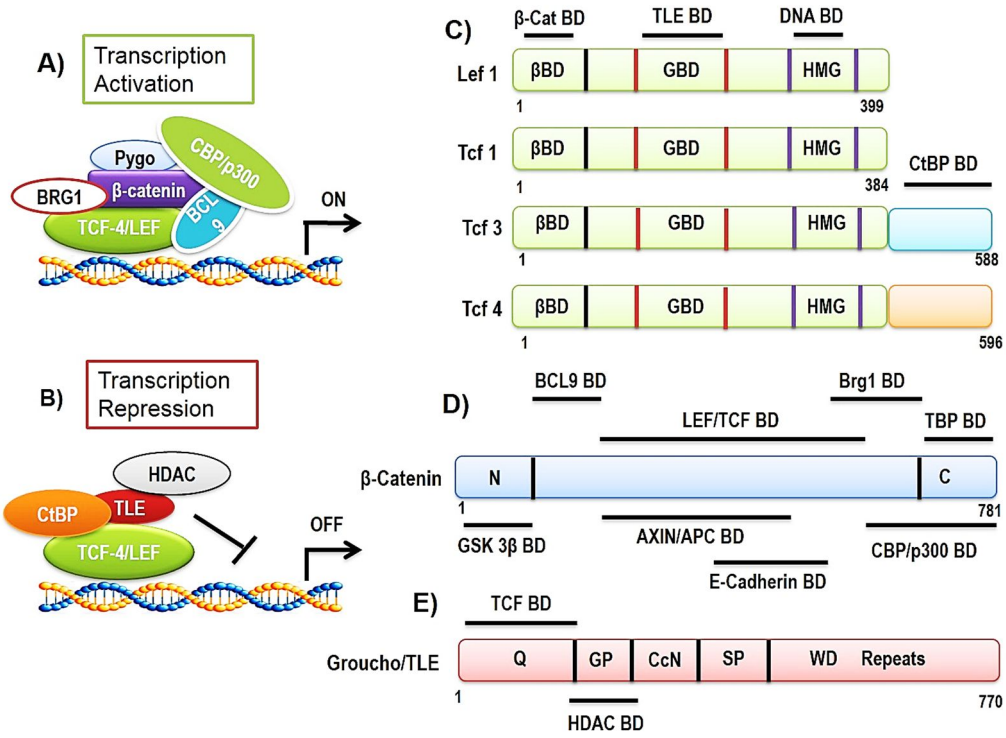


Figure 1-4: Structural organization and transcriptional regulation of canonical Wnt regulators. Schematic illustrates the formation of transcriptional activation or repression complex of LEF/TCF on Wnt target genes. **A)** In the activation mode, β-catenin binds with a member of the LEF/TCF family of DNA-binding proteins thereby recruiting transcription activators histone modifiers CBP/p300 and BRG1 as well as BCL9 and Pygo. **B)** In the absence of β-catenin, TCF/LEF members interact with the transcriptional repressor Groucho/TLEs which in turn recruit CtBP as well as histone deacetylase (HDAC) to yield an inactive chromatin state for the target

genes leading to transcriptional repression of Wnt target genes. Structural depiction of **C)** LEF/TCF, **D)** β-catenin and **E)** Groucho/TLE with their respective binding domains are also shown. Adapted from (Lien and Fuchs, 2014)**.**

1.2.6 Non canonical Wnt signalling pathway

Apart from the canonical Wnt-pathway, specific Wnt-ligands can also trigger non-canonical pathways, which are also referred to as β-catenin independent pathways. As earlier mentioned, the Wnt ligands consists of a large family of 19 secreted glycoproteins that are cysteine-rich and highly hydrophobic. It is not entirely understood which particular Wnt ligand participates in either of the Wnt-pathways, however, some Wnts (Wnt1 and Wnt3a) preferentially trigger canonical signalling, whereas others (such as Wnt5a and Wnt11) initiate the β-catenin-independent pathways (Kikuchi et al., 2011). The non-canonical Wnt pathway is further divided into three other distinct branches namely, the Wnt/Ca^{2+}, the Wnt/JNK and the Wnt/planar cell polarity (PCP) pathways (Figure 1-5). Upstream, the activation of non-canonical Wnt pathways also involve Wnt/Fz, however, the mechanism of downstream signal transduction through these pathways occurs in a less understood manner although scientific evidences suggest the 3 branches of the non-canonical pathway function dependently of each other (Rao and Kühl, 2010).

Generally, non-canonical pathways have been implicated in the regulation of cell movement and polarity (Mayor and Theveneau, 2014; Sugimura and Li, 2010). For instance, in the planar cell polarity pathway, frizzled activates JNK, directs asymmetric cytoskeletal organization, and coordinated polarization of cells

within the plane of epithelial sheets via activation of small GTPases of the rho family including rac, cdc42, and rho. This leads to release of intracellular Ca^{2+}, via G-proteins which in-turn activates calcium dependent enzymes like calcium/calmodulin-dependent kinase (CaMKII), PKC or calcineurin (Komiya and Habas, 2008; Yamanaka et al., 2002). Consequently, through calcineurin, the Wnt/calcium pathway activates NFAT (nuclear factor of activated T cells) transcription factor, which translocates to the nucleus to regulate multiple processes such as T-cell differentiation and proliferation (Figure 1-5). Interestingly, the non-canonical Wnt signalling antagonizes the β-catenin-dependent Wnt signalling pathway by either or both CaMKII pathway and NFAT-mediated transcriptional regulation (Sugimura and Li, 2010), however, some studies also suggest that the PCP pathways can also antagonize the canonical Wnt cascade (Sato et al., 2010). The CaMKII pathway suppresses β-catenin-TCF-dependent transcription through phosphorylation of TCF transcription factors (Ishitani et al., 2003), while NFAT is reported to inhibit β-catenin-dependent transcription (Saneyoshi et al., 2002). All these findings simply highlight the possible crosstalk among various types of Wnt signalling.

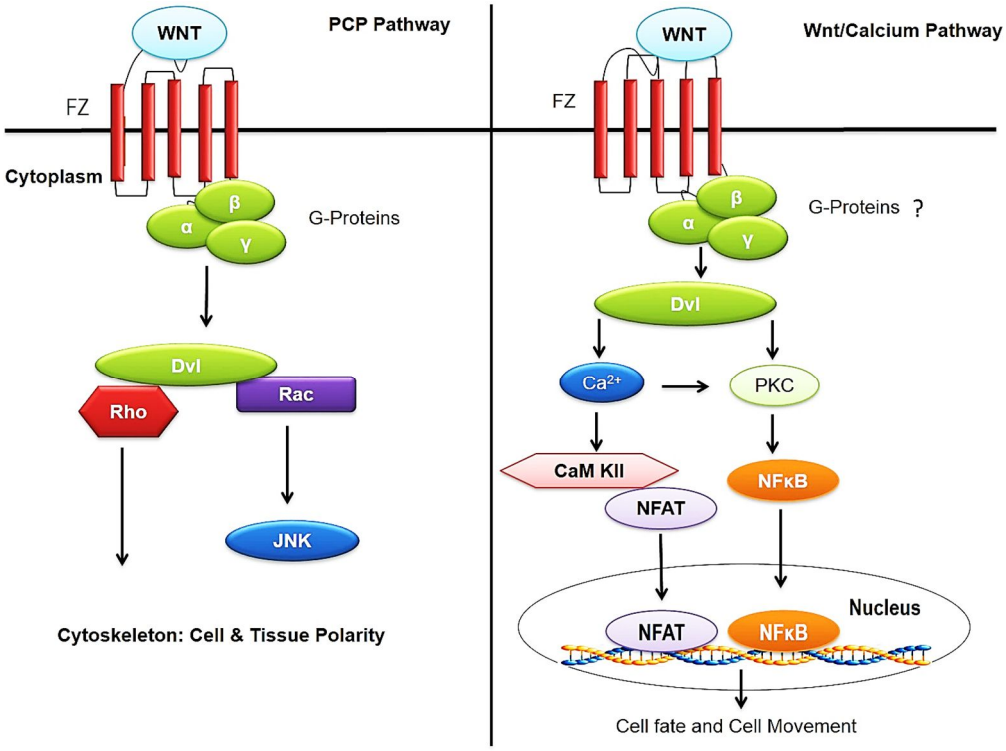


Figure 1-5: Schematic of Non-Canonical Wnt pathway. In the PCP pathway, Fz activates Dvl through G-proteins in the absence of LRP receptors. Subsequent activation of the Rho GTPases, Rho and Rac results to the induction of cytoskeletal changes. In the Wnt/Calcium pathway, Dvl activates protein kinase C (PKC) to release intracellular calcium and calcium/calmodulin-dependent protein kinase II (CaMKII). However, it is still unclear whether G-proteins are involved in this particular pathway. Taken from (Onyido et al., 2016).

The Wnt signalling pathways (both canonical and non-canonical) are among the most essential pathways generally implicated in various aspects of development, cell biology and in a deregulated or mutated state, the pathways promote tumorigenesis. However, for this purpose, the Wnt/β-catenin signalling is of particular relevance to the normal function of the intestinal architecture and homeostasis with the following sections explaining this in more detail.

1.3 Influence of the Canonical Wnt Signalling Pathway in the Maintenance of Normal Intestinal Architecture

Development and homeostasis in all multicellular organisms is based on an intricate interplay between a plethora of processes involved in migration, cell proliferation, differentiation, adhesion, and cell apoptosis. A number of intercellular signals mostly coordinates this multitude of cellular responses. Scientific evidences from several laboratories have proven that the Wnt/β-catenin signalling pathway not only drives tumorigenesis when mutated but also plays a crucial role in all aspects of intestinal biology ranging from cellular homeostasis to normal development and carcinogenesis determined by the context of activation and surrounding microenvironment (Figure 1-6).

1.3.1 Role of Wnt signalling in Intestinal Crypts Cell Migration & Positioning

Generally, intestinal epithelia homeostasis is strongly maintained by specific signalling pathways. In particular, the activity of Notch, BMP and Wnt signalling pathways are required for a proper balance of proliferation and differentiation between cell lineages in the intestine that maintain balance between processes of cell proliferation and differentiation.

The role of Wnt/β-catenin signalling pathway in the maintenance of pluripotency and stem cell proliferation have long been firmly established according to *in-vivo* and *in-vitro* studies (Clevers et al., 2014). For instance, studies in mice have

shown Wnt activity elevates the Lgr5+ stem cell population as observed following inoculation of RSPO1, a Wnt agonist (Kim et al., 2005). Genetic mutation of β-catenin (*CTNNB1*) (Fevr et al., 2007; Ireland et al., 2004), TCF4 (van Es et al., 2012) and other components of the cytoplasmic destruction complex are particularly associated with the demise of the intestinal crypts. Similarly, aberrant ectopic expression of Wnt ligand can contribute to the collapse of the intestinal architecture (Kuhnert et al., 2004), hence a balance in the Wnt ligand secretion is highly essential.

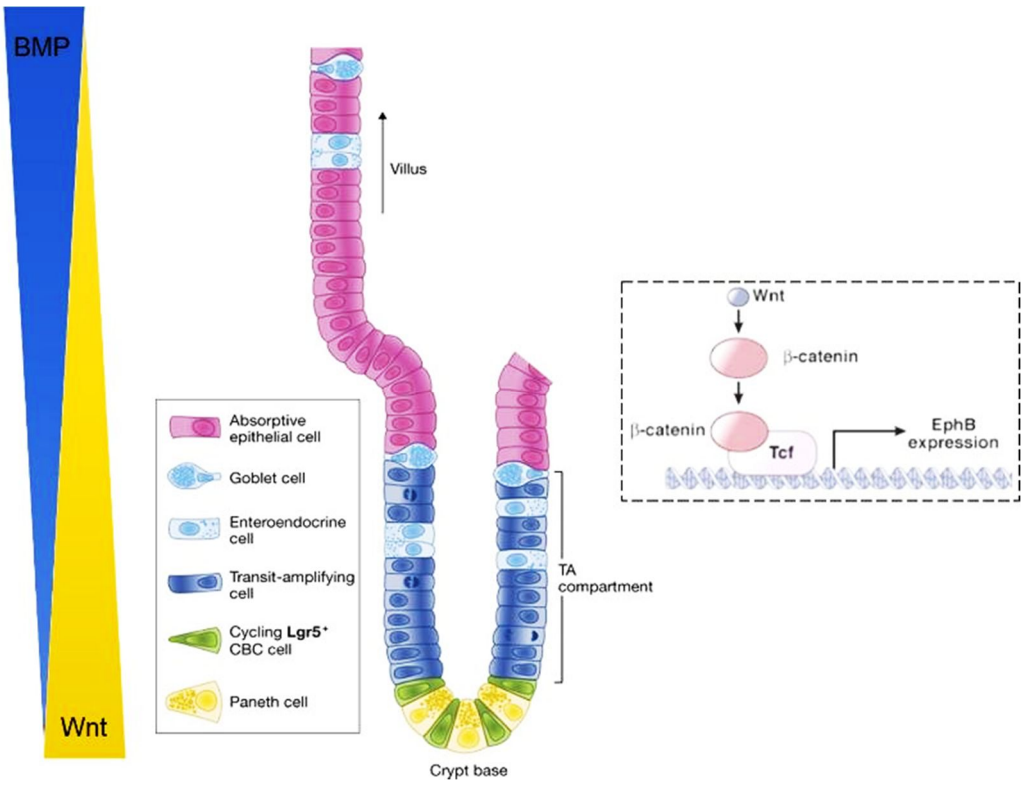


Figure 1-6: Wnt/β-catenin signalling regulation in Intestinal Stem Cells (ISCs). ISCs, including CBCs, Lgr5+and +4 LRCs, and their niche Paneth cells are located at the crypt base. An opposing gradient involving Wnt and BMP expression exists at the crypt base. Wnt levels are usually high which consequently facilitates EphB expression. Among LEF/TCF family proteins, TCF4 has been shown as a key regulator of adult intestinal epithelial cells homeostasis. Adapted from (Schuijers and Clevers, 2012).

Furthermore, stem cell studies suggest that the expression of stem cell markers such as Tert, EphB2, Bmi1 and Lgr5 are controlled by the Wnt/β-catenin signalling pathway (Krausova and Korinek, 2014). In addition, identification of ISCs directly correlated to TCF-β-catenin-responsive genes analysis in human tumour cells with the interpretation of the results also established in mouse intestinal tissue (van de Wetering et al., 2002). Under normal conditions, the strength of the Wnt cascade becomes subdued in CBC cells by a negative feedback-loop mechanism involving the upregulation of the β-catenin negative regulator and a component of the destruction complex, Axin2 (Lustig et al., 2002) as well as the expression of Frizzled specific ubiquitin ligases Rnf43 and Znfr3 (Glinka et al., 2011; Koo et al., 2012), which reduces Frizzled stability via ubiquitin-mediated destruction. Consequently, simultaneous conditional knock-out of both Rnf43 and Znrf3 induced expansion of the proliferative zone of the crypts which eventually led to development of intestinal adenomas in mouse intestines (Koo et al., 2012).

The Wnt signalling cascade is tightly governed to maintain a balance of proliferation and quiescence of ISCs (Merrill, 2012; Nusse et al., 2008) (Figure 1-6) . Numerous scientific evidence shows the expression of Wnt diminishes as cells migrate along the crypt-villus axis (Krausova and Korinek, 2014). The Wnt pathway output is controlled by co-operative activity of Bone Morphogenic Protein (BMP) and Hedgehog cascades (Clarke, 2006; Katoh, 2007). As the progenitor cells further migrates away from the crypt base, the Hedgehog-induced, mesenchyme-to-epithelium BMP signalling promotes differentiation while preventing proliferation (Clarke, 2006). This mechanism explains why

differentiation of different cells in the intestinal epithelium occurs away from the crypt base. Importantly, ISCs located in the colon are also locally protected from the pro-differentiation BMP signals by secretion of BMP antagonists; gremlin 1/2 and chordin-like 1 (Larman et al., 2009). The balance in the activity of Wnt pathway and the Hedgehog/BMP cascade must be maintained in order to preserve the integrity of the intestinal epithelium as inappropriate activation of any of the pathways involved would result to cancer development (Figure 1-7). The dual cell fate decisions between absorptive versus secretory cell lineages are modulated by the cross-talk between the Wnt and Notch pathways (Yeung et al., 2011).

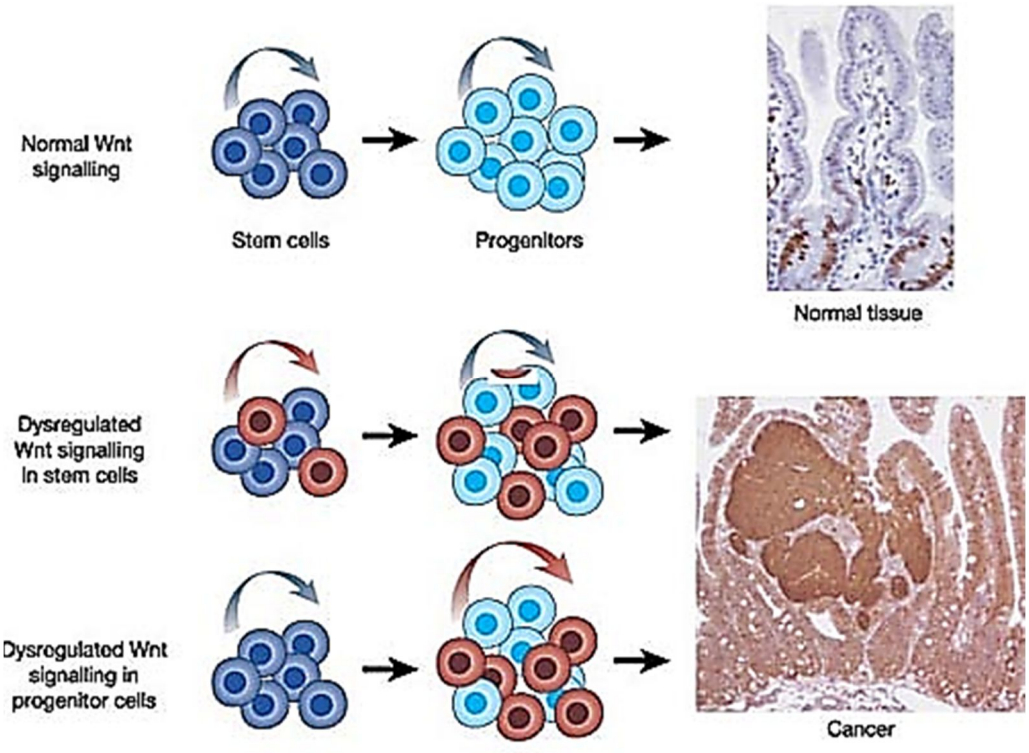


Figure 1-7: Importance of Wnt signalling in the regulation of stem cells. The Wnt/β-catenin signalling pathway has been implicated as a niche factor that maintains the integrity of various types of stem cells in a self-renewing manner. Hence, uncontrolled Wnt signalling can result to aberrant stem cell pool expansion. Taken from (Reya and Clevers, 2005).

1.4 Zinc Finger Family of Proteins

Many proteins capable of binding to specific DNA sequences have been revealed to date via high throughput bioinformatics analysis. This has enabled the identification of distinct amino acid motifs on these proteins capable of recognizing, and binding to specific DNA sequences via hydrogen bond interaction in DNA major and minor grooves. A typical example of such motif widely recognized to participate in DNA binding is the zinc finger (ZF) motif.

The zinc finger family of proteins are characterized by the presence of zinc ions as structural components (Figure 1-8). There are approximately 10 different classes of zinc-binding motifs identified having been either totally or partially characterized, however, the C_2H_2 (TFIIIA/Krüppel) zinc finger motif appears to be the most abundant and mostly studied DNA-binding motif among putative eukaryotic transcription factors (Krishna et al., 2003a; Razin et al., 2012). The DNA/RNA binding capability was initially identified in Xenopus TFIIIA (Hanas et al., 1983; Lu et al., 2003), the first zinc/finger transcription factor before the subsequent characterization of the C_2H_2 zinc finger motif (Miller et al., 1985). The tandem arrays of the C_2H_2 motif is represented in this sequence Y/F-X-C-X2–4-C-X3-F-X5-L-X2-H-X3–5-H, where X indicates variable amino acid residues.

Structurally, each zinc finger motif consists of two perpendicular β-strands followed by an α-helix. The conserved cysteine and histidine residues (C_2H_2) form coordinate bonds with the zinc ion within the motif (Figure 1-8). This bond forms a hydrophobic core to maintain stabilization of the protein structure. Absence of these zinc ions would eventually result in unfolding of the domain,

hence rendering the protein non-functional. These proteins also possess a highly conserved seven-amino-acid H/C link (also referred to inter-finger spacer, TGEKP(Y/F)X) which has been proven to undergo phosphorylation on its threonine residue during the mitotic stage of the cell cycle, resulting in protein inactivation (Dovat et al., 2002), thus suggesting a potential inactivation mechanism of the C_2H_2 family.

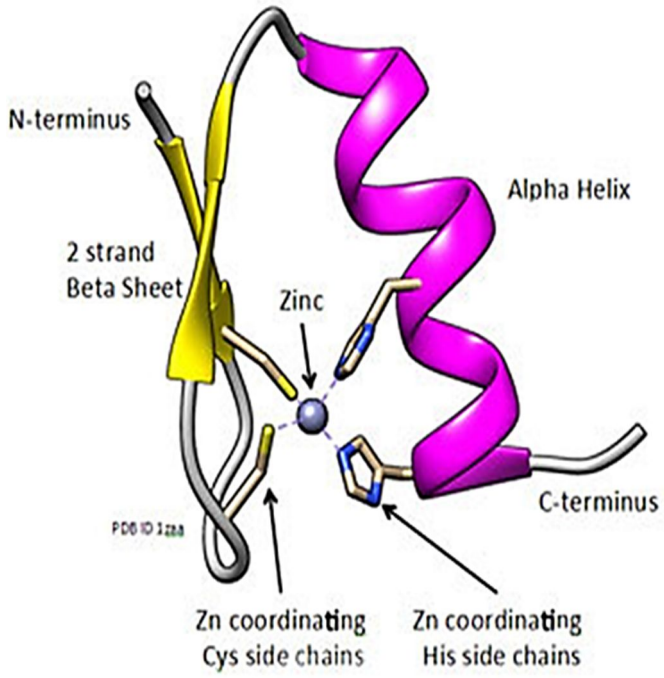


Figure 1-8: C_2H_2 zinc finger motif. A C_2H_2 zinc finger showing the alpha helix (pink), antiparallel Beta sheets (yellow) and the zinc molecule (grey) bound by two histidine (His) amino acids and two cysteine (Cys) amino acids (Gaj et al., 2013).

As indicated earlier, one of the most fascinating property of C_2H_2 zinc finger appears to be its sequence specific DNA binding affinity (Najafabadi et al., 2015). For instance, Egr-1 (Zif268) possessing three zinc finger motifs as well as having an influence on the brain and cardiovascular system, specifically binds

to a 9 base-pair (bp) CG-rich sequence, with each zinc finger simultaneously binding to a sub-site along the major groove of DNA (Elrod-Erickson et al., 1996; Pavletich and Pabo, 1991). This zinc finger-DNA binding mode suggests the possibility of the presence of a DNA recognition region/code, which provides a framework for the design of novel zinc finger recognition target sites. However, considerable amount of effort devoted to this field of study has established that a single DNA recognition code for mC_2H_2 does not exist. There are other forms of zinc fingers which uniquely bind to DNA sites of AT-rich sequences (e.g. TATAZF) (Wolfe et al., 2001). The general binding affinity of a mC_2H_2 is largely determined by the association between zinc fingers, as well as the linkers (Laity et al., 2000; Papworth et al., 2006). However, the actual conformation and binding motif of the generic mC_2H_2 zinc finger protein with DNA is not completely understood (Persikov et al., 2009; Persikov and Singh, 2013).

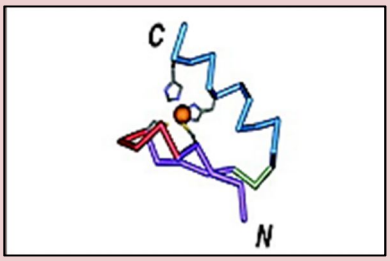
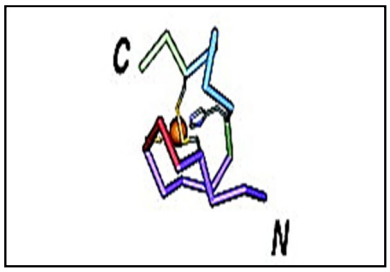
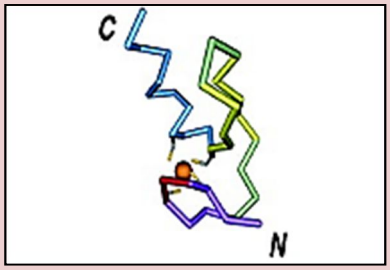
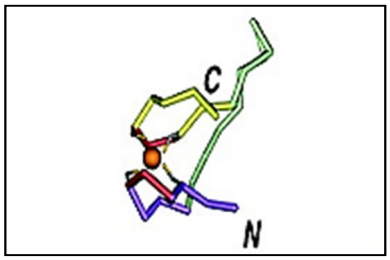
The first co-crystal structure (Zif268-DNA complex) to be determined was a polypeptide containing three C_2H_2 motifs of Zif268/Egr1/Krox-24 containing the DNA double-helix binding region within the major groove enveloped by the zinc fingers (Pavletich and Pabo, 1993). In this structure, each zinc finger appears to independently bind DNA with contact residues at three amino acid positions: -1, + 3, and + 6, where -1 is the first residue of the α-helical region (Ganss and Jheon, 2004).

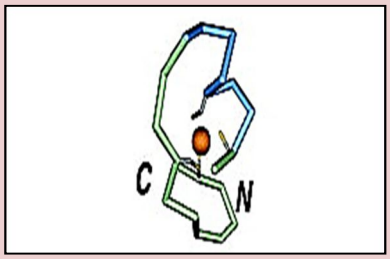
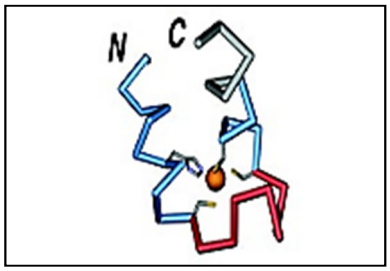
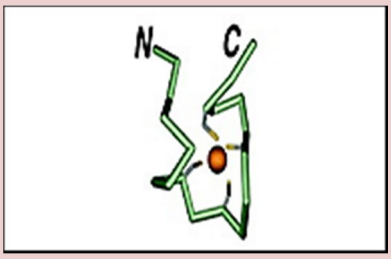
Although the zinc finger motifs have largely been identified as DNA-binding domains (Gaj et al., 2013), there still exists evidences suggesting these motifs also participates in RNA binding as well as protein-protein interaction (Brayer

and Segal, 2008a; Krishna et al., 2003b). For instance, zinc fingers motifs in Sp1 and YY1 have been implicated in both DNA and protein interaction (Brayer and Segal, 2008b; Lee et al., 1993). As a result of the above mentioned function, zinc finger-containing proteins have been broadly involved in various cellular biological activities such as but not restricted to gene expression regulation, replication and repair, signal transduction, differentiation, post-transcription modification processes and proliferation (Lupo et al., 2013; Urrutia, 2003)

As our knowledge of zinc fingers continues to expand, different classes and subfamilies of these proteins have been identified (Table 1-1). Therefore, due to zinc finger motifs being functionally and structurally diverse and present among a plethora of proteins, scientists have attempted to classify them based on specific criteria such as the type or number of amino acids participating in the zinc coordination (Leon and Roth, 2000) or based on the structural properties of the protein backbone present in the folded domain region (Krishna et al., 2003b). The current classifications of zinc finger domains are listed below:

Table 1-1: Structural classification of zinc fingers. Taken and adapted from (Krishna et al., 2003b).

Fold groups	Representative structure	Brief description
C_2H_2 like		Two zinc ligands contribute to form a zinc knuckle at the end of the beta-hairpin while the other two ligands form the C-terminus end of the alpha-helix.
Gag knuckle		Two N-terminal zinc ligands contribute to form zinc knuckle and two others form a short helix.
Treble clef		Beta-hairpin at the N-terminus and an alpha-helix at the C-terminus. Two ligands form a zinc knuckle while two more ligands form N-terminal turn of the helix.
Zinc ribbon		Two ligands contribute to form two zinc-knuckles. The beta-hairpins further form two structurally identical zinc-binding sub-sites.

Zn2/Cys6		A pair of ligands forms the N-terminus of a helix while another pair forms a loop giving rise to Zinc-binding domains.
TAZ2 domain like		Zinc-binding domains formed by the association of two ligands forming the termini of two alpha-helices.
Zinc Binding Loops		Four ligands contribute to form a loop.

1.5 FLYWCH Zinc Finger Protein

1.5.1 Discovery & Description

The FLYWCH zinc finger motif is a recently discovered member of the zinc finger family isolated from the Drosophila modifier of mdg4 [mod (mdg4)] encoded proteins (Dorn and Krauss, 2003). The designation "FLYWCH" is derived from the presence of four hydrophobic amino acids residues [**F** (phenylalanine), **L** (Leucine), **Y** (tyrosine) and **W** (tryptophan)] located at conserved positions of the Cys_2His_2 motif. It is composed of a conserved

sequence F/Y-X_n-L-X_n-F/Y-X_n-WXCX_{6-12}CX_{17-22}HXH where X signifies the presence of any amino acid. The Mod (mdg4) isoforms consists of a leucine zipper and a BTB domain (Beaster-Jones and Okkema, 2004a). Mod (mdg4) maintains complex phenotypes enabling it to carryout roles suggested to consist of regulation of gypsy insulator sequences, apoptosis, viability, as well as regulation of homeotic gene expression involving either gene activation or gene silencing (Dorn and Krauss, 2003). This DNA/protein binding zinc finger domain is located either on the N-terminus or C-terminus of different mammalian and drosophila proteins (Mongelard et al., 2002).

FLYWCH motifs have also been identified in two other proteins derived from *Caenorhabditis elegans* (*C. elegans*) namely; FLYWCH transcription factors; FLH-1, FLH-2, and FLH-3 (Ow et al., 2008b) and PEB-1 (Beaster-Jones and Okkema, 2004b). Furthermore, the FLYWCH motifs have also been discovered in a highly conserved uncharacterized protein in mammals designated FLYWCH1 (Gene ID: 84256).

Here, for the first time, Dr. Nateri's lab have identified a FLYWCH-type zinc finger protein (FLYWCH1), which binds to nuclear β-catenin hindering β-catenin/TCF4 signalling via competitive inhibition (Muhammed et al, submitted). Apart from the initial discovery of proteins with FLYWCH domain in *Drosophila* and *C. elegans*, there are limited published data about the function of FLYWCH protein particularly in human or any other mammals. Therefore, the current work further demonstrate the characterization and functional analysis of FLYWCH1 in CRC cells after the initial research project previously carried on in Dr Nateri's lab (Muhammed, et al., submitted).

1.5.2 Bioinformatics of human FLYWCH1 motif

Based on bioinformatics analyses, human FLYWCH1 gene (Gene ID: 84256, http://www.ncbi.nlm.nih.gov/gene/84256) is composed of 2,151 nucleotides (2.1 kb) encoding a protein of 716 amino acid (aa) residues (Muhammed et al., submitted) and shows homology with a variety of organisms (Table 1-2, Figure 1-10). Bioinformatics resources such as protein family (Pfam, http://pfam.sanger.ac.uk/) (Finn et al., 2010) and Domain Mapping of Disease Mutations (DMDM, http://bioinf.umbc.edu/dmdm/) (Peterson et al., 2010) were utilized for the purpose of defining the amino acid sequence within which the conserved FLYWCH1 domains are located. The analysis showed FLYWCH1 contains a distribution of a tandem array of five FLYWCH-type zinc finger motifs (Muhammad et al., submitted). Further validation to confirm the presence of the conserved FLYWCH domains via sequence alignment of FLYWCH1 motif was performed with results showing the FLYWCH consensus sequence (**F**, **L**, **Y**, **W**, **C**, & **H**) was conserved within the zinc finger motif of the protein (Figure 1-9 B). Identification of the putative nuclear localization signal (NLS) motif (KRAK) within the amino acid sequence of FLYWCH1 was revealed by Predict-Protein database (available at www.predictprotein.org) (Figure 1-9 A). This NLS sequence is similar to the classical NLS motif (K-R/K-X-K/R) (Hodel et al., 2001).

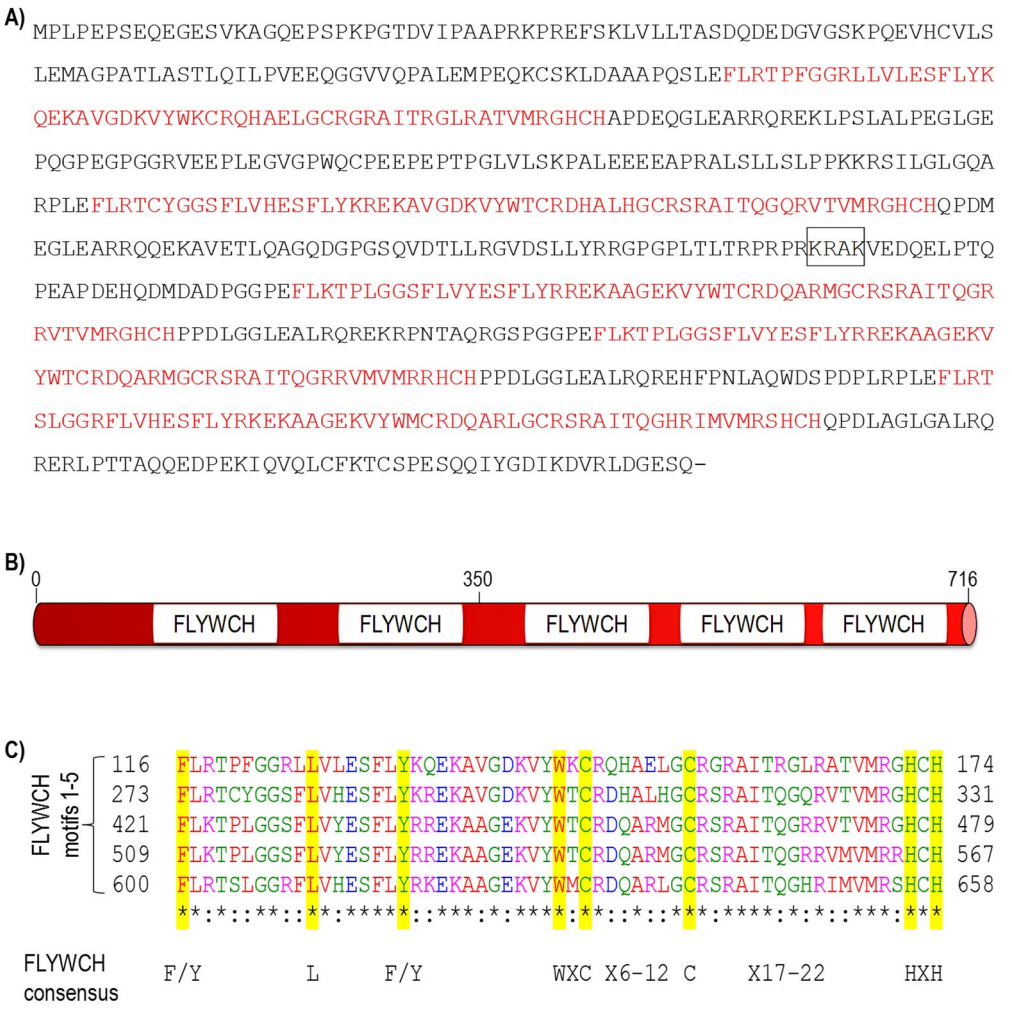


Figure 1-9: Characterization of FLYWCH motifs within human FLYWCH1 protein. A) Amino acid sequence of full-length human FLYWCH1. The amino acid region of FLYWCH motifs are indicated in red and the proposed NLS motif (KRAK) is boxed. Translation of the FLYWCH1 nucleotide sequence was performed using ExPASy translation tool (http://expasy.org/). **B)** Schematic showing tandem repeats of five FLYWCH encoding domains across human FLYWCH1 protein. **C)** Alignment of FLYWCH domain sequences showing core amino acid residues (F, L, Y, W, C, and H) of FLYWCH consensus sequence (yellow). The residue numbers for each domain represent the amino acid numbering within the FLYWCH1 protein sequence (Muhammad et al., submitted).

Table 1-2 : FLYWCH1 homology vs other mammals. The HomoloGene automated system was utilized to analyse the similarities between protein and nucleotide sequence. The level of similarity (identity) is indicated in percentage (%) (Muhammad et al., submitted).

Gene		**Identity (%)**	
Species	**Symbol**	**Protein**	**DNA**
Homo sapiens	*FLYWCH1*		
vs. *Pan troglodytes*	*FLYWCH1*	98.5	98.8
vs. *Canis lupus familiaris*	*FLYWCH1*	81.9	83.9
vs. *Bos taurus*	*FLYWCH1*	78.6	83.7
vs. *Mus musculus*	*Flywch1*	73.1	76.4
vs. *Rattus norvegicus*	*Flywch1*	74.2	78.3

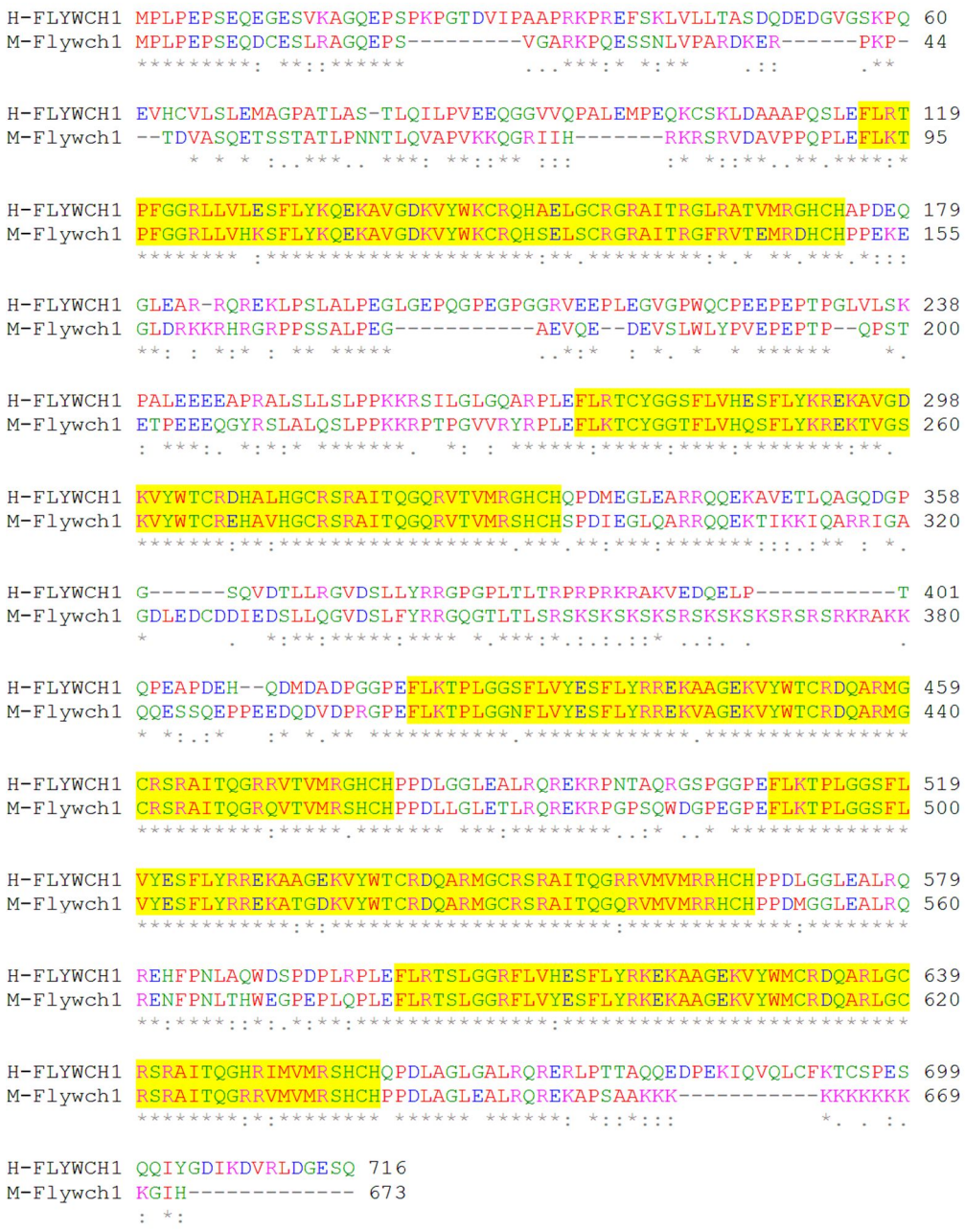


Figure 1-10: FLYWCH1 amino acid sequence alignment in human and mouse. Alignment showing the five conserved FLYWCH motifs (highlighted in yellow). Asterisks (*) indicate positions having single or fully conserved residue, colons (:) indicate conservation between groups having strong similar properties. Periods (.) indicate conservation between groups having weak similar properties (Muhammad et al., submitted).

1.5.3 Functions & Properties

Initially, the FLYWCH motif was identified in the *Drosophila* mod (mdg4) gene which encodes a family of approximately 26 alternatively spliced protein isoforms (Krauss and Dorn, 2004). The Mod (mdg4) protein possesses a common N-terminal region of 400 amino acid residues which consists of a highly conserved BTB domain and a C-terminus containing the C_2H_2 motif FLYWCH domain within a peptide of 60 amino acid residue (Büchner et al., 2000; Dorn et al., 2001). The discovery of *Drosophila* Mod (mdg4) was further boosted by the possible mRNA trans-splicing activity in arthropods thus suggesting mod (mdg4) may represent a form of a gene structure in which different conserved protein domains encoded by independent transcripts are fused via trans-splicing. Mod (mdg4) also maintains complex phenotypes which enables it to carryout roles suggested to consist of regulation of gypsy insulator sequences, apoptosis, viability, as well as regulation of homeotic gene expression involving either gene activation or gene silencing (Dorn and Krauss, 2003). Additionally, the *Drosophila* Mod (mdg4) has been suggested to participate in chromatin modulation mainly through the BTB/POZ (BTB) N-terminal region (Dorn and Krauss, 2003). Although the actual role of the FLYWCH domain is still poorly understood, the C-terminal regions of different Mod (mdg4) protein isoforms, mostly containing the FLYWCH motif, are postulated to participate in protein-protein interaction, thereby facilitating targeting of various proteins to different chromatin sites.

The FLYWCH domain has also been identified in another *Drosophila* protein, *Drosophila* GST-containing FLYWCH zinc finger protein (dGFZF) (Dai et al.,

2004a). This protein is unique in the sense that it possesses a tandem array of four FLYWCH motifs at the N-terminus expressed in every stage of *Drosophila* embryonic development, while also possessing a C-terminus domain that shares a 46% homology with glutathione SH-transferase (GST). The presence of GST domain promotes the speculation that this protein may play a crucial role in detoxification due to the fact that glutathione SH-transferase, a member of ROS (Reactive Oxygen Species) defence mechanism is responsible for the conjugation of reduced glutathione to hydrophobic and electrophilic substrates that are less reactive to oxygen (Townsend et al., 2009). However, the dGFZF protein lack the nuclear localization signal (NLS) motif hence, is localized in *Drosophila* S2 cells. The absence of the NLS suggests that this protein may not be directly involved in gene regulation via direct binding to DNA but may participate in gene regulation via interaction with other transcription factors and protein-protein interaction (Krauss and Dorn, 2004; Provost et al., 2006).

Based on the above mentioned *Drosophila* and *C. elegans* studies, the FLYWCH motifs may function in protein-protein interactions and serves as DNA-binding domains. Accordingly, it can be predicted that human FLYWCH1 may have similar biological activities due to harbouring of five FLYWCH motifs.

1.6 A Brief Overview of microRNA

Approximately 95% of the human genome is comprised of noncoding DNA, which differs from one species to another (Kellis et al., 2014). Numerous genes located in these non-protein-coding regions encode microRNAs (miRNAs),

which participate in RNA-mediated gene silencing through RNA interference (RNAi)-like pathways. MiRNAs are small single-stranded regulatory RNAs capable of carrying out post-transcriptional modification of intracellular messenger RNAs (mRNAs) via either complete or partial complementarity. They can be exploited for the design of new therapies against viral mutations and cancer polymorphisms. With the availability of high-throughput sequencing, over 25,000 miRNAs have been identified in plants, animals, and even microbes (Ameres and Zamore, 2013).

1.6.1 MicroRNA Biogenesis

MiRNAs are composed of ~22 nucleotide sequences in length and belong to the class of non-coding endogenous small RNAs. The functions of miRNAs in posttranslational gene regulation involves the direct interaction of miRNA with the 3' un-translated region (UTR) of the target messenger RNAs (Cai et al., 2004; Pillai, 2005). In mammals, impartial base pairing between the miRNA and the target mRNA or gene also results in translational repression of the target gene (Förstemann et al., 2005). To date, more than 2,500 miRNAs have been identified in the human genome (Ha and Kim, 2014; Thomas et al., 2015). The miRNA biogenesis is primarily mediated by the microprocessor complex composed of two RNase III endonucleases; Drosha and DGCR8 (Ha and Kim, 2014; Meister and Tuschl, 2004). In the first step of miRNA biogenesis, miRNAs are initially transcribed by RNA polymerase II resulting in the production of primary miRNA (pri-miRNA). Shortly after transcription and prior to translocation from the nucleus into the cytoplasm, the pri-miRNA undergoes

modifications and transformation to a ~ 60-100 nucleotide hairpin structure precursor miRNA (pre-miRNA) via the activity of Drosha. Once the pre-miRNA is transported to the cytoplasm by Exportin-5 (Pillai, 2005), it undergoes further modifications by Dicer, a multi-domain ribonuclease III enzyme. The cleavage event carried out by Dicer results to final product consisting of a 22 nucleotide double-stranded miRNA composed of a mature miRNA strand and its complementary miRNA strand (Meister, 2013). Following interaction with the miRNA-induced silencing complex (miRISC), miRNAs repress target mRNA translation thereby enabling acceleration of mRNA decay. The subsequent degradation of the mRNA is initiated by shortening of the poly(A) tail by the CCR4–NOT deadenylase complex followed by the 5′ cap structure removal and exonucleolytic decay of the mRNA (Rouya et al., 2014).

Interestingly, recent experimental advances have suggested that in specific cell types and conditions, some miRNAs could upregulate gene expression via a mechanism involving micro ribonuclear proteins (miRNPs) (Valinezhad Orang et al., 2014). For instance, during muscle differentiation, miR-145 facilitates myocardin gene upregulation (Cordes et al., 2009).

Additionally, apart from the canonical miRNA biogenesis pathways described above, alternative mechanisms, particularly through mRNA splicing (Flynt et al., 2010), have been discovered to generate miRNAs or other non-coding RNAs (Xie and Steitz, 2014; Yang and Lai, 2011). The revelation of unconventional miRNA biogenesis has been made possible via deep sequencing of small RNAs from cells deficient in Drosha, Dgcr8 or Dicer which can be produced in a Dicer-independent or microprocessor-independent manner.

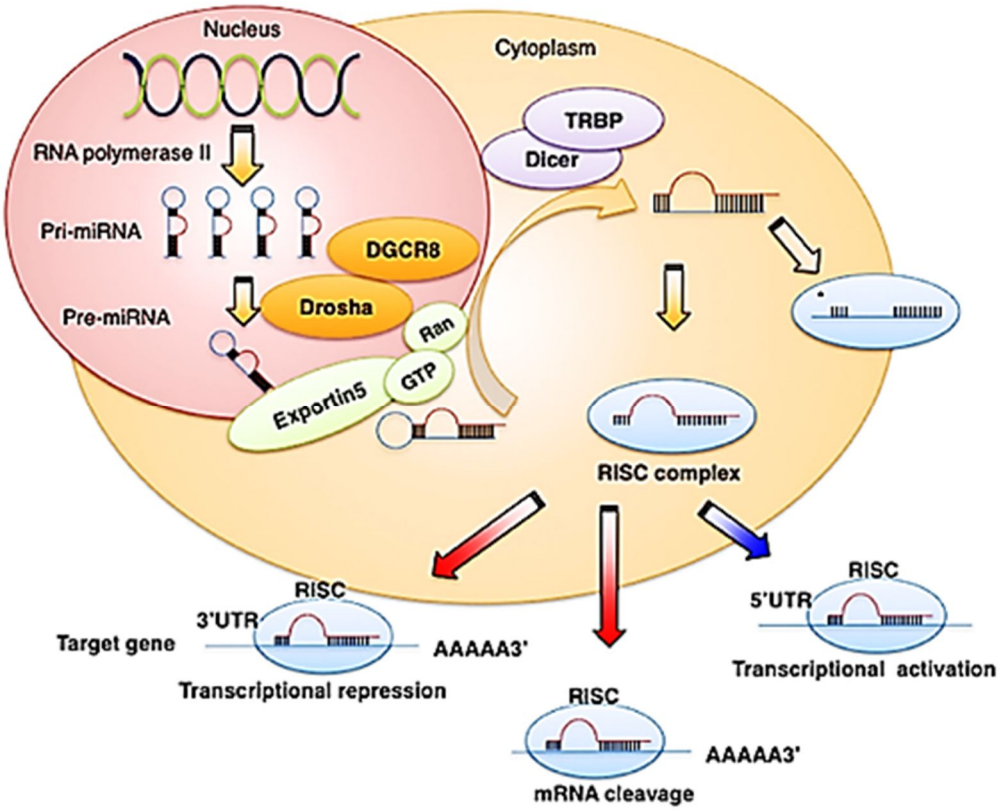


Figure 1-11: Biogenesis of miRNA. During biogenesis of miRNA, RNA polymeraseII transcribes pri-miRNA, which is subsequently processed by nuclear microprocessor complex into pre-miRNA and transported from the nucleus to the cytoplasm by Exportin 5. In the cytoplasm, Dicer facilitates generation of the mature double stranded miRNA prior to incorporation to the RISC complex which mediates gene silencing via degradation and mRNA cleavage or transcriptional activation. Taken from (Takahashi et al., 2014).

1.6.2 MiRNA-mediated Regulation of Wnt/β-catenin signalling

The relevance of miRNA in embryonic and developmental processes cannot be ignored. Experimental evidence from various experimental studies have highlighted the significance of miRNAs in a variety of complex processes such as regulation of apoptosis during development and cell cycle proliferation, cell fate regulation and differentiation and most importantly, participation in the gene

regulatory network, just to mention a few (Rolle et al., 2016). Moreover, certain miRNAs have been implicated as regulators of the Wnt signalling pathway in the context of embryonic (Kim et al., 2011a), bone (Lin and Hankenson, 2011) and cardiac development (Olson, 2006), amongst involvement in other organ developmental processes and normal cellular functions as well as regulation of tumorigenesis (Song et al., 2015). This discovery have been made possible partly by the advent of bioinformatics approaches that have been utilized in recent advances to identify and characterize Wnt/β-catenin-regulated miRNAs.

For instance, miR-200a has been identified as a potential negative regulator of the Wnt/β-catenin signalling pathway. This miRNA targets mRNAs of ZEB1 and ZEB2, which are repressors of E-cadherin. Therefore, by degrading ZEB1 and ZEB2 mRNA, E-cadherin becomes available for binding with β-catenin thereby forming E-cadherin-β-catenin complex which promotes cell-cell adhesion while negating metastasis (Su et al., 2011). The recruitment of β-catenin in the formation of this complex is beneficial towards reducing cytoplasmic β-catenin, which would eventually translocate to the nucleus and trigger the transcription of Wnt genes (Liu et al., 2011). Recent studies have reported the role of miRNAs in governing the differentiation of mesenchymal stem cells (MSCs) into osteoblasts with several miRNAs been identified to promote osteoblast differentiation by activating the Wnt signalling pathway (Song et al., 2015). For instance, miR-142-3p, miR-27 and miR-135a-5p target *APC* which results in the accumulation of β-catenin and activation of Wnt signalling to promote osteoblast differentiation in human fetal osteoblastic cells (Chen et al., 2014; Hu et al., 2013a; Wang and Xu, 2010). In cardiac

development, overexpression studies revealed miR-19b control of the left-right symmetry and cardiac development by directly suppressing β-catenin (*CTNNB1*) of the Wnt signalling pathway in zebrafish embryo (Li et al., 2014). While miR-431 was discovered to promote regenerative axon growth in the brain by suppressing *Kremen1* (*DKK1*), a negative regulator of the Wnt/β-catenin signalling pathway (Wu and Murashov, 2012).

A fundamental comprehension of miRNA functions in regulating the canonical Wnt signalling transduction pathways may lead to the revelation of new insights into crosstalks of regulatory mechanisms essential for normal development and disease pathophysiology leading to the discovery of anti-miRNA-based diagnostics and therapeutics suitable for cancer treatment and other human disease.

1.7 MiRNA Dysregulation in Cancer

Over the past decade, dysregulation of certain miRNAs have been implicated in human malignancies. The underling mechanisms that drives this phenomenon includes transcriptional control variations, chromosomal abnormalities, epigenetic changes and mutational defects in the miRNA biogenesis machinery (Peng and Croce, 2016).

MiRNA expression is tightly regulated by a plethora of transcription factors, hence abnormal expression of some key transcription factors including, but not restricted to c-Myc and p53 due to mutations could have a profound influence on miRNA expression in cancer state. For instance, upregulation of c-Myc has

been discovered in many malignancies thereby activating the transcription of oncogenic *miR-17–92* cluster via direct binding to E-box elements in *miR-17–92* promoter (Peng and Croce, 2016). Also, the p53-miR-34 regulatory axis has been discovered as another example of the transcriptional factor mediated regulation of miRNA expression to promote tumour suppressive properties (He et al., 2007). Some miRNAs also acts as oncogenes to facilitate tumour progression, for instance, miRNA-1908 has been implicated as a glioblastoma oncogene by antagonizing the PTEN tumour suppressor pathway (Xia et al., 2015)

The role of miRNA in the regulation of stemness of CSCs is another aspect of miRNA activity currently under investigation. Reports suggest that miR-193a expression inhibits tumourigenicity and invasiveness by directly targeting KRAS and plasminogen activator urokinase (PLAU), respectively, with these two factors highly expressed in human colon adenocarcinomas (Deng et al., 2014). In addition, miR-451 appears to be another regulator of CSC properties such as drug resistance, self-renewal and tumourigenicity. Experiments carried out in spheroid cell cultures, showed reduced expression of miR-451, triggering the up-regulation of macrophage migration inhibitory factor (MIF) and COX-2 which are involved in deregulation of canonical Wnt pathway in CSCs (Bitarte et al., 2011; de Sousa et al., 2011).

It has been established that a major consequence of dysregulation of certain miRNAs could affect target genes via specific signalling pathways such as Wnt/β-catenin signalling pathway that govern growth, proliferation and differentiation to facilitate tumour initiation and progression.

1.7.1 Alterations of miRNAs/ β-catenin signalling in cancer

The network involving both miRNAs and Wnt-signalling pathway have been implicated in regulating tumorigeneses in various forms of cancer (Hayes et al., 2014) (Table 1-3). For instance, experimental evidence have implicated miR-374a in promoting EMT and metastasis by activating the Wnt/b-catenin pathway breast cancer cell lines (Cai et al., 2013b). This result suggests that miR-374a may be responsible for the degradation of APC or one of the other components of the destruction complex, hence leading to the translocation of β-catenin to the nucleus thereby enhancing the transcriptional activity of LEF/TCF4 (He et al., 2005).

MiR-200a directly targets β-catenin leading to translation repression and blockade of the Wnt/β-catenin signalling, which is frequently involved in cancer (Saydam et al., 2009). Consequently, downregulation of miR-200a facilitates the increased expression of β-catenin and downstream target cyclin-D1, both involved in cell proliferation. Additionally, activation of LIN28 has been shown to be necessary for Wnt-β-catenin pathway mediated let-7 repression and cell proliferation (Zhang et al., 2007). Interestingly, let-7 miRNAs have also been implicated as a potential regulator β-catenin in cancer cells as overexpression of let-7a in Wnt activated MDA-MB-231 cells was observed to inhibit β-catenin-activated cell growth and colony formation, thus emphasising the significance of let-7 miRNAs as downstream regulators of Wnt-β-catenin pathway in the regulation of cell proliferation (Cai et al., 2013a). Furthermore, miR-34 has been discovered to attenuate the canonical Wnt-signalling via corporation with p53 in

A549 and MCF-7 carcinoma cell lines. Knockdown and/or deletion of functional miR-34a gene resulted in the increased expression of WNT1, LRP6 and β-catenin mRNA in these cells (Wang et al., 2010). The significance of the above findings suggests interplay between Wnt signalling pathways and miRNAs in cancer development. These results all suggest that miR-34, miR-320, miR-200 and Let-7 could be exploited for the development of therapeutic agents with specific focus on targeting the canonical Wnt-signalling pathway in cancer.

As critical biological modulators, it is no more news that miRNAs act to suppress or facilitate cancer and tumour development by interacting with targets of the Wnt-signalling pathway. A summarized description showing the alterations of miRNAs/Wnt/β-catenin signalling in cancer has been provided (Table 1-3). A more detailed explanation on the Wnt/miRNA network in carcinogenesis has been provided in recent studies (Ghahhari and Babashah, 2015; Song et al., 2015).

Table 1-3: Alterations of miRNAs/Wnt/β-catenin signalling in cancer. Inhibition and activation of carcinogenesis in the context of Wnt/β-catenin signalling.

Cancer Type	miRNA	Wnt-signalling Target	Inhibits /Activates Carcinogenesis via Wnt signalling	Reference
Colorectal	miR-224	cdc42	Inhibits	(Song et al., 2015)
Colorectal	miR-574-5p	Qki6/7, p27, β-catenin	Activates	(Ji et al., 2012)
Colorectal	miR-7,miR-34	Ying Yang	Activates	(Wang et al., 2014; Zhang et al., 2013a)
Colorectal	miR-29b	BCL9	Inhibits	(Subramanian et al., 2014)
Liver	miR-155, miR-106b	*APC*	Activates	(Shen et al., 2013; Zhang et al., 2012b)
Liver	miR-148b, miR-122	Wnt1	Inhibits	(Xu et al., 2012; Zhang et al., 2015a)
Liver	miR-139	TCF4	Inhibits	(Gu et al., 2014)

Breast	miR-31, miR145	RhoA, β-catenin, c-myc	Inhibits	(Kim et al., 2011b; Valastyan and Weinberg, 2010)
Breast	miR-142	*APC*	Activates	(Isobe et al., 2014)
Prostate	miR320	β-catenin	Inhibits	(Hsieh et al., 2012)
Lung	miR-191	Wnt1	Activates	(Xu et al., 2015b)
Thyroid	miR-146b-5p	ZNRF3	Activates	(Deng et al., 2015)
Ovarian	miR-181a	VNGL1	Activates	(Parikh et al., 2014)
Oesophage-al	miR-141	SOX17	Activates	(Jia et al., 2012)

1.8 Rational and objectives of this study

1.8.1 Rational

The Wnt/β-catenin pathway is closely regulated at both transcriptional-level regulations and post-translational modification; thus aberrant Wnt activity often results in developmental disorders and diseases including but not limited to

cancer (Dey et al., 2013; Novellasdemunt et al., 2015; Sheikh et al., 2014). For instance, during metastatic processes, epithelial cancer cells require certain characteristics such as elevated expression of mesenchymal markers as well as other alterations in their microenvironment to enable invasion of adjacent tissues and progression to metastatic high-grade tumours. Inappropriate Wnt signals coupled with a loss of E-cadherin promotes an increase in cytoplasmic and nuclear β-catenin levels where it interacts with the epithelial-mesenchymal transition (EMT) regulators, such as E-cadherin repressors: Snail, twists and ZEBs (Lamouille et al., 2014; Yang et al., 2015b). Recent advances in biomedical research have allowed experimental and bioinformatics approaches to identify short non-coding RNAs such as miRNAs as regulators of components of the Wnt-signalling pathways and vice versa. Thus, both miRNAs and Wnt-signalling pathways form a network involved in the regulation of key biological processes. Although, individual interactions between components of the Wnt/β-catenin pathway and miRNAs in normal and cancer state have already been established (Kang and Hata, 2015), we have simply just began to comprehend the role of miRNAs, not only in normal human development but also in tumour progression mediated by the Wnt/β-catenin signalling and vice-versa especially due to the fact that multiple components are involved in this complex network. Therefore, more efforts are required to identify the mechanism that controls miRNA/canonical Wnt-signalling network.

The first evidence of a FLYWCH1/β-catenin interaction comes from a large scale screen using a modified yeast-2-hybrid based RRS (Muhammed et al 2016, submitted). Following the earlier discovery in our lab that FLYWCH1

negatively regulates the Wnt/β-catenin signalling pathway by directly binding to unphosphorylated β-catenin to prevent interaction with TCF4 (Muhammed et al., submitted), we then sought to further characterize FLYWCH1, mechanisms and its biological importance in cultured CRC cells.

1.8.2 Aims & Objectives

The FLYWCH gene was recently described and, apart from the publication in coronary heart disease (Asl et al., 2015), there is very little known about its function in human and other mammalian cells. Hence, my PhD project is aimed to explore and investigate the cellular and molecular role of FLYWCH1 in CRC cells by antagonizing the Wnt/β-catenin signalling. This was accomplished by utilizing different *in-vitro* approaches as well as analysis of normal vs primary/metastatic human tissue samples that may aid to uncover novel mechanisms and pathways that are involved in early cancer development and lead to the discovery of better diagnostic tools for disease and potential anti-cancer drug targets.

Therefore, the present project was aimed to study the role of FLYWCH1 in CRC cells through:

1) Examining and re-evaluate the FLYWCH1-mediated morphological changes under different *FLYWCH*1 status via Phalloidin staining of the actin filament organization, in fibroblasts (TIG119) and CRC cell lines SW480 and HCT116 cells with FLYWCH1 knockdown ($FLYWCH1^{shRNA}$) and overexpression ($FLYWCH1^{O/E}$).

2) Examining the EMT-associated cell morphology, attachments and migration caused by aberrant expression of FLYWCH1, via western blotting analysis and their correlation with CRC development by transcriptional analyses in normal, primary and metastatic human tissue samples.

3) Studying the role of FLYWCH1 in colon cancer stemness activity by colonosphere formation efficiency and the expression of some of differentiation and stem cell markers via immunofluorescence microscopy.

4) Investigating the association of FLYWCH1 foci with different nuclear signalling and biological signalling via extensive immunofluorescence co-localization assays.

5) Exploring the role of FLYWCH1 in miRNA biosynthesis via FLYWCH1 foci co-localisation with the splicing factor SC35, utilizing RNA-Immuno-precipitation (RIP) combined with miRNAs qRT-PCR for 84 of mature cancer-associated miRNAs expression analysis. The findings have been consolidated following further validation and correlation of FLYWCH1 expression with the let-7 miRNAs in normal, primary and metastatic human tissue samples.

2 CHAPTER 2

Materials & Methods

All procedures were performed under aseptic conditions under the guidance of strict safety regulations. Standard protocols of various techniques used throughout the thesis were followed from previously established templates and modified were necessary or otherwise, developed in our lab.

2.1 Materials

2.1.1 Reagents and buffers

All buffers, liquids and solid reagents used for biochemical, molecular and cellular purposes were purchased from Sigma (UK) unless otherwise stated (Table 2-1).

Table 2-1: Non-commercial buffers and solutions used in this study**.**

Materials	Composition	Stock Conc.	Working Conc.	Storage temperature. (°C)
Antibiotics	Kanamycin (50 mg/mL)	1000X	1X	4
	Ampicillin (50 mg/mL)			-20
TSD Buffer 1 **(used for chemical competent cells preparation)**	12 g Rubidium-chloride, 9 g Manganese-chloride X2H_2O, 2.94 g Potassium-acetate, 1.5 g Calcium-chloride X2H_2O, 150 g Glycerol, dH_2O to 900 mL, adjust pH to 5.8 then complete to 1 Litre with dH_2O.	1X	1X	4
TSD Buffer 2 **(used for chemical competent cells preparation)**	2.09 g Mops, 1.2 g Rubidium-chloride, 11 g Calcium-chloride X2H_2O, 150 g Glycerol, dH_2O to 900 mL, adjust pH to 6.8 then complete to 1 Litre with dH_2O.	1X	1X	4
Agarose gel loading buffer	3 ml glycerol (30%), 25 mg Bromophenol blue (0.25%), dH_2O to 10 mL	10X	1X	4
RNA gel electrophoresis running buffer	0.4M MOPS pH 7.0, 0.1M sodium acetate, 0.01 M EDTA, 18 mL 37% formaldehyde (12.3M) then complete to 1 Litre with dH_2O.	10X	1X	RT

DNA gel electrophoresis running buffer	48.4g Tris base, 11.4 mL glacial acetic acid (17.4M), 3.7g EDTA, then complete to 1 Litre with dH_2O.	10X	1X	RT
SDS-PAGE loading buffer	10% w/v SDS (sodium dodecyl sulfate), 10 mM Beta-mercaptoethanol, 20 % v/v Glycerol, 0.2 M Tris-HcL pH 6.8, 0.05% w/v Bromophenol blue, dH_2O to the desired volume.	5X	1X	-20
SDS-PAGE semi-transfer buffer	30.3 g Trizma-base, 144 g Glycine, then complete to 1 Litre with dH_2O.	10X	1X	RT
TBS buffer	24.2 g Trizma-base, 80 g Glycine, dH_2O to 1Litre, pH 7.6.	10X	1X	RT
RIPA buffer	150 mM NaCl, 25 mM Tris-HcL pH 7.6, 1% NP-40, 0.1% SDS, dH_2O to the desired volume.	1X	1X	4
Luria Broth (LB) medium	10 g Tryptone, 5g Yeast extract, 10g NaCl, then complete to 1 Litre with dH_2O, autoclave before use.	1X	1X	4
LB Agar medium	Luria Broth with 1% bacteriological agar.	1X	1X	4
1.5 M Tris-HcL, pH 8.8 (stock buffer for resolving	181.65g Tris base, adjust pH to 8.8 with concentrated HcL, then complete to 1 Litre with dH_2O	1X	1X	4
1.5 M Tris-HcL, pH 6.8 (stock buffer for stacking	90.8g Tris base, adjust pH to 6.8 with concentrated HcL, then complete to 500 mL with dH_2O	1X	1X	4

2.1.2 Cell lines

HEK293T (Human Embryonic Kidney), a transformed human cell line, normal human skin fibroblast cells (TIG119 cells), and two human CRC cell lines (HCT116, and SW480) were utilized throughout the duration of this study. Transformation of rapid-growing HEK293T cell line was originally performed via transduction of sheared DNA from adenovirus type 5 normal human embryonic kidney cells (Graham et al., 1977). Due to the straightforward and relatively easy manner in which these cells are cultured and easy to transfect, HEK293T cell lines are the most preferred hosts for biochemical studies (Soni and Lai, 2011). Two CRC cell lines were utilized; SW480 cell lines possessing wild type TGFβR2 with microsatellite stability (MSS) (SW480 is also mutated for APC) and HCT116 cell lines possesses mutated TGFβR2 with microsatellite instability (MSI) (HCT116 is also mutated for β-catenin phosphorylation site). The CRC cell lines were initially isolated from primary colon tissue tumours and purchased originally from the American Type Culture Collection (ATCC) (Babaei-Jadidi et al., 2011). Also, wild type human 'TIG119' skin fibroblast cells were kind gifts from Dr Axel Behrens laboratory (LRI, London) (Nateri et al., 2005).

Most importantly, regular mycoplasma tests were performed on a regular basis especially prior to commencement of any experiment and the morphology of the cell lines was closely monitored with the replacement of fresh medium when necessary.

2.1.3 Human Tissue Specimen

Normal, tumour and metastatic tissue samples derived from colorectal cancer patients and obtained from Nottingham tissue bank. All samples including normal and cancerous tissue samples were obtained from patients who underwent colectomy at Queens Medical Center (QMC), Nottingham University Hospital, Nottingham, UK with informed consent (Babaei-Jadidi et al., 2011).

2.1.4 Plasmid Constructs

Let-7 reporter plasmids were utilized to analyse and validate the expression patterns of let-7 in the presence of FLYWCH1. Plasmids used include psiCHECK2-let7-8x (which possesses a 3' UTR let-7 target (8x) site which triggers *Renilla* luciferase activity upon direct interaction with let-7 miRNAs (Iwasaki et al., 2009), let-7 inhibitor sponge (Kumar et al., 2008), let-7a-1 (Wang et al., 2011b), let-7b-GFP (Addgene #25404) and let-7g (Addgene #14784) (Nishino et al., 2008). Other plasmids utilized includes plasmids cloned with GFP-FLYWCH1 (Appendix 2) and GFP (for control) (Appendix 1) and pEGFP-FLYWCH1-ΔC350 (Muhammed et al., submitted) (Appendix 3). The pcDNA and *Renilla* plasmids were used while performing luciferase assay as previously described in (Babaei-Jadidi et al., 2011). PLVX-Puro were purchased from Clontech (Appendix 4), pLVX-Puro-GFP (Appendix 5) and pLVX-Puro-FLYWCH1-GFP (Appendix 6) were constructed throughout this study for stable transfection (Muhammed et al., submitted). In addition, firefly luciferase reporter plasmid constructs used includes pTN24 (a kind gift from Nasim)

(Nasim and Eperon, 2006), Luc-I and Luc plasmids (Younis et al., 2010) and HMGA-2 reporter constructs (a kind gift from Victoria James) (James et al., 2010). Scrambled piLenti-shRNA-GFP (LV015-G) and piLenti-shRNA-FLYWCH1-GFP Lentivectors (i008000) are from Applied Biological Materials (ABM) Inc.

2.1.5 Antibodies

Different types of primary and secondary antibodies were used throughout this study for both Western blotting and immunofluorescent analysis. Details about the source of these antibodies and the dilution factors used are given in details (Table **2-2**).

Table 2-2: Comprehensive list of primary antibodies used for Western blotting and Immunofluorescent analysis. "NA" means not applicable**.**

Primary antibodies	Source & catalogue number	Dilution used	
		WB	IF
FLYWCH1 (V18)	Goat Polyclonal (Santa Cruz # sc-242855)	1:500	1:50
Vimentin (V9)	Monoclonal Mouse antibody (Santa Cruz #sc-6260)	1:1,000	1:100
GFP	Polyclonal Mouse antibody (Invitrogen)	1:1,000	NA
Fibrillarin	Monoclonal Rabbit (Cell Signalling #2639P)	1:500	1:50

E-Cadherin	Monoclonal Mouse IgG2a, κ (BD Biosciences, # 610181)	1:5,000	1:100
Phospho GSK-3β (S9)	Monoclonal Rabbit mAb (Cell Signalling #9322)	1:2,000	1:50
GSK-3β (T216)	Monoclonal Rabbit mAb (Cell Signalling #9315)	1:2,000	1:50
β-actin	Mouse monoclonal (AC-15) to beta Actin (Abcam, # ab6276)	1:10,000	NA
α/β-Tubulin	Polyclonal Rabbit antibody (Cell Signalling #2148)	1:1,000	NA
β-catenin (Clone 8E7)	Rabbit Polyclonal (Santa Cruz #sc-220)	1:2,000	1:100
ZEB1 (H-102)	Rabbit Polyclonal (Santa Cruz # sc-25388)	1:1,000	1:50
ZEB2 (E-11)	Mouse monoclonal (Santa Cruz #sc-271984)	1:1,000	1:50
U1 snRNP70 (c-3)	Mouse Monoclonal (Santa Cruz # sc-390899)	1:2,000	NA
LIN28A	Rabbit Polyclonal (abcam ab46020)	1:1,000	1:100
LIN28B	Rabbit Polyclonal (LifeSpan BioSciences LS-B3423)	1:1,000	1:100
SC-35	Mouse Monoclonal (abcam, ab11826)	1:1,000	1:100
HP1α	Rabbit Polyclonal (abcam ab9057)	1:1,000	1:100
H2AXγ (phospho S139)	Rabbit Polyclonal (abcam ab11174)	1:2,000	1:100

BMP4 (D-6)	Mouse Monoclonal (Santa Cruz #sc-393329)	1:2,000	1:100
CD44	Rabbit Polyclonal (abcam aab24504)	1:2,000	1:100
MUC2 (F-2)	Mouse Monoclonal (Santa Cruz #sc-515032)	1:1,000	1:50

Table 2-3: Comprehensive list of secondary antibodies used for Western blotting and Immunofluorescent analysis.

Secondary antibodies	**Source & catalogue number**	**Dilution used**	
		WB	**IF**
Goat anti-mouse IgG-HRP	(Santa Cruz, # sc-2005)	1:5,000	NA
goat anti-rabbit IgG-HRP	(Santa Cruz, # sc-2004)	1:5,000	NA
Rabbit anti-Goat IgG-HRP	(DakoCytomatio, # P 0160)	1:2,000	NA
Rabbit Anti-Mouse IgG (H+L)	Alexa Fluor® 488 (Invitrogen, # A11059)	NA	1:400
Goat Anti-Mouse IgG (H+L)	Alexa Fluor® 594 (Invitrogen, # A11005)	NA	1:400
Goat Anti-Rabbit IgG (H+L)	Alexa Fluor® 594 (Invitrogen, # A11037)	NA	1:400

2.1.6 Oligonucleotides

The FLYWCH1 oligonucleotides used in this study (Table 2-4) where designed using primer3 web based primer design tool (Version 0.4.0, available at http://frodo.wi.mit.edu/primer3/) for standard PCR and quantitative real time polymerase chain reaction (qRT-PCR) and purchased from Sigma. MiRNA primer assays (containing oligos) were purchased from Qiagen. The specificity of the primers was checked by blasting the primer sequences against the NCBI human transcript database (http://www.ncbi.nlm.nih.gov/tools/primer-blast/). Upon arrival, apart from the let-7 assays, primers were spun down, re-suspended in an appropriate volume of Sigma distilled water to give a final concentration of 100 µM as a stock, and stored at -20°C until use.

Table 2-4: Primers Used in this study. Let-7 & miRNA internal control primers and PCR primers used to amplify the FLYWCH1 mRNA.

miRNA Target genes	**Mature miRNA sequences 5'- 3'**
Hs-let-7a-2 (MIRLET7A1)	UGAGGUAGUAGGUUGUAUAGUU
Hs-let-7b-1 (MIRLET7B)	UGAGGUAGUAGGUUGUGUGGUU
Hs-let-7c-1 (MIRLET7C)	UGAGGUAGUAGGUUGUAUGGUU
Hs-let-7d-1 (MIRLET7D)	AGAGGUAGUAGGUUGCAUAGUU
Hs-let-7e-3 (MIRLET7E)	UGAGGUAGGAGGUUGUAUAGU
Target genes	**Primer sequences 5'- 3'**
FLYWCH1	**Forward**: CTGGATGCAGCCCCTCAGT **Reverse**: TTGGCGGCACTTCCAGTAC
HPRT	**Forward:** AGATGTGATGAAGGAGATG **Reverse**: GTGTCAATTATATCTTCCA
EPHA4	**Forward**: CGACAAAGAGCGTTTCATCA **Reverse**: GCTTCACCCAAGTGGACATT
ZEB1	**Forward**: GCATACACCTACTCAACTACGG **Reverse**: TGGGCGGTGTAGAATCAGAGTC
U1snRNA	**Forward**: GGGAGATACCATGATCACGAA GGT **Reverse**: CCACAAATTATGCAGTCGAGT TTC CC

2.2 Methods

2.2.1 General Tissue Culture Techniques

2.2.1.1 Human cell culture conditions

Human skin fibroblast cells (TIG119) and CRCs (HCT 116 and SW480) cell lines were all cultured in RPMI growth medium (Sigma, #R0883). The RPMI growth medium used was supplemented with of 1% Penicillin-Streptomycin (Invitrogen, #15140-122, 10 mg/mL), 10% Fetal Bovine Serum (FBS) (Sigma, #F7524) and 1% L-Glutamine (Invitrogen, #25030-024). The growth medium was regularly changed twice a week and the cells were passaged using 1X Trypsin/EDTA solution (Invitrogen, #15400-054).

Depending on the nature of subsequent experiments, cell lines were cultured in T-75 flasks and incubated at 37°C with 5% CO_2 in a tissue culture specific incubator (Corning Incorporation, UK). Once the cells attained up to 85%-90% confluency, they were passaged. This was accomplished with an initial rinse with sterile phosphate buffer saline (PBS) (Sigma, #D8537) after which 3 mL of 1X Trypsin/EDTA solution (Invitrogen, #15400-054) was added in order to detach the cells. Following incubation, cells were incubated at 35ºC for 5 minutes (10-15 minutes for SW480 cell lines). The effect of the Trypsin/EDTA solution was subsequently neutralized via the addition of 10 mL of medium to the detached cells. The mixture was gently mixed and 10 mL was discarded from the mixture after which fresh 10 mL medium was added to the remaining mixture.

For storage purposes, 10 mL of the trypsinized cells was removed from the flasks, transferred to a separate 15 mL centrifuge falcon tubes, and centrifuged for 5 minutes at 1,300 rpm. Following centrifugation, the supernatant was discarded and the pellet re-suspended in 1,000 µL of freezing media [composed of 90% serum + 10% dimethyl sulfoxide (DMSO)] and later stored at either -150^{o}C or liquid nitrogen.

2.2.1.2 Cell Counting

Neubauer haemocytometer (Marienfeld, Germany) and Trypan blue viability dye (Sigma T8154) were utilized to determine the concentration/number of the cells. The trypsinized cells were passed through a 5 mL syringe in order to prevent clumping-up of cells. This was followed by addition of 50 µL of cell suspension into a new Eppendorf tube containing 50 µL Trypan blue and mixed. About 10 µL of the cell/Trypan blue mixture was loaded into the haemocytometer slide composed of four large corner squares (each large square is divided into 16 smaller squares) and viewed with 10X magnification under the light microscope (Figure 2-1). The principle of counting using haemocytometer is designed so that the cells in a single set of 16 squares correspond to the number of cells x 10^4 / mL:

For instance, in order to obtain the count, the total cells in 4 sets of 16 small squares = (cells/mL x 10^4) x 4 squares from a single haemocytometer grid:

- Divide the count by 4,
- Multiply by 2 in order to adjust to the 1:2 dilution from the trypan blue

However, the above two steps is equivalent to dividing the total cell count by 2.

For instance, if the total cell count is 165, then the cell density is:

$$\frac{165}{2} = 8.2 \times 10^4/\text{mL}$$

2.2.1.2.1 Viability

Dark blue cells within the grid being counted are considered as dead cells. Percentage viability was obtained by dividing number of live cells by the total number of cells and multiplying by 100.

For instance;

Live cells = 30×10^4 mL

Total cells = 39×10^4 mL

$$\frac{30\ x\ 10^4 ml}{39\ x\ 10^4/ml}\ X\ 100 = 76.9\%\ viability$$

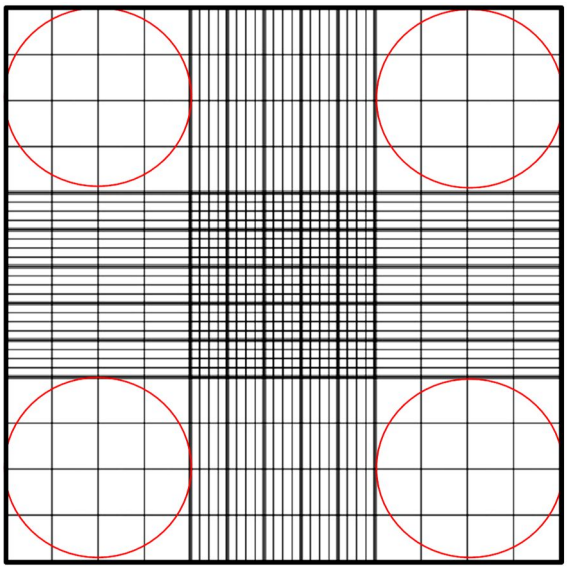


Figure 2-1: Layout of the Neubauer haemocytometer slide grid. Red squares indicate the regions within which the cells are counted. Cells appearing just on the border of the grid lines are not counted.

2.2.1.3 Colonospheres Formation

Formation of colonospheres derived from SW480 cells was examined as described by Shaheen et al. (Shaheen et al., 2016), and Kanwar et al. (Kanwar et al., 2010). Colonospheres were generated by incubating a small number of parental cells at a concentration of 100 cells per 200 µL in serum-free stem cell medium (SCM) containing DMEM/F12 (1:1) supplemented with B27 (Life Technologies, Gaithersburg, MD), 20 ng/ml EGF (Sigma cat no. E9644, St Louis, MO), 10 ng/mL fibroblast growth factor (Sigma), and antibiotic-anti-mycotic in 24-well plates (Corning Inc, Lowell, MA) for 14 days. Medium was changed with freshly prepared complete stem cell medium every 3-4 days in a careful manner while the colonospheres grow as floating spheroid colonies.

2.2.1.4 Transient transfection

The transient transfection of various plasmid DNAs into different human cell lines was performed using polyethyenimine (PEI) (Sigma, #408727) and instructions were followed according to the manufacturer's guidelines. Two days prior to transfection, cells were trypsinized and sub-cultured in RPMI growth medium in 24 well plate, 6 well plate, T-75 flasks or cell culture dishes depending on the nature of subsequent experiments to be performed. Cells were allowed to attain ~70% confluency to attain optimum transfection efficiency.

The transfection mixture was prepared as follows: For cells grown in 6 well plates, for each well two sterile 1.5 mL Eppendorf tubes were prepared. In the first tube 4 µg of the plasmid DNA was mixed with 250 µL of 1X OPTI-MEM® medium (Invitrogen, #31985-047). The second sterile Eppendorf tube was composed of 12 µL of PEI transfection reagent combined with 250 µL of 1X OPTI-MEM® medium. The contents in both tubes were immediately mixed together and incubated at RT for 20 minutes. Shortly before transfection, the RPMI growth medium in which the cells were cultured was removed after which the cells were washed with PBS. At the end of the 20-minute incubation period, the transfection mixture was added in a drop-wise manner into the well containing the cells to be transfected. The plate was immediately incubated in tissue culture incubator at 37^{o}C for 6-7 hours after which the 1X OPTI-MEM® medium was replaced with 3 mL of RPMI medium per well and incubated for 24 - 36 hours. The volume of each content was slightly optimized while using 10 cm culture dish. The transfected cells were later used for different experiments.

Subsequently, the transfection was analysed in two ways; firstly the transfection efficiency was assessed by the number of GFP^{+VE} cells (if the plasmid express GFP) using the fluorescent microscope and secondly the western blotting analysis was utilized to analyze the protein expression. Experiments with low transfection efficiency (less than 30%) were neglected and repeated. Based on the transfection efficiency, the above described technique could be subject to optimization by utilizing different transfection agents such as either lipofectamine™ 2000 or FuGENE® HD.

.

2.2.1.5 RNAi Transfection

The procedure for siRNA/shRNA transfection was similar to the procedure carried out for transient plasmid transfection. However, the only difference was after the 6-hour incubation period with 1X OPTI-MEM® medium, the cells were incubated in fresh RPMI media for 48-72 hours depending on the cell lines used. A longer period is required for the siRNA to degrade the target mRNA thereby inhibiting its translation and resulting to gene silencing compared to DNA plasmid transfection.

2.2.1.6 Generation of stable cell lines (Puromycin selection)

PLVX-puro, an HIV-1 based lentiviral expression vector expressing GFP and GFP-FLYWCH-1 as well as FLYWCH1-set shRNA lentivector were utilized in the generation of stable cell lines. All lentivectors contained a Puromycin

resistant gene which when picked up by cells and integrated into the host cell's genome acquire resistance to Puromycin drug depending on the concentration of the drug.

Firstly, each cell line was cultured in separate 6 well plate with RPMI growth medium. For instance, SW480 cells were cultured in 6 wells with 3 wells used as positive control while the remaining 3 wells were used as negative controls (not transfected). The cells were later transfected (following the procedure from section 2.2.1.4) with 1.5 µg of either PLVX-GFP or PLVX-GFP-FLYWCH-1 or FLYWCH1-set shRNA lentivector and left to grow under non-selective conditions for 48 hours followed by selection via introduction of Puromycin every 48 hours depending on the cell line. This was repeated depending on the different cells used. TIG119 cells were treated with 3 µg of Puromycin whereas CRCs were treated with 5 µg of Puromycin. Usually, cells that failed to integrate the resistant gene died upon exposure to the drug. Treatment with the drug was repeated weekly until all the cells had developed resistance to the drug (for up to 3 weeks). Cells were also viewed under the fluorescent microscope to confirm GFP expression in all the cells. The cells were then transferred to T75 culture flasks, cultured and amplified appropriated and stored in -150^{o}C or under liquid nitrogen storage. Validation of the stable cell lines were carried out via western blot analysis and immunofluorescence techniques.

Unfortunately, consistent with previous efforts in our laboratory (Muhammed et al., submitted), the stable overexpression of full-length FLYWCH1 attempted in TIG119, SW480 and HCT116 cells using GFP-FLYWCH1 lentiviral vector

(pLVX-GFP-FLYWCH1-Puro^{R}) based on Puro selection occurred without success.

2.2.1.6.1 Single cell cloning via serial dilution

Due to the different GFP expression patterns of the stable cell lines, single cell cloning via serial dilution was performed. Firstly, cells were trypsinized and the required volume of RPMI media was prepared to make a 1:10 dilution. The diluted RPMI cell mixture was then thoroughly pipetted up and down to sort 1 cell into each well. The solution was added to a 96-well plate for single cell seeding (50 µL/well) ensuring adequate coverage of the surface. The cells were then incubated under normal tissue culture conditions for expansion of single cell colony (Section 2.2.1.1).

2.2.1.7 Freezing and thawing cells

For storage purposes, 10 mL of the trypsinized cells was removed from the flasks, transferred to a separate 15 mL centrifuge falcon tubes, and centrifuged for 5 minutes at 1,300 rpm. Following centrifugation, the supernatant was discarded and the pellet re-suspended in 1,000 µL of freezing media [composed of 90% serum + 10% dimethyl sulfoxide (DMSO), mixed well, and later stored at -150^{o}C or liquid nitrogen.

For recovery of cells from a frozen stock, the cells were defrosted in a water bath at 37°C and immediately transferred to 10 ml of pre-warmed complete medium before plated in T75 flasks and incubated at 37°C and 5% CO_2 incubator.

2.3 DNA preparation

2.3.1 DNA transformation and amplification

Chemically prepared competent DH5α *Eschericha coli* (E. coli) cells were utilized for the purpose of transformation of various plasmids. The plasmids and the competent bacteria cells were thawed on ice before 1.5 µL of the plasmid of choice was mixed with 100 µL of the competent cells in a sterile 1.5 mL Eppendorf tube and incubated on ice for 30 minutes. The mixture was subjected to heat shock in a water bath at 42°C for 1 minute prior to adding 500 µL of Luria Broth (LB) medium. The tube with LB, was then placed in a shaking thermos-mixer set at 37°C for 1 hour. An agar plate was prepared within which the desired antibiotic [Ampicillin (50 µg/mL) or Kanamycin (30 µg/mL)] was added and incubated at RT. The bacterial mixture was later spread carefully and evenly over the agar and following a 5-minute incubation period, it was placed upside down in a bacterial growth incubator overnight. Alternatively, following heat shock, the mixture was directly added into 500 µL of Luria Broth (LB) medium with the desired amount of antibiotic and incubated in a shaking incubator overnight.

2.3.2 DNA plasmid isolation & purification using midi prep kits

DNA plasmids were isolated with Genopure plasmid midi prep kit (Roche #15945100) and utilized strictly according to the manufacturer's instructions. The midi prep protocol was utilized to yield a product of more than 100 µg. Product yield less than 100 µg was isolated using mini prep kit. A single colony was later selected and re-cultured in 250 mL LB medium with the appropriate antibiotic and placed in a shaking incubator at 220 rpm overnight. Plasmid extraction was accomplished following the protocol below;

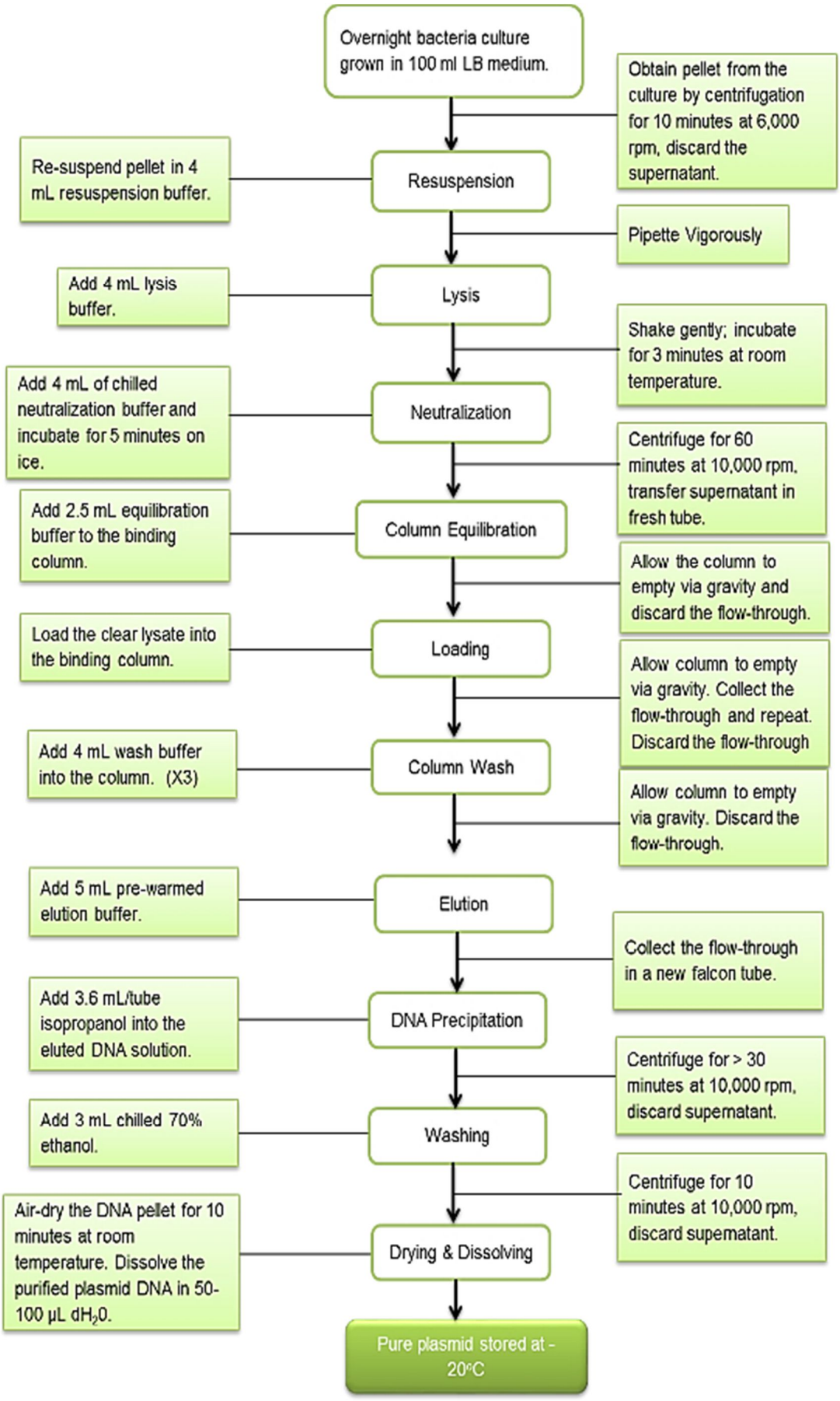

Overnight bacteria culture grown in 100 ml LB medium.
Obtain pellet from the culture by centrifugation for 10 minutes at 6,000 rpm, discard the supernatant.
Re-suspend pellet in 4 mL resuspension buffer.
Resuspension
Pipette Vigorously
Add 4 mL lysis buffer.
Lysis
Shake gently; incubate for 3 minutes at room temperature.
Add 4 mL of chilled neutralization buffer and incubate for 5 minutes on ice.
Neutralization
Centrifuge for 60 minutes at 10,000 rpm, transfer supernatant in fresh tube.
Add 2.5 mL equilibration buffer to the binding column.
Column Equilibration
Allow the column to empty via gravity and discard the flow-through.
Load the clear lysate into the binding column.
Loading
Allow column to empty via gravity. Collect the flow-through and repeat. Discard the flow-through
Add 4 mL wash buffer into the column. (X3)
Column Wash
Allow column to empty via gravity. Discard the flow-through.
Add 5 mL pre-warmed elution buffer.
Elution
Collect the flow-through in a new falcon tube.
Add 3.6 mL/tube isopropanol into the eluted DNA solution.
DNA Precipitation
Centrifuge for > 30 minutes at 10,000 rpm, discard supernatant.
Add 3 mL chilled 70% ethanol.
Washing
Centrifuge for 10 minutes at 10,000 rpm, discard supernatant.
Air-dry the DNA pellet for 10 minutes at room temperature. Dissolve the purified plasmid DNA in 50-100 µL dH_2O.
Drying & Dissolving
Pure plasmid stored at -20°C

Figure 2-2: Plasmid DNA isolation using Genopure midiprep kit. Steps showing isolation and purification of pure plasmid DNA using Roche Genopure Plasmid Midi Kit. Centrifugations were performed at 2-8ºC using an ultra-centrifuge at speeds indicated.

2.3.3 DNA quantification and storage

The concentrations of the plasmids of interest were determined via the use of Nanodrop spectrophotometer (ND-1000 UV-Vis, Labtech International Ltd, and Ringmer, UK) machine. The absorbance of the sample (1 µL) was measured at 260 nm and 280 nm while the ratios were determined at A260/A280 with a baseline correction of 340 nm. The 260/280 ratio is an ideal way to evaluate the purity of both DNA and RNA. A ratio of 1.8 or higher is generally accepted as "pure" for DNA while a ratio of 2.0 or higher is generally accepted as "pure" for RNA. In addition, the values of 260/230 ratio which is a secondary measure of nucleic acid purity was also used with as satisfactory range of 1.8 - 2.2. Ratios with lower values may indicate the presence of contaminants such as alcohol and isopropanol used in the precipitation of DNA sample, hence appropriate washing is recommended to avoid this issue. All DNA samples were stored at -20°C for long-term storage.

2.3.4 Restriction enzyme digestion

Plasmid DNAs were digested mostly to confirm that the appropriate plasmids of interest have been isolated following DNA cloning. For this, specific restriction endonucleases purchased from NEW ENGLAND BioLabs (NEB) were used

according to manufacturer's guidelines. The single or double digestion of the plasmids to be analyzed was performed with different restriction enzymes depending on the site available to be cut by the restriction enzymes (Table 2-5). Normally, 1 µL of a restriction enzyme was used to digest 1 µg of a plasmid DNA within 4 hours in a 20 µL reaction mixture containing 1X NEB buffer. The appropriate NEB buffer, BSA and incubation temperature were used for each particular restriction enzyme according to the manufacturer's instruction (NEW ENGLAND BioLabs catalog & technical reference guide). Subsequently, the efficiency of the enzymes was validated by running the digested samples on 1% agarose gel.

Table 2-5: Restriction enzymes used for plasmid validation.

Restriction Enzyme	Catalouge Number	Buffer	Incubation Conditions
EcoR1	#R0101S	NEB Buffer 3	37°C
Nhe1	#R0131S	NEB Buffer 2	37°C
BglII	#R0142S	NEB Buffer 3	37°C
HindIII	#R3104S	NEB Buffer 2	37°C

2.3.5 DNA Agarose gel electrophoresis

To visualize the DNA bands, 1% agarose gel [composed of 1g agarose + 100 mL of 1X Tris Acetate EDTA (TAE) buffer] was prepared. The solution was heated and dissolved in the microwave machine for 1-2 minutes after which 10 µL of Ethidium Bromide (Sigma #E1385) was added. Meanwhile, a gel

apparatus with an appropriate comb was prepared. The mixture was poured carefully into a tray with the appropriate comb attached before incubated at RT to solidify.

Size of the DNA plasmid was determined by loading 10 µL of either 1 kb or 100 bp DNA ladder (Figure 2-3) into the first well while 20 µL of the DNA samples were loaded carefully with 10 µL of 10X loading buffer into each wells and run at 80 volts for 70 min. 1X TAE was used as the running buffer while the loading buffer served the purpose of making the DNA samples heavy enabling them to sink to the bottom of the well. For PCR products (100 – 130 bp), 2 - 2.5% agarose gel was used.

Visualization of DNA & RNA bands was performed using Bio-Rad gel-Doc EZ system following gel electrophoresis.

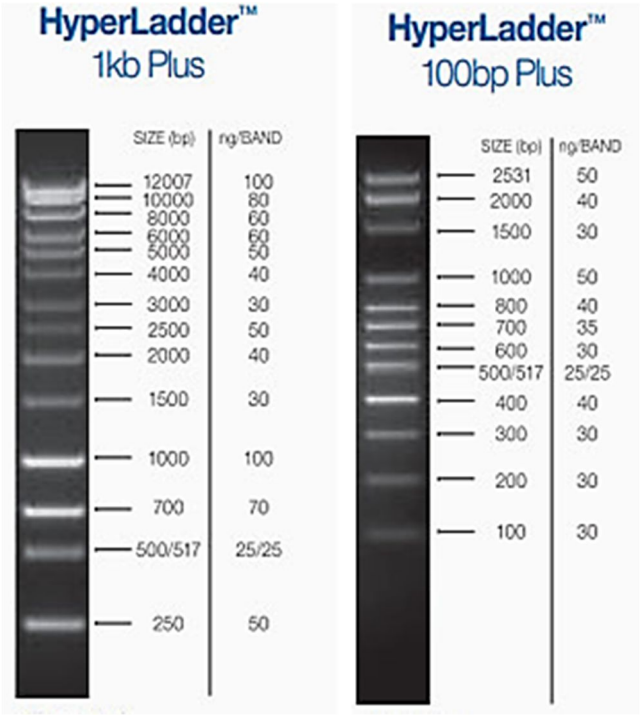


Figure 2-3: DNA Ladders (HypperLadder ™ Bioline). Different DNA ladders used for gel electrophoresis depending on agarose percentage.

2.3.6 Standard polymerase chain reaction (PCR)

All standard polymerase chain reactions (PCR) were performed using GoTaq® PCR master mix kit (#M4021) and Thermal Cycler machine (Applied Biosystems). A typical single sample reaction mixture consisted of the following: Sigma distilled water (to complete the volume of the reaction to the required final volume), 10X PCR Buffer, 25 mM $MgCl_2$, 0.25 mM dNTPs, 100 mol/µL from each forward and reverse primers, 0.1 - 0.5 µg DNA template, and 0.25 - 1.0 µL of DNA Taq-Polymerase enzyme (5 units/µL). The cycling parameters for a typical PCR reaction are shown in (Table 2-6). However, depending on the type of reaction, for instance primer optimization, melting temperature as well as the size of the amplicon, some of the amplification parameters such as the elongation time and the annealing temperature were amended. Finally, for each set of reaction, the housekeeping gene HPRT was used as the loading control while samples without cDNA were used as negative controls. For low complexity templates (i.e. plasmid), 1 pg – 10 ng of DNA per 50 µL reaction was used for PCR reactions.

Table 2-6: Cycling parameters to perform standard polymerase chain reaction.

Cycle Steps	Temperature (°C)	Time	Number of cycles
Initial Denaturation	95	5.0 minutes	1
Denaturation	95	20 seconds	35
Annealing	55	20 seconds	
Extension	72	1.0 minute	
Final Extension	72	7.0 minutes	1
Cooling	4	∞	_

2.4 Ribonucleic acid (RNA) isolation and reverse transcription

2.4.1 RNA Isolation

The total RNA was isolated depending on the number of cells as well as the appropriate cell lines using TRIzol® reagent protocol (Figure 2-4). Cells were washed once with PBS and lysed directly upon addition of the appropriate amount of TRIzol® reagent according to the manufacturer's protocol as illustrated below;

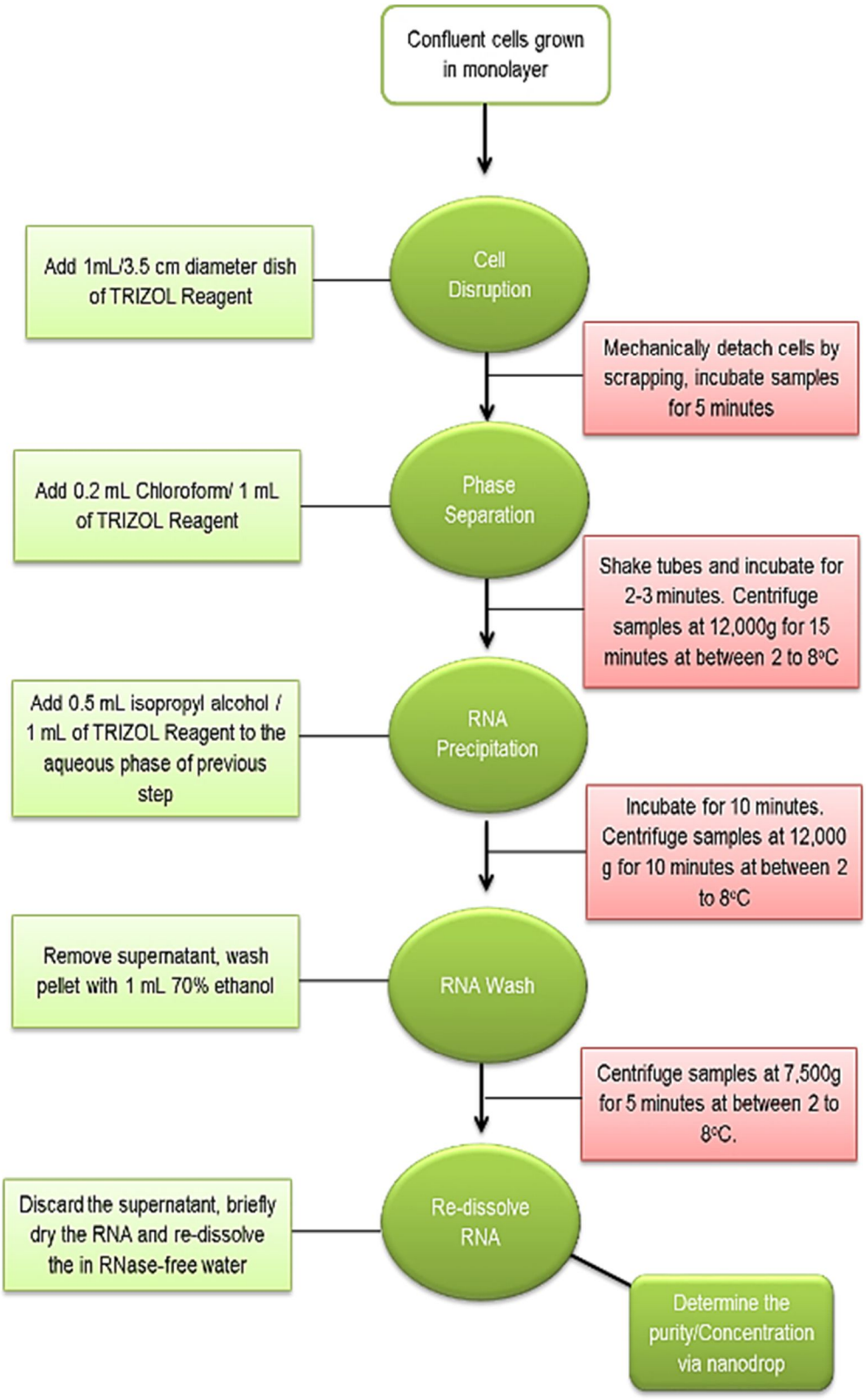


Figure 2-4: Total RNA extraction using TRIzol®. Stepwise description of total RNA extraction. Centrifugations were performed at 2-8°C using an ultra-centrifuge at speeds indicated.

Quantification and quality control of the RNA samples were carried out using Nanodrop and running at least 5 µL of each sample on Agarose gel.

2.4.2 RNA gel electrophoresis

For RNA gel electrophoresis, 1X MOPS (see section 2.1.1) was used as the running buffer. Formamide is a component in the loading dye for RNA while Formaldehyde is a component of the running buffer. Formamide is used as an RNA stabiliser in gel by deionizing RNA whereas formaldehyde acts as a denaturising agent by preventing secondary structure formation in RNA.

2.4.3 Reverse transcription and complementary Deoxyribo-nucleic acid (cDNA) synthesis

For cDNA synthesis, PrimeScript™ RT reagent Kit (TAKARA #RR037A) was utilized. 1 µg of total RNA was used in addition to a master mix of reagents consisting of 2 µL 5x PrimeScript buffer, 0.5 µL PrimeScript RT enzyme mix, 0.5 µL oligo dT primers (50 µL), 0.5 µL random-6-mers (100 µM), variable amounts of RNase free water and total RNA making a total volume of 10 µL per sample. The Veriti Thermal Cycler (Applied Biosystems) provided the precise temperature control and rapid temperature to acquire cDNA. The resulting cDNA samples were directly used for either PCR or qRT-PCR otherwise stored long-term at -20^{o}C. Stepwise procedure of the cDNA synthesis is illustrated in (Figure 2-5);

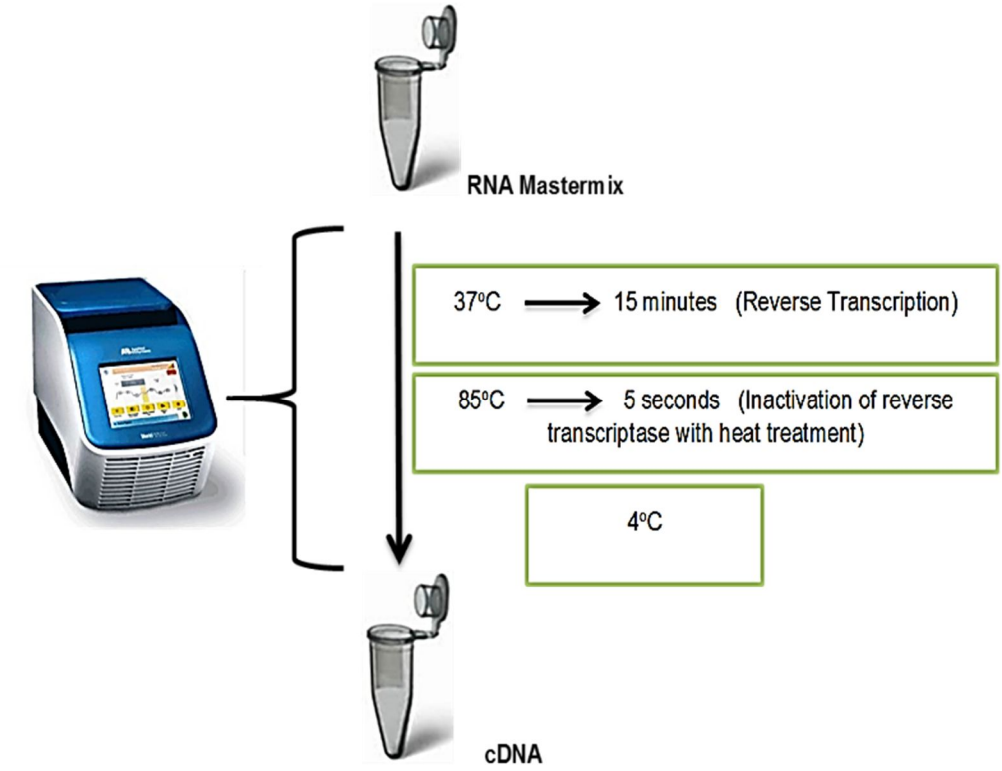


Figure 2-5: cDNA synthesis. Stepwise description of total cDNA synthesis. Centrifugations were performed at 2-8°C using an ultra-centrifuge at speeds indicated. Thermal Cycler image obtained from https://www.thermofisher.com/uk/en/home/life-science/pcr/thermal-cyclers-realtime-instruments/thermal-cyclers.html.

2.4.4 Quantitative real time polymerase chain reaction (qRT-PCR)

2.4.4.1 Primer design

Primers were designed using Primer3 and Blast design tool available at http://www.ncbi.nlm.nih.gov/tools/primer-blast/. Primers were generated from the mRNA sequence of the gene of interest such that the pair of primers (forward & reverse) was selected from two different exon regions (to prevent

amplification of contaminating genomic DNA) with the total size of the resulting amplicon strictly between the range of 100-200 bp. The specificity of the designed primer/s was analysed using NCB1 blast tool.

2.4.4.2 Reaction Preparation

The reaction mixture per sample consisted of 1.5 µL dH_20 PCR grade (Roche, # 04707516001), 0.5 µL of reverse and forward primers each, 5 µL 2X LightCycler® 480 SYBR Green I Master Mix (Roche, # 04707516001) and 2.5 µL of cDNA bringing the total volume up to 10 µL. Reactions were performed in triplicate per sample using 96 well plates provided by Roche (LightCycler® 480 Multi-well plate 96) and run under the appropriate amplification parameters (Table 2-7). Similar to the standard PCR procedure, the internal control housekeeping gene HPRT was used while samples without cDNA were used as negative controls. Each sample was placed in the appropriate well in the 96 well plate before properly sealed with LightCycler® 480 sealing foil (Roche, #04729757001) and run using a LightCycler® 480 II RT-PCR machine (Roche) under the guidance of standard protocol provided by the manufacture.

Table 2-7: Amplification parameters used for the quantative real time polymerase chain reaction (qRT-PCR).

Cycle Steps	Temperature (°C)	Time	Number of cycles
Pre-incubation	95	5.0 minutes	1
Amplification	95	10 seconds	40
	55	10 seconds	
	72	10 seconds	
Melting curve	95	5.0 seconds	1
	65	1.0 minutes	
	97	_	
Cooling	40	30 seconds	1

2.4.4.3 Data Analysis

The qRT-PCR data was analyzed using the comparative Ct ($2^{-\Delta\Delta CT}$) method in which the Ct values obtained from two different experimental RNA samples (control & experimental) are directly normalized to a housekeeping gene and then compared (Johnston et al., 2012). These Ct values were first generated from the LightCycler® 480 software (Roche, release 1.5.0) before been fully analysed in Microsoft Excel with further calculations in order to determine the mRNA expression and fold change between samples. All assays were performed in triplicate at least three times.

2.4.5 miRNA PCR Arrays

2.4.5.1 Pathway-focused miScript miRNA PCR array for mature miRNA expression profiling

Human miFinder miScript miRNA PCR array (MIHS-001ZF) enables profiling of the expression of the 84 most abundantly expressed miRNAs according to miRBase (www.miRBase.org). Each of these miRNAs can regulate one or more messenger RNA transcripts, and conversely a given mRNA can be regulated by one or more miRNAs. Overexpressed GFP and GFP-FLYWCH1 cells (TIG119 GFP^{+VE} & TIG119 GFP-$FLYWCH1^{O/E}$) were utilized for this experiment. The total RNA associated with FLYWCH1 of each cell lines was isolated using RNA immunoprecipitation (see section 2.7) in which the RNA/protein complex of FLYWCH1 was precipitated before isolation of the RNA which includes non-coding RNAs such as miRNAs.

Using a special kit provided by Qiagen (miScript® II RT kit # 218160) which utilizes total RNA that contains miRNA as a starting material for cDNA synthesis. The reverse-transcription reaction components per sample consisted of 4 µL 5x miScript HiSpec buffer, 2 µL 10x miScript Nucleics mix (contain oligo dT primers), 2 µL miScript reverse transcriptase mix (containing an optimized mixture of poly (A) polymerase and reverse transcriptase) and variable mixture of RNase free water and template RNA bringing the total volume to 20 µL. Quantity of RNA required is between 125-250 ng per RNA sample. The reverse transcriptase PCR conditions includes incubation of each samples for 60 minutes at 37ºC followed by incubation for 5 minutes at 95ºC to

inactivate the miScript reverse transcriptase mix before finally placing the cDNA on ice.

Following conversion of miRNA to cDNA, using miScript SYBR® Green kit (# 218073) the cDNA was combined with 1,375 µL 2x QuantiTect SYBR Green PCR master mix, 275 µL 10x miScript universal primer, 100 µL template cDNA and 1000 µL of RNase free water bringing the final volume to 2,750 µL per sample for 96-well format. This was promptly followed by aliquoting the mixture across the miScript PCR array (MIHS-001ZF).

A set of controls (SNORD61, SNORD68, SNORD72 and SNORD95) present on this array where used for data nominalization using delta CT method of relative comparison. Additionally, the controls aided in analysis using the ΔΔCT method of relative quantification, assessment of reverse transcription performance, and assessment of PCR performance.

2.4.5.2 Heat map Generation

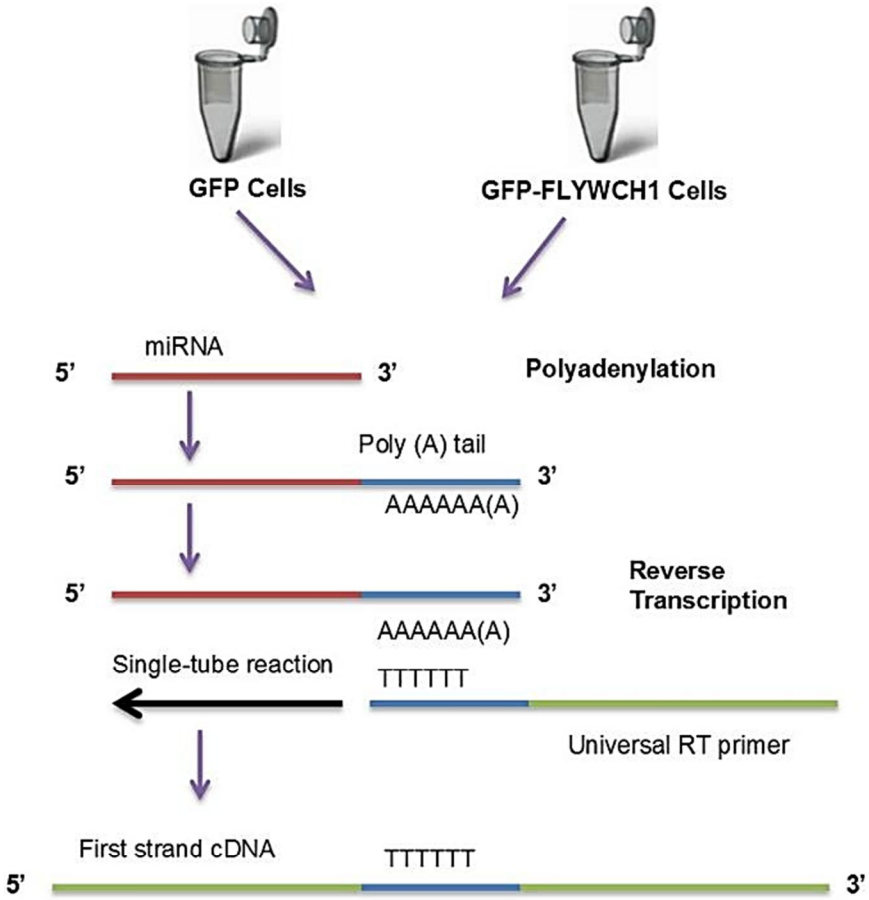
The heat-map of the miRNA expression profile in TIG119 GFP^{+VE} and TIG119 GFP-$FLYWCH1^{O/E}$ cells was generated via the PCR Array Data Analysis Web Portal provided by SA Biosciences. Intense red indicates over expression while intense green indicates under expression.

2.4.5.3 Validation of Pathway-Focused miScript miRNA PCR Array

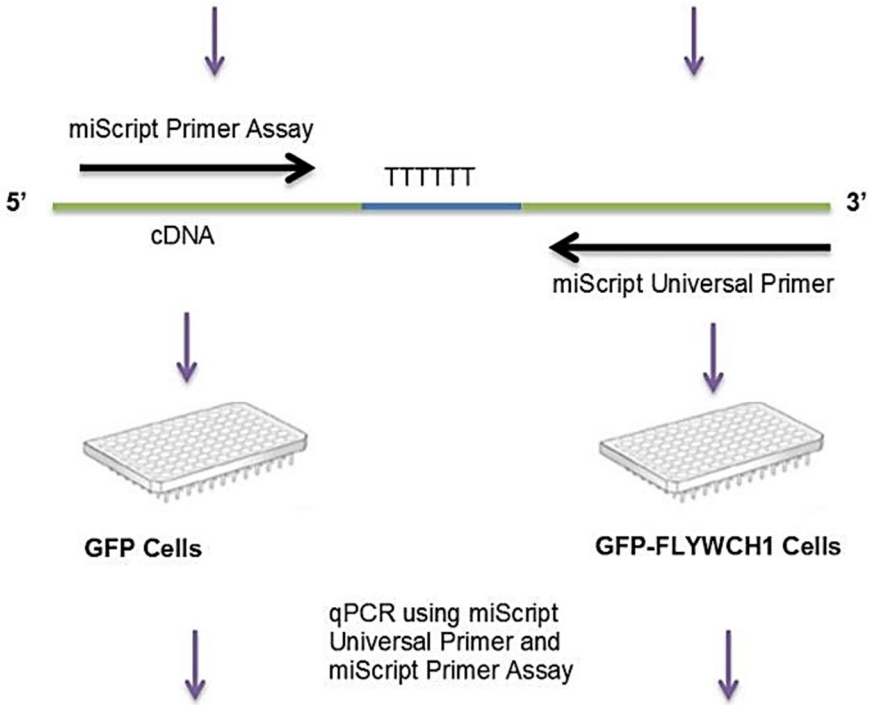
Validation of the experiment explained in section 2.4.5.1 was carried by firstly, selecting a group of genes to focus on and in this case all of the let-7 gene where up-regulated in TIG119 GFP-FLYWCH1$^{O/E}$. Cells under different conditions (TIG119 GFP^{+VE}, GFP-FLYWCH1$^{O/E}$ and GFP-FLYWCH1^{shRNA} cells) were cultured in normal media until the cells attained 80-90% confluency. Total RNA was isolated using TRIzol® reagent protocol. At this point the total RNA also contains miRNAs hence, the miRNAs are converted to cDNA using the miScript® II Reverse Transcriptase kit (# 218160) following the procedure explained in section 2.4.5.1 (Figure 2-6). The cDNA was then combined with 12.5 µL 2x QuantiTect SYBR Green PCR master mix, 2.5 µL 10x miScript universal primer, 2.5 µL 10x miScript let-7 primer assay, 2.5 µL template cDNA and a variable amount of RNase free water bringing the final volume to 25 µL per sample. The reaction samples where then run using the appropriate amplification parameters (Table 2-8).

The Ct values were then generated from the LightCycler® 480 software (Roche, release 1.5.0). For normalization, two assays were used (SNORD68 and SNORD95). The same procedure under appropriate conditions was carried out with CRCs.

1) miRNA conversion to cDNA via single tube reverse transcription reaction using miScript (RT) kit.



2) Combination of cDNA with QuantiTect SYBR Green PCR master mix, miScript universal primer and RNase-free water distributed equally across the miScript miRNA PCR array.





3) Run in real time PCR cycler and analyse data

Figure 2-6: Conversion of mature miRNAs into cDNA following manufacturer' recommendations. 1). A Poly-A polymerase contained in the HiSpec buffer adds a poly(A) tail to the miRNA sequence. A primer, containing oligo(dT) as well as a universal PCR primer sequence, anneals to the poly-adenylated RNA. **2)** Synthesis of the cDNA commences via reverse transcription while appending to the DNA primer sequence complementary to the miRNA. **3)** Finally, the a poly(dT) tract, the miRNA complement sequence and the universal PCR primer sequence are contained in the final first strand cDNA product. It is then utilized for mature miRNA expression profiling via real-time PCR utilizing a miRNA-specific primer. Image adapted and taken from http://www.sabiosciences.com/mirnaArrayDataAnalysis.php.

Table 2-8: Cycling parameters for the real-time polymerase chain reaction for profiling of mature miRNA expression.

Reaction Steps	Time	Temperature	Additional comments
Initial activation step	15 minutes	95ºC	This heating step enables the activation of HotStar Taq DNA Polymerase
Denaturation	15 seconds	94ºC	
Annealing	30 seconds	55ºC	
Extension	30 seconds	70ºC	Collection of fluorescence data
Cycle number	40 cycles		Number of cycles is dependent on the abundance of target and amount of template cDNA

2.5 Protein lysate preparation and analysis

2.5.1 Protein extraction and purification

Complete cellular protein lysate was prepared from different cell lines (transfected or un-transfected) via RIPA lysis buffer (Sigma #R0278) containing protease inhibitor (Sigma # P8340). The culture medium was removed and the cells were rinsed once prior to lysis with PBS. Depending on condition of the experiments, appropriate amounts (250 - 350 µL per one well of 6-well plate, 1 mL per one 10 cm petri dish) of freshly prepared RIPA lysis buffer was directly applied with the cells subjected to mechanical detachment with a scraper and incubated on a rocker for 5 - 10 minutes at 37^{o}C. The cell lysate was transferred into new 1.5 mL Eppendorf tubes and subjected to centrifugation at 13,000 rpm for 10 minutes at 4°C. The supernatant (containing total cell lysate) was transferred into separate Eppendorf tubes and labelled properly.

2.5.2 Protein Quantification

Protein quantification was performed using Bio-Rad Protein Assay reagent (Bio-Rad, # 500-0006) following the manufacturer's instructions. Firstly, the Bio-Rad reagent was diluted 1:5 in distilled water (dH_2O) and a series of standard dilutions of BSA (Bovine Serum Albumin) (Sigma, # A4503) (0.05, 0.1, 0.15, 0.2 and 0.25 µg/µL) were also prepared, diluted in dH_2O and added into the respective wells in a 96-well micro test plate (Scientific laboratory supplies, # MIC9038). The blank was prepared by adding 20 µL of dH_2O to the first well of

a 96-well micro test plate. This was followed by the addition of the various samples with the addition of 20 µL of dH_20 in the first well (Blank) prior to the addition of each protein samples diluted (1/10) by mixing 2 µL of the protein lysate with 18 µL dH_2O.

Subsequently, the protein-dye mixture was formed by adding 200 µL of the diluted Bio-Rad reagent in the wells upon which the protein samples were added in the microplate before determination of the absorbance measured at 595 nm by Infinite F50 TECAN machine with the software Magellan for F50. The protein concentration was then determined based on the BSA standard curve generated after which the samples were directly used for western blot analysis/protein immunoprecipitation or stored at -20^{o}C for future use.

2.5.3 Western blotting (WB) analysis

2.5.3.1 Sample preparation and SDS-PAGE electrophoresis

Following protein quantification, protein samples were prepared by mixing small portions of the cell lysates (ranging from 30 µg – 100 µg depending on the nature of the experiment) with appropriate amount of 5X loading buffer. The final concentration of the loading buffer in the sample should be 1X. Samples were placed on a heating block, heated for 4 minutes at 95°C to enable partial denaturation of the protein, and cooled down on ice for 5 minutes. Subsequently, the SDS-PAGE gel which is composed of two parts, the stacking and the resolving gels was prepared (Table 2-9, Table 2-10).

Table 2-9: Preparation of Tris-glycine staking gel for SDS-PAGE.

Solution components	Component volumes (mL) per gel Mol/d volume of				
	1 mL	**2 mL**	**3 mL**	**4 mL**	**5 mL**
H_2O	0.68	1.4	2.1	2.7	3.4
30% acrylamide mix	0.17	0.33	0.5	0.67	0.83
Tris (1.0 M, pH 6.8)	0.13	0.25	0.38	0.5	0.63
10% SDS	0.01	0.02	0.03	0.04	0.05
10% ammonium persulfate	0.01	0.02	0.03	0.04	0.05
TEMED	0.001	0.002	0.003	0.004	0.005

Table 2-10: Preparation of Tris-glycine resolving gel for SDS-PAGE.

Solution components	Component volumes (mL) per gel volume				
	5 mL	**10 mL**	**15 mL**	**20 mL**	**25 mL**
8%					
H_2O	2.3	4.6	6.9	9.3	11.5
30% acrylamide mix	1.3	2.7	4	5.3	6.7
Tris (1.5 M, pH 8.8)	1.3	2.5	3.8	5	6.3
SDS (10%)	0.05	0.1	0.15	0.2	0.25
10% ammonium persulfate	0.05	0.1	0.15	0.2	0.25
TEMED	0.003	0.006	0.009	0.012	0.015

Solution components	Component volumes (mL) per gel volume				
	5 mL	**10 mL**	**15 mL**	**20 mL**	**25 mL**
10%					
H_2O	1.9	4	5.9	7.9	9.9
30% acrylamide mix	1.7	3.3	5	6.7	8.3
Tris-Cl (1.5 M, pH 8.8)	1.3	2.5	3.8	5	6.3
SDS (10%)	0.05	0.1	0.15	0.2	0.25
10% ammonium persulfate	0.05	0.1	0.15	0.2	0.25
TEMED	0.002	0.004	0.006	0.008	0.01

An appropriate gel cassette (Amersham Biosciences or BioRad) in which the gel would be poured into was assembled prior to the preparation of both gels. The resolving gel was incubated at RT for 45 minutes to polymerize prior to the addition of the staking gel and insertion of a 10-well comb and incubated for another 15 minutes. Proteins with a molecular weight of >120 kDa was run on 8% resolving gel for easy separation. Protein markers (Bio-Rad Precision Plus Protein™ Standards) were normally poured in the first well followed by the addition of the previously heated protein samples (Figure 2-7).

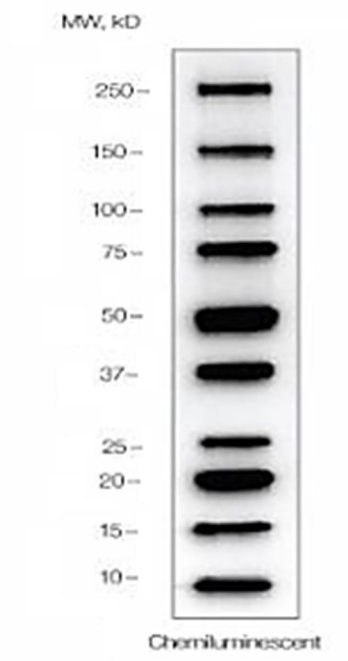


Figure 2-7: Protein markers used for SDS-PAGE analysis. Representation of pre-stained, chemiluminescent and fluorescent protein standard from Bio-Rad.

The outer and inner compartment of the gel electrophoretic unit (miniVE Vertical Electrophoresis System, Amersham/Biosciences, # 80-6418-77) were filled with 1X TGS running buffer (Tris/Glycine/SDS buffer, Bio-Rad, # 161-0772) and the gel was run at 130 V for ~2 hours and 30 minutes using a Bio-Rad PowerPac supply until the desired separation of the pre-stained marker was observed. Upon completion of the run, the proteins of interest were transferred to a Hybond-P PVDF membrane (GE Healthcare, # RPN303F) using a semi-dry transfer system (Bio-Rad, UK) at 14 V for 70 minutes while two membranes were transferred at the same time at 19 V for 75 minutes. Gels run on BioRad

cassettes were transferred at 14 V for 30 minutes (2 membranes were run as 19 V).

Upon completion of the transfer, membranes were blocked with a blocking buffer for 1 hour at RT. The blocking reagent was prepared by adding 0.1% Tween-20 (Sigma, # P1379), and 5% milk or 2% BSA with TBS-T (Tris buffer saline-Tween-20). Blocking buffer can also be prepared by dissolving 5% BSA in dH_2O. For detection of phosphorylated levels of proteins, 5% BSA was used.

2.5.3.2 Immunoblotting

Following blocking procedure, membranes were immunoblotted with primary antibodies to detect bands corresponding to the proteins of interest. Due to the different primary antibodies used different dilutions and incubation times were utilized according to the manufacturer instructions. These dilutions vary mainly due to the strength of the protein signal of interest. Details of different types of primary and secondary antibodies and their dilution factors used throughout this study are described in (see section 2.1.5).

Membranes were incubated in appropriate amounts of specific primary antibodies diluted in 5 mL blocking reagent and incubated under constant rotation for either a short period (1 hour) at RT or a longer period (overnight) at 4°C using a Roller mixer (Stuart SRT6, UK). Following incubation, membranes were washed three times with TBS-T for 5-10 minutes each and subsequently incubated with appropriate addition of secondary antibodies also diluted in blocking reagent for 1 hour at RT. Upon completion of incubation, the

membranes were washed again three times with TBS-T (washing buffer) for 5-10 minutes each before washing finally with dH_2O for 10 minutes. The proteins were then visualized via chemiluminesence method using ECL AdvanceTM Western Blotting detection Kit (GE Healthcare, # RPN2135) on LI-COR Odyssey®Fc dual mode western imaging system according to the manufacturer guidelines. In addition, different exposure times were used for visualization depending on the abundance of the protein of interest.

2.6 Sub-cellular Fractionation

Nuclear/cytosol separation was performed using Bio-Vision Nuclear/cytosol fractionation kit (# K266-25) as described in (Kalin et al., 2006; Takahashi et al., 2006). Below is the description of the components of the kit;

Table 2-11: Fractionation kit contents

Components	Volume (For 25 Assays)
Cytosol Extraction Buffer A (CEB-A)	5 mL
Cytosol Extraction Buffer B (CEB-B)	300 µL
Nuclear Extraction Buffer A (NEB)	2.5 mL
DTT (1M)	100 µL
Protease Inhibitor Cocktail	1 vial

2.6.1 Cytoplasmic Extraction

Firstly, NEB mix and CEB-A mix were prepared by adding 2 µL protease inhibitor cocktail and 1 µL DTT into each of 1 mL NEB and 1 mL CEB-A respectively on ice. Cells were then collected via centrifugation at 600 x g at 4^{o}C for 5 minutes. This was followed by the addition of 0.2 mL of CEB-A mix after which the cells were re-suspended by vortexing at the highest setting for 20 seconds and later incubated on ice for 10 minutes. 11 µL of ice cold CEB-B was added to the cells prior to vortexing for 10 seconds and incubation for 1 minute on ice. The sample was then exposed to 5 seconds of vortexing followed by centrifugation at 16,000 x g for 5 minutes. The resultant supernatant, which contains the final cytoplasmic extract, was then transferred into a new Eppendorf tube, labelled and stored on ice. The pellet contains nuclei extract.

2.6.2 Nuclear Extraction

Following manufacturers' recommendation with respect to cytoplasmic extraction, the pellet was later re-suspended in 100 µL of ice-cold NEB mix with vortexing for 15 seconds and incubation on ice. This was repeated 6 times over a 30 minutes period. The sample was subsequently centrifuged at 16,000 x g for 10 minutes. The resultant supernatant (containing the nuclear extract) was immediately transferred to a clean tube and temporarily stored on ice. Long-term storage of both the cytoplasmic and nuclear extracts were at -80^{o}C.

2.7 RNA Immunoprecipitation (RIP)

2.7.1 Nuclei Isolation & Nuclear pellet lysis

RNA immunoprecipitation (RIP) was performed using Magna RIP™ RNA-Binding Protein immunoprecipitation kit (#17-700). Following manufacturers' recommendation, total cell lysates were prepared using 100 µL RIP-lysis buffers (protease inhibitor cocktail and RNase inhibitor) and collected via centrifugation at 1,500 rpm for 5 minutes at 4^{o}C. The pellet was re-suspended by vortexing until a clear homogenous mixture was observed. The lysate was incubated on ice to enable the hypotonic RIP buffer to swell the cells before aliquoting 200 µL of the cell lysate into nuclease free micro centrifuge and stored at -80^{o}C for long-term use.

2.7.2 Agarose Beads

For RIP, Protein A/G PLUS-magnetic beads (Millipore, # CS203178) was utilized to pull down exogenous GFP-tagged proteins (GFP and GFP-FLYWCH1) along with the RNA associated with the protein. The cell lysate (0.5 mg) was first mixed with a specific amount of the primary antibody of interest (6-8 µg) in 1 mL RIPA lysis buffer. Following 1 hour of incubation at 4°C, 60 µL of the re-suspended Protein A/G PLUS-Agarose beads was added to the mixture and incubated with rotation for 2-3 hours at 4°C.

2.7.3 Formation of bead-antibody complex

Separate Eppendorf tubes were labelled and prepared depending on the nature of the experiments prior to the addition of 50 µL of magnetic beads A/G and 500 µL of RIP wash buffer in appropriate tube and placed on a magnetic separator before the supernatant was discarded after bead aggregation. The washing step was repeated twice before the beads were re-suspended with 100 µL wash buffer and addition of 5 µg of the primary antibody of interest and incubated with rotation for 30 minutes at RT. For negative control, anti-SNRNP70, which detects the U1 ribonucleoprotein was utilized. The beads were later washed twice with magnetic separator before the supernatant was discarded leaving the bead-antibody complex. The bead-antibody complex was immediately re-suspended with RIP immunoprecipitation buffer per sample.

2.7.4 Immunoprecipitation

The total cell lysate acquired from the initial step was thawed and centrifuged at 14,000 rpm for 10 minutes at 4^{o}C before 100 µL of the supernatant was removed and added to the bead-antibody complex in the RIP immunoprecipitation buffer and incubated under constant rotation overnight at 4^{o}C. However, prior to the addition of RIP immunoprecipitation buffer, a separate 10-20 µL of the total cell lysate was stored in a separate tube and used as input. Additionally, 5% of the bead-antibody complex with RIP immunoprecipitation buffer was stored SDS-PAGE analysis along with the input.

2.7.5 Isolation and purification of RNA bound to immunoprecipitated RBP

Upon completion of the conjugated beads, the tubes were placed on the magnetic separator and the supernatant discarded followed by washing with 500 µL RIP wash buffer on the magnetic separator. This was repeated twice. The immunoprecipitate was re-suspended in 150 µL proteinase K buffer (117 µL RIP wash buffer, 15 µL of 10% SDS and 18 µL of 10 µg/µL proteinase K) and incubated on a thermoplate at 55^{o}C for 30 minutes with constant shaking. Afterwards, the tubes were centrifuged briefly with the supernatant transferred into new tubes followed by the addition of 250 µL of RIP wash buffer with the supernatant. Addition of 400 µL of phenol:chloroform:isoamyl alcohol into each of the tubes was closely followed prior to centrifugation at 14,000 rpm for 10 minutes at RT to separate the phases. Upon separation, 350 µL of the aqueous phase was placed into new tubes with the addition of 400 µL of chloroform each and centrifuged at 14,000 rpm for 10 minutes at RT (The bottom phase containing protein isolated by the beads can be detected by western blot analysis). Following centrifugation, 300 µL of the aqueous phase was placed in new sets of tubes and RNA precipitation was performed by the addition of 50 µL salt solution I, 15 µL of salt solution II, 5 µL of precipitate enhancer and 850 µL of absolute ethanol per sample. The precipitate was isolated via centrifugation at 14,000 rpm for 30 minutes at 4^{o}C after which the supernatant was discarded carefully.

Finally, the pellet was washed once with 80% ethanol and exposed to centrifugation at 14,000 rpm for 15 minutes at 4^{o}C after which the supernatant

was discarded and the pellets air dried for 10 minutes. The RNA pellet was then re-suspended in 10-20 µL RNase-free water and stored on ice.

2.7.6 PCR Analysis of RIP

The immunoprecipitated RNA to cDNA synthesis was acquired with TAKARA PrimeScript™ RT reagent kit (#RR037A) under PCR conditions stated in section 2.3.6. For visualization, the amplified PCR product was run on 2% agarose gel with PCR product of SNRNP70 used as negative control.

2.8 Protein Immunoprecipitation

PureProteome™ Protein A/G Mix Magnetic beads (Millipore #2562415) were utilized to pull down GFP tagged proteins such as GFP and GFP-FLYWCH1. Here, the beads were manually conjugated to a desired antibody, mixed vigorously before addition of 50 µL of the homogenized beads to an Eppendorf tube, and placed on the magnetic separator to separate the beads from the storage buffer. The supernatant was discarded and the beads were re-suspended in 500 µL PBS-T (PBS, 0.1% Tween 20) solution containing appropriate concentration of a primary antibody of interest (normally 5 µg). Tubes were incubated with continuous rotation for 45 minutes at RT. The acquired beads-Ab complex was washed twice in 500 µL PBS-T solution twice by gentle pipetting with the magnetic separator used to separate the supernatant from the beads in-between each wash. The conjugated beads was then mixed with 550 µg of cell lysate of

choice and incubated overnight under constant rotation at 4ºC. Upon overnight incubation, the beads were washed once with PBS-T on the magnetic separator after which the supernatant was discarded followed by the addition of 60 µL of denaturation buffer suitable for electrophoresis (Sigma sample laemmli buffer, #SLBL1656V) per sample and heated at 90ºC for 10 minutes. The tubes were then placed in the magnetic separator and the supernatant carefully extracted and run on SDS-PAGE gel.

2.9 Functional analysis

2.9.1 *In-vitro* scratch assay

Briefly, cells were sub-cultured under different conditions and grown in 6-well plates in triplicate. CRC GFP^{+VE} cells were used as control in parallel CRC GFP-$FLYWCH1^{shRNA}$ cells were used as the experimental cells. The cells were later starved overnight in a serum free RPMI medium 48 hours after the initial culture in order to synchronize the cells at G0 (Langan and Chou, 2011).

Once the cells attained 80-90% confluency a narrow (1,000 µL) tip was used to create three parallel wounds on the bottom of the wells. Afterwards, the cells were washed with PBS and maintained in complete RPMI medium. The wounds were immediately examined under the bright-field and fluorescence microscope (Nikon, Model ECLIPSE TE2000-S) and the first batch of images (t = 0) were acquired using the 10X lens of a phase-contrast and GFP filter. The images were taken directly above the wound and below each marker line to recognize the

specific area captured at t = 0. The wound was observed and the imaging process was repeated after 24 and 48 hours.

Quantitative analysis of the images acquired was performed using ImageJ software (Rasband, W.S., ImageJ, U. S. National Institutes of Health, Bethesda, Maryland, USA, http://imagej.nih.gov/ij/, 1997-2011). The distances between each side of the scratch in each image were measured using the "Freehand Selections" command of the Image J software at the different time intervals (e.g. 0, 24 and 48 hours). The rate of cell migration for the cells under experimental condition was determined by comparing the average of the percentage of cell movement of at least five readings for each well.

The percentage of wound confluence/closure at each time interval was calculated using the equation below:

$$Percentage\ wound\ clusure = (\frac{A - B * 100}{A})$$

Where:

A= Initial wound scratch (t_O)

B= Wound scratch at time X (t_X)

2.9.2 Luciferase Reporter assay

For further gene regulation studies, an indirect transcriptional activity was assessed using the firefly-luciferase reporter system by the Dual-luciferase kit (Dual-Luciferase® Reporter Assay, Promega, # E1910) according to the

manufacturer's instruction as well as described previously (Nateri et al., 2005). Cells were seeded (3 x 10^5) and grown to a cell density of 60-70% in 24-well plates. Depending on the nature of the experiments, transient transfection was performed (as outlined above in section 2.2.1.4) with the plasmid of interest along with the reporter constructs of the genes of interest. In this experiment, only 0.2 µg of all plasmid DNAs was used while 0.05 µg of *Renilla* construct was used due to its high sensitivity. However, reporter plasmids that contained both fused firefly and *Renilla* luciferase did not require separate transfection of *Renilla* plasmids. Transfections were carried out in triplicate and the cells were harvested 36 hours post transfection using varying amounts of 1X passive lysis buffer provided within the Dual-Luciferase kit. The samples were mechanically lysed with a scrapper, incubated on a rocker at RT for 10-15 minutes before exposure to centrifugation at 15,000 rpm for 15 minutes before finally transferred to fresh Eppendorf tubes, and stored at -20^{o}C.

The activity of the firefly luciferase reporter was measured first by adding 50 µL/well Luciferase Assay Reagent II (LAR II) followed by the addition of small amounts of freshly prepared lysates (10 µL/well) in Microplate FluoroNunc 96 well plate (Fisher, # MPA-560-040A) in triplicate. The LAR II enabled the generation of a stabilized luminescent signal, which can be detected and read by a Luminoskan Ascent Microplate Luminometer (Thermo Scientific, UK). Immediately after the successful quantification of the firefly luminescence, the reaction was quenched with 70% ethanol and dH_20. In a similar manner as earlier described, 10 µL/well of fresh lysate was added and the *Renilla* luciferase reaction was concomitantly initiated by the addition of 50 µL/well Stop & Glo®

Reagent to the samples in the same plate. This allowed the activities of both firefly and *Renilla* luciferases to be measured sequentially from the same samples.

2.9.3 Cell cycle analysis

Propidium iodide (PI) staining method was utilized to analyze the effect of FLYWCH1 on the cell cycle progression of CRC cells as described previously (Babaei-Jadidi et al., 2011; Ibrahim et al., 2012b; Nateri et al., 2004). Cells were either transfected with the appropriate plasmid DNAs or cells stably expressing a plasmid of interest, and cultured in triplicate in a 10cm culture dish. Suitable amounts of the transfected cells (~3 x 10^5 cells) were detached via trypsinisation and collected in 15 mL Eppendorf tubes. The cells were centrifuged at 1,200 rpm for 5 minutes to produce a solid cell pellet with the supernatant discarded. The cells were washed and re-suspended with 2 mL/tube of PBS and centrifuged again at 1,200 rpm for 5 minutes. Cells were subsequently fixed with 2 mL of 70% cold ethanol dropwise while vortexing the sample then left at 4°C for at least 30 minutes or at -20^{o}C for maximum of 1 week.

The fixed cells were washed twice in 1 mL PBS, and each wash samples were spun down for 5 minutes at 1,000 rpm. Cells were stained with 300 µL of diluted (50 µg/mL) propidium iodide (PI) solution (Sigma, # P4864) in PBS containing 0.1 µg/µL of RNase A. The number of stained cells in each step of the cell cycle was determined by a Coulter FC 500 flow cytometer (BEKMAN COULTER,

UK). Finally, further statistical analysis was performed by using Weasel Java™ platform software and Microsoft Excel 2010 for statistical analysis.

2.9.4 Electric Cell-substrate Impedance Sensing (ECIS) for Cell Attachment Quantification

ECIS is an impedance-based, real-time, label-free method to analyze the properties of cells ranging from morphological alterations, cell migration, and other characteristics directed by cellular cytoskeleton grown in tissue culture. Following manufacturers' recommendation (Applied Biophysics Inc, Troy NY, USA), 200 µL/well 10 mM L-cysteine was added to each well of the ECIS array and incubated for 15 minutes at room temperature (RT). The cysteine modifies and cleans the electrode surface thereby, providing a reproducible and high electrode capacitance. This was followed by wash with 500 µL/well of ultra-pure water/ sigma water prior to coating of electrodes with 200 µL/well with warm 1% gelatine and incubated for 30 minutes at RT. Following incubation, the gelatine was completely removed and washed once immediately with ultra-pure water (see section 3.2.5 for description of ECIS).

2.9.4.1 Array Stabilization

Stabilization on the array(s) was performed prior to an experiment to prevent electrode drift, and to improve signal-to-noise ratio and improve well-to-well reproducibility. 200 µL/well of complete medium was added with the array placed in the array holder in the incubator. The measurement software (Applied

Biophysics ECIS Software) was opened while pressing "***set-up button"*** to ascertain the array was connected properly to measure impedance (Z) for DC circuit, Resistance (R) for AC circuit and Capacitance (C). The electrodes were stabilized by pressing "***Stabilize button"*** in the "collection data" section of the software. At this point, a high current (3 mA), high frequency (64 kHz) pulse was applied by the system to clean the electrodes.

2.9.4.2 Inoculation of Cells

Following stabilization, the medium was removed and cells were seeded as a single cell suspension in 400 µL/well ($5x10^4$ cells per mL) in complete cell culture medium in the ECIS array (Figure 2-8). The array was then placed into the array holder in the incubator and secured properly by ensuring the adjustment screw was hand tight. Subsequently, the measurement software was opened and instructions for measurement set-up and data acquisition were followed according to the manufacturer's guidelines and reliable protocols (Szulcek et al., 2014). The system was run for a period of 24 hours after which data analysis and quantification in terms of cell attachment and spreading was carried out.

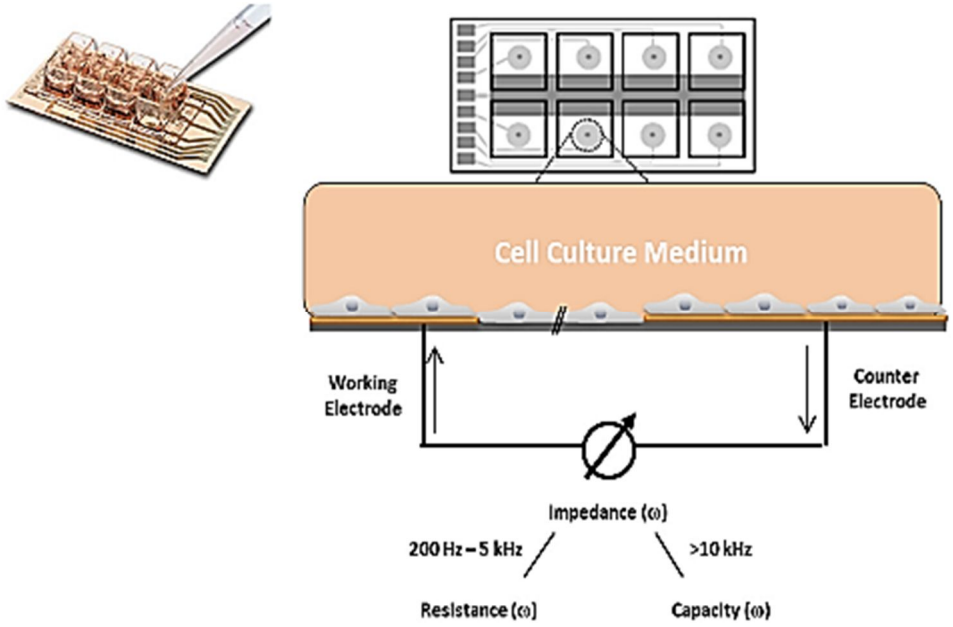


Figure 2-8: Schematic representation of the principles of ECIS. Applied BioPhysics, Inc http://www.biophysics.com/ecis-theory.php and (Benson et al., 2013).

2.9.5 Cytotoxicity & Viability Assay

Sulforhodamine-B (SRB) (Sigma) colorimetric assay for cytotoxicity screening was performed as described in (Li et al., 2015). Firstly, SW480 GFP^{+VE} and GFP-$FLYWCH1^{O/E}$ cells were cultured in 10 cm plates until 70-80% confluent. 24 hours post-transfection, cells were transferred in triplicates into a 96-well plate, ensuring the cell count was 3,000 cells/well. Cells were starved in serum-free medium for 18 hours to synchronise the cells to the same stage of cell growth. Serial dilutions of TDZD-8 were then prepared and 200 µL of each dilution was added to the corresponding well. A range of concentrations from 0-100 µM of TDZD-8 was used to enable calculation of the IC_{50} values. The cells were checked 6 hours following TDZD-8 treatment (corresponding to the

approximate half-life indicated for the drug) and the following day, cells were fixed by adding 50 µL of cold 30 % TCA to the inhibitor and incubating for 1 hour at 4^{O}C. The TCA and drug solution was then removed and the plate was washed with tap water and air-dried. 50µL of SRB solution at 0.4% in 1% acetic acid was later added to the wells, which were then incubated for 20 minutes at RT. (The TCA and acetic acid provide the acidic environment enabling SRB to bind basic amino acids).

The dye was removed by washing the wells 5 times with 1% acetic acid and air-drying. Finally, 200 µL of 10 mM Trizma Base was added to solubilise the protein-bound dye and absorbance values were measured at 540 nm of wavelength, from which percentage control values were obtained. Plotting a dose-response curve of the negative log concentration of TDZD-8 against the percentage control values enabled determination of the IC_{50} value.

2.9.6 Immunofluorescent (IF) analysis

2.9.6.1 Cell Preparation

An optimized IF protocol was applied to stain the cells in three steps as previously described in (Ibrahim et al., 2012b). Coverslips were sprayed with 70% ethanol before washing with 1 mL PBS. 800 µL/1mL of Poly-L-lysine was added to each well of a 6 well plate with the coverslip (22 x 22 mm) and incubated for 2 hours at room temperature under the hood after which the Poly-

L-lysine was discarded gently. Cells were seeded and grown on coverslips in 6 well plates and transfected with the appropriate plasmids/siRNA.

2.9.6.2 Fixation & Permeabilization

Cells were subsequently washed twice with PBS (1 mL/well) before fixation with 4% Paraformaldehyde (PFA) for 30 minutes at RT. Another fixation agent, Glutaraldehyde was used for filopodia detection. This was followed by another wash with PBS prior to permealization of the cells by addition of 500 µL/well of 0.1% TRITON X 100 in dH_2O for 30 minutes at RT and later washed twice for 5 minutes in PBS.

2.9.6.3 Blocking Buffer

The permealized cells were blocked with the addition of 300 µL/well of 2% BSA (Bovine Serum albumin) diluted in PBS on top of each coverslip and incubated for 1 hour at RT to block. This was followed by 500 µL/well PBS wash for 5 minutes.

2.9.6.4 Staining with Primary and Secondary antibodies

Following blocking, primary antibody was prepared. The dilutions were prepared in 2% BSA (diluted in PBS) with the addition of 300 µL of the mixture per well prior to incubation at 4^oC conditions for 1 hour or overnight depending on the antibody. Primary antibody was not added to cells that were used as

negative controls. Following exposure to the primary antibody, the cells were washed 4 times for 10 minutes in 1% BSA 0.1% Tween 20, 300 µL/well diluted in PBS at RT. In the absence of light the secondary antibody was diluted in 2% BSA and 350 µL/well was added. The plate was carefully wrapped with an aluminium foil and incubated without light at RT for 1 hour. The secondary antibody was also added in the cells used as negative controls. The cells were later washed 5 times for 10 minutes each with 1% BSA 0.1% Tween 20 diluted in PBS. The slides were carefully removed from the 6 well plate with a bent needle and placed upside down directly on a drop of DAPI stain (ThermoFisher Scientific) on a clean slide and incubated for 15 minutes at RT prior to storage at 4^{o}C conditions. Subsequently, slides were mounted and analysed using Leica DMI3000 B Inverted microscope (Leica Microsystems, UK) following the manufacture's instruction.

2.9.6.5 Immunofluorescence Staining of Colonospheres

Following 14 days of culture and deriving colonospheres (section 2.2.1.3), the stem cell medium was aspirated carefully from the edges of the 6-well plate and washed once with 1 mL PBS. 4% paraformaldehyde (PFA) in PBS was prepared and 800 µL of 4 % PFA was added to the side of the well and incubated for 30 min at RT. The colonospheres were washed once in 1 mL PBS. Following aspiration and emptying the collected PFA, the colonospheres were incubated for 5 min at RT after which 800 µL of 0.5 % Triton x-100 (diluted in PBS) was added to permeabilize the colonospheres at RT for 5 minutes. The permeabilized colonospheres were blocked by adding 800 µL of 1 % BSA in PBS to each well

and incubated for 30 min at RT. Following permealization, the 6-well plate was tilted at approximately 45° to carefully aspirate BSA/PBS from each well. At this point, the colonospheres are now ready for immunofluorescent staining.

Note: During the whole process, aspiration of stem cell media, PBS was performed with extreme caution, as colonosphere do not attach to the plate surface.

2.10 Phalloidin staining

Phalloidin is a commonly used dye for cytoskeletal and morphological analysis. It binds to F-actin to display the shape of the cells. The initial step of Phalloidin staining is similar to the IF protocol in which the cells were initially grown on coverslips, fixed, and permeabilized with 0.1% Triton X-100 (see section 2.9.6.2). Following permeabilization, cells were incubated with diluted (50 µg/ml, in PBS) fluorescent Phalloidin conjugate solution (Sigma, # 1951) for 40 minutes in dark. Subsequently, the stained cells were washed 2-3 times in PBS for 5 minutes at room temperature prior to mounting the cover slips upside down on a slide with a drop of DAPI and analyzed with the Leica microscope as described above in (section 2.9.6.4). Furthermore, 1% glutaraldehyde was added with the fluorescent Phalloidin conjugate solution to analyse filopodia in relation to epithelial mesenchymal transition (EMT) analysis.

2.11 Patient sample Analysis

Colorectal cancer patient samples of each condition (normal, primary and metastatic) were provided by gastrointestinal (GI) surgery department, QMC, Nottingham University Hospital. The samples were subsequently subjected to tissue homogenization.

Upon final tissue extraction, each tissue was immediately sliced into pieces preferably not wider than 0.5 cm and stored in RNAlater® stabilization solution (Thermo Fisher Scientific) and incubated overnight or stored for up to 4 weeks at 2 - 8^{o}C. At least 1 mL TRIzol® reagent /50 - 100 mg tissue to be homogenized was transferred into RNase-free homogenization tubes. Homogenization was accomplished via utilization of Polytron tissue homogenizer and prior to use, the probe was cleaned by running the homogenizer with DEPC treated water and absolute ethanol for 1 minute each. Once homogenized, solutions of each sample were aliquoted into RNase-free 1.5 mL Eppendorf tubes and incubated for 5 - 10 minutes at RT in order to allow for the complete dissociation of nucleoprotein complexes. Phase separation, RNA precipitation, RNA wash, re-suspension, quantification and quality control were all executed according to the protocol explained in (Section 2.4.1**)**. RNA purification was carried out with Qiagen RNeasy and followed strictly according to manufacturer's protocol.

Following RNA isolation, cDNA of each sample (normal, tumour & metastasis) was obtained to investigate the different levels of FLYWCH1 expression in each sample. Additionally, RNA samples were used to acquire cDNA of miRNA using miScript® II RT kit (# 218160) to measure the expression of let-7 in the

different samples and subsequently correlate the data with FLYWCH1 expression levels.

2.12 Statistical analysis

Statistical evaluations were accomplished by applying the independent-samples *t-test* (2-tailed) method using Microsoft Excel (Microsoft Office 2013, 2016). Box and whisker plots were generated via GraphPad Prism and Microsoft Excel 2016 version. Statistical significance where determined as follows; P value ≤ 0.05 (*) was considered statistically significant, P ≤ 0.01 (**) highly significant and P ≤ 0.001 (***) very highly significant. The error bars shown for all charts represent the standard deviation (STDEV) for the sample's mean unless stated otherwise. Experiments were performed in triplicates for each case and repeated on at least 2-3 independent occasions. GraphPad prism software was used to evaluate IC_{50} values as described in https://graphpad.com/support/faq/how-to-determine-an-icsub50sub/.

2.12.1 Quantitative Image Analysis of Colonospheres, Immunofluorescence data & Western blot

Quantification of fluorescence intensity was performed by calculating the corrected total cell fluorescence (CTCF) as described in (Abashidze et al., 2014; Roulois et al., 2015) using ImageJ software as follows;

CTCF = Integrated Density - (Area of selected cell X Mean fluorescence of background readings).

The selected parameters (Area, mean gray value, integrated density and the background measurements) of the appropriate expression makers were measured in colonspheres derived from SW480 GFP^{+VE} and SW480 $FLYWCH1^{shRNA}$ cells. The CTCF data presented (Chapter 4) is a representation of the CTCF average of a total of 4 colonospheres from triplicate in each condition (per expression markers).

Co-localization quantification (Figure 5-1 & Figure 5-2) was performed by calculating the Pearson co-localization coefficient (PCC) with ImageJ as described in (Dunn et al., 2011; Moser et al., 2016). PCC values close to 1.0 indicates absolute co-localization while PCC close to 0.0 indicates poor co-localization.

Box and whisker plot was used (Figure 3-14 & 5-17) to describe the distribution of values across the patient samples used for the analysis. While histograms require a large sample size of at least 30 to be useful, box plots require a sample size of only 5, and provides more detail in the tails of the distribution (Krzywinski and Altman, 2014). The five most important descriptive values provided by box and whisker plot includes the minimum value, the first quartile (25^{th}), the median, the third quartile (75^{th}), and the maximum value. Outliers are also revealed. Additionally, this was suitable in the data described in Figure 5-17 as a cohort of 9 normal, primary and metastatic samples were used.

For quantification of western blot bands, first the loading control in each lane was quantified followed by normalizing the band intensity of interest with the corresponding loading control in order to obtain the ratio via Licor Odessey software Image Studio 3.1.

3 CHAPTER 3

Human FLYWCH1 controls cell morphology and migration

3.1 Brief Introduction

Alterations in cell morphology and motility are initial steps toward metastasis and invasion, which are key hallmarks of cancer (Hanahan and Weinberg, 2011). It can be hypothesized that changes in biomechanical properties, including changes in expression of adhesion proteins and changes in cytoskeletal properties correlates with changes in cell shape. Studies have shown that changes in gene expression of certain genes with cytoskeletal function results to cell morphology alterations which may be signatures of metastatic capacity (Brandhagen et al., 2013).

During tumorigenesis, epithelial mesenchymal transition (EMT) facilitates invasiveness and motility of cancer cells (Boyer et al., 2000). The motile capability acquired by these cells can be attributed to remodelling of actin filaments and stress fibre formation (Haynes et al., 2011; Vallenius, 2013). The processes that occur in EMT during normal development closely resemble the EMT processes occurring during metastasis and tumour progression especially the change in morphology from an epithelial to a mesenchymal phenotype. However, due to certain preferential oncogenic pathways, the molecular program resulting to EMT in cancer state may be characterized by the augmentation of only a hand-full of some aspects necessary for EMT to occur during normal development.

The Wnt/β-catenin signalling pathway, through multiple mechanisms, is often associated to regulation of various biological activities such as modulation of cell branching and collective cell migration and (Aman and Piotrowski, 2008; Humtsoe et al., 2010; Matsuda et al., 2009). Indeed, signalling through this

pathway governs the expression of a plethora of genes that regulate filopodia formation and consequently cell morphology, migration, and invasion. Activated Wnt signalling plays a crucial role in cellular homeostasis and carcinogenesis depending on the context of activation and the surrounding microenvironment. More importantly, β-catenin participates in linking cadherins to the cytoskeleton, thereby facilitating tight intercellular as well as surface adhesion, and together with members of the TCF/LEF-transcription factors (TCFs) controls several associated genes in the context of canonical Wnt signalling.

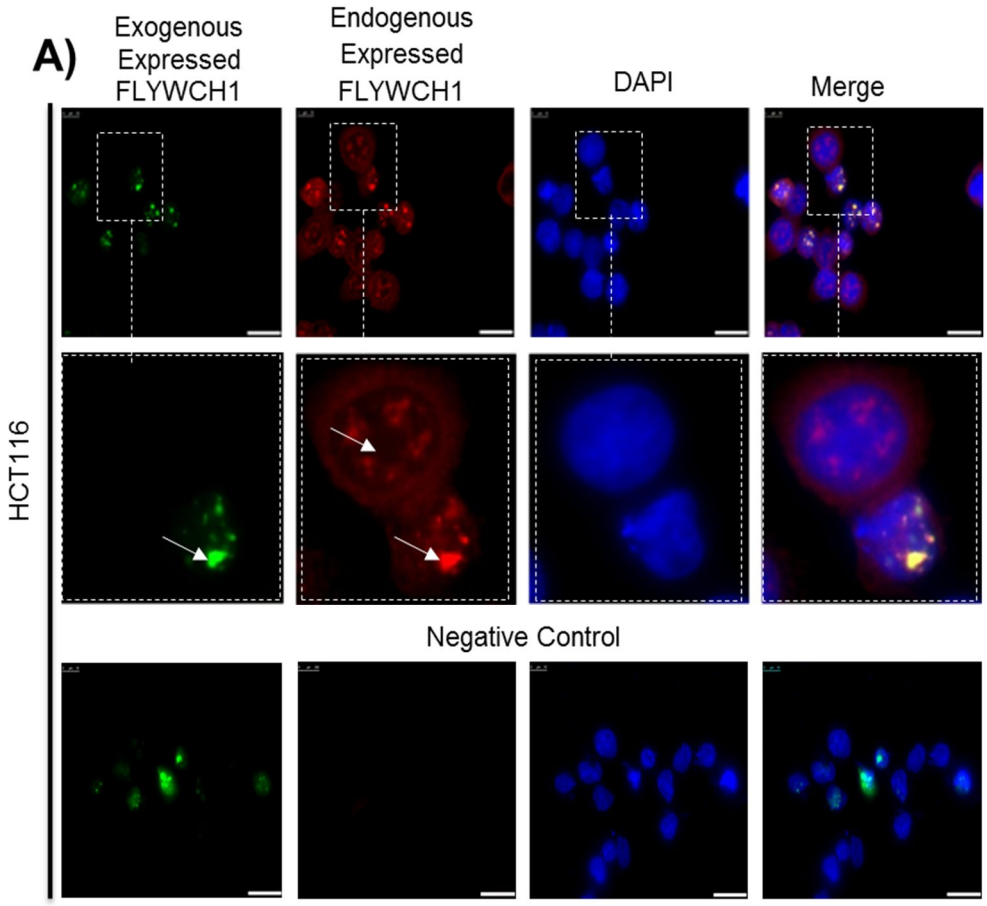
Therefore, due to the FLYWCH1-mediated negative regulation of Wnt/β-catenin signalling pathway (Muhammed et al., submitted), this chapter focuses on describing the involvement of FLYWCH1 in modulating cellular adhesion and migration properties via cell morphology and probably via negatively regulating the β-catenin/TCF4 complex thereby inhibiting ZEB1 transcriptional activation.

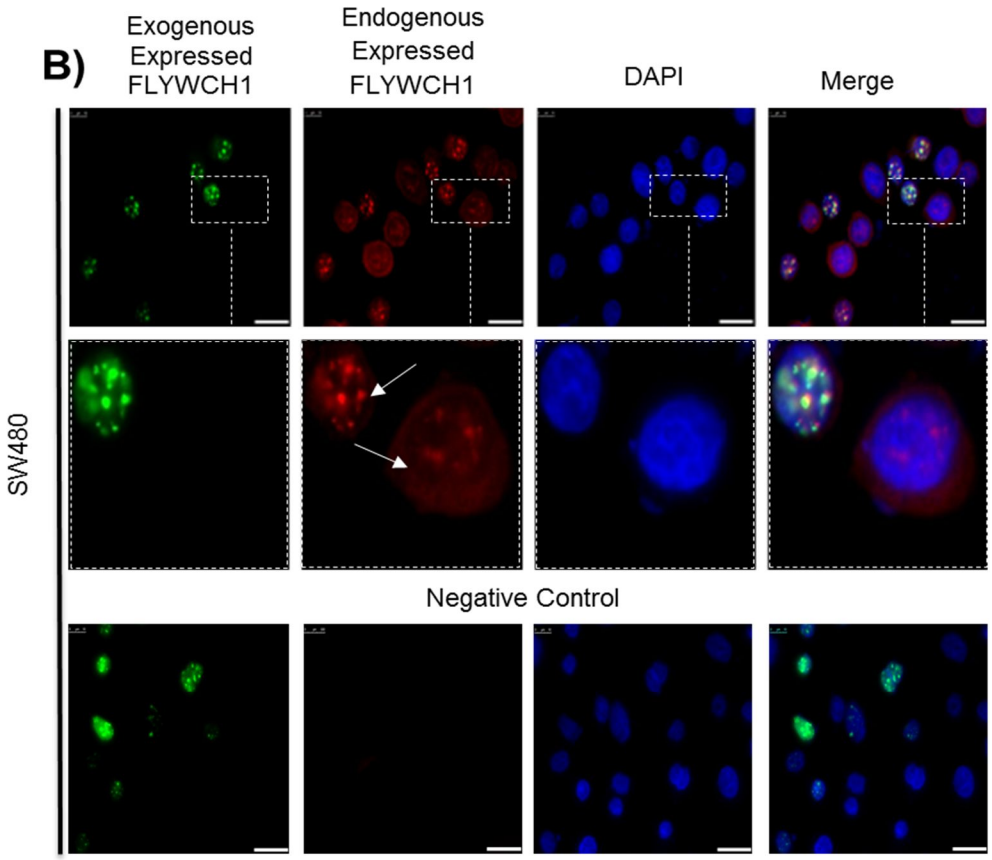
3.2 Results

3.2.1 Endogenous nuclear localization of FLYWCH1 in human cell lines

Prior to the generation of FLYWCH1^{shRNA} cells, we sought to evaluate the ability for the FLYWCH1 antibody (Table 2-2), to detect both endogenous and exogenous expression of FLYWCH1 in normal fibroblast and CRC. Immunofluorescence technique was employed to visualize the endogenous and exogenous (via transient transfection) FLYWCH1 expression in TIG119, SW480 and HCT116 cell lines. The results reveal that endogenous and

exogenous expression of FLYWCH1 was detectable in the nucleus with a characteristic speckle-like pattern in each of the cell lines used. Also, following the use of the FLYWCH1 antibody, high intensity of FLYWCH1 expression on individual cells expressing GFP-FLYWCH1 is suggestive of detection of endogenous and exogenous expression of FLYWCH1 by the antibody used (Figure 3-1). Taken together, these results simply confirms the nuclear localization and speckle-like pattern of FLYWCH1.




B)
Exogenous Expressed FLYWCH1
Endogenous Expressed FLYWCH1
DAPI
Merge
SW480
Negative Control

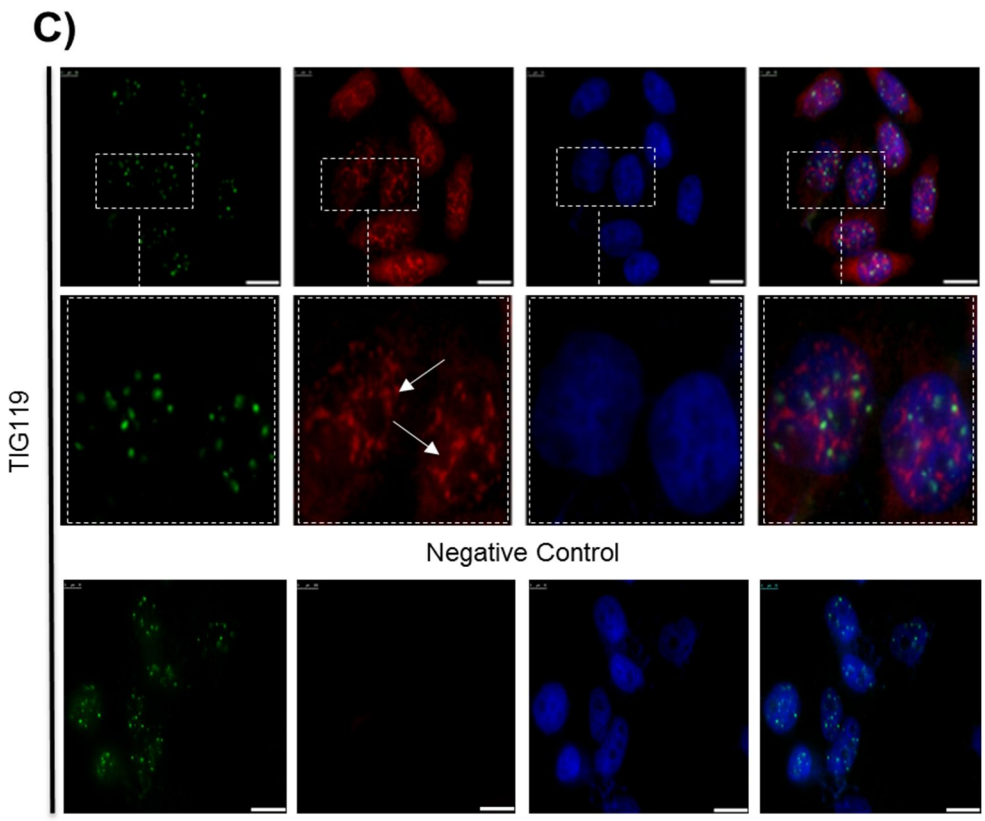

C)
TIG119
Negative Control

Figure 3-1: Nuclear localization of FLYWCH1 foci in normal and CRC cells. Detection of exogenous (Green) and endogenous (Red) FLYWCH1 expression in **A)** HCT116, **B)** SW480 and **C)** TIG119 cells using FLYWCH1 antibodies. Negative controls were used in the absence of primary antibody. Scale bars, 10 µm. Arrows show the FLYWCH1 foci. Increased intensity of FLYWCH1 expression is suggestive of the endogenous & exogenous detection of FLYWCH1 by the antibody utilized. Quantitative analysis is not required.

3.2.2 Generation of cells stably expressing GFP for gain-of-function and piLenti-FLYWCH1^{shRNA} for loss-of-function studies of FLYWCH1

To investigate the effects of FLYWCH1 gain-of-function in cancer cells, stable overexpression of full-length FLYWCH1 had been attempted in SW480 and HCT116 cells using GFP-FLYWCH1 lentiviral vector (pLVX-GFP-FLYWCH1-PuroR) and based on Puro selection without success. Additionally, FLYWCH1 in the selected Puro-resistant cells showed different cellular localisation pattern in these cell lines and basically failed to form the FLYWCH1 foci in these cells (Muhammed et al, submitted).

Several lines of evidence point to speckles as key storage/assembly/modification compartments that may regulate the splicing factors supply to active transcription sites (Mao et al., 2011). These findings suggest that either genomic alterations of the genome-integrated FLYWCH1 cDNA or post-transcriptional modifications of FLYWCH1 protein product might have possibly happened in these Puro^{R} cell lines. However, whether natural *in-vivo* mutations of FLYWCH1 gene may occur in human cancer cells, further studies should be carried out to support these notions. Hence in this study, we approached transient

transfection for FLYWCH1-GFP expression in CRC cell lines for FLYWCH1 gain-of-function study.

Furthermore, to effectively elucidate the loss-of-function properties of FLYWCH1, we took advantage of the iLenti™ RNAi expression system (Chapter 2, section 2.2.1.6). The double promoter piLenti-FLYWCH1^{shRNA} (Appendix 7) contains opposing modified RNA polymerase III promoters (H1 & U6) directly flanked the shRNA target sequence, where possessing a 5'LTR terminator sequence located upstream of the transcriptional start sites (Figure 3-2 A, Top panel). Usually, following transcription the resulting double stranded (ds)-shRNA product possesses similar structure as 'natural' double stranded shRNA thus bypassing the dicer-processing step (Liu et al., 2013). Inclusion of the two promoters enhances the shRNA template insert stability. The vector also retains a Puromycin resistant gene useful for generating stable cell lines as well as the inclusion of GFP to enable assessment of transfection efficiency by the fluorescent microscopy.

To further understand the biological role of FLYWCH1, stable FLYWCH1-knockdown CRC cell lines (FLYWCH1^{shRNA}) was generated by pGFP-C-shLenti vector following Puro-resistant gene selection driven by a SV40 promoter and a tGFP gene driven by a CMV-promoter. Firstly, 4 x 500 ng FLYWCH1-set shRNA lentivector containing the FLYWCH1 target sequence was amplified using the midi-prep protocol (Chapter 2, section 2.3.2). Briefly, TIG119, SW480 & HCT116 cells were transfected with the expression plasmids containing FLYWCH1 target sequences enabling the knockdown of FLYWCH1 expression. At 24-36 hours post-transfection, infected cells were maintained and

selected with Puromycin. The transfection efficiency of all the cells used was high (>70%) and monitored via fluorescence microscopy. However, the GFP expression was not uniform with some cells losing the GFP fluorescence intensity during selection. Therefore, single cell cloning via serial dilution was performed by choosing, maintaining and expanding the cells with the best GFP expression and cultured initially in 96 well plates. Following successful selection, cells of each well were gradually transferred and sub-cultured into one well of a 6-well plate and considered as P0 (passage zero) and finally transferred to T75 flasks during expansion and used for further characterization and validation. Furthermore, the expression of piLenti-shRNA-FLYWCH1-GFP was evaluated within a very limited passage number, (between P0 to P2).

To evaluate the stable expression of piLenti-shRNA-FLYWCH1-GFP in TIG119, SW480 & HCT116 cell, fluorescence microscopy was performed (Figure 3-2 A; bottom panel). Following single cell cloning selection and amplification, cells were initially observed using fluorescence microscopy. Although endogenous and exogenous FLYWCH1 expression presents a speckle-like nuclear pattern, the piLenti-shRNA-FLYWCH1-GFP protein appeared to be diffused both in the nucleus and cytoplasm and lost FLYWCH1 foci formation. The GFP expression has no effect in the knock-down efficiency of the plasmid.

Generation of stable SW480 GFP^{+VE}, HCT116 GFP^{+VE} and TIG119 GFP^{+VE} cells using pLVX-Puro-GFP plasmids were performed (Figure 3-2 B; bottom panel) in the same manner as earlier explained in the generation of cells stably expressing piLenti-shRNA-FLYWCH1-GFP. These cells were used as control cells for subsequent gain-of-function and loss-of-function experiments.

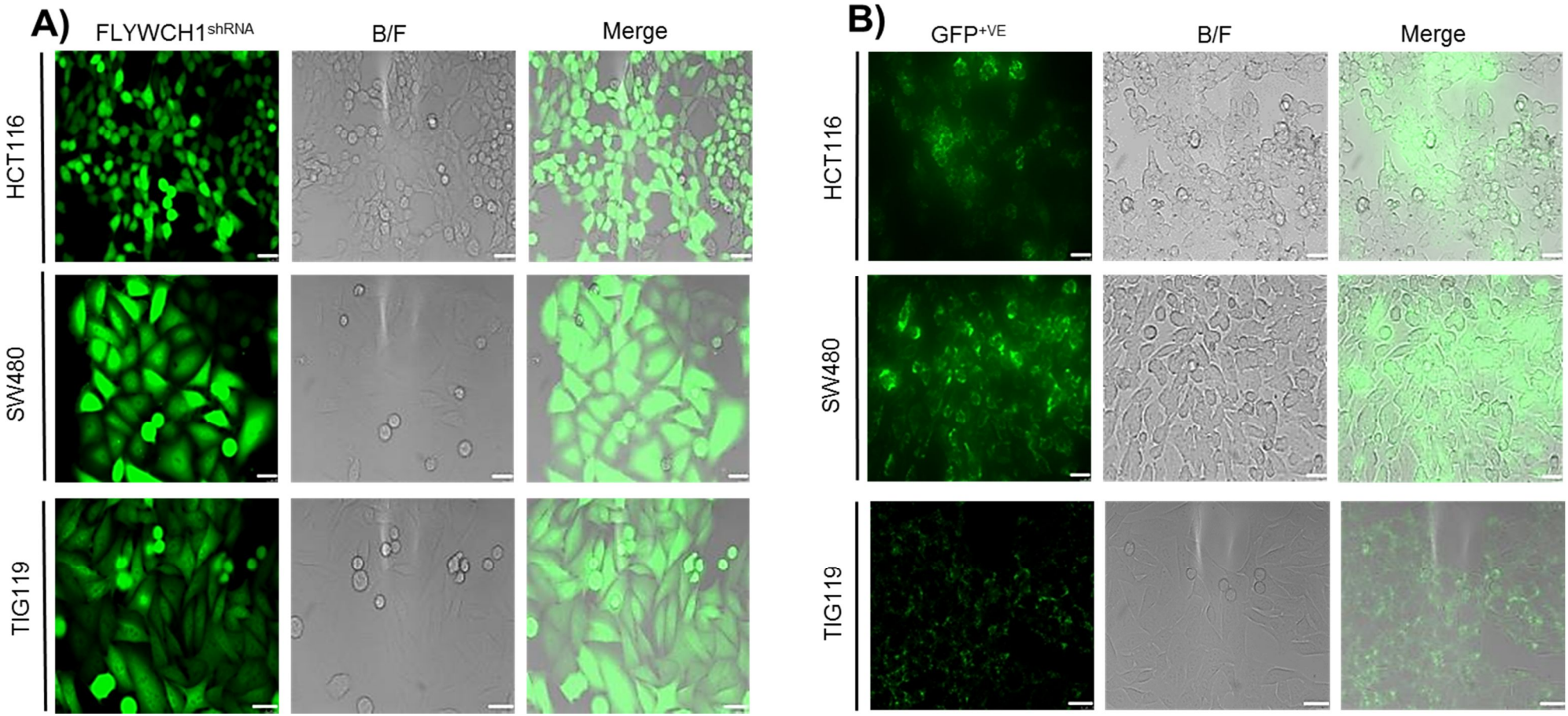
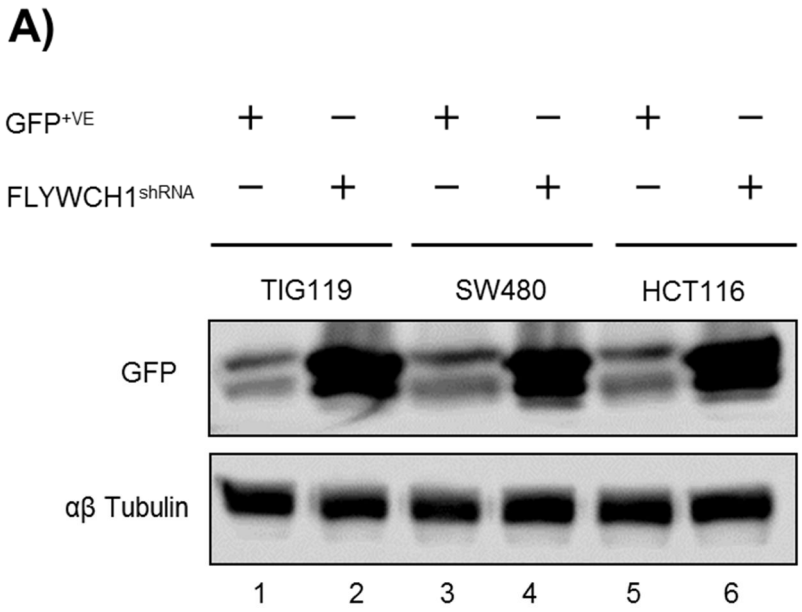

A)
FLYWCH1shRNA
B/F
Merge
HCT116
SW480
TIG119
B)
GFP+VE
B/F
Merge
HCT116
SW480
TIG119

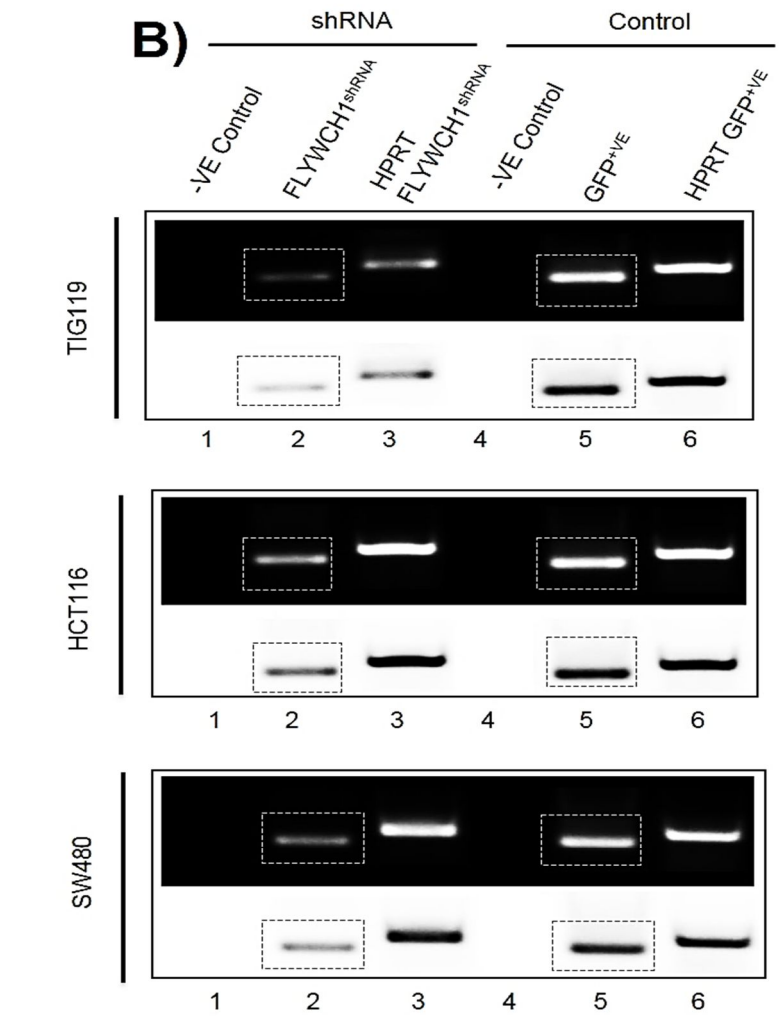
Figure 3-2: Expression and localization patterns of GFP in stable cell lines generated for FLYWCH1^{shRNA} and GFP expression. **A)** HCT116, SW480 and TIG119 cell lines were transiently transfected with piLenti-shRNA-FLYWCH1-GFP plasmid. The GFP expression (green) of these proteins were monitored under fluorescent microscope as indicated. The GFP of piLenti-shRNA-FLYWCH1-GFP plasmid is driven by a CMV promoter while the shRNA is driven by U6 and H1 promoter (Appendix 7). Magnification; 40x. Scale bar, 75 µm. **B)** HCT116, SW480 and TIG119 cell lines stably expressing pLVX-GFP plasmid (Appendix 5). Magnification; 40x. Scale bars, 75 µm. Data represents images taken following 3 weeks of Puromycin selection and amplification.

3.2.3 Validation of cells stably expressing piLenti-FLYWCH1^{shRNA}

Following the generation of FLYWCH1^{shRNA} cell lines, we sought to validate the different cells by examining the endogenous expression of *FLYWCH1* mRNA in GFP^{+VE} vs FLYWCH1^{shRNA} cells. This was accomplished via quantitative RT-PCR, standard RT-PCR and fluorescent immunostaining techniques. Unfortunately, western blot analysis could not be performed for validation due to the inability of the FLYWCH1 antibody to detect the endogenous protein on the blotting membrane. Specific primers (Forward: 5'-CTGGATGCAGCCCCTCAGT-3' and reverse: 5'-TTGGCGGCACTTCCAGTAC-3') were designed to quantify the gene expression/mRNA levels of FLYWCH1 utilizing standard RT-PCR and qRT-PCR techniques using cDNA derived from TIG119, SW480 and HCT116 cells under different conditions. Following the PCR annealing temperature from our previous work in the lab (Muhammad et al., submitted), the expression of *FLYWCH1* in GFP^{+VE} vs FLYWCH1^{shRNA} cells in TIG119, SW480 and HCT116 cells were performed by using 54^{o}C. Following detection of GFP protein

expression in all the stable cell lines (Figure 3-3 A), using standard RT-PCR, successful knock-down of *FLYWCH1* was observed indicated by the reduced expression of FLYWCH1 product (40%-80% compared with controls) in FLYWCH1^{shRNA} cells (Figure 3-3 B). Successful knock-down was also observed using qRT-PCR (Figure 3-3 C). Additionally, immunofluorescence analysis using anti-FLYWCH1 antibodies further confirmed the FLYWCH1 knockdown (Figure 3-4 A vs B) in FLYWCH1^{shRNA} cells compared to control GFP^{+VE} cells.




B)
shRNA
Control
-VE Control
FLYWCH1shRNA
HPRT FLYWCH1shRNA
-VE Control
GFP+VE
HPRT GFP+VE
TIG119
HCT116
SW480
1
2
3
4
5
6

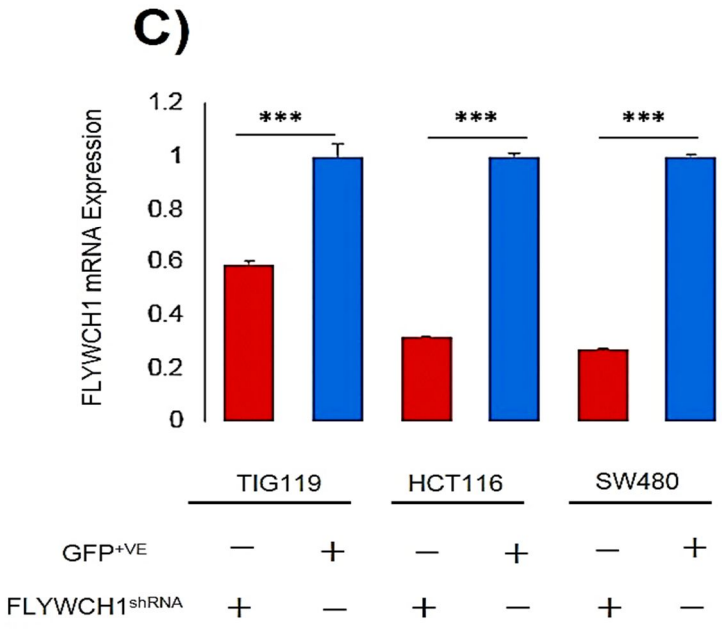
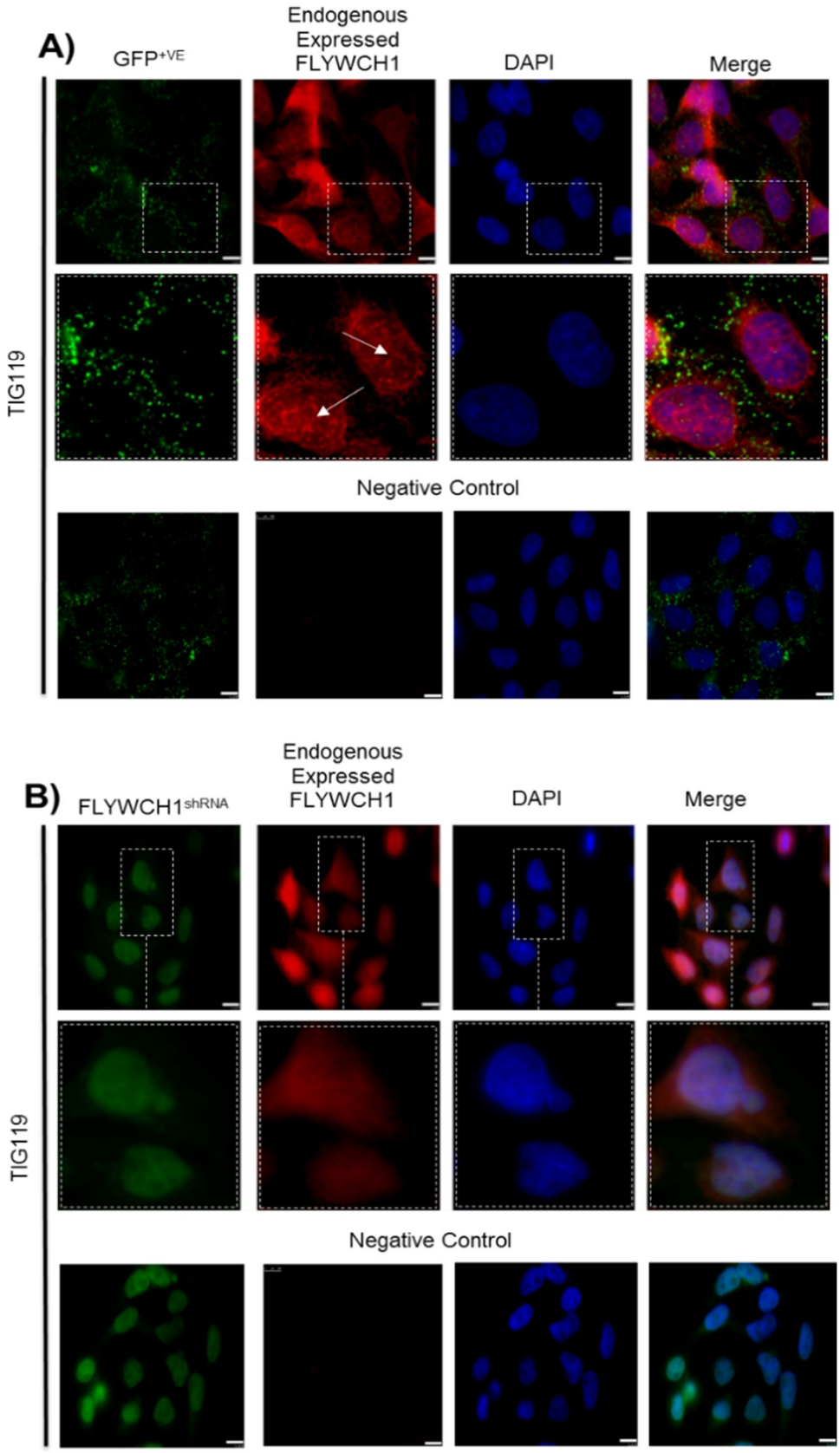

C)
FLYWCH1 mRNA Expression
1.2
1
0.8
0.6
0.4
0.2
0
***
***
***
TIG119
HCT116
SW480
GFP+VE
FLYWCH1shRNA

Figure 3-3: Downregulation of *FLYWCH1* expression in stable FLYWCH1^{shRNA}. A) Evaluation of piLenti-shRNA-FLYWCH1-GFP protein expression. Detection of GFP expression in FLYWCH1^{shRNA} stable cells (TIG119, SW480 and HCT116) with anti-GFP, while anti-αβ-tubulin was used a loading control. Lysate derived from GFP^{+VE} cells were used as controls. **B)** Standard RT-PCR validation of knock-down expression of FLYWCH1 in TIG119 (Top panel), HCT116 (Middle panel) & SW480 (Bottom panel) cells. GFP^{+VE} cells were used as controls. For negative controls, PCR were performed with RNA samples amplified in the absence of reverse transcriptase. This indicated a lack of genomic DNA. Boxes showing the reduction of FLYWCH1 expression. **C)** Subsequently, the mRNA level in the different cell lines was quantified by qRT-PCR. Data are mean ± SD (***, $P < 0.001$). Experiment was repeated at least on two independent occasions.


A)
GFP+VE
Endogenous Expressed FLYWCH1
DAPI
Merge
TIG119
Negative Control
B)
FLYWCH1shRNA
Endogenous Expressed FLYWCH1
DAPI
Merge
TIG119
Negative Control

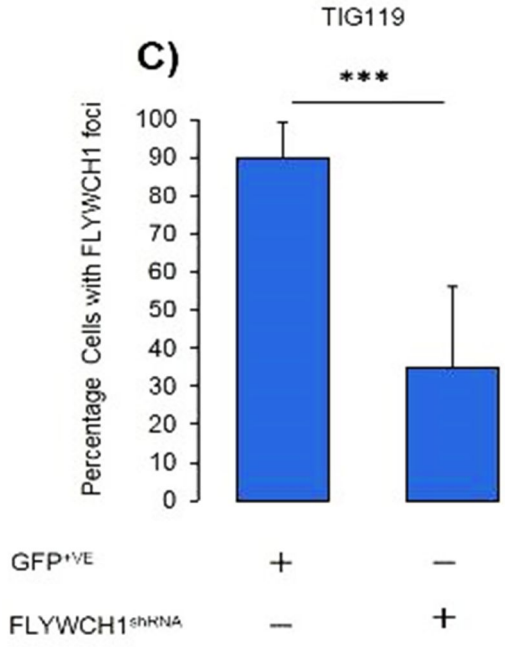
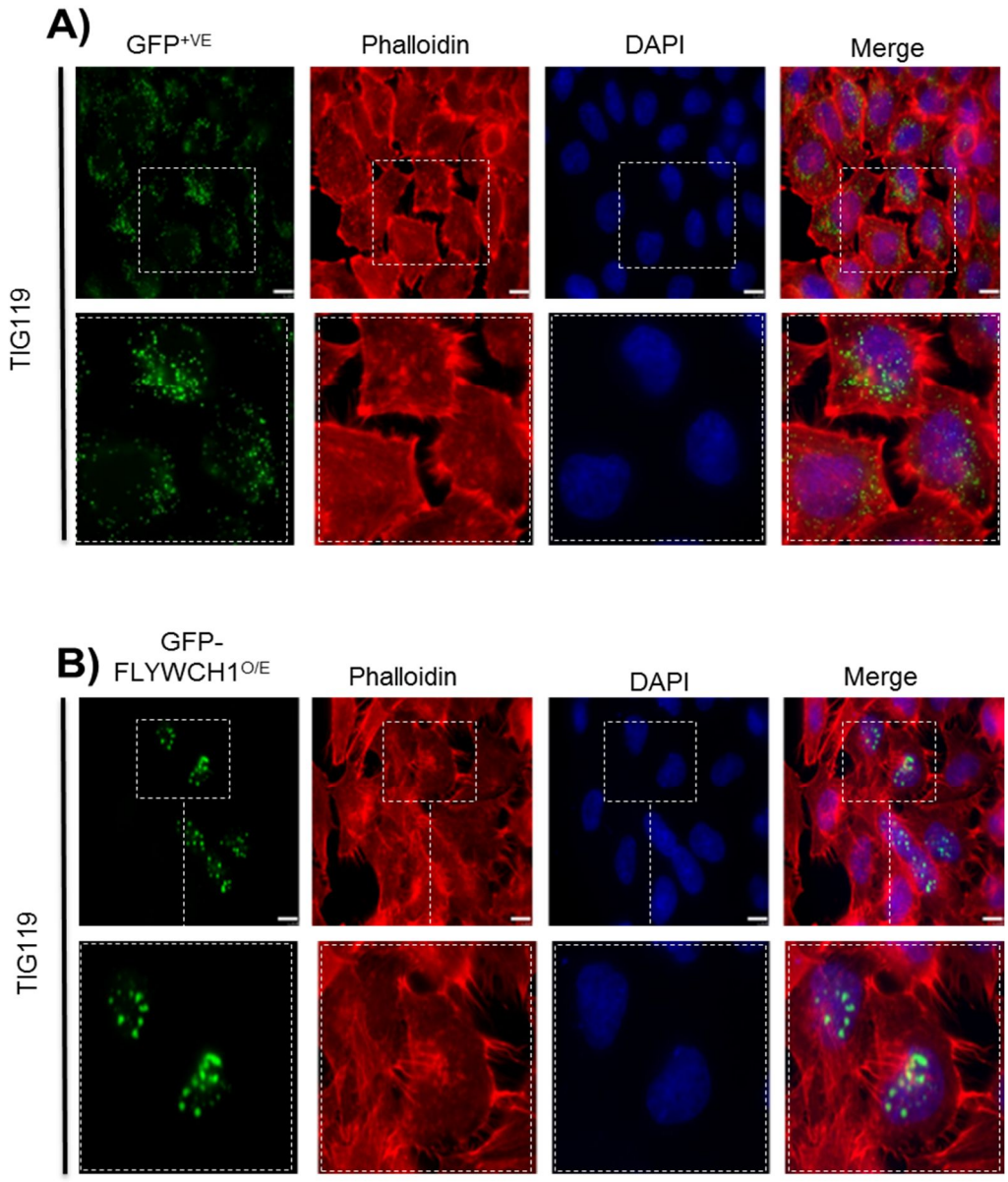


Figure 3-4: Validation of FLYWCH1 in FLYWCH1^{shRNA} TIG119 cells. Immunofluorescence staining using anti-FLYWCH1 antibody (red) showing, **A)** the normal expression pattern of FLYWCH1 in control GFP^{+VE} cells. Boxed cells are magnified individual cells. Arrows show detection of FLYWCH1 foci. **B)** Knocked-down expression pattern of FLYWCH1 in FLYWCH1^{shRNA} cells. Boxed cells are magnified individual cells. The FLYWCH1 foci is diffused indicating successful FLYWCH1 knockdown at protein level. Negative controls were used in the absence of primary antibody. Magnification; 100x. Scale bar, 25 µm. **C)** Quantitative analysis of foci presence in individual GFP^{+VE} vs FLYWCH1^{shRNA} cells. Data are represented as mean of 30 individual cells. Data are mean ± SD (***, $P < 0.001$).

3.2.4 Ectopic FLYWCH1 expression mediates change in morphology of CRC cells as well as formation of actin stress fibres in TIG119 cells.

To investigate whether differential expression of FLYWCH1 alters cell morphology via actin re-assembly, we performed an extensive fluorescent microscopic analysis using GFP-FLYWCH1$^{O/E}$ vs FLYWCH1^{shRNA} cells.

Herein, SW480 and TIG119 cells were initially utilized due to the display of mesenchymal phenotype, which enables better observation, and quantification of cell morphology changes. Hence, GFP^{+VE} (Control), GFP-$FLYWCH1^{O/E}$ and $FLYWCH1^{shRNA}$ cells were cultured on cover slips and stained afterwards with Phalloidin [a high affinity F-actin probe conjugated to the red-orange fluorescent dye, tetramethylrhodamin (TRITC)] and observed via fluorescence microscopy as described in chapter 2, section 2.10. The microscopy analysis revealed that knockdown of FLYWCH1 protein expression mediated morphological changes via possible F-actin organization (visualized by Phalloidin stain). In fibroblast TIG119 cells, $FLYWCH1^{shRNA}$ (Figure 3-5 C)**,** exhibited high alteration of actin stress fibre-like structures, basically lost branched network relative to GFP^{+VE} (Figure 3-5 A)**,** and GFP-$FLYWCH1^{O/E}$ cells (Figure 3-5 B). Taken together, these results suggest that FLYWCH1 may facilitate cytoskeleton re-arrangement via ventral stress fibre formation.


A)
GFP+VE
Phalloidin
DAPI
Merge
TIG119
B)
GFP-
FLYWCH1O/E
Phalloidin
DAPI
Merge
TIG119

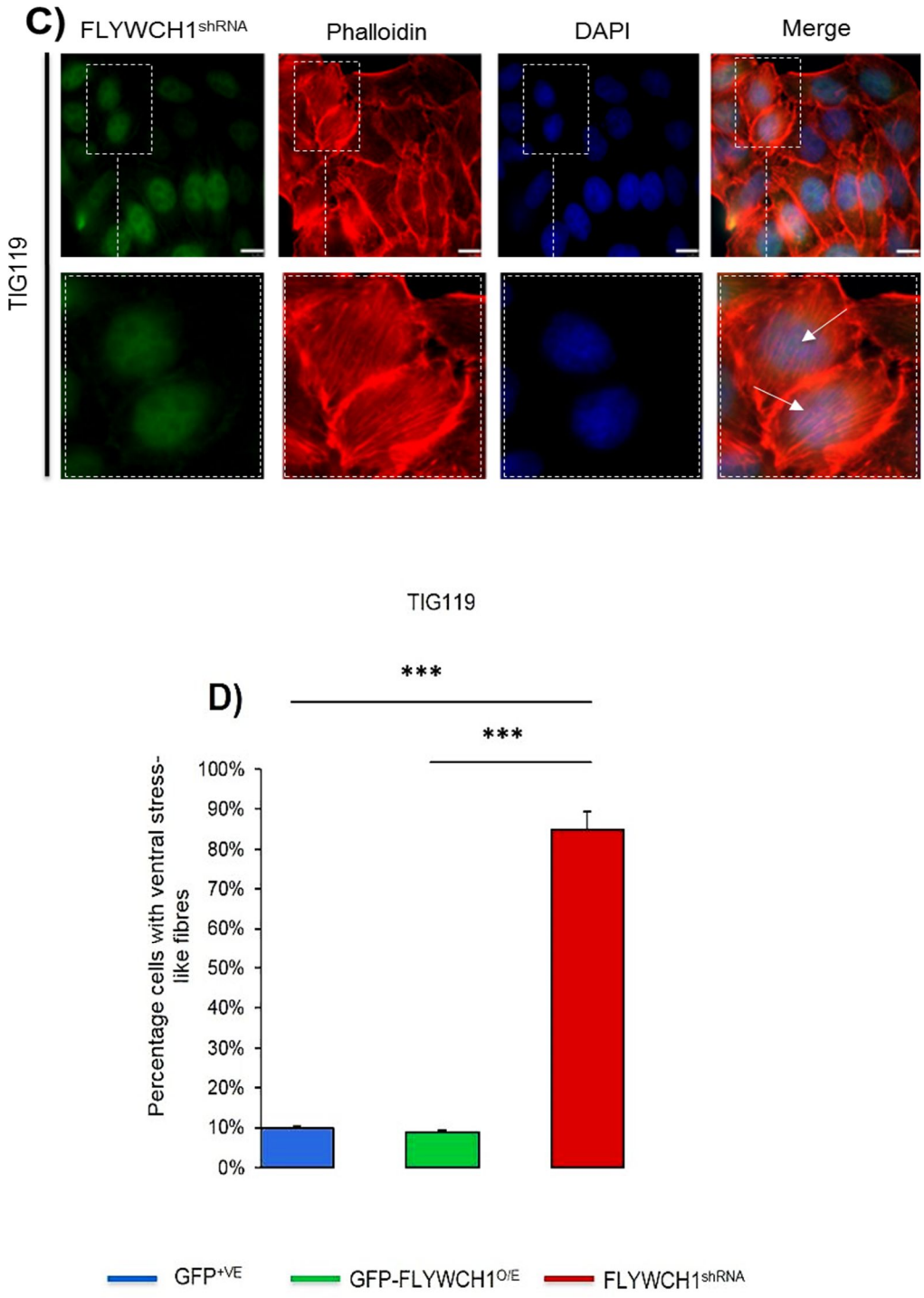


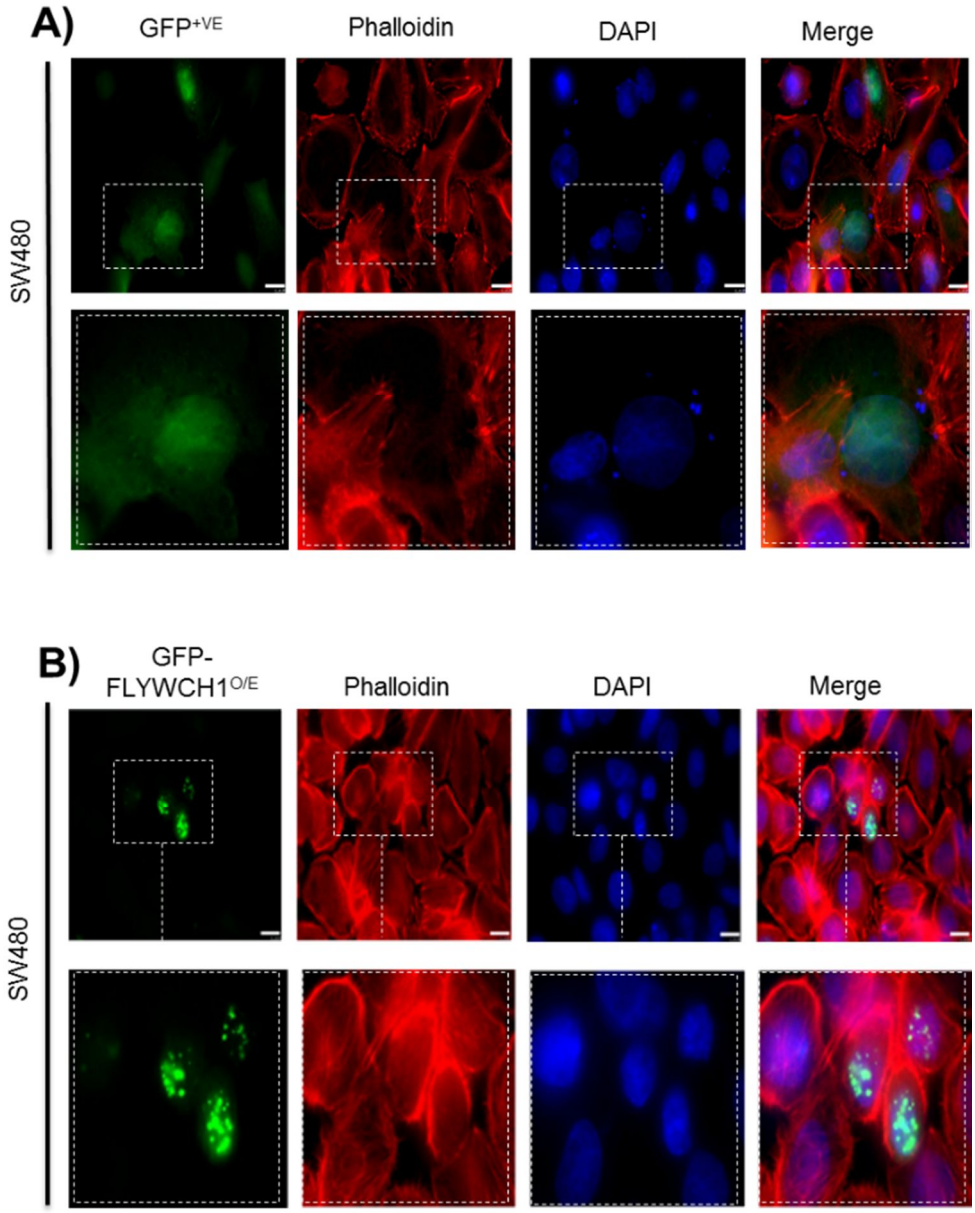
Figure 3-5: Knockdown of FLYWCH1 triggers formation of ventral stress fibres. TIG119 cells under different conditions, **A)** GFP^{+VE} (control) **B)** GFP-FLYWCH1$^{O/E}$ and **C)** FLYWCH1^{shRNA} were cultured and stained with Phalloidin (red) and DAPI (blue) and observed under the fluorescence microscope. Dotted lines represent enlarged individual cells in the bottom panels. Arrows indicate

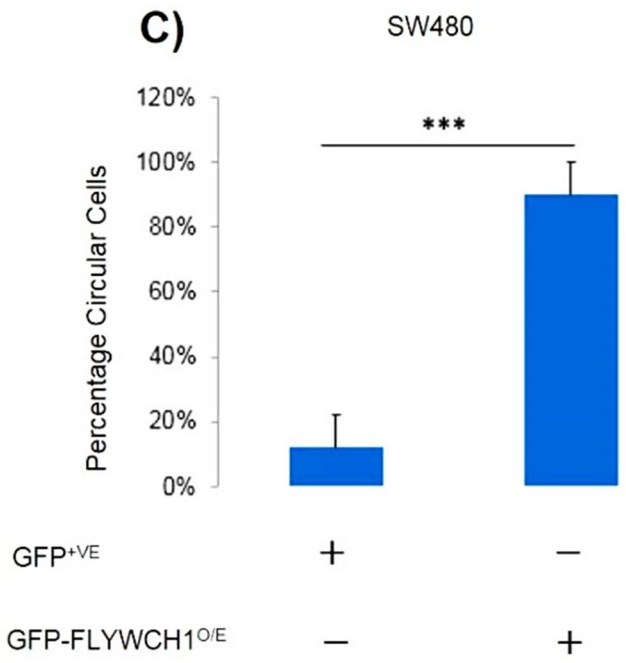
the presence of stress fibre-like structures. Magnification; 100x**.** Scale bars, 25 µm. Arrows indicates the presence of stress fibres. **D)** Quantitative analysis of cells exhibiting ventral stress fibre-like structures. Data are represented as mean of 40 individual cells under different conditions. Data are mean ± SD (***, P < 0.001). Experiment was repeated at least on two independent occasions.

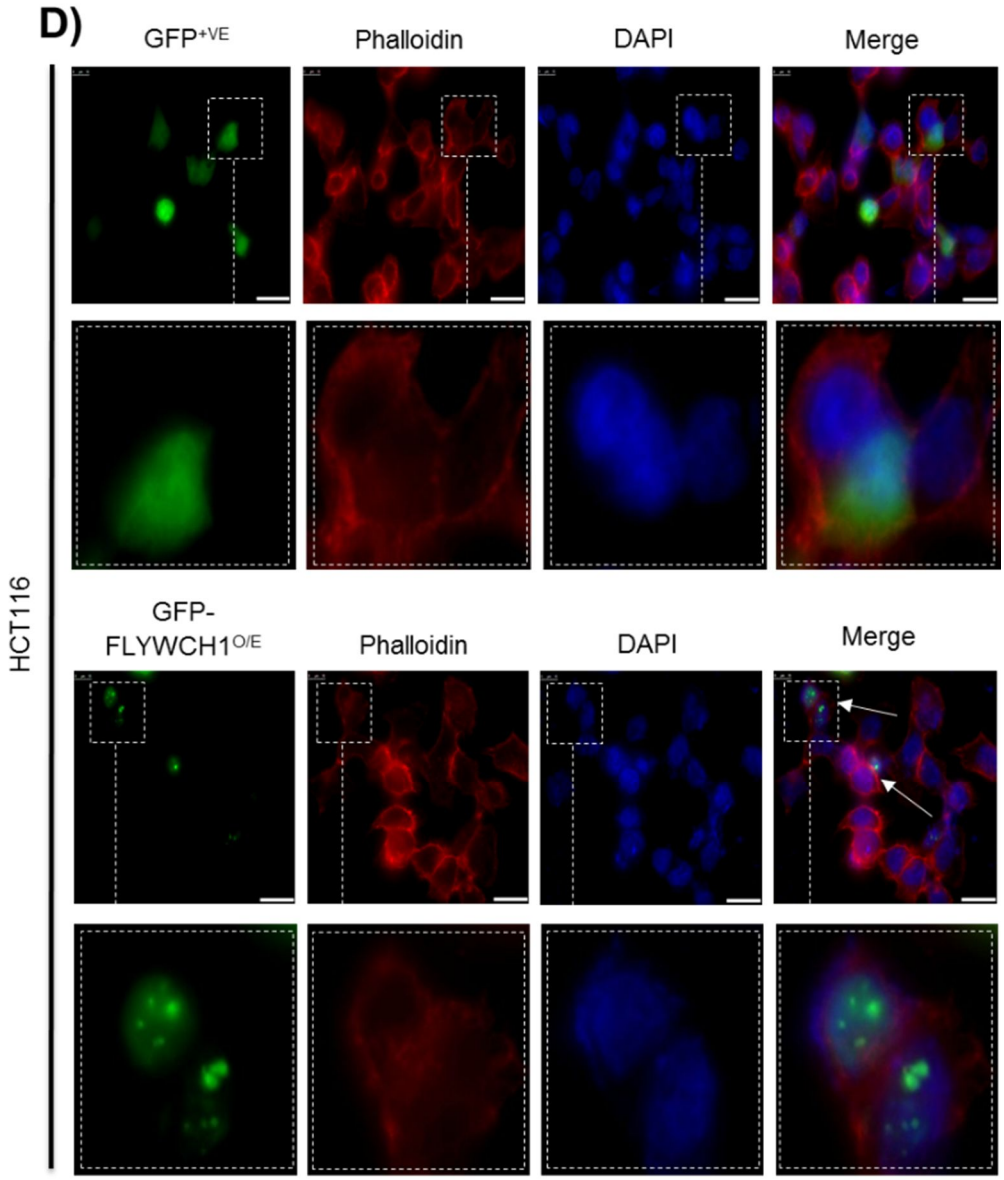
Next, to investigate whether CRCs cells would exhibit morphological changes mediated possibly by actin re-organization observed in TIG119 cells, SW480 and HCT116 cell also under different conditions were cultured, fixed and stained with Phalloidin.

Firstly, SW480 GFP^{+VE} (control) vs SW480 $FLYWCH1^{O/E}$ cells were examined. The result showed GFP-$FLYWCH1^{O/E}$ cells (Figure 3-6 B & Figure 3-6 C) were characterized with a less elongated, more circular epithelial-like phenotype where as GFP^{+VE} (Figure 3-6 A & Figure 3-6 C) retained a more mesenchymal-like phenotype. Furthermore, the Phalloidin stain revealed that GFP^{+VE} cells showed prominent presence of dorsal stress fibres concentrated at the periphery of the cells (Figure 3-6 A), which are required for cellular migration (Huang et al., 2002). Therefore, the data suggest that an overexpression of FLYWCH1 may inhibit cancer cell migration in SW480 cells.

Additionally, HCT116 GFP-$FLYWCH1^{O/E}$ were utilized to determine whether FLYWCH1-mediated morphological changes would occur, however, there were no significant changes relative to control GFP^{+VE} cells (Figure 3-6 D & Figure 3-6 E). These observations in both fibroblast and SW480 cells compared with HCT116 cells all indicate that FLYWCH1 may modulate cell morphology by altering actin cytoskeleton re-organization in a cell-specific manner.


A)
GFP+VE
Phalloidin
DAPI
Merge
SW480
B)
GFP-
FLYWCH1O/E
Phalloidin
DAPI
Merge
SW480


C)
SW480
120%
100%
80%
60%
40%
20%
0%
Percentage Circular Cells
***
GFP+VE
+
−
GFP-FLYWCH1O/E
−
+


D)
GFP+VE
Phalloidin
DAPI
Merge
HCT116
GFP-
FLYWCH1O/E
Phalloidin
DAPI
Merge

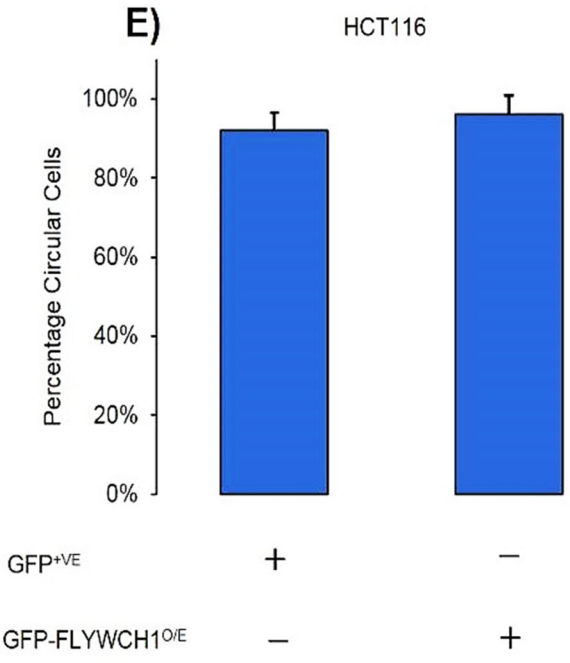
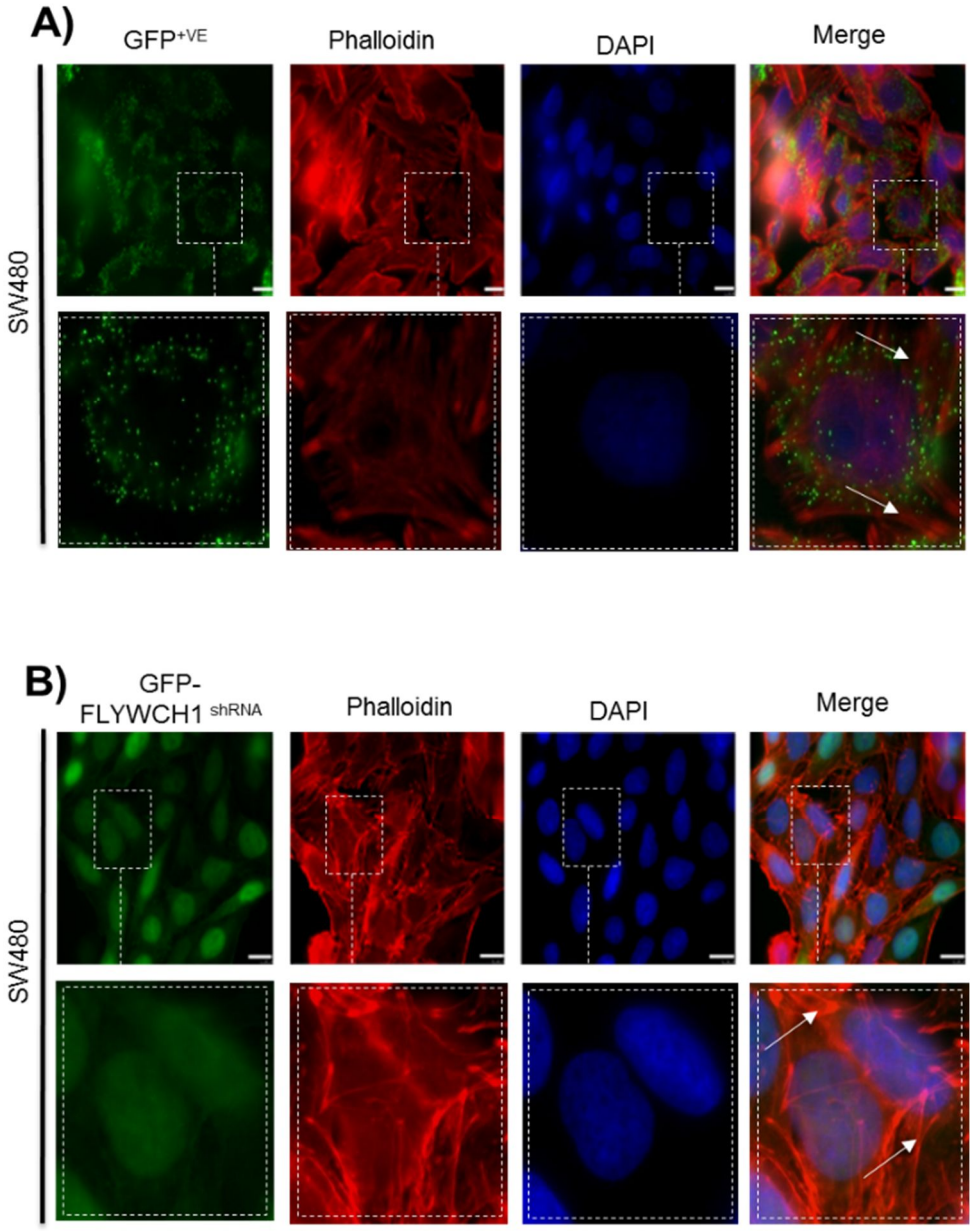


Figure 3-6: FLYWCH1 triggers morphological changes in CRC SW480 cells, but not in HCT116 cells. SW480 cells under different conditions were utilized to examine the biological activity of FLYWCH1 with respect to morphology changes. **A)** SW480 GFP^{+VE} and **B)** SW480 GFP-FLYWCH1$^{O/E}$ cells were fixed and stained with Phalloidin (Red) and DAPI (blue). Dotted lines represent enlarged individual cells in the bottom panels. **C)** Quantitative analysis of the morphological changes in SW480 GFP^{+VE} vs SW480 GFP-FLYWCH1$^{O/E}$ ectopically expressing cells. Data are represented as mean of 30 individual cells under different conditions. Data are mean ± SD (***, P < 0.001). Experiment was repeated at least on two independent occasions. **D)** HCT116 GFP^{+VE} cells (top panels) and GFP-FLYWCH1$^{O/E}$ cells (bottom panels) were also subjected to Phalloidin staining with no noticeable change in cytoskeletal re-arrangement or morphology observed. Magnification; 100x Scale bars, 10µm. Arrows showing cells ectopically expressing FLYWCH1. **E)** Quantitative analysis of the morphological changes in HCT116 GFP^{+VE} vs HCT116 GFP-FLYWCH1$^{O/E}$ ectopically expressing cells. Data are represented as mean of 30 individual cells under different conditions. Data are mean ± SD. Experiment was repeated at least on two independent occasions.

We have then examined, SW480 GFP^{+VE} (control) vs SW480 FLYWCH1^{shRNA} cells. The results revealed SW480 FLYWCH1^{shRNA} cells retained an irregular phenotype as well as dense stress fibres (similar to that observed in fibroblast FLYWCH1^{shRNA} cells) at the periphery of the cells relative to the control GFP^{+VE} (Figure 3-7 B).



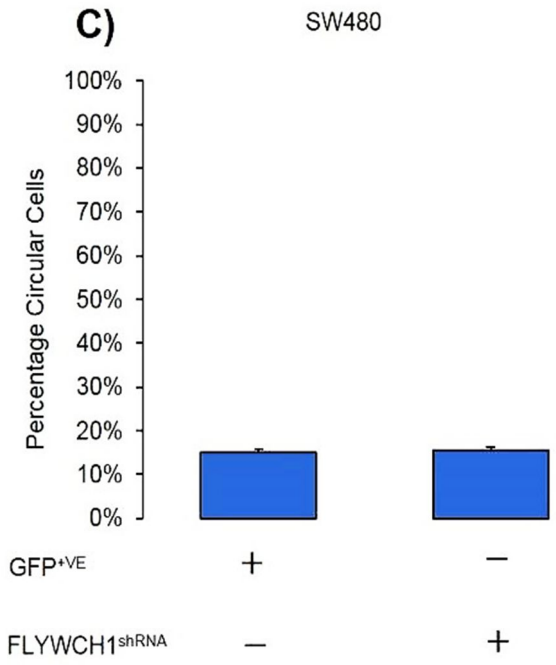


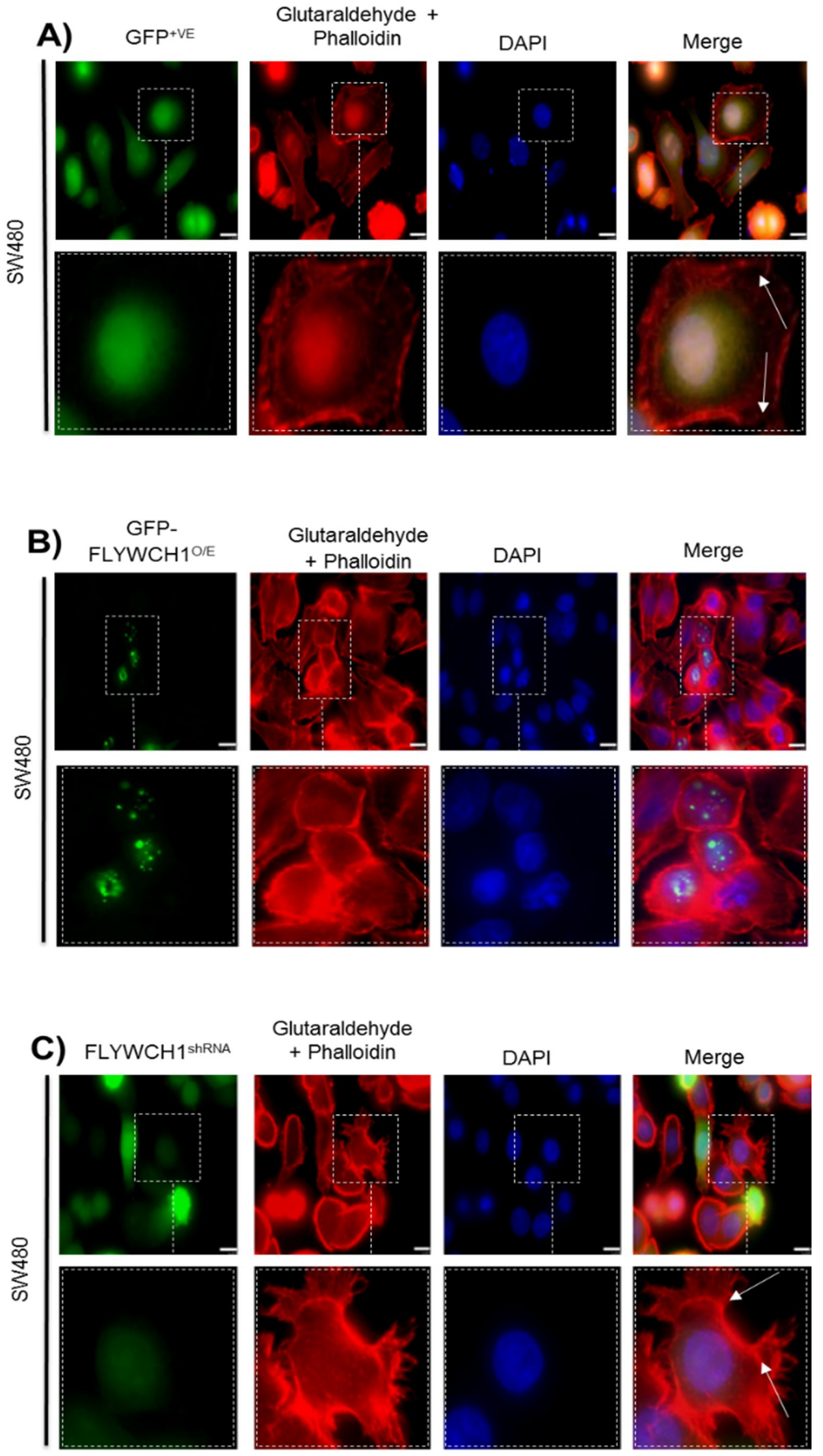
Figure 3-7: FLYWCH1 knockdown condition maintains an irregular, mesenchymal-like phenotype in SW480 cells. SW480 cells under different conditions were utilized to examine the biological activity of FLYWCH1 with respect to morphology changes. **A)** Fixed SW480 GFP^{+VE} and, **B)** SW480 FLYWCH1^{shRNA} cells were subject to Phalloidin stain (red) and DAPI (blue). Dotted lines represents enlarged individual cells in the bottom panels. Arrows showing dense stress fibres on the cell periphery**.** Magnification; 100x**.** Scale bars, 10µm. **C)** Quantitative analysis of the morphological changes in SW480 GFP^{+VE} vs FLYWCH1^{siRNA} cells. Most cells retained their irregular morphology. Data are represented as mean of 30 individual cells under different conditions. Data are mean ± SD (***, P < 0.001). Experiment was repeated at least on two independent occasions

3.2.4.1 Knock-down of FLYWCH1 expression triggers filopodia formation in CRC SW480 cells

Because of the changes observed in terms of characteristic stress fibre formation particularly in SW480 FLYWCH1^{shRNA} cells, further investigations were focused on filopodia formation. Filopodia are thin, actin-rich plasma-membrane

protrusions vital for cell migration, in addition to other processes such as wound healing, extracellular matrix attachment and guidance towards chemo-attractants (Jacquemet et al., 2015). Hence, investigations on whether filopodia formation correlates with FLYWCH1-mediated stress fibre formation was required.

Therefore, to test the possible relationship between FLYWCH1 and filopodia formation status in CRCs, SW480 GFP^{+VE}, GFP-$FLYWCH1^{O/E}$ cells and $FLYWCH1^{shRNA}$ cells were all simply fixed with 4% paraformaldehyde and 1% glutaraldehyde. Results showed that individual GFP-$FLYWCH1^{O/E}$ cells (Figure 3-8 B) not only exhibited an epithelial-like phenotype but also were devoid of filopodia relative to control GFP^{+VE} which exhibited lamellipodial-like protrusions (Figure 3-8 A). On the other hand, $FLYWCH1^{shRNA}$ cells showed a significant presence of filopodia protrusions (Figure 3-8 C), thus signifying a key metastatic characteristic. Taken together, these observations indicate that FLYWCH1 may participate in regulation of filopodia formation via cytoskeleton re-organization necessary for possible metastatic and invasive characteristics.


A)
GFP+VE
Glutaraldehyde + Phalloidin
DAPI
Merge
SW480
B)
GFP-FLYWCH1O/E
Glutaraldehyde + Phalloidin
DAPI
Merge
SW480
C)
FLYWCH1shRNA
Glutaraldehyde + Phalloidin
DAPI
Merge
SW480

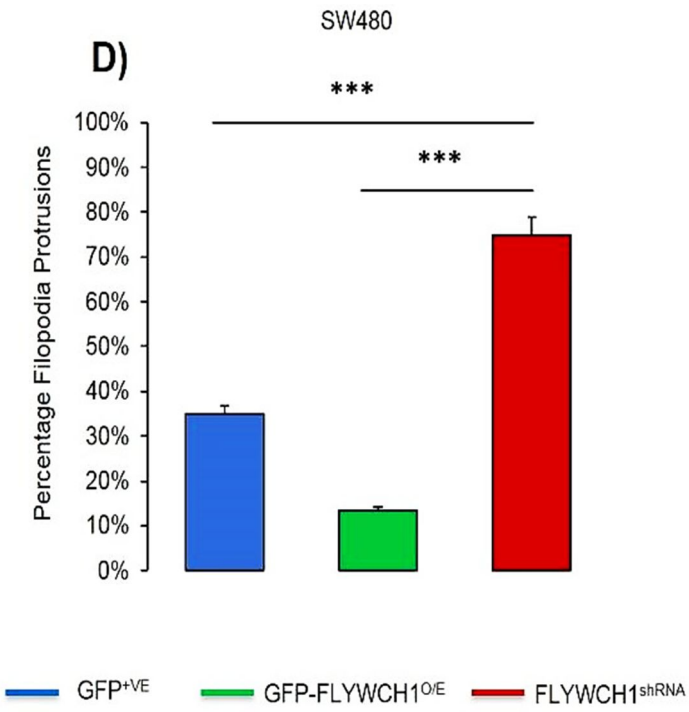


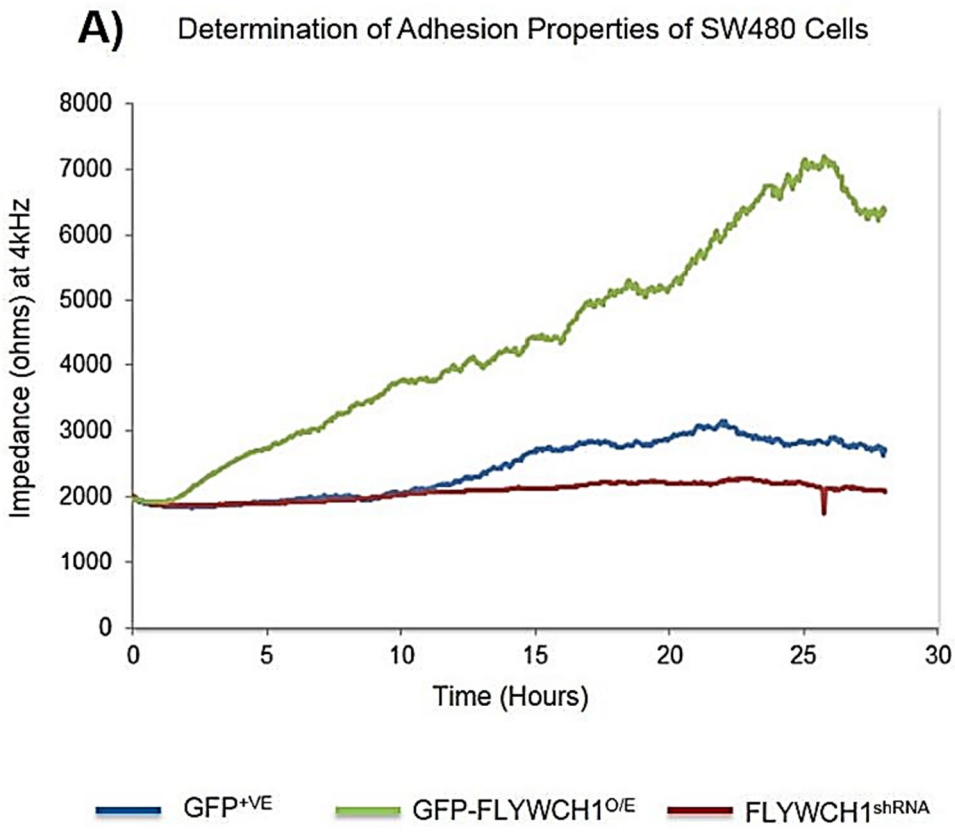
Figure 3-8: Knockdown of FLYWCH1 expression promotes filopodia formation. SW480 cells under different conditions; **A)** GFP^{+VE} (control) vs **B)** $GFP\text{-}FLYWCH1^{O/E}$ vs **C)** $FLYWCH1^{shRNA}$, were fixed with paraformaldehyde and glutaraldehyde before subsequently stained with Phalloidin (red) to examine filopodia presence. Dotted lines represents enlarged individual cells in the bottom panels. Magnification; 100x. Scale Bar, 10 µm. Arrows shows the presence of lamellapodia and/or filopodia-like structures. **D)** Quantitative analysis of cells exhibiting filopodia protrusions. Data are represented as mean of 30 individual cells under different conditions. Data are mean ± SD (***, $P < 0.001$). Experiment was repeated at least on two independent occasions.

3.2.5 FLYWCH1 influences the cell spreading & attachment properties

To investigate via experimental means the influence of FLYWCH1-associated cell morphology on the spreading and attachment properties of CRCs to artificial surfaces, quantitative analysis was performed. The Electric Cell-Substrate

Impedance Sensing (ECIS) method (Chapter 2, section 2.9.4) was used to accomplish this assessment which detects the attachment and spreading of cells upon artificial surfaces in real time with special emphasis on the kinetic aspects of this phenomenon (Wegener et al., 2000).

SW480 (GFP^{+VE}, GFP-$FLYWCH1^{O/E}$ and $FLYWCH1^{shRNA}$) cells were cultured on the ECIS plates with the impedance and capacitance monitored over a period of 24 hours in order for the attachment and cell spreading properties to be quantified. The analysis showed that the impedance measurement of SW480 GFP-$FLYWCH1^{O/E}$ cells was significantly higher than GFP^{+VE} cells due to restriction of current flow as the cells attach to the surface, while $FLYWCH1^{shRNA}$ cells possessed the lowest impedance reading (Figure 3-9 A). The alteration of impedance experienced in GFP-$FLYWCH1^{O/E}$ and $FLYWCH1^{shRNA}$ cells suggests that FLYWCH1 may improve the adhesiveness of the cells. Additionally, SW480 GFP-$FLYWCH1^{O/E}$ cells exhibited the highest cell spreading capability as indicated by the R^2 value while $FLYWCH1^{shRNA}$ cells showed the lowest cell spreading capacity (Figure 3-9 B). Also, the results observed in SW480 cells are in accordance with the previous Phalloidin staining of glutaraldehyde-fixed cells (Figure 3-8) showing the presence of extensive filopodia and presence of stress fibres in $FLYWCH1^{shRNA}$ cells thereby FLYWCH1 knockdown may facilitate cancer cell migration. Taken together, these data suggests FLYWCH1 enhances cell adhesion via actin re-modelling.


A)
Determination of Adhesion Properties of SW480 Cells
Impedance (ohms) at 4kHz
8000
7000
6000
5000
4000
3000
2000
1000
0
0
5
10
15
20
25
30
Time (Hours)
GFP+VE
GFP-FLYWCH1O/E
FLYWCH1shRNA

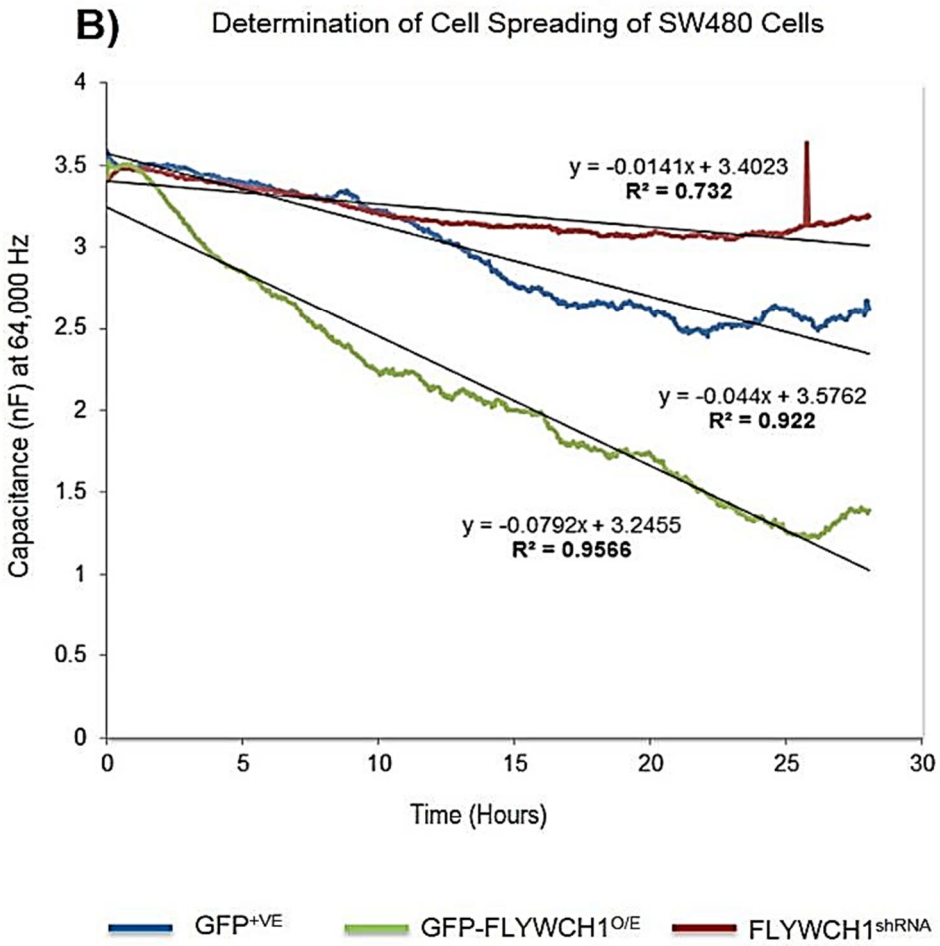


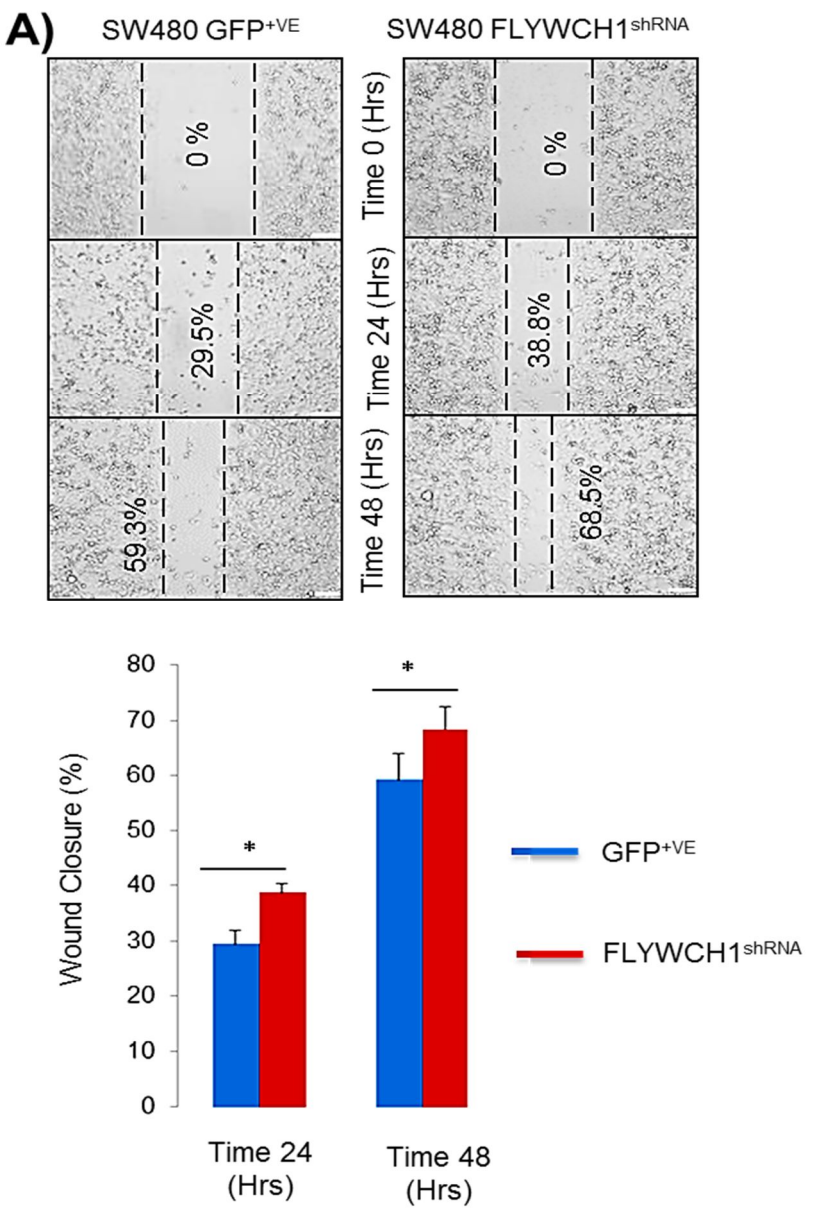
Figure 3-9: FLYWCH1 influences cell attachment and spreading. The impedance reflecting **A)** cell adhesion, and capacitance reflecting **B)** cell spreading, were measured for SW480 cells expressing GFP (control, blue), GFP-FLYWCH1 (green) and FLYWCH1^{shRNA} (red) using ECIS, over 30 hours. (Data shows mean of duplicate wells of representative ECIS plates). The majority of GFP-FLYWCH1$^{O/E}$ cells were attached in 2-3 hours and cell spreading was readily detected by an impedance increase, compared with GFP^{+VE} (control) and FLYWCH1^{shRNA} cells.

3.2.6 Knock-down of FLYWCH1 increases wound healing capacity

A major question in cancer biology has been whether a link exists between cell metastasis and cell cycle control. There exists a notion that cell metastasis is strictly regulated by cell cycle as studies have demonstrated a correlation between metastasis and cell cycle progression (Lawson et al., 2015), however the mechanisms that drives this phenomenon still remains largely unclear (Boehm and Nabel, 2001; Ridenour et al., 2014). Therefore, as part of the loss-of-function studies of FLYWCH1, we first sought to examine the effect of knockdown of FLYWCH1 on the motility of cancer cells via the *in-vitro* wound healing assay before analysing the changes in cell cycle profiles.

Firstly, HCT116 and SW480 GFP^{+VE} and $FLYWCH1^{shRNA}$ cells were cultured and incubated for 48 hours in serum free RPMI medium for cells to be synchronized at G0 phase before scratch assay was performed as outlined in (section 2.9.1).

The results revealed that there was a significant increase in wound closure in SW480 $FLYWCH1^{shRNA}$ cells (38.8% & 68.5%) compared to control SW480 GFP^{+VE} cells (29.5% & 59.3%) after 24 and 48 hours respectively (Figure 3-10 A). There was also a significant increase of wound closure observed in HCT116 $FLYWCH1^{shRNA}$ cells (57.5% & 89.9) compared to control HCT116 GFP^{+VE} cells (24% & 64.8%) after 24 and 48 hours respectively (Figure 3-10 B). Taken together, these data indicate possible spreading defects and increased cell-cell attachment caused by FLYWCH1.


A)
SW480 GFP+VE
SW480 FLYWCH1shRNA
Time 0 (Hrs)
Time 24 (Hrs)
Time 48 (Hrs)
0 %
0 %
29.5%
38.8%
59.3%
68.5%
Wound Closure (%)
80
70
60
50
40
30
20
10
0
*
*
Time 24 (Hrs)
Time 48 (Hrs)
GFP+VE
FLYWCH1shRNA

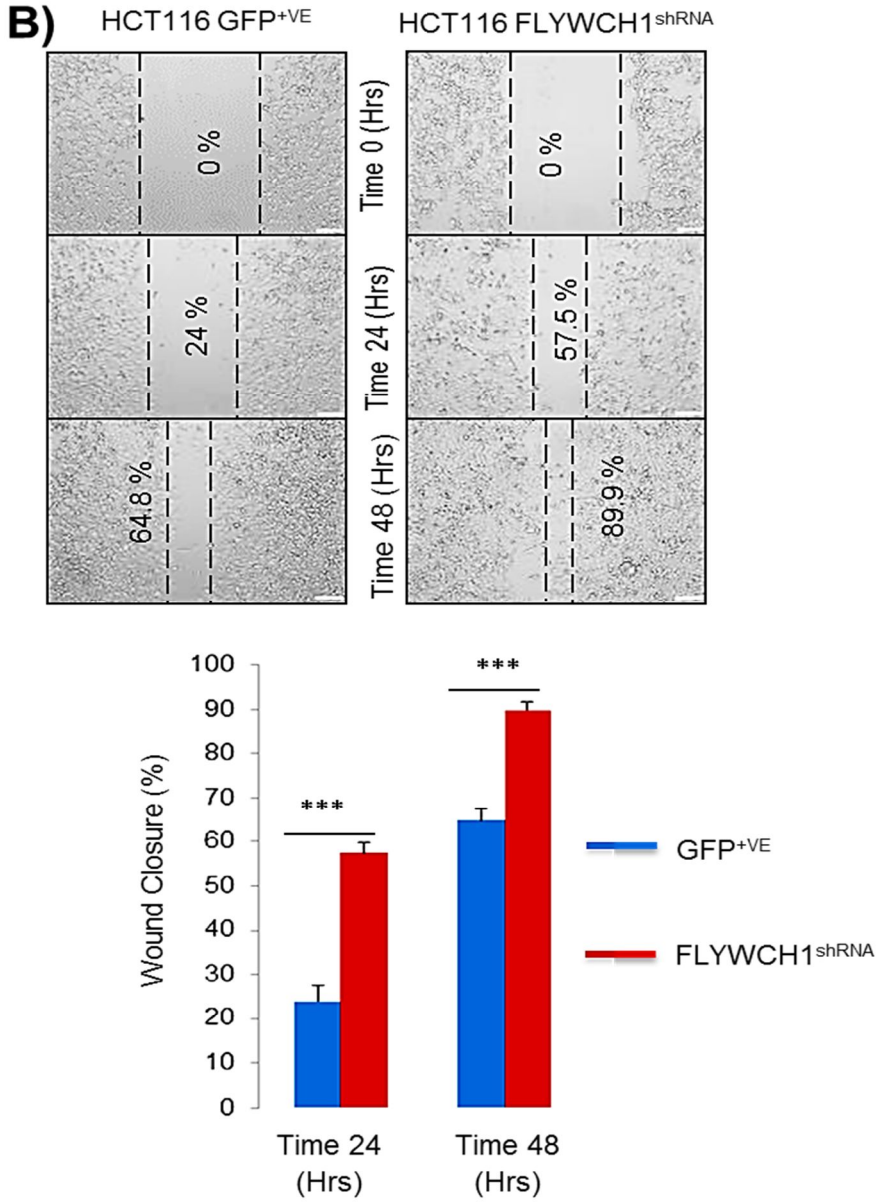

B)
HCT116 GFP+VE
HCT116 FLYWCH1shRNA
Time 0 (Hrs)
Time 24 (Hrs)
Time 48 (Hrs)
0 %
0 %
24 %
57.5 %
64.8 %
89.9 %
Wound Closure (%)
100
90
80
70
60
50
40
30
20
10
0
***
***
Time 24 (Hrs)
Time 48 (Hrs)
GFP+VE
FLYWCH1shRNA

Figure 3-10: FLYWCH1 reduces wound-closure capacity of CRC cells. CRC GFP^{+VE} and FLYWCH1^{shRNA} cells were subjected to wound/scratch assay. Representative images of wounds at time 0 – time 48 hours in, **A)** SW480 & **B)** HCT116 cells are shown. Charts showing the percentage wound closure in SW480 and HCT116 cells are shown (Bottom panel). Data are mean ± SD (*, $P < 0.05$; ***, $P < 0.001$). Experiment run in triplicate and repeated at least on two different occasions. Scale bars, 25 µm.

3.2.7 FLYWCH1 has varying cell cycle effect in CRC cell lines

To determine whether the cytoskeletal re-arrangement as well as morphological changes from mesenchymal to epithelial phenotype in CRCs exogenously expressing GFP-FLYWCH1 was facilitated via changes in cell cycle processes and related to defects in cell proliferation, cell cycle analysis of normal fibroblast and CRC cell lines was performed. GFP^{+VE} and FLYWCH1^{shRNA} cells were cultured fixed and subjected to cell cycle analysis using Propidium iodide (PI) staining as previously described in (Chapter 2, section 2.9.3).

Our analyses revealed no significant changes were observed in SW480 GFP^{+VE} vs FLYWCH1^{shRNA} cells in different cell cycle phases (Figure 3-11 A).

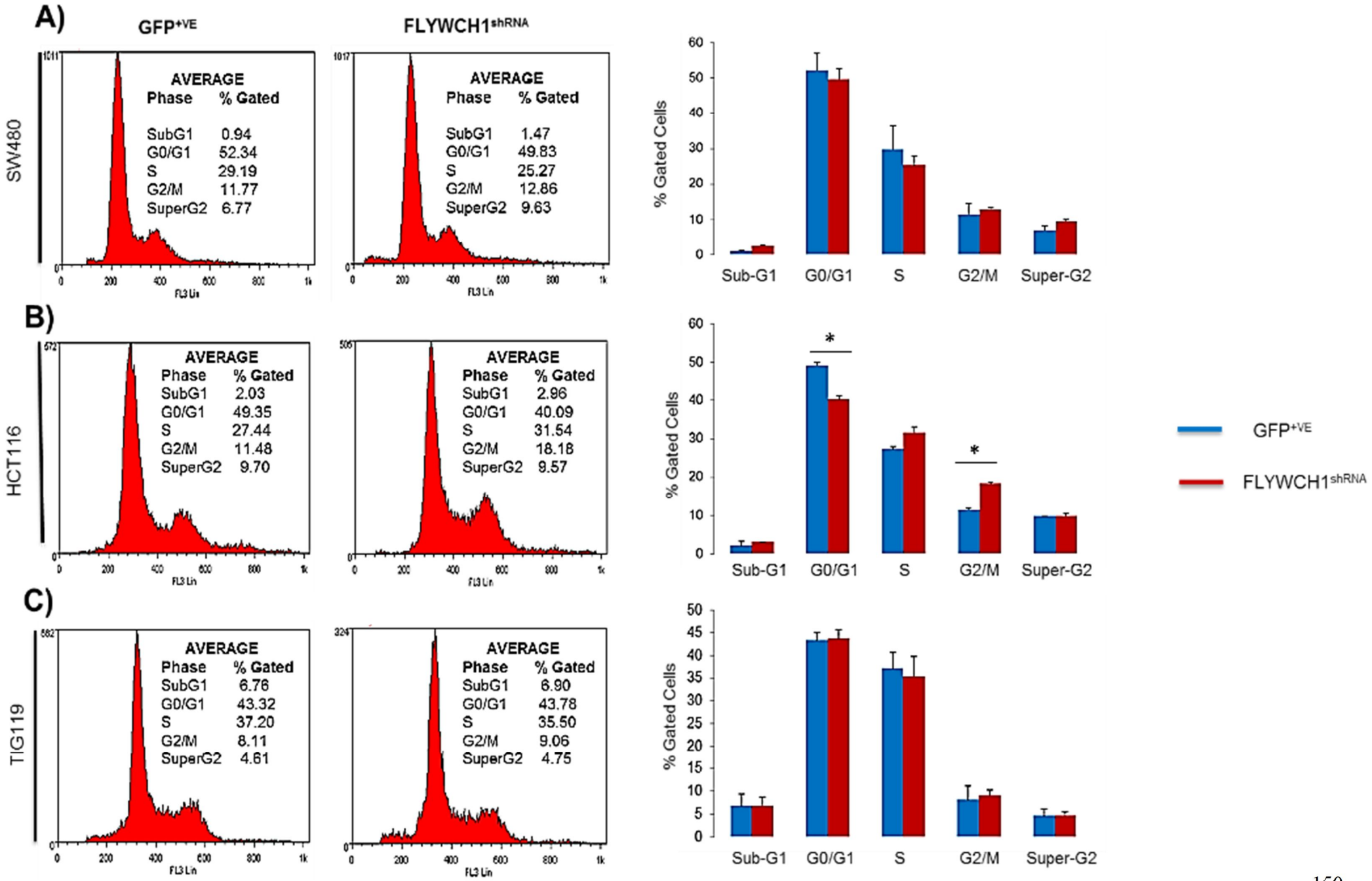

A)
GFP+VE
FLYWCH1shRNA
SW480
AVERAGE
Phase % Gated
SubG1 0.94
G0/G1 52.34
S 29.19
G2/M 11.77
SuperG2 6.77
AVERAGE
Phase % Gated
SubG1 1.47
G0/G1 49.83
S 25.27
G2/M 12.86
SuperG2 9.63
% Gated Cells
Sub-G1 G0/G1 S G2/M Super-G2
B)
HCT116
AVERAGE
Phase % Gated
SubG1 2.03
G0/G1 49.35
S 27.44
G2/M 11.48
SuperG2 9.70
AVERAGE
Phase % Gated
SubG1 2.96
G0/G1 40.09
S 31.54
G2/M 18.18
SuperG2 9.57
*
*
% Gated Cells
Sub-G1 G0/G1 S G2/M Super-G2
C)
TIG119
AVERAGE
Phase % Gated
SubG1 6.76
G0/G1 43.32
S 37.20
G2/M 8.11
SuperG2 4.61
AVERAGE
Phase % Gated
SubG1 6.90
G0/G1 43.78
S 35.50
G2/M 9.06
SuperG2 4.75
% Gated Cells
Sub-G1 G0/G1 S G2/M Super-G2
GFP+VE
FLYWCH1shRNA

Figure 3-11: Influence of FLYWCH1 on cell cycle progression in normal & CRC cells. Representative cell cycle histogram for each cell lines as follows; **A)** SW480, **B)** HCT116 & **C)** TIG119 cells are shown following treatment of cells to Prodidium iodide staining for cell cycle analysis. Statistical analysis of the percentages of cells in different cell cycle phases under different conditions are shown. Data are mean ± SD (*, $P < 0.05$). Experiments were repeated at least on two different occasions.

The morphological features of the different classes of cells are not the same with some appearing to be more mesenchymal-like than the others are and vice versa depending on the function and location of these cells. For instance, SW480 cells possess a more mesenchymal-like phenotype characterized with extensive cytoskeletal arrangements, on the other hand, HCT116 cells appear to possess a less mesenchymal properties. As already shown in previous data (Figure 3-6 D & E), ectopic expression of FLYWCH1 did not trigger any significant morphological changes in HCT116 cells. Following these observations, we sought to compare the changes in cell cycle progression profile in both HCT116 and SW480 cells under different conditions.

In HCT116 cells, data revealed more percentages of cells were accumulated in G0/G1 (49.35%) and less cells in G2/M phases (11. 48%) in GFP^{+VE} cells while less percentage of cells were observed in G0/G1 (40.09%) and more cells in G2/M phases (18.18%) in $FLYWCH1^{shRNA}$ cells (Figure 3-11 B). This is suggestive of possible cell cycle arrest in G0/G1 phase mediated by FLYWCH1. This data may suggest a FLYWCH1-mediated regulation of cell cycle progression in HCT116 cells. Consequently, these FLYWCH1-mediated cell cycle progression changes may not drive FLYWCH1-mediated morphological changes in HCT116 cells as ectopic expression of FLYWCH1 in HCT116 did

not instigate any significant morphological changes (Figure 3-6 D & E), while mediating changes in cell cycle dynamics in the same cells (Figure 3-11 B).

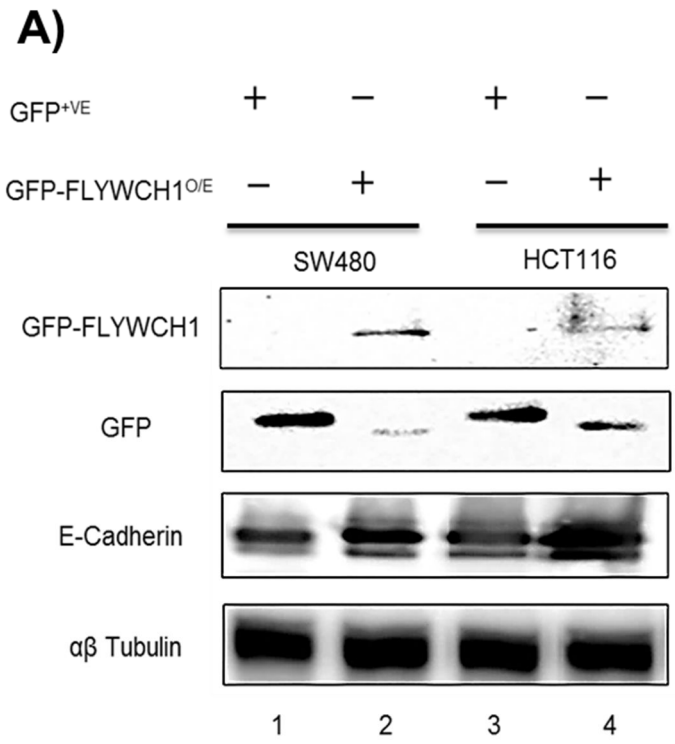
The cell cycle profile of TIG119 GFP^{+VE} and $FLYWCH1^{shRNA}$ cells were also investigated with no significant changes observed in both sets of cells (Figure 3-11 C). Following the cytoskeletal changes observed in TIG119 $FLYWCH1^{shRNA}$ cells, the lack of changes in cell cycle profiles in TIG119 cell lines as well as SW480 cells proves that cytoskeletal changes may occur independent cell cycle activity. Additionally, these results also suggest that FLYWCH1 may not facilitate cell cycle progression in normal cells and specific CRCs.

3.2.8 FLYWCH1 modulate cell morphology by targeting E-cadherin antagonist ZEB1

The trans-differentiation of highly adherent epithelial cells into motile mesenchymal cells, via EMT, is crucial in wound healing, embryonic development and stem cell behaviour (Lamouille et al., 2014). It also contributes pathologically to cancer progression. This change in cell differentiation and behaviour is controlled and maintained at the transcriptional, post-transcriptional as well as translational and post-translational levels. Epithelial cells undergoing EMT lose the expression of epithelial markers (E-cadherin and ZO-1) while acquiring expression of mesenchymal markers (N-cadherin, α-SMA and vimentin) (Liu et al., 2016; Smith and Bhowmick, 2016; Yu et al., 2015).

To support the hypothesis that the alterations in actin organization via filopodia and stress fibre formation mediated by FLYWCH1 is as a result of EMT/MET

processes, firstly, protein expression levels of specific epithelial (E-cadherin) markers were analysed via western blotting. The protein lysates derived from GFP^{+VE} and $GFP\text{-}FLYWCH1^{O/E}$ cells were immunoblotted with anti-GFP, and anti-E-cadherin antibodies. Our western blot data revealed that there was an up-regulation of E-cadherin in $GFP\text{-}FLYWCH1^{O/E}$ cells (Figure 3-12 A & B). Taken together, these data suggests the stress fibres and cell morphology changes observed predominantly in SW480 cells may be caused by FLYWCH1 mediated upregulation of E-cadherin.



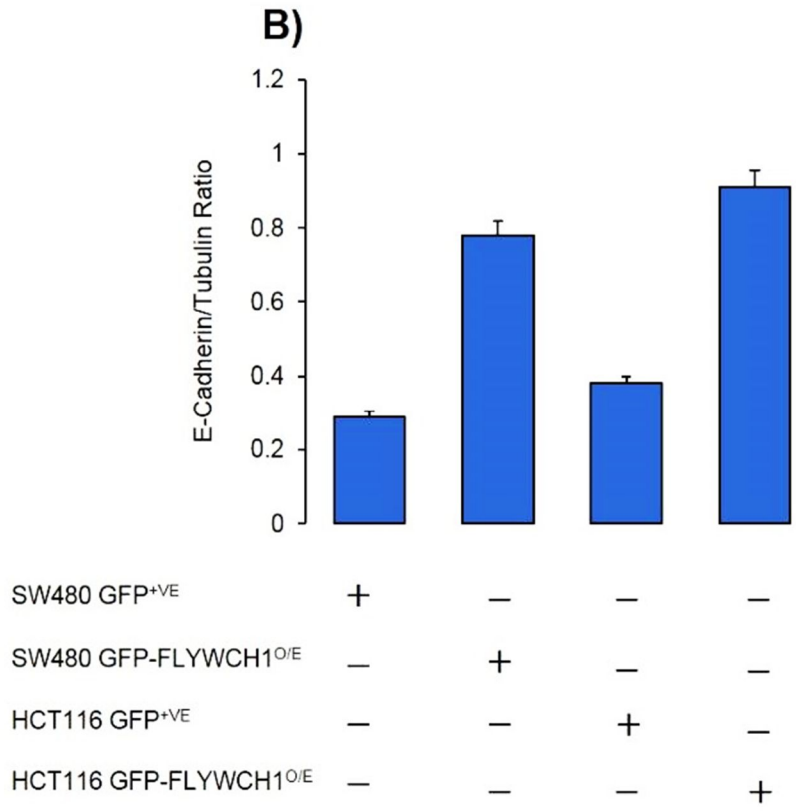
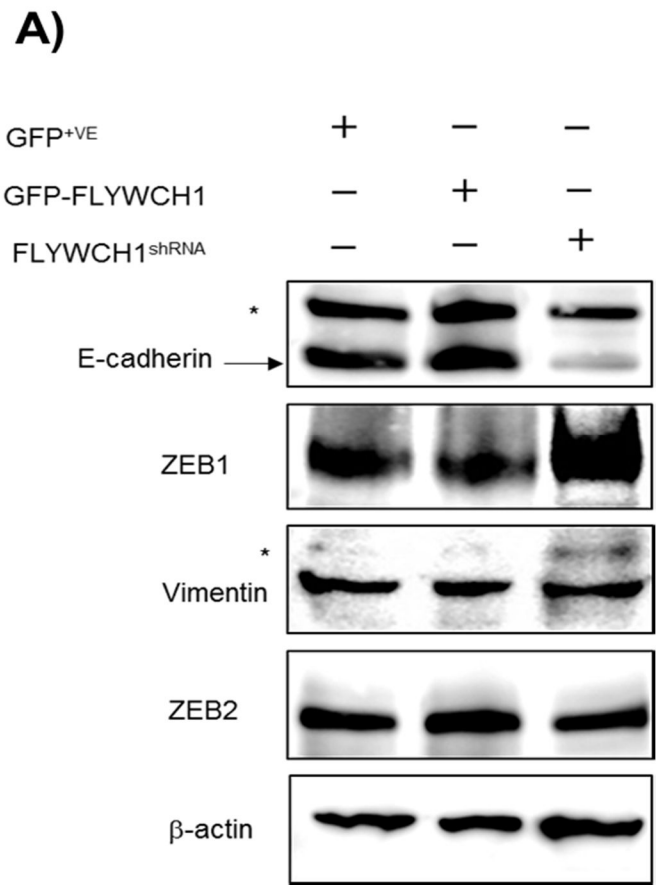


Figure 3-12: FLYWCH1 positively regulates E-cadherin. A) SW480 and HCT116 cells were transiently transfected to express GFP-FLYWCH1 (Lane 2, 4). The protein lysate obtained was immunoblotted with anti-GFP, anti-E-cadherin and αβ-tubulin antibodies with the expression patterns compared with SW480 GFP^{+VE} (lane 1) and HCT116 GFP^{+VE} (lane 3) control cells. **B)** Histograms show band intensity following E-cadherin normalization with tubulin. Data are represented as mean of two independent experiments +/- SD.

Defects in cell migration and actin cytoskeleton rearrangement, could also be related to epithelial-mesenchymal transition (EMT) (Nelson et al., 2008). The process of MET (mesenchymal-epithelial transition) is characterized by up-regulation of epithelial-specific proteins, including E-cadherin, and down-regulation of mesenchymal-specific molecules, such as Vimentin (Mani et al., 2008; Mendez et al., 2010; Nelson et al., 2008).

Our biochemical analyses however reveal no significant differences in the levels of Vimentin and ZEB2 proteins in response to the presence and/or absence of FLYWCH1 expression (Figure 3-13 A - E). These results suggest that the FLYWCH1-mediated E-cadherin regulation does not trigger EMT despite changes in ZEB1 expression. These data gives the view that FLYWCH1 modulates cell morphology by targeting E-cadherin suppressor ZEB1.



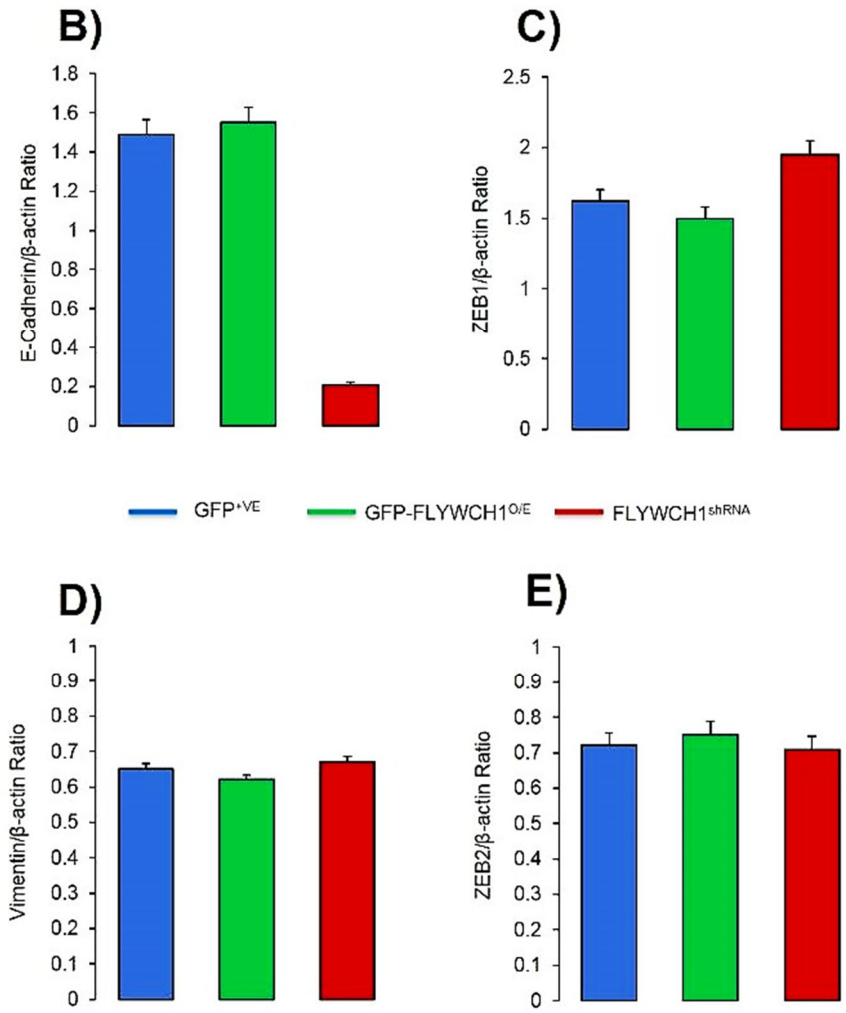


Figure 3-13: FLYWCH1 negatively regulates ZEB1 expression in SW480 cells. **A)** Western blot analysis was performed to detect the changes in expression of EMT markers and regulatory factors in SW480 cells. Endogenous FLYWCH1 repressed the endogenous ZEB1 expression at protein level. By contrast, the E-cadherin protein is upregulated by FLYWCH1. On the other hand, the vimentin and ZEB2 expression remained unchanged. * indicates precursor and/or unspecific band. **B)** Histograms shows band intensity following normalization with β-actin. Data are represented as mean of two independent experiments +/- SD.

Upregulation of ZEB1 and EPHA4, as well as the resulting repression of E-cadherin, has been revealed to be crucial in cell polarity and cell migration (de

Marcondes et al., 2016a; Sanchez-Tillo et al., 2011). We wondered how expression of FLYWCH1 would correlate with ZEB1 and EPHA4 expressions in human pathological samples. We therefore investigated the expression pattern of FLYWCH1, ZEB1 and EPHA4 mRNAs in a cohort of thirty three; normal, primary and metastatic tumour tissues derived from patients in Nottingham, UK. Our data revealed that *ZEB*1 expression is elevated in advanced tumour tissues. Interestingly, there is a significant linear correlation between *FLYWCH*1 down-regulation and *ZEB*1 and *EPHA*4 up-regulation in normal and advanced stage of CRCs but not in primary tumours (Figure 3-14). These data is suggestive of a FLYWCH1-mediated repression of ZEB1 in CRC cells.

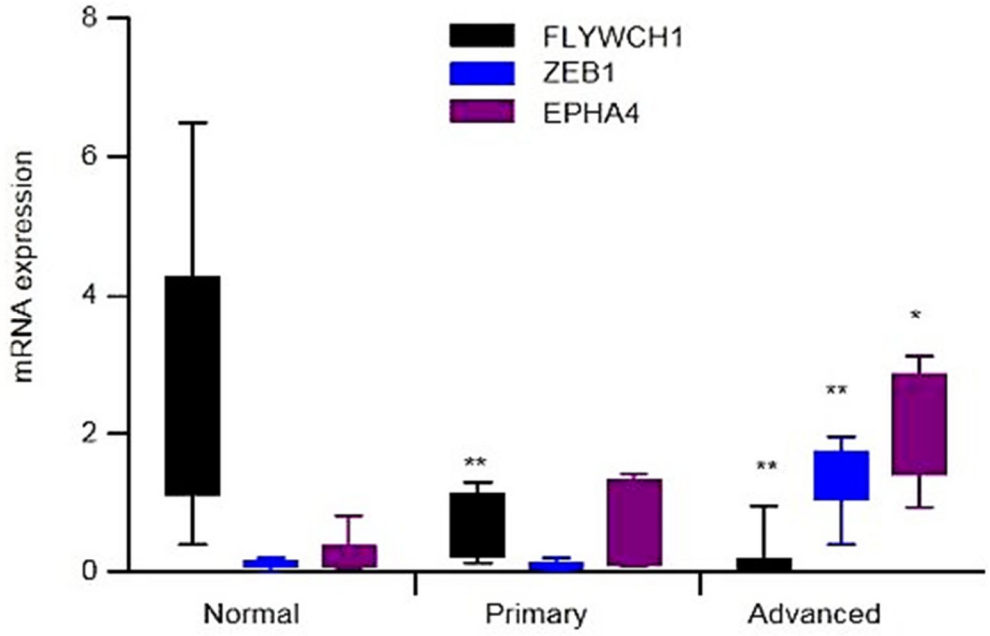


Figure 3-14: qRT-PCR analysis of FLYWCH1, EPHA4 and ZEB1 mRNA expression in a cohort of thirty three; normal, primary and metastatic tumour tissues from patients in Nottingham, UK, normalized to HPRT. Data are mean ± SEM (n = 3; *p ≤.05; **, p ≤.01; ***, p ≤.001). Experiments were performed in triplicate for each sample and repeated on two independent occasions. Experiments performed in collaboration with Dr. Roya Babaei-Jadidi.

3.3 Discussion

Investigation of protein localization at the subcellular level is highly essential, as it provides a better understanding of protein activity, cellular signalling cascades and interaction networks. Therefore, we attempted to identify the cellular localization and endogenous expression levels of FLYWCH1 in normal vs. cancer cell lines via immunofluorescence technique as it is widely used and is considered as one of the best methods for visualization of endogenous proteins with specific antibodies (Stadler et al., 2013). Our analysis revealed FLYWCH1 as a nuclear protein with a characteristic speckle-like pattern in TIG119, SW480 and HCT116 wildtype cell lines. As expected, fluorescent immunostaining revealed the endogenous FLYWCH1 expression co-localized with exogenously expressed GFP-FLYWCH1, thus eliminating any unreasonable doubt based on the nuclear localization of FLYWCH1 (Figure 3-1 A, B & C) and enabling additional functional analysis performed to elucidate the biological function of FLYWCH1.

Cell migration, morphological changes, and adhesive properties are closely regulated and dependent on continuous actin cytoskeleton remodelling. While investigating the cellular localization of FLYWCH1, it was observed that some morphological alterations including formation of ventral stress fibres and dense actin concentrated at the boundary of the cells while retaining a more mesenchymal-like phenotype was evident upon knockdown of FLYWCH1 in normal skin fibroblast cells (Figure 3-5 C). In contrast, SW480 cells exhibited a more rounded and epithelial-like morphology in addition to displaying less stress fibres with increased enrichment of actin on the periphery of the cells following

overexpression of FLYWCH1 (Figure 3-6 B). The exhibition of different patterns of actin appeared to be cell-dependent as the stress fibres observed in the absence of ectopic expression of FLYWCH1 in SW480 cells (Figure 3-7) appeared to be concentrated on the boundaries of the cells in contrast to the ventral stress fibres observed in normal skin fibroblast cells in the absence of ectopic FLYWCH1 expression (Figure 3-5 C). Stress fibres are contractile actomyosin bundles, essential for alterations in cell morphology during cell migration. Several types of stress fibres have been identified with ventral stress fibres been the most commonly observed (Burridge and Wittchen, 2013). Dorsal stress fibres and transverse arcs are the other types of stress fibres (Figure 3-15). In contrast to relatively well-characterized filopodia and lamellipodia, the assembly mechanisms and primary function of actin stress fibres remain poorly understood. Although studies have suggested the enrichment of stress fibres in motile cells (Tojkander et al., 2012), recent scientific evidences have implicated ventral stress fibres as drivers of mesenchymal cell migration (O'Connor and Chen, 2013; Vallenius, 2013), a major signature of metastasis.

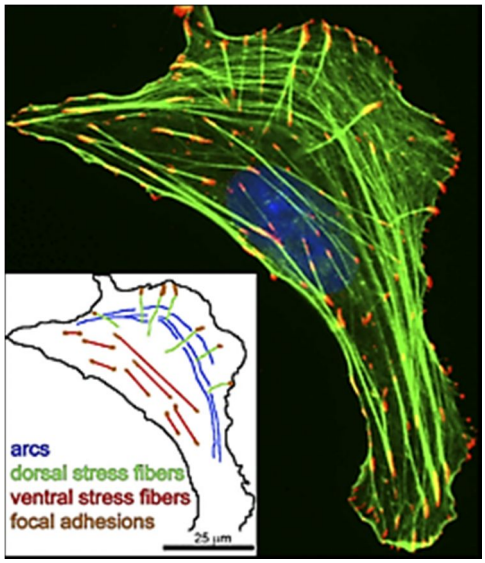


Figure 3-15: Stress fibres. U2OS human osteosarcoma cells exhibiting exhibiting ventral stress fibres as well as other types of stress fibres. (Inset) Schematic drawing depicting the SF subtypes. Taken from (Burridge and Wittchen, 2013).

Extensive studies over the past years supported with microscopic evidences have shown that actin filaments mediate cell migration via lamellipodial actin network at the cell periphery, unipolar filopodial bundles on the plasma membrane and presence of contractile actin stress fibres (Ridley et al., 2003; Vallenius, 2013). Studies have also shown the presence of ventral stress fibres in motile fibroblast cells which appears to drive tail retraction during the process of migration (Guo and Wang, 2012; Pellegrin and Mellor, 2007). Hence, current studies show that FLYWCH1 might indirectly negatively influence actin formation essential for migration. Interestingly, there were no obvious changes in cytoskeletal re-organisation observed in HCT116 in upon ectopic expression of FLYWCH1 (Figure 3-6 D). Although for the purpose of the current study, one major genetic alteration in HCT116 cells is the TGFβR2 mutation as well as mutations on β-

catenin phosphorylation sites (section 2.1.2), the direct link between these mutations and the less mesenchymal-like phenotype of HCT116 cells is yet to be determined.

Additionally, the acquisition of a more epithelial-like phenotype with less stress fibre formation observed in SW480 with ectopic expression of FLYWCH1 relative to control cells is suggestive of the possible involvement of FLYWCH1 in EMT/MET processes as mesenchymal phenotype promotes migration and metastasis. This was also supported by the presence of more extensive filopodia protrusions in the absence of FLYWCH1 visualized via Phalloidin staining following cell fixation with 1% glutaraldehyde (Figure 3-8). As already established, apart from dissolution of the epithelial cell–cell junctions, loss of apical–basal polarity amongst other features, a key characteristic event in EMT also includes increased cell protrusions such as filopodia and lamellipodia, thus enabling directional motility and cell elongation (Lamouille et al., 2014; Yilmaz and Christofori, 2010). Because EMT is characterized by actin stress fibre formation and increased cell contractility, the microscopic data presented indicates that loss of FLYWCH1 expression may trigger cytoskeleton re-modelling that facilitates cell migration and metastasis.

The ECIS platform has widely been utilized in the areas research focused on cell attachment and spreading, cell layer barrier functions, cell motility as well as for *in-vitro* toxicological studies and drug screening. Given the morphological changes observed upon ectopic expression of FLYWCH1 in SW480 cells, we attempted to investigate the role of FLYWCH1 in cell attachment/adhesion. Following the use of Electric cell-substrate impedance sensing (ECIS) studies

(Szulcek et al., 2014; Wegener et al., 2000), our data also reveal that overexpression of FLYWCH1 resulted to the most cellular adhesiveness by restricting the current flow indicative of high impedance while the reverse was observed following knockdown of FLYWCH1 (Figure 3-9 A). Consequently, the rapid adhesion of these cells causes a reduction in capacitance characterized by a higher slope value (Figure 3-9 B). The slope of the capacitance curve illustrates the rate of proliferation and cell spreading (Wegener et al., 2000). These data not only suggests the loss of FLYWCH1 positively regulates cell adhesion and restricts metastasis of cancer cells but it also supports recent studies' claim that actin stress fibres is key in the mechanism of migration, metastasis and invasion. Although the ECIS system was utilized to study the cell attachment and proliferative influence of FLYWCH1, potential improvement of these technical approaches should be considered such as examining the effect of FLYWCH1 on cell attachment and migration in the presence of pharmacologic inhibitors/activators that influence cancer cell adhesion (Spencer and Baker, 2016). However, the full molecular mechanisms explaining this discovery remain to be elucidated.

Cell morphology regulates cellular response to a plethora of stimuli ranging from, proliferation, differentiation and cell death (via apoptosis or necrosis), cell division, nuclear organization and morphogenesis (Sero et al., 2015). EMT is a phenotypic alteration involving detachment of epithelial cells from the underlying basement membrane thereby becoming more migratory and motile (Radisky, 2005; Thiery, 2002). Ordinarily, EMT is extremely crucial for metazoan embryonic development during gastrulation and in vertebrates, where

multipotent migratory neural crest cells exfoliate from the neural ectoderm to form diverse tissue derivatives (Lim and Thiery, 2012). However, both EMT and MET processes are reliant on E-cadherin expression, as epithelial cells exhibit high levels of E-cadherin while the reverse is observed in mesenchymal cells. Experimental evidences have shown that transcription of the E-cadherin gene is repressed in various forms carcinomas, while enforced expression of E-cadherin in carcinomas *in-vitro* appears to be sufficient in reducing the tumour cells aggressiveness (Larue and Bellacosa, 2005). These observations all suggest E-cadherin may possess tumour suppressor activity.

Considering the morphological changes (that are signatures of MET) modulated by FLYWCH1, we decided to explore the possible mechanism/s responsible for these changes. Our western blotting data showed elevated levels of E-cadherin upon ectopic expression of FLYWCH1 in both SW480 and HCT116 cells (Figure 3-12) with the reverse observed upon knockdown of FLYWCH1 expression (Figure 3-13). However, the E-cadherin expression levels observed are consistent with previous preliminary studies elucidating the biological activities of FLYWCH1 utilizing both western blotting and qRT-PCR techniques (Muhammad et al., submitted). The role of E-cadherin and the adherens junctions in mediating epithelial differentiation, by establishment of cellular adhesion and polarity, is well recognised. Additionally, E-cadherin has a role in signal transduction by restricting the cellular localisation of β-catenin. In normal epithelial cells, β-catenin is localised to the membrane, associated with E-cadherin. However, upon loss of E-cadherin, β-catenin can translocate to the nucleus, where it functions as a transcriptional activator with the TCF/LEF

protein family, as part of Wnt signalling (Schmalhofer et al., 2009). Consistent with our observations, upregulation of E-cadherin by different mechanisms has been widely associated to reduced cell motility and invasion in addition to morphological changes from mesenchymal-like to epithelial-like shape in various types of cancer (Kajiyama et al., 2003; Mao et al., 2008; Wong et al., 2010). Interestingly, this is in agreement with our findings in which knockdown of FLYWCH1 provoked an increase in the rate of wound healing in CRCs (Figure 3-10) without having much effect on proliferation (Figure 3-11 A, Figure 3-11 B). Since ectopic FLYWCH1 expression did not provoke any sort of cytoskeletal re-arrangement in HCT116 cells (Figure 3-6 D), it is feasible to suggest the FLYWCH1-mediated modulation of cytoskeleton may not play a dominant role in metastasis compare to tumour microenvironment. Additionally, data acquired from the *in-vitro* wound healing/scratch assay re-affirms the involvement of FLYWCH1 in cytoskeletal changes while re-affirming migration is not dependent upon cell cycle activities.

Further western blot analysis also revealed significant differences of E-cadherin and ZEB1 expression (Figure 3-13), in response to the absence and/or present of FLYWCH1 expression. This was expected as it has been established that high levels of ZEB1 corresponds to a low expression of E-cadherin and vice-versa (Romero-Pérez et al., 2013; Singh et al., 2011). ZEB proteins are sequence-specific DNA-binding transcription factors of E-cadherin. Expression and binding of ZEB1 to the E-cadherin E-boxes has been implicated in the regulation of E-cadherin expression at transcriptional level resulting to an induction of epithelial-to-mesenchymal transition in multiple human cancers (Comijn et al., 2001; Wong et al., 2014). Therefore, this study proves that the reduction of ZEB1

and concomitant induction E-cadherin via FLYWCH1 over-expression lead to a re-assembly of cell adherens junctions, reorganization of the actin cytoskeleton, and acquisition of a less motile and invasive phenotype in a ZEB1-mediated mechanistic manner. To further strengthen the FLYWCH1-mediated repression of ZEB1, we show an inverse correlation between FLYWCH1, ZEB1 and EPHA4 in a cohort of normal, primary and metastatic tumour samples (Figure 3-14). Increased *EPHA4* expression/activity has been implicated in various forms of cancers, including CRC, facilitating the progression of malignant events in several tumours (de Marcondes et al., 2016b). Surprisingly, no significant changes were observed in mesenchymal marker, vimentin and ZEB2 in response to the absence and/or present of FLYWCH1 expression (Figure 3-13). This was unexpected as upregulation of mesenchymal markers such as N-cadherin and vimentin as well as ZEB2 are key prerequisites for EMT activation (Chu et al., 2013; Lamouille et al., 2014). Therefore, results in this study suggest that FLYWCH1-mediated changes in ZEB1 expression does not trigger EMT but may facilitate morphological alterations that facilitates migration via crosstalk with key signalling pathways. However, expression patterns of other EMT transcription factors such as Twist, Snail and Slug upon FLYWCH1 over expression and knock-down requires further investigations.

To sum up, the data in this chapter have shown that FLYWCH1 possesses an anti-migratory role by modulating actin cytoskeleton re-modelling and stress fibre formation resulting to transition from a mesenchymal to a more epithelial phenotype. The expression levels of E-cadherin and subsequent reduction of ZEB1 expression thereby prompting the formation of an E-cadherin-dependent adhesion complex with a plethora of transmembrane glycoproteins, such as β-

catenin, which is a prerequisite for cell-cell adhesion, may mediate the morphological changes instigated by FLYWCH1 (Figure 3-16) . Although ZEB2 and mesenchymal marker, vimentin remained marginally unchanged upon FLYWCH1 overexpression, the morphological changes observed may occur in a ZEB1 dependent manner. As changes in cell motility are crucial toward metastasis and invasion, based on these results, FLYWCH1 may possess a potential metastasis-suppressing ability, which could be beneficial to the therapeutic field of colon cancer to restrict the dissemination of cancer.

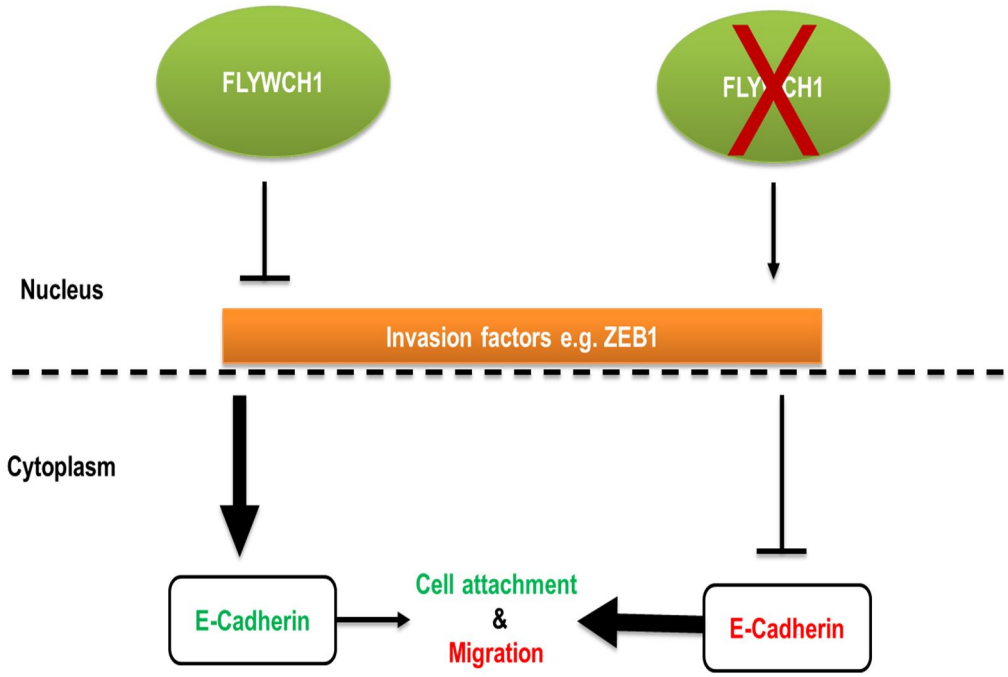


Figure 3-16: Possible mechanism illustrating FLYWCH1-mediated involvement in cell migration and attachment. FLYWCH1 represses a number of TCF/LEF target genes, including ZEB1, which is mainly associated with polarity, cellular migration and invasion.

4 CHAPTER 4

Phosphorylation and Inactivation of Glycogen synthase kinase (GSK-3β) by FLYWCH1 in cultured human colorectal cancer cell lines

4.1 Brief Introduction

During embryogenesis, β-catenin is a key requirement for stem cells in mediating the response to Wnt signalling for their transition from a pluripotent state. In adult stem cells, the function of Wnt signalling at various hierarchical levels contributes to specialized cell formation in different tissues (Holland et al., 2013). This is suggestive that the tightly controlled self-renewal property mediated by Wnt/β-catenin signalling in stem and progenitor cells is undermined in cancer cells to facilitate malignant progression. Nevertheless, intensive research is currently being undertaken to determine how Wnt/β-catenin signalling controlled by intrinsic and extrinsic factors coordinate the stem and cancer stem cell states (Holland et al., 2013).

Despite the multiple roles of GSK-3 in cellular physiology, its actual role in cancer progression still remains poorly understood. GSK-3 suppresses the Wnt/β-catenin pathway by phosphorylating β-catenin resulting in the ubiquitin/proteasome-dependent degradation of β-catenin. In some studies, ectopic expression of constitutively-active GSK-3 mutants increased cell cycle arrest, and reduced tumorigenicity of breast cancers although chemo-sensitivity, which is a key hallmark of cancer stem cell were also increased (Dal Col and Dolcetti, 2008). Suppression of active GSK-3 has been associated with tumour progression leading to the stabilization of β-catenin and subsequent transcription of Wnt-target genes such as c-Myc, cyclin-B1 and survivin that facilitate proliferation and tumorigenesis (McCubrey et al., 2014). Additionally, ZEB1, an effector of β-catenin/TCF4 signalling in EMT and tumour progression is also activated due to the stabilization of β-catenin (Sánchez-Tilló et al., 2011).

Coupled with earlier discoveries in our lab via *in-situ* hybridization that flywch1 mRNA is highly expressed in intestinal crypts (Muhammed et al., submitted), we investigated the effect of FLYWCH1 expression via possible crosstalk with GSK-3β and β-catenin activities in modulating cancer stem-like cell (CSC) properties using colonsphere formation assays.

As outlined, the previous studies in our lab showed that the human FLYWCH1 interacts with nuclear β-catenin via the C-terminal domain, and further transcriptional assays revealed that FLYWCH1 plays a potential negative regulator role of the canonical β-catenin signalling pathway (Muhammed et al., submitted). Herein, to understand the role of β-catenin phosphorylation mediated by GSK-3β we carried out further biochemical experiments on CRC cell lines (SW480 and HCT116 cell lines), which may also relate to cell shape changing mediated by FLYWCH1 overexpression in SW480 cells (addressed in chapter 3).

Taken together, our data suggest that FLYWCH1 may possess tumour suppressor activity via colorectal CSCs regulator activity by directly repressing the Wnt/β-catenin signalling pathway and in a GSK-3β dependent manner in cultured SW40 cells.

4.2. Results

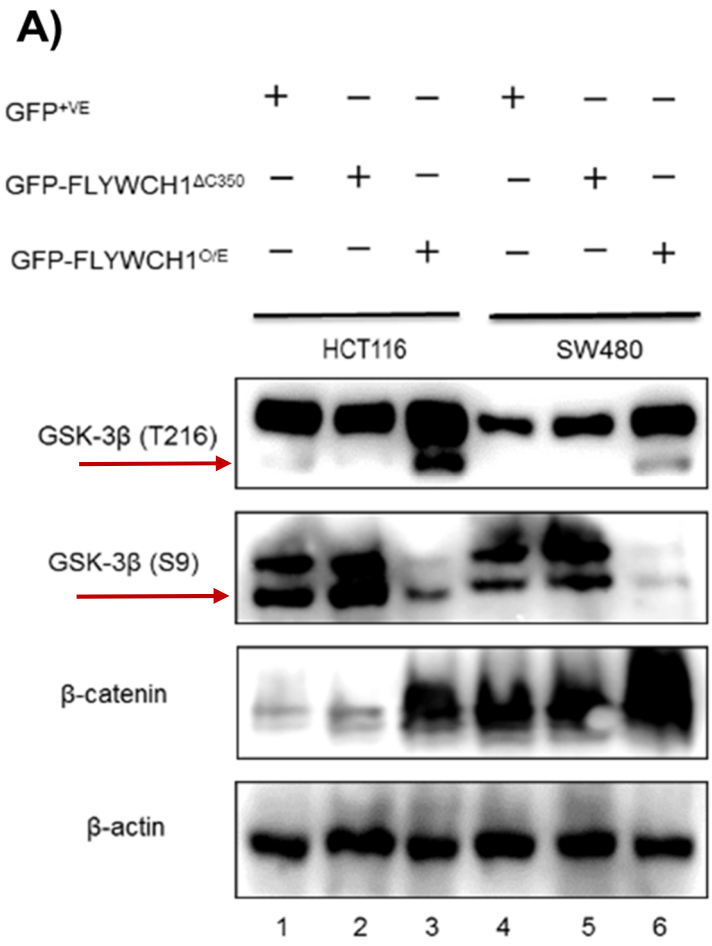
4.2.1 FLYWCH1 inhibits the serine 9 phosphorylation of GSK-3β that results in the induction of phosphorylated β-catenin

Recent experiments utilising TOP-FLASH reporters carried out in our lab have shown that FLYWCH1 protein interacts with β-catenin and represses β-catenin/TCF4 activity (Muhammed et al., submitted). In order to consolidate the proof of interaction between FLYWCH1 and β-catenin, here we performed further biochemical experiments which may also relate the cell shape changing mediated through overexpression of FLYWCH1 in CRC SW480 cell lines.

Using the overexpression-based system, cells were transfected with pEGFP-C2 (GFP positive control) and pEGFP-FLYWCH1-ΔC350 (loss of β-catenin interacting domain as negative control) plasmids. The pEGFP-FLYWCH1-ΔC350 plasmids are mutant FLYWCH1 variants with deleted 350 amino acids in the C-terminal. The pEGFP-FLYWCH1-ΔC350 plasmid was used because recent studies carried out in our lab suggested that the 350 amino acid sequence on the C-terminus of FLYWCH1 protein is crucial for β-catenin interaction (Muhammed et al., submitted). Western blot analysis carried out on both CRC cell lines with the appropriate antibodies clearly showed that GFP-FLYWCH1$^{O/E}$ cells exhibited an elevated protein expression of GSK-3β (Tyr-216) relative to both GFP^{+VE} and GFP-FLYWCH1$^{\Delta C350}$ cells (Figure 4-1). The data showed that HCT116 GFP-FLYWCH1$^{O/E}$ cells exhibiting a higher expression of GSK-3β (Tyr-216) compared to the corresponding SW480 cells (Figure 4-1; lane 3 vs lane 6).

Conversely, western blot analysis was performed to investigate the expression of inactive GSK-3β (Ser-9) with the use of phospho-GSK-3β antibody and it was discovered that GFP-FLYWCH1$^{O/E}$ cells showed a significantly reduced induction of phospho-GSK-3β (Ser-9) relative to both GFP^{+VE} and GFP-FLYWCH1$^{\Delta C350}$ cells (Figure 4-1). Further analysis were carried out to determine the effect this would have on the protein level of total β-catenin and it was discovered through western blot analysis that GFP-FLYWCH1$^{O/E}$ cells showed significantly high protein levels of β-catenin (with a pick shift on the gel considered to be phosphorylated β-catenin) relative to the controls. Moreover, immunofluorescence (IF) analysis was performed on the same cell lines and the results revealed consistency with the western blot analysis results (Figure 4-2).

Taken together, our data suggest that FLYWCH1 prevents the phosphorylation of GSK-3β at the Ser-9 position, thus promoting the phosphorylation of β-catenin and subsequent degradation. However, further studies are required to explore how the nuclear FLYWCH1 may cross-talk with nuclear form of GSK-3β while complexed with β-catenin protein


A)
GFP+VE
GFP-FLYWCH1ΔC350
GFP-FLYWCH1O/E
HCT116
SW480
GSK-3β (T216)
GSK-3β (S9)
β-catenin
β-actin
1 2 3 4 5 6

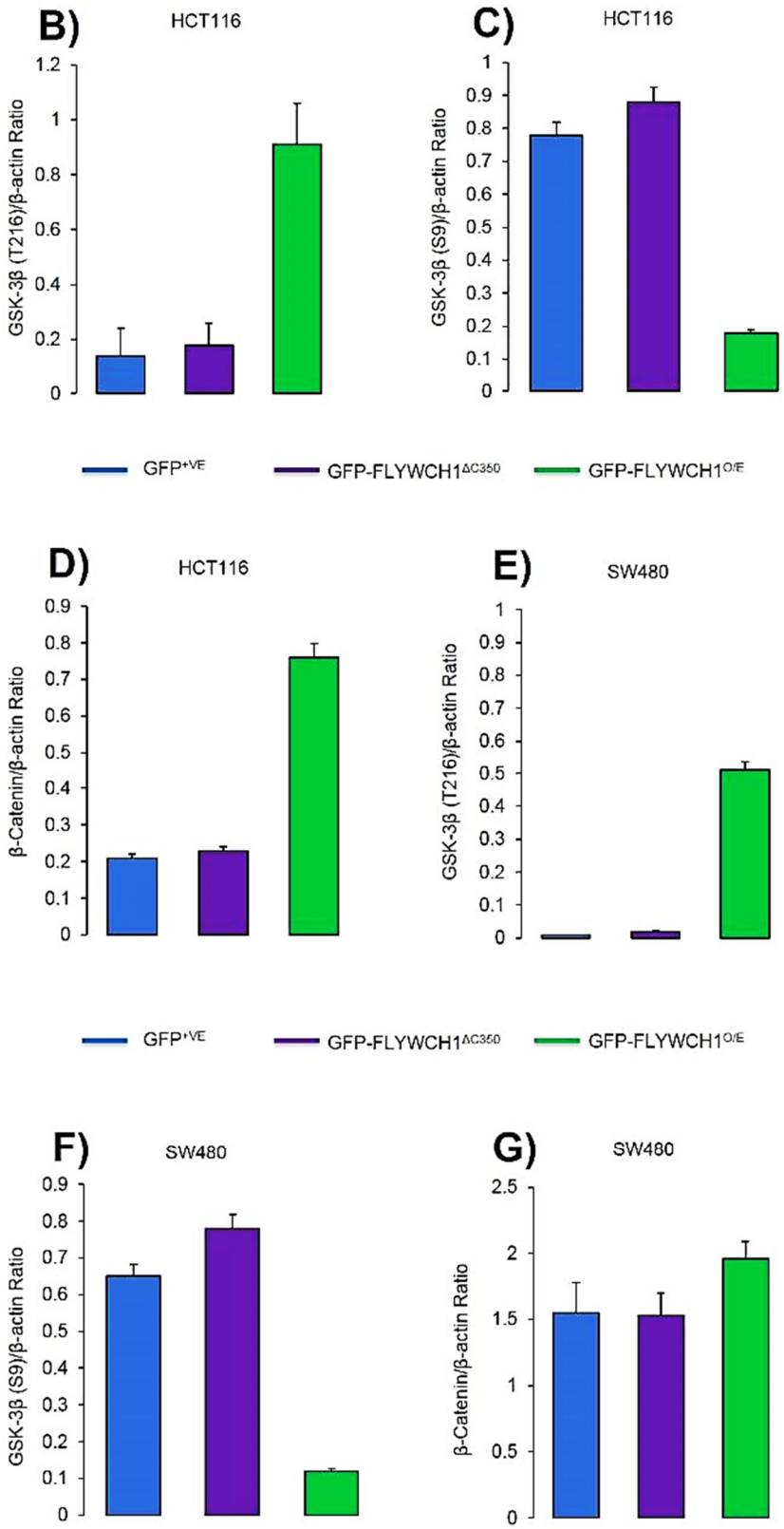
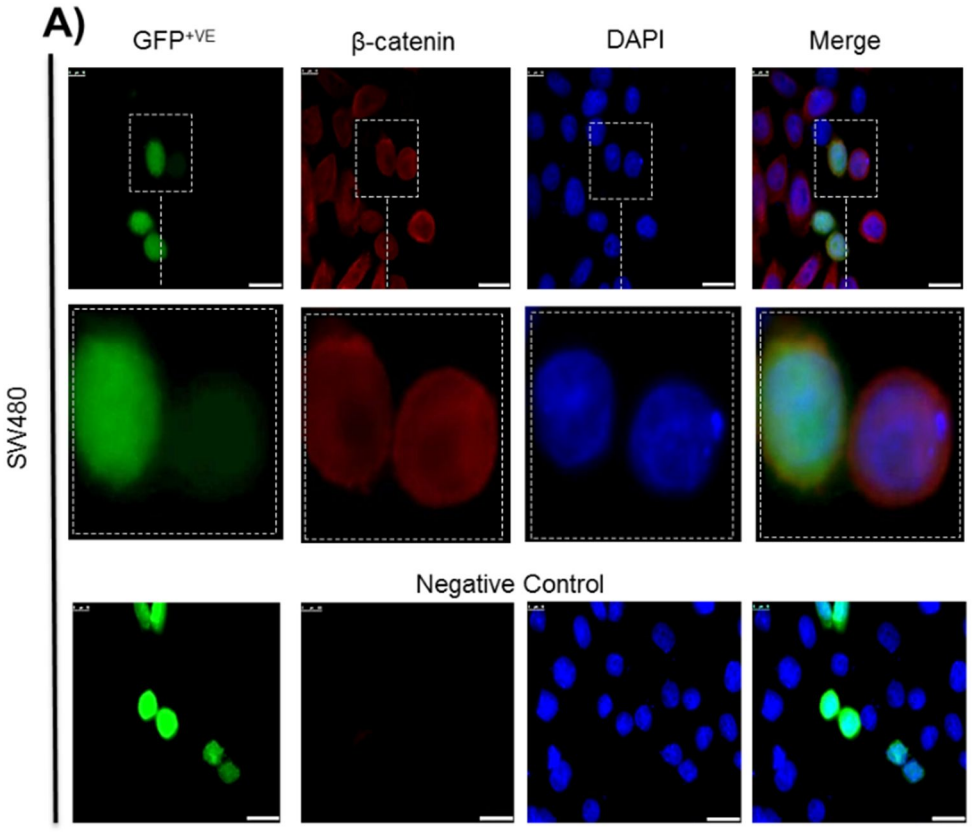
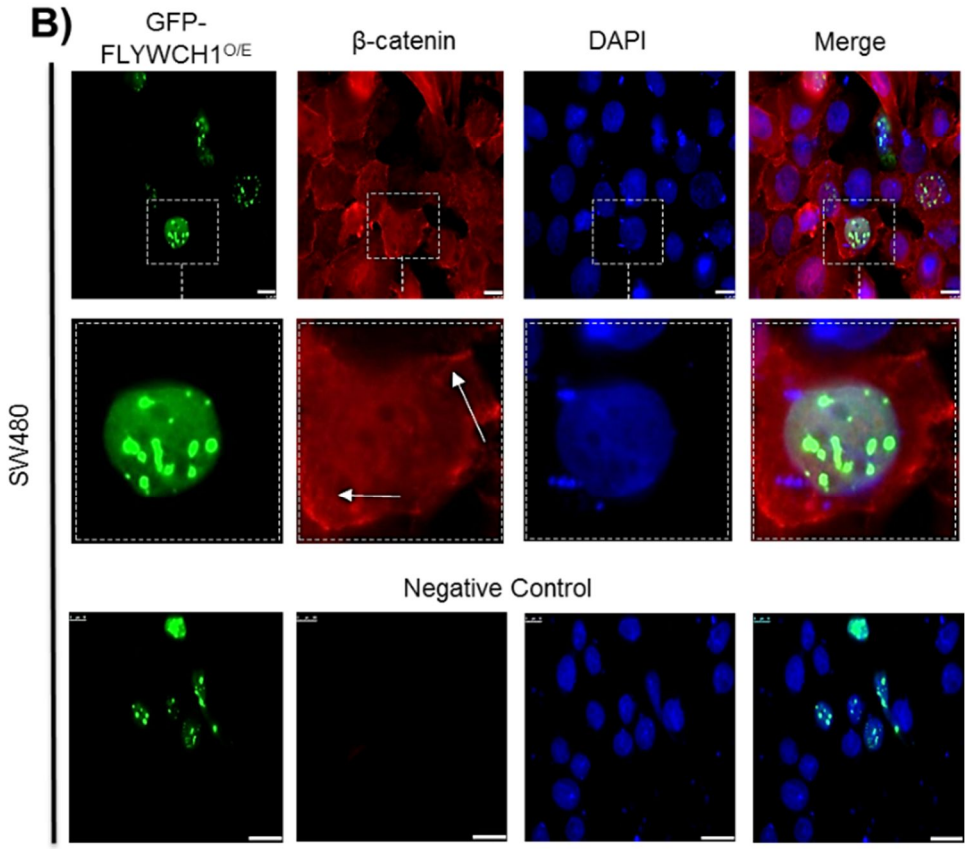


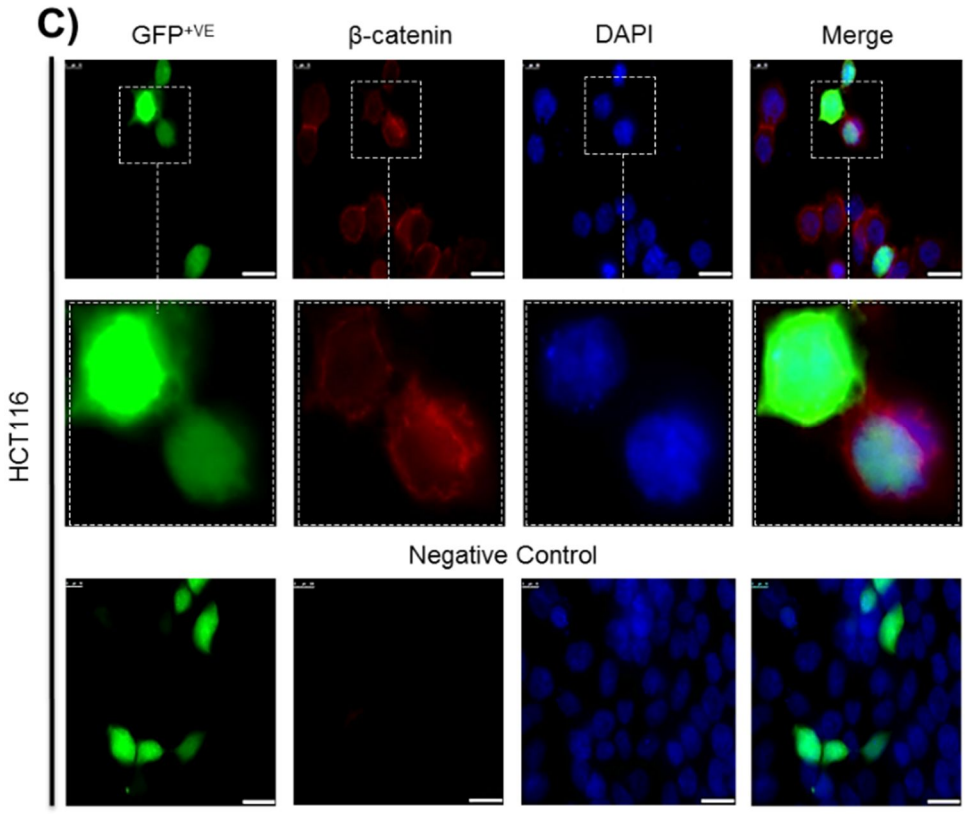
Figure 4-1: Phosphorylation and inactivation of GSK-3β by FLYWCH1 overexpression. A) HCT116 and SW480 GFP^{+VE}, GFP-FLYWCH1$^{\Delta C350}$ and GFP-FLYWCH1$^{O/E}$ cells were cultured and the cell lysate was immunoblotted

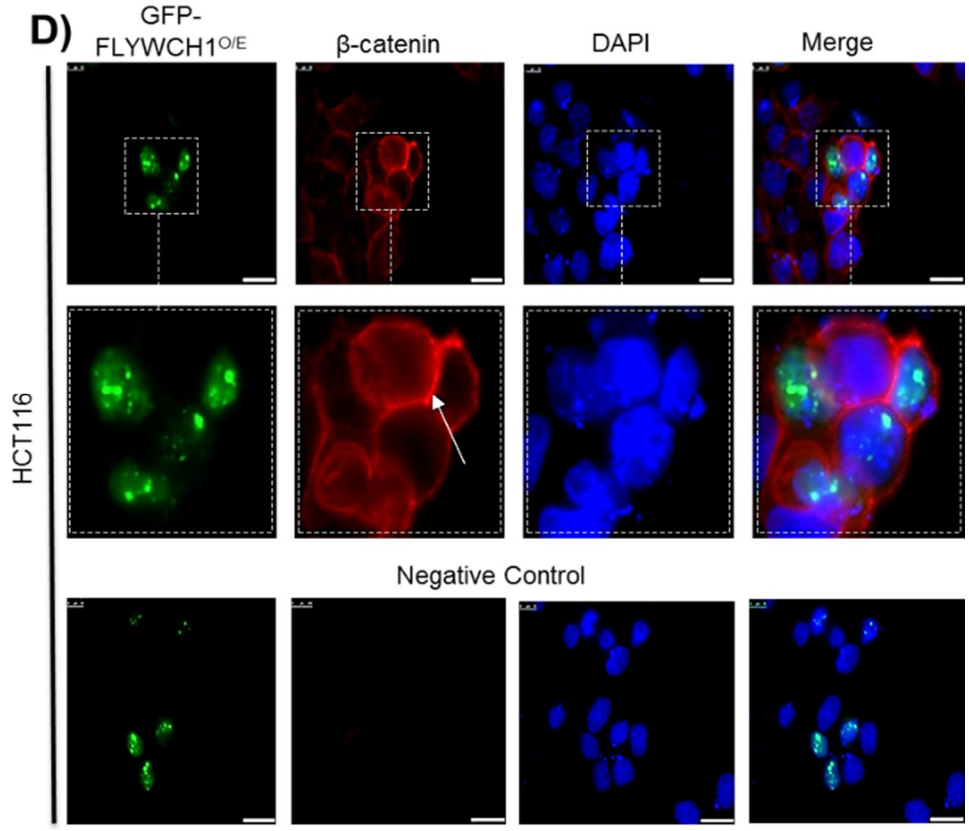
with anti-GSK-3β (T216), anti-phospho-GSK-3β (S9) and anti-β-catenin antibodies. Red arrows indicates GSK-3β bands. Experiments were repeated on two independent occasions. **B - G)** Histograms show band intensity following normalization with β-actin. Data are represented as mean of two independent experiments +/- SD.

.


A)
GFP+VE
β-catenin
DAPI
Merge
SW480
Negative Control


B)
GFP-FLYWCH1O/E
β-catenin
DAPI
Merge
SW480
Negative Control


C)
GFP+VE
β-catenin
DAPI
Merge
HCT116
Negative Control


D)
GFP-FLYWCH1O/E
β-catenin
DAPI
Merge
HCT116
Negative Control

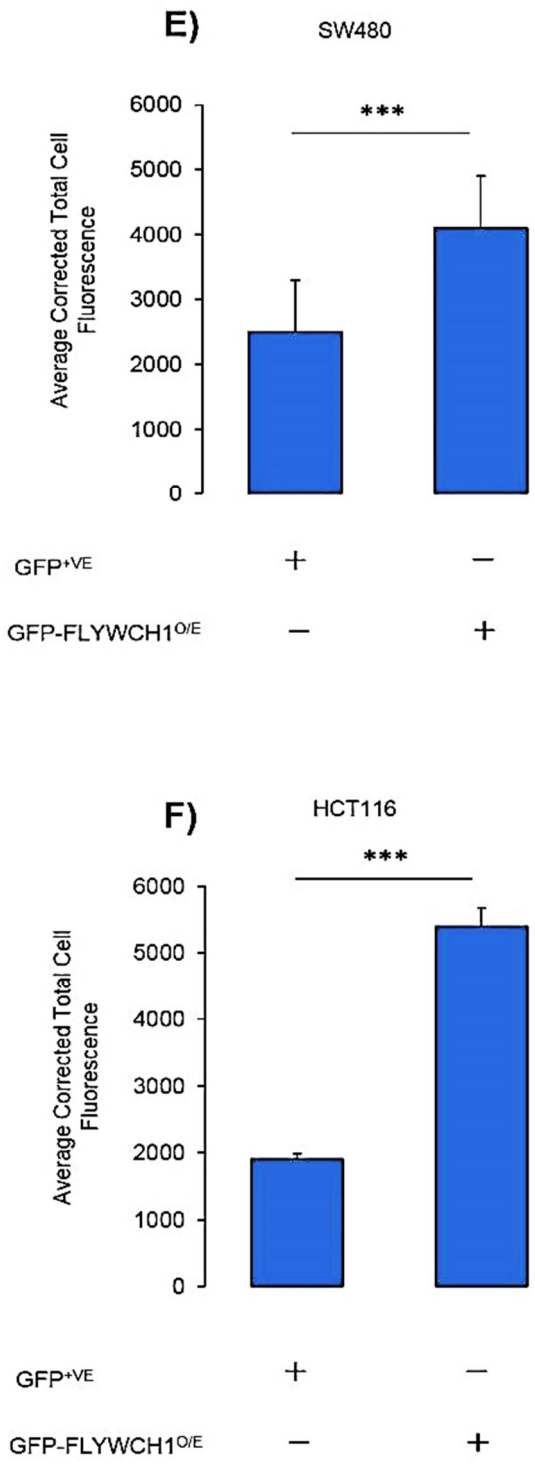


Figure 4-2: FLYWCH1 increased membrane bound phosphorylated β-catenin. Also, SW480 **A)** GFP^{+VE} and **B)** GFP-FLYWCH1$^{O/E}$ cells as well as HCT116 **C)** GFP^{+VE} and **D)** GFP-FLYWCH1$^{O/E}$ cells, were cultured, fixed on cover slips and stained with DAPI (blue), β-catenin (red) and GFP expression (green). Dotted lines indicates enlarged cell/s. Negative controls were used in

the absence of primary antibody. Arrows indicate the increase of membrane pool of β-catenin. Magnification; 100x. Scale bars, 10 μm. **E - F)** Quantitative analysis of β-catenin fluorescence intensity in SW480 and HCT116 cells was determined by calculating the Corrected Total Cell Fluorescence [CTCF = Integrated intensity – (area x fluorescence mean)] using ImageJ. Data are represented as mean of 30 individual cells under different conditions. Data are mean ± SD (***, P < 0.001). Experiment was repeated at least on two independent occasions.

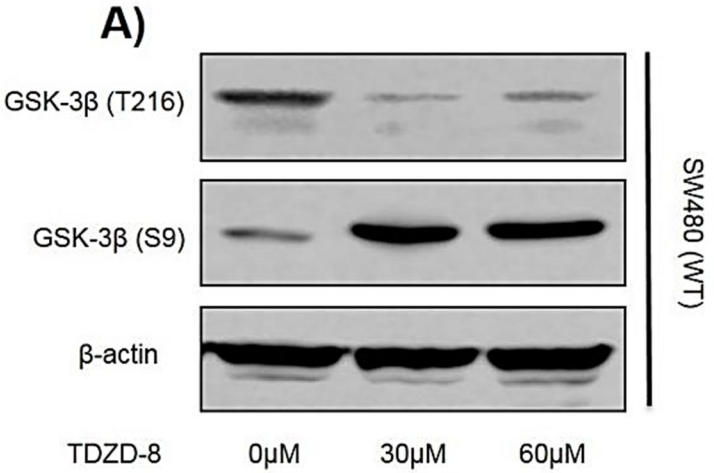
4.2.2 FLYWCH1 overexpression reduces sensitivity of SW480 CRC cells to GSK-3β drug inhibitor

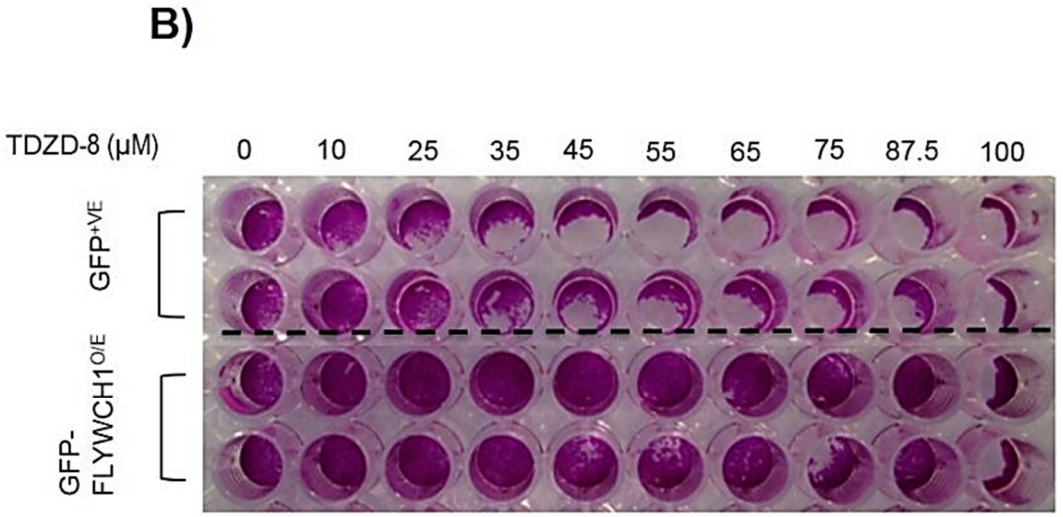
Our earlier results suggests that FLYWCH1 promotes the induction of GSK-3β in CRC cell lines (Figure 4-1 & Figure 4-2) Additionally, studies have shown GSK-3β mediates drug sensitivity/resistance in cancer chemotherapy (Luo, 2009; McCubrey et al., 2014). Therefore, next, we investigated the effect of FLYWCH1 on the viability of SW480 colorectal cancer cells treated with the GSK-3β inhibitor drug, TDZD-8, by using already established sulforhodamine B (SRB) cytotoxicity assay. The SRB survival assay was used to measure the IC_{50} of TDZD-8 (the concentration of drug producing 50% of the maximum response of inhibited cell survival activity) in SW480 GFP^{+VE} and GFP-$FLYWCH1^{O/E}$ cells. The assay was chosen, as it is a sensitive test, providing good linearity with cell number. Although the multi-step technique may lead to human error, when performed well, the SRB assay is commonly regarded as the ideal test for measuring *in-vitro* cytotoxicity (Vichai and Kirtikara, 2006).

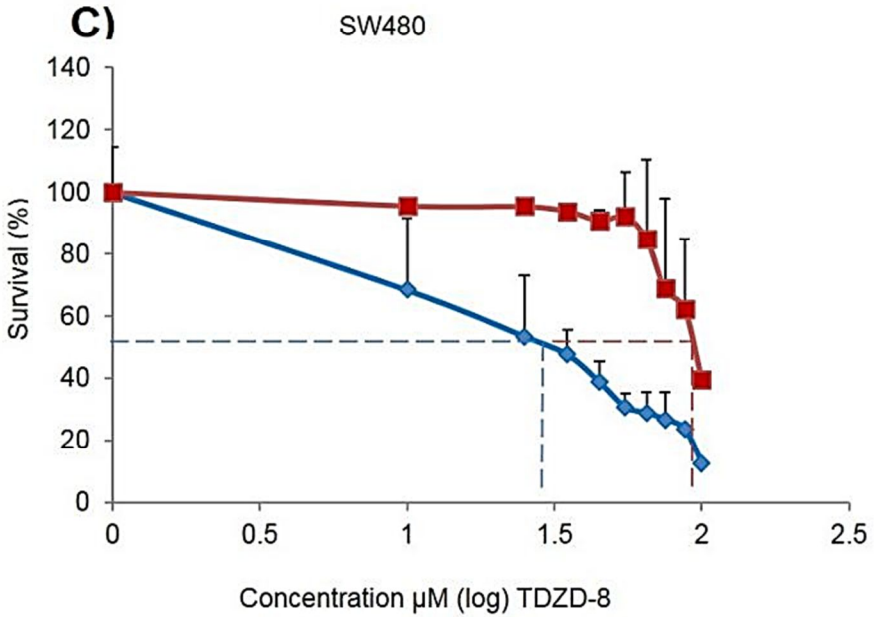
Prior to the application of the SRB assay, validation of TDZD-8 carried out on SW480 wild type cells showed a down regulation of GSK-3β (T216) in cells treated with 30-60 μM of TDZD-8 with an opposite effect on inactive GSK-3β

(S9) Figure 4-3 A). The SRB dye-staining pattern was observed on SW480 GFP^{+VE} and GFP-$FLYWCH1^{O/E}$ cells as described in (Chapter 2.9.5). The results of the assay showed that in GFP^{+VE} cells SRB dye staining gradually decreases, indicating a gradual decrease in cell number and a response of progressive inhibition of cell survival activity. On the other hand, GFP-$FLYWCH1^{O/E}$ cells stained with SRB dye remained relatively unchanged until it suddenly decreases at a concentration of 75μM of TDZD-8 (Figure 4-3 B), indicating a suppressive activity of FLYWCH1 overexpression in cell death response to TDZD-8 drug (Figure 4-3 B). Additionally, the IC_{50} values obtained from the dose-response curves confirm that SW480 GFP-$FLYWCH1^{O/E}$ cells (IC_{50} = 91.3 μM) showed a suppressed toxicity activity to TDZD-8 compared with control SW480-GFP^{+VE} cells (IC_{50} = 26.35 μM) (Figure 4-3 C & D).

Taken together, these results suggest a restoration of sensitivity for TDZD-8 drug-induced cytotoxicity by overexpressing of FLYWCH1 in SW480 cells. It is intriguing to hypothesize that there may be a significant cross-talk between FLYWCH1 and GSK-3β in understanding the molecular basis of drug resistance in colorectal cancer cells.







D)

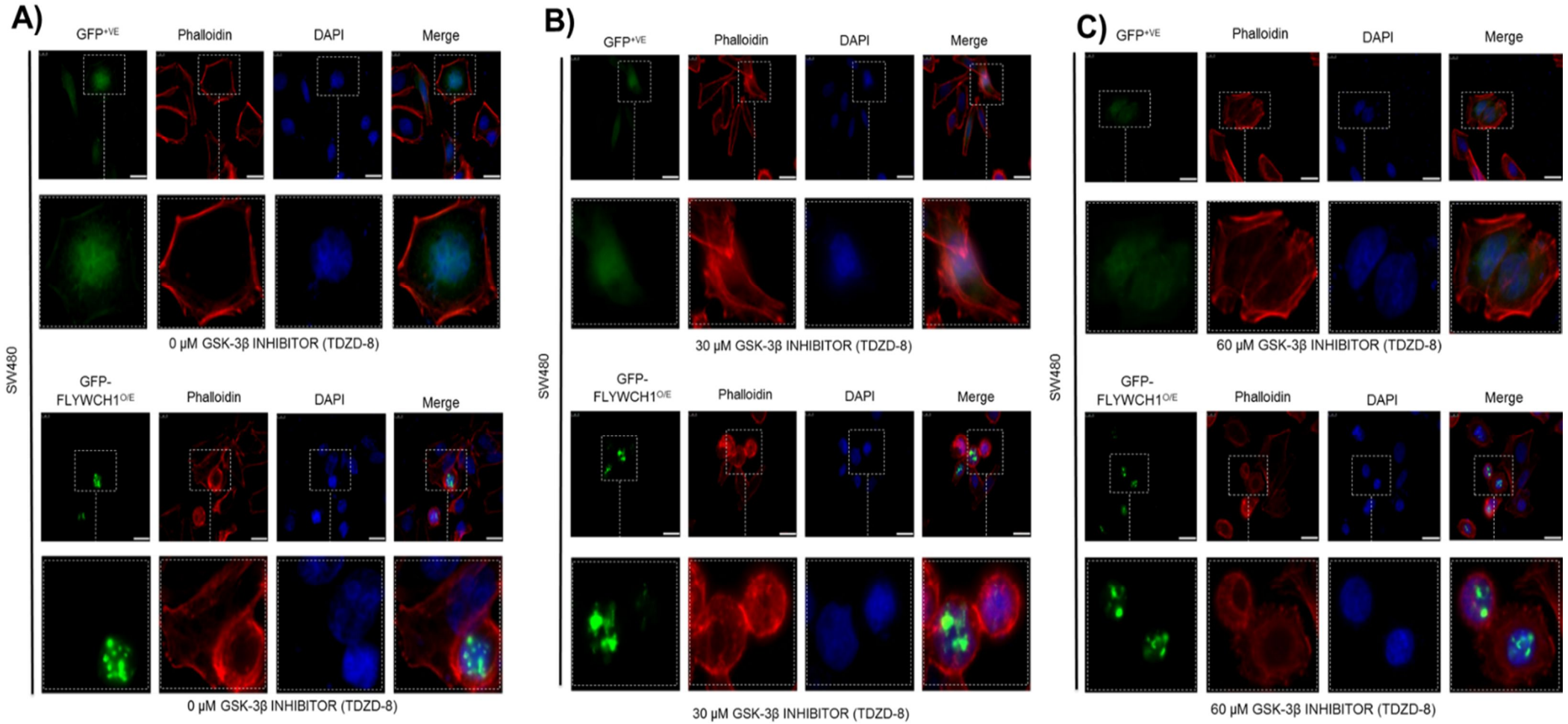
	IC_{50} Value (μmol/L) (Mean +/- SEM)
SW480 GFP^{+VE}	26.35 +/- 8.1
SW480 GFP-FLYWCH1$^{O/E}$	91.3 +/- 6.1

Figure 4-3: FLYWCH1 overexpression confers GSK-3β inhibitor resistance in SW480 CRC cell lines. A) Western blot analysis showing the validation of GSK-3β inhibitor (TDZD-8) on GSK-3β activity in SW480 wild-type cell lines. **B)** Cytotoxicity of TDZD-8 under different concentrations was analyzed via SRB assay on GFP^{+VE} and GFP-$FLYWCH1^{O/E}$ cells. **C, D)** Determination of IC_{50} values, indicated in the table, were determined via GraphPad Prism software. Experiments were performed in duplicate and repeated at least in three independent occasions. Data are mean ± standard error of the mean.

4.2.3 FLYWCH1-mediated cell morphology alteration is independent of its effect on GSK-3β activity

In the previous chapter, we reported the FLYWCH1-mediated morphological changes in SW480 cells. Hence, the current study was performed to investigate the effects of small-molecule GSK-3β inhibitor (TDZD-8) on morphology alteration specifically in SW480 cells. This would also aid to ascertain whether the FLYWCH1-mediated morphological changes occurred in a GSK-3β dependent manner.

SW480 GFP^{+VE} (control) and GFP-$FLYWCH1^{O/E}$ cells were cultured in cover slips under different concentration (0 µM, 30 µM & 60 µM) of GSK-3β inhibitor (TDZD-8), stained afterwards with Phalloidin, and observed via fluorescence microscopy. Interestingly, the microscopy analysis revealed no significant GSK-3β-mediated cell morphological changes in FLYWCH1 overexpressing cells (Figure 4-4 A-C, bottom panel), although increase in TDZD-8 caused a reduction in the phenotype of SW480 GFP^{+VE} cells Figure 4-4 A-C, top panel). These data suggests that FLYWCH1-mediated alteration of cellular morphology occurs in a GSK-3β independent manner.


A)
GFP+VE
Phalloidin
DAPI
Merge
SW480
0 μM GSK-3β INHIBITOR (TDZD-8)
GFP-FLYWCH1O/E
Phalloidin
DAPI
Merge
0 μM GSK-3β INHIBITOR (TDZD-8)
B)
GFP+VE
Phalloidin
DAPI
Merge
SW480
30 μM GSK-3β INHIBITOR (TDZD-8)
GFP-FLYWCH1O/E
Phalloidin
DAPI
Merge
30 μM GSK-3β INHIBITOR (TDZD-8)
C)
GFP+VE
Phalloidin
DAPI
Merge
SW480
60 μM GSK-3β INHIBITOR (TDZD-8)
GFP-FLYWCH1O/E
Phalloidin
DAPI
Merge
60 μM GSK-3β INHIBITOR (TDZD-8)

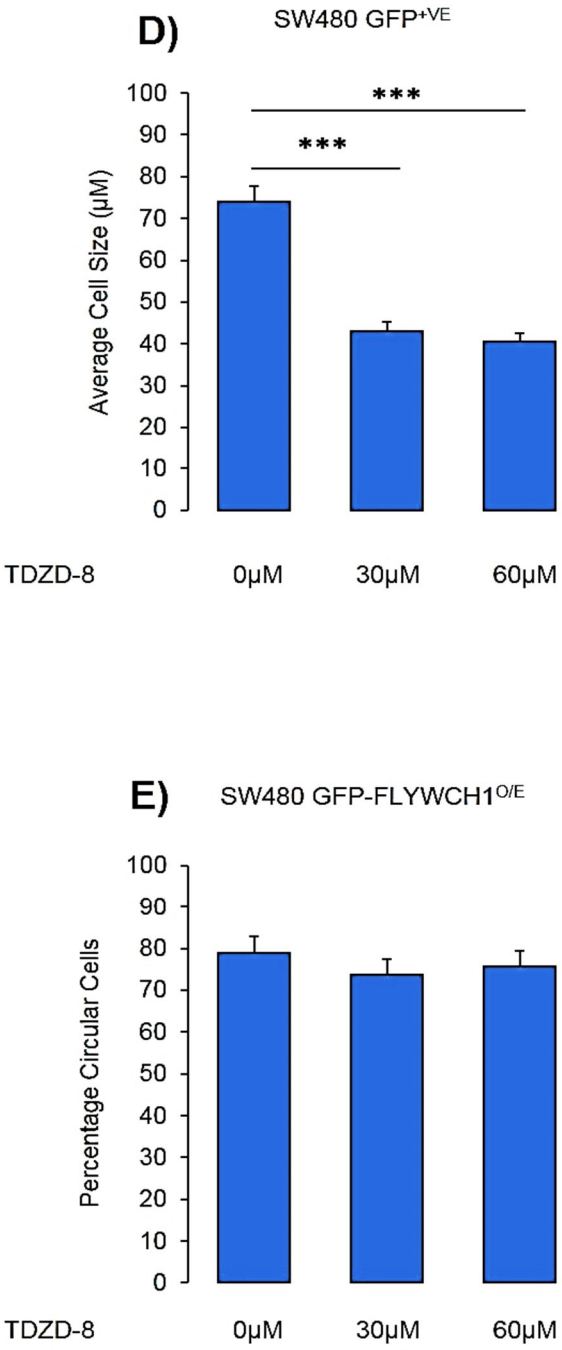


Figure 4-4: FLYWCH1-mediated morphology changes occur in a GSK-3β independent manner. SW480 GFP^{+VE} and GFP-FLYWCH1$^{O/E}$ were fixed, stained with Phalloidin and observed under fluorescence microscopy in the following conditions; **A)** 0µM TDZD-8, **B)** 30µM TDZD-8, **C)** 60µM TDZD-8. Scale bars, 25 µm. Magnification; 100x. Dotted lines indicates enlarged cell/s. concentration of TDZD-8. Quantitative analysis of morphological changes in **D)** SW480 GFP^{+VE} and **E)** SW480 GFP-FLYWCH1$^{O/E}$ cells under different TDZD-

8 concentrations were performed. Data are represented as mean of 30 individual cells under different conditions. Data are mean ± SD (***, P < 0.001). Experiment was repeated at least on two independent occasions.

4.2.4 FLYWCH1 knock-down enhances the colonosphere formation efficiency

The GSK-3β and β-catenin pathways play crucial roles in the regulation of stem cell/progenitors, cell self-renewal and maintenance in a plethora of systems (Reya and Clevers, 2005). For instance, Wnt3a via β-catenin was shown to foster the formation of embryonic stem cell (ESC)-like colonies (Sato et al., 2004). Cancer stem cells (CSC) possess features associated with normal stem cells. However, a major similarity between normal stem cells and CSCs is the fact that they both function via common signalling pathways such as Wnt & Notch pathways that aids in the maintenance of proliferation of stem cells (Nguyen et al., 2012). Given that FLYWCH1 has been shown to negatively regulate the β-catenin and GSK-3β signalling, we sought to investigate the effect of knockdown of FLYWCH1 expression on CSC properties using colonosphere formation approach. Colonospheres are spherical structures composed of several colonic mucosal epithelial cells. The 3D-colonosphere culture model represents *in-vitro* conditions for the spontaneous cluster of cancer cells in spheroids and offers a platform for observation of CSC properties (Shaheen et al., 2016).

To do this, SW480 cell lines derived colonospheres were generated as described in section (2.2.1.3). The colonospheres began to form towards the end of the incubation period (14 days) after which they were evaluated for the number and size by light microscopy. The average size and the number of colonospheres

formed per well was determined and it was observed that colonospheres formation derived from parental SW480 GFP^{+VE} cells were delayed as $FLYWCH1^{shRNA}$ derived colonospheres appeared to be more in number and larger in size (Figure 4-5). Taken together, results suggest that FLYWCH1 may play a role in the regulation of CSCs by probably restricting stemness capacity via inhibiting β-catenin activity.

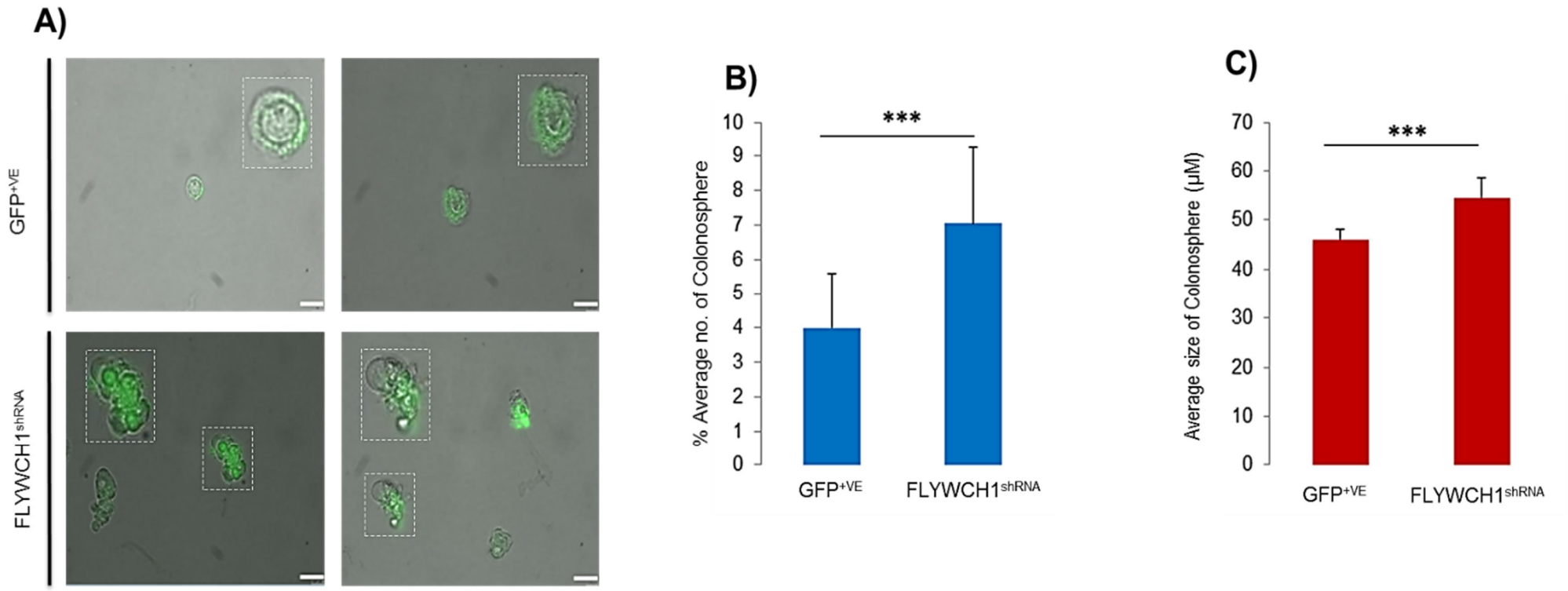


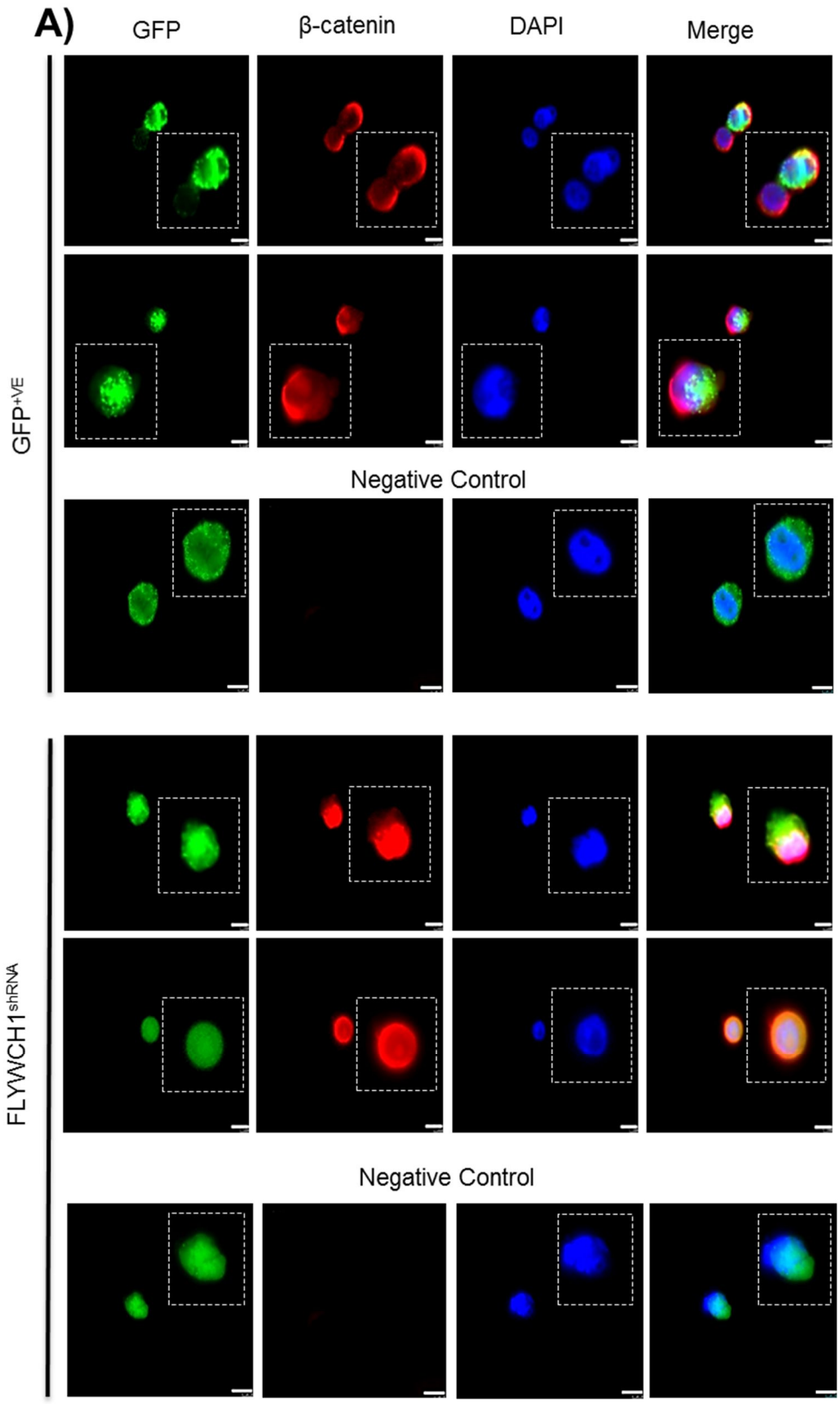
Figure 4-5: Loss of FLYWCH1 expression caused morphological changes in SW480-derived colonospheres. **A)** Bright field view of cultured colonospheres in 48-well plate derived from GFP^{+VE} (Top panel) & FLYWCH1^{shRNA} (Bottom panel) SW480 parental cells. Quantitative data illustrating the; **B)** Percentage average number of colonospheres per well (96 well plate) and **C)** Measurement of average size of colonospheres in GFP^{+VE} vs FLYWCH1^{shRNA}. Experiment was repeated at least on three independent occasions. Dotted lines indicates enlarged cell/s. Data are mean ± SD (n = 3; ***, P < 0.001). Scale bars, 10 µm. Magnification: 40x. Cell size (per pixel) = Physical length / Diameter of Field of View.

4.2.4.1 Evaluation of loss of FLYWCH1 effect on self-renewal and differentiation activities in colonospheres.

Human CRCs are characterized with a heterogeneous selection of cancer cells (Perez et al., 2013). CSCs (also known as cancer initiating cells) form a small sub-population of CRC cells possessing self-renewing properties and are poorly differentiated (Medema, 2013). Ordinarily, spheroids/colonospheres display increased levels of CSC markers. Moreover, the spheroid-forming assay has been established as a gold standard in CSC research as it enables the evaluation of differentiation and self-renewal capabilities at the single-cell level. Using this approach, the role of FLYWCH1 in stemness and differentiation was investigated by analysing the expression patterns of signature stem cell markers.

Colonospheres derived from SW480 GFP^{+VE} and SW480 $FLYWCH1^{shRNA}$ were cultured on coverslips after which fluorescent immunostaining was performed for selected stem cell and differentiation markers including β-catenin (stem cell associated marker), ZEB1 (EMT marker), BMP4 (differentiation marker), CD44 (stem cell marker) and MUC2 (differentiation marker).

Interestingly, there was an elevated expression of ZEB1, nuclear β-catenin, and CD44 in colonospheres derived from SW480 $FLYWCH1^{shRNA}$ relative to the control. In particular, the expression of ZEB1 and β-catenin were in agreement with the expression patterns observed in the corresponding parental cells (Chapter 3). Additionally, a decreased expression of MUC2 and BMP4 were observed in colonospheres derived from SW480 $FLYWCH1^{shRNA}$ relative to the GFP^{+VE} cells.


A)
GFP
β-catenin
DAPI
Merge
GFP+VE
Negative Control
FLYWCH1shRNA
Negative Control

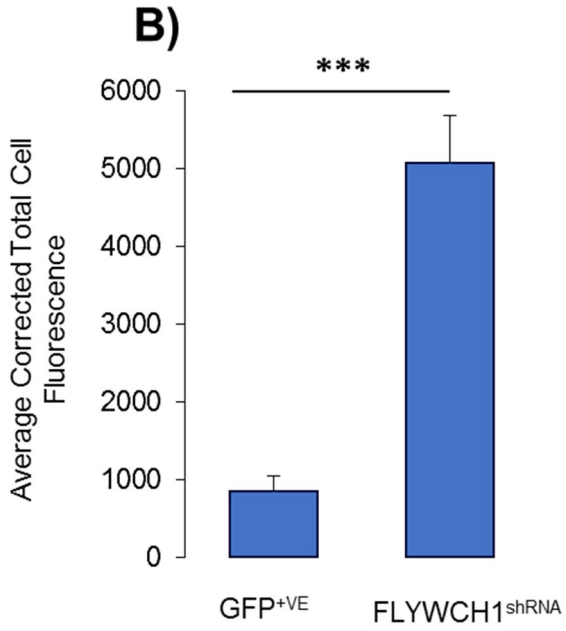


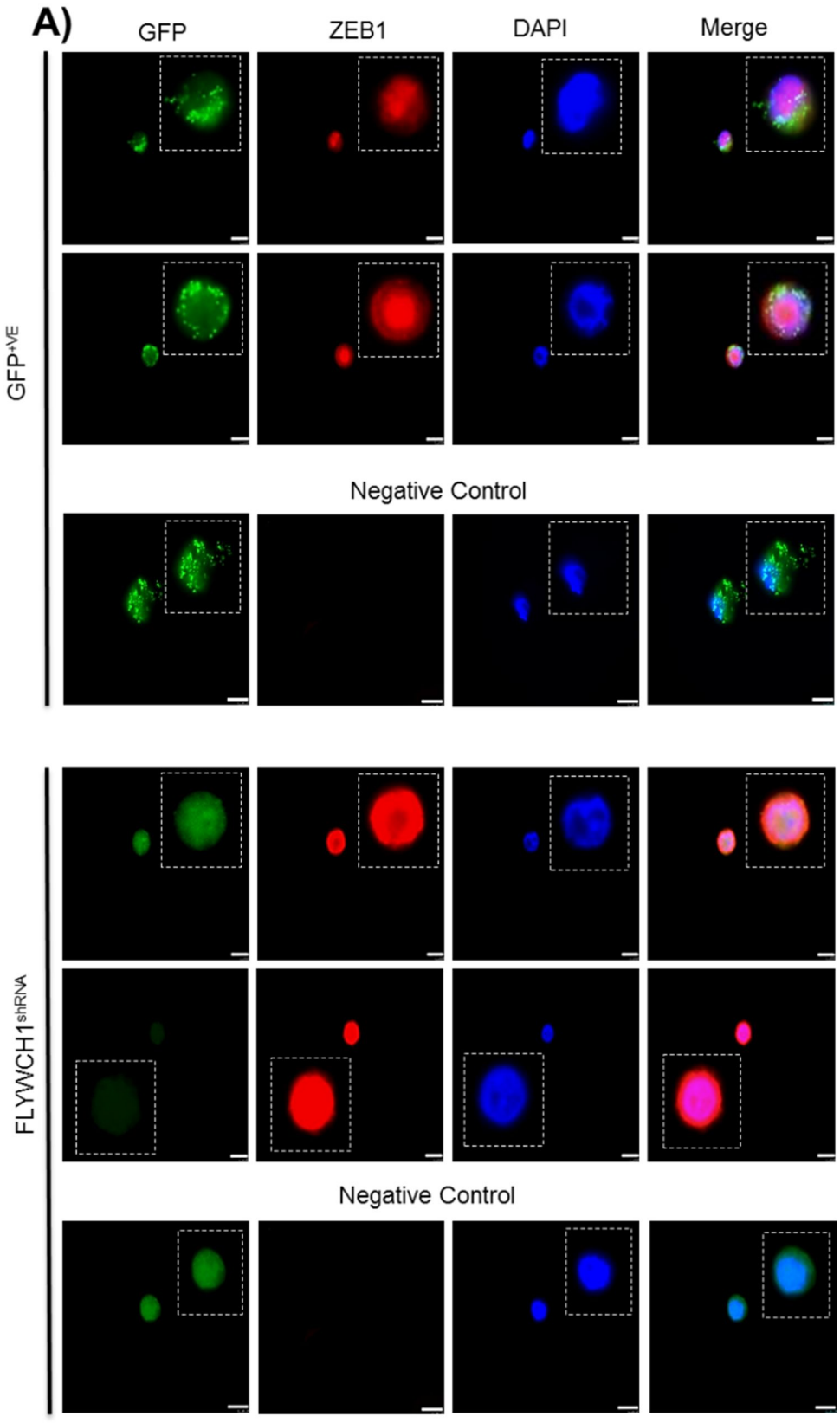
Figure 4-6: Knockdown of FLYWCH1 expression increases β-catenin expression patterns in colonospheres. A) Expression patterns of β-catenin (red) in GFP^{+VE} vs $FLYWCH1^{shRNA}$ were observed following fixation. Dotted lines indicates enlarged cell. Negative controls were used in the absence of primary antibody. Scale Bar, 25 µm. Magnification; 100x. **B)** Fluorescence intensity of β-catenin was determined by calculating the Corrected Total Cell Fluorescence [CTCF = Integrated intensity – (area x fluorescence mean)] using ImageJ. Data are represented as mean of 4 individual colonospheres under different conditions. Data are mean ± SD (***, $P < 0.001$). Experiment was repeated at least on two independent occasions.

It is widely acknowledged that the Wnt/β-catenin signalling plays a crucial role in the maintenance and homeostasis of intestinal stem cells. Importantly, β-catenin is required during embryogenesis while transiting from a pluripotent to a self-renewal state (Davidson et al., 2012). Also, studies suggests a dominant role for Wnt/β-catenin signalling in differentiation as opposed to self-renewal of hESCs, while some experimental data show that the relative level of Wnt/β-catenin signalling is significantly augmented in certain CSCs relative to bulk

cancer cells and implicated as a poor prognosis marker (Jang et al., 2015; López-Knowles et al., 2010).

Therefore, to further evaluate the role of FLYWCH1 in self-renewal and differentiation, the expression patterns of β-catenin in SW480 GFP^{+VE} and $FLYWCH1^{shRNA}$ derived colonospheres were investigated. In agreement to earlier report suggesting that FLYWCH1 is a negative regulator of Wnt/β-catenin signalling pathway (Figure 4-1 & Figure 4-2), GFP-$FLYWCH1^{shRNA}$ derived colonospheres exhibited an increased expression pattern of nuclear β-catenin relative to the control (Figure 4-6). However, although this result may suggest a role of FLYWCH1 in inhibition of differentiation, further validation with alternate differentiation markers is required.

Although numerous studies have confirmed ZEB1 as an EMT activator and promotor of tumour cell dissemination, recent studies also suggests ZEB1 facilitates migration of cancer stem cells by linking EMT-activation or cell polarity activation to initiate the transition of non-CSCs to CSC state (Chaffer et al., 2013; Li et al., 2012). Since it was reported that knockdown of FLYWCH1 expression augments ZEB-1 expression (Chapter 3), we sought to investigate the molecular relationship between FLYWCH1 loss-of-function effect and EMT and stemness properties. Colonospheres derived from SW480 GFP^{+VE} and $FLYWCH1^{shRNA}$ cells were stained with ZEB1 antibody and observed under fluorescent microscopy. It was observed that $FLYWCH1^{shRNA}$ colonospheres displayed a higher expression of ZEB1 relative to GFP^{+VE} colonospheres (Figure 4-7). This loss-of-function result indicates that FLYWCH1 may play a crucial role in regulation of cell polarity in CSCs.


A)
GFP
ZEB1
DAPI
Merge
GFP+VE
Negative Control
FLYWCH1shRNA
Negative Control

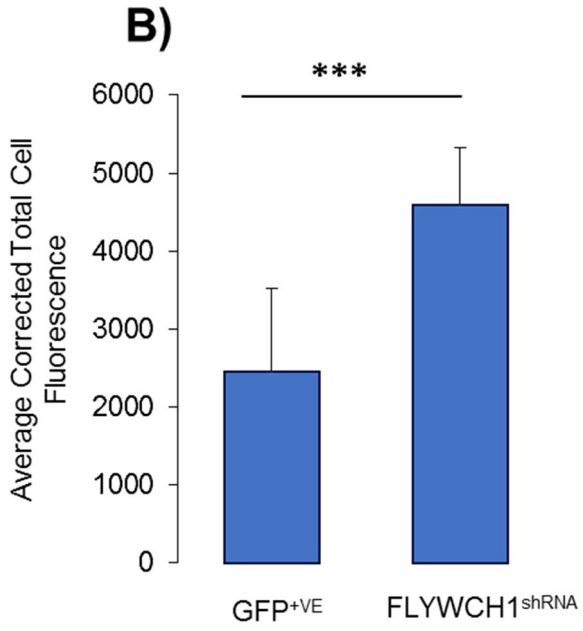
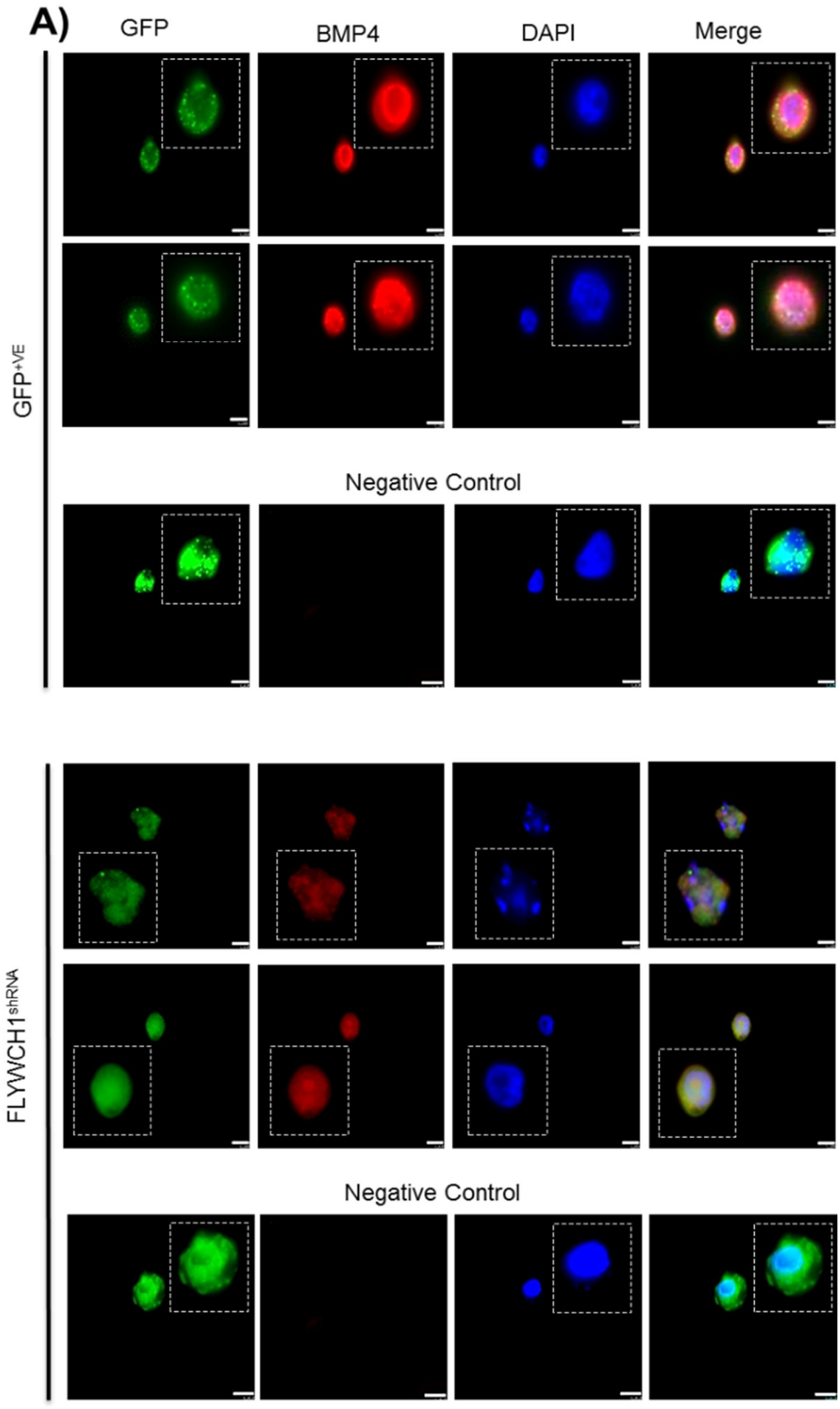


Figure 4-7: Knockdown of FLYWCH1 expression increases ZEB1 expression patterns. A) Colonospheres where fixed and stained with ZEB1 antibodies (red) followed by observation of expression patterns via immunofluorescence microscopy. Dotted lines indicates enlarged cell. Negative controls were used in the absence of primary antibody. Magnification; 100x. Scale Bar, 25 µm. **B)** Fluorescence intensity of ZEB1 was determined by calculating the Corrected Total Cell Fluorescence [CTCF = Integrated intensity – (area x fluorescence mean)] using ImageJ. Data are represented as mean of 4 individual colonospheres under different conditions. Data are mean ± SD (***, $P < 0.001$). Experiment was repeated at least on two independent occasions.

BMP4 belongs to the TGF-β superfamily of proteins. Like other bone morphogenetic proteins, TGF-β is primarily involved in bone and cartilage development and fracture repair. BMP4 facilitates differentiation resulting in the inhibition of intestinal stem cell self-renewal through suppression of Wnt/β-catenin signalling (He et al., 2004; Zhang et al., 2015b). Interestingly, studies have equally shown that BMP4 promotes differentiation with consequent inhibition of self-renewal properties (Zhang et al., 2012a). To investigate the

possible regulation of differentiation in CSCs by FLYWCH1, GFP^{+VE} and $FLYWCH1^{shRNA}$ derived colonospheres were stained with BMP4 differentiation marker and analysed under fluorescent microscopy. Results obtained revealed a reduction in BMP4 expression in $FLYWCH1^{shRNA}$ derived colonospheres relative to the control (Figure 4-8). This result is also in agreement with the expression patterns of β-catenin reported in (Figure 4-6) as BMP4 signalling is negatively regulated by Wnt/β-catenin signalling in the intestinal crypts (Krausova and Korinek, 2014). Taken together, this result further indicates that FLYWCH1 may promote differentiation.


A)
GFP
BMP4
DAPI
Merge
GFP+VE
Negative Control
FLYWCH1shRNA
Negative Control

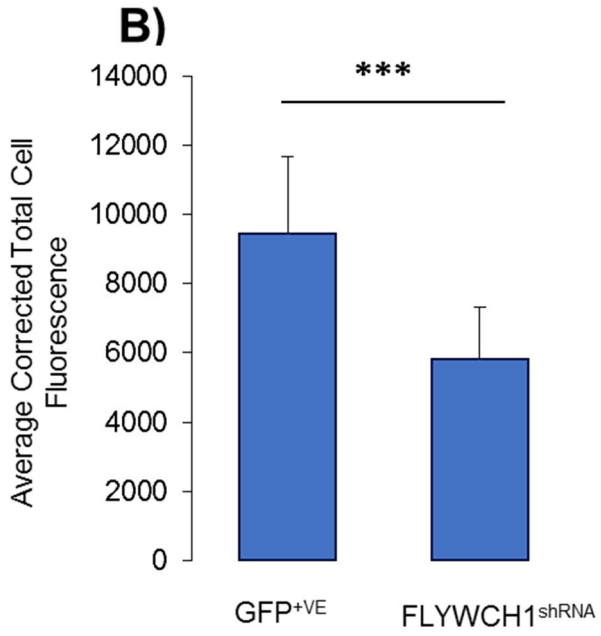
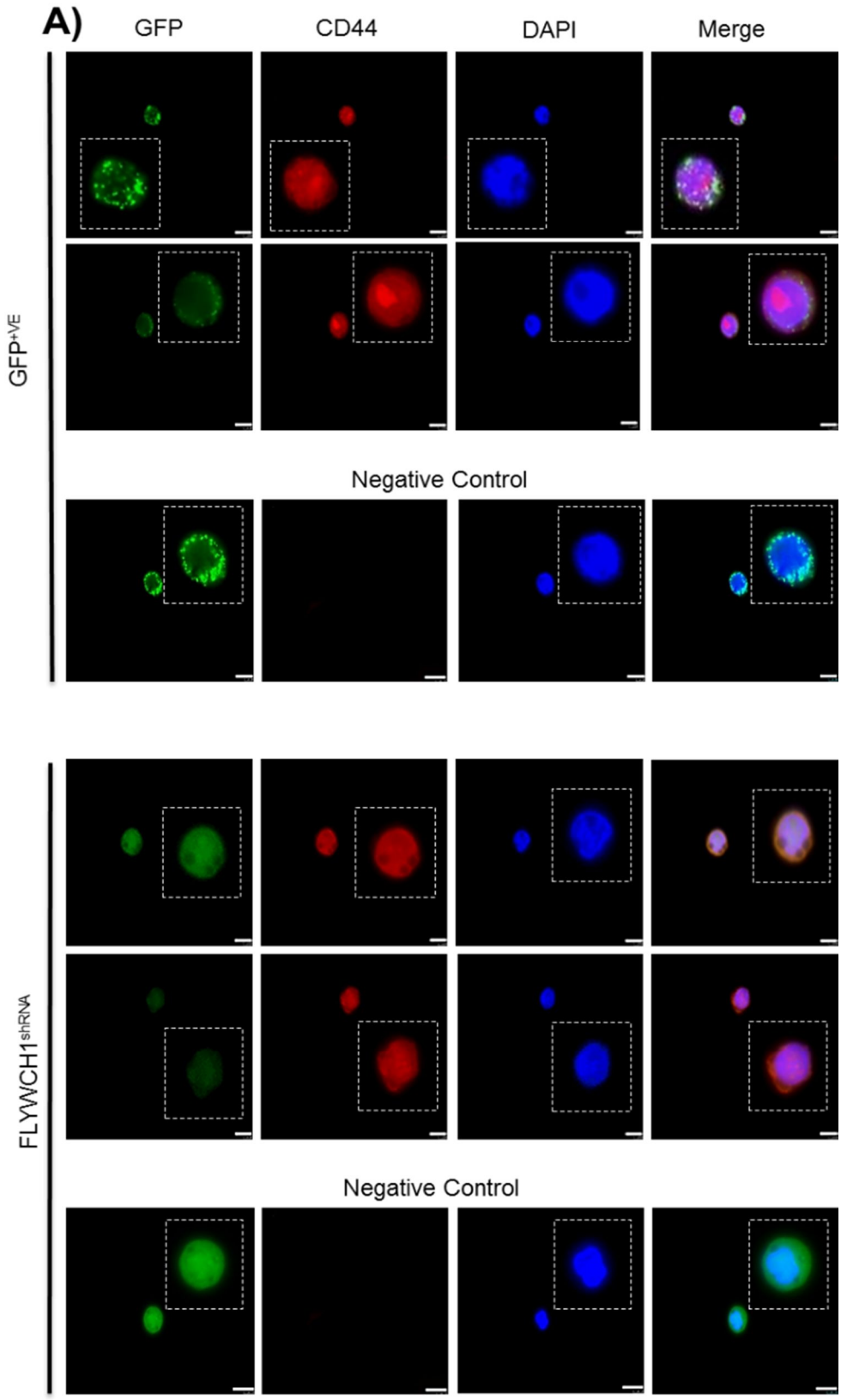


Figure 4-8: FLYWCH1 knockdown reduces BMP4 expression. **A)** Following culture and fixation on cover slips, BMP4 expression patterns were analysed in GFP^{+VE} vs $FLYWCH1^{shRNA}$ derived colonospheres. Dotted lines indicates enlarged cell. Negative controls were used in the absence of primary antibody. Magnification; 100x. Scale Bar, 25 µm. **B)** Fluorescence intensity of BMP4 was determined by calculating the Corrected Total Cell Fluorescence [CTCF = Integrated intensity – (area x fluorescence mean)] using ImageJ. Data are represented as mean of 4 individual colonospheres under different conditions. Data are mean ± SD (***, $P < 0.001$). Experiment was repeated at least on two independent occasions.

CD44, particularly CD44v isoforms are CSC surface markers and critical players in the regulation of CSCs properties including tumour initiation, metastasis, chemo/radio-resistance and self-renewal (Yan et al., 2015). Since studies have identified a feedback loop that employs CD44-mediated activation of ZEB1 expression to facilitate tumour-sphere initiation capacity (Preca et al., 2015), coupled with the observed increase in ZEB1 expression in $FLYWCH1^{shRNA}$

derived colonosphere we decided to investigate whether FLYWCH1 knockdown correlates to increased expression of CD44 stem cell marker.

Following staining of colonospheres with CD44 stemness marker, it was observed that FLYWCH1^{shRNA} derived colonosphere exhibited an increased expression pattern of CD44 relative to control GFP^{+VE} (Figure 4-9), thus suggesting FLYWCH1 may control self-renewal properties.


A)
GFP
CD44
DAPI
Merge
GFP+VE
Negative Control
FLYWCH1shRNA
Negative Control

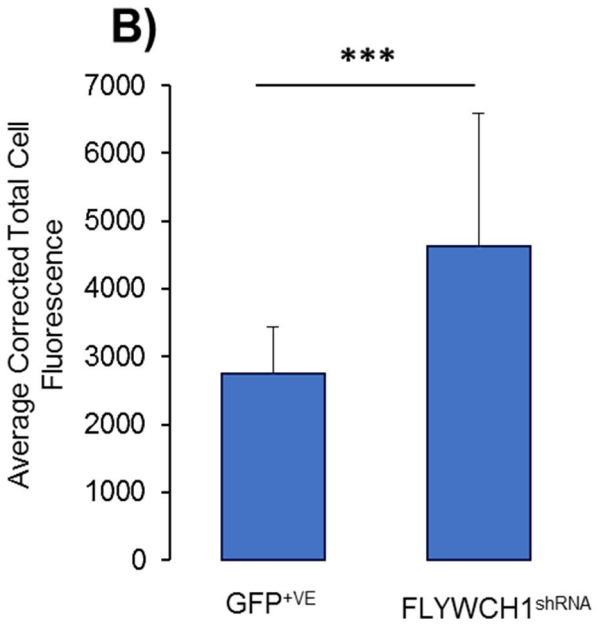
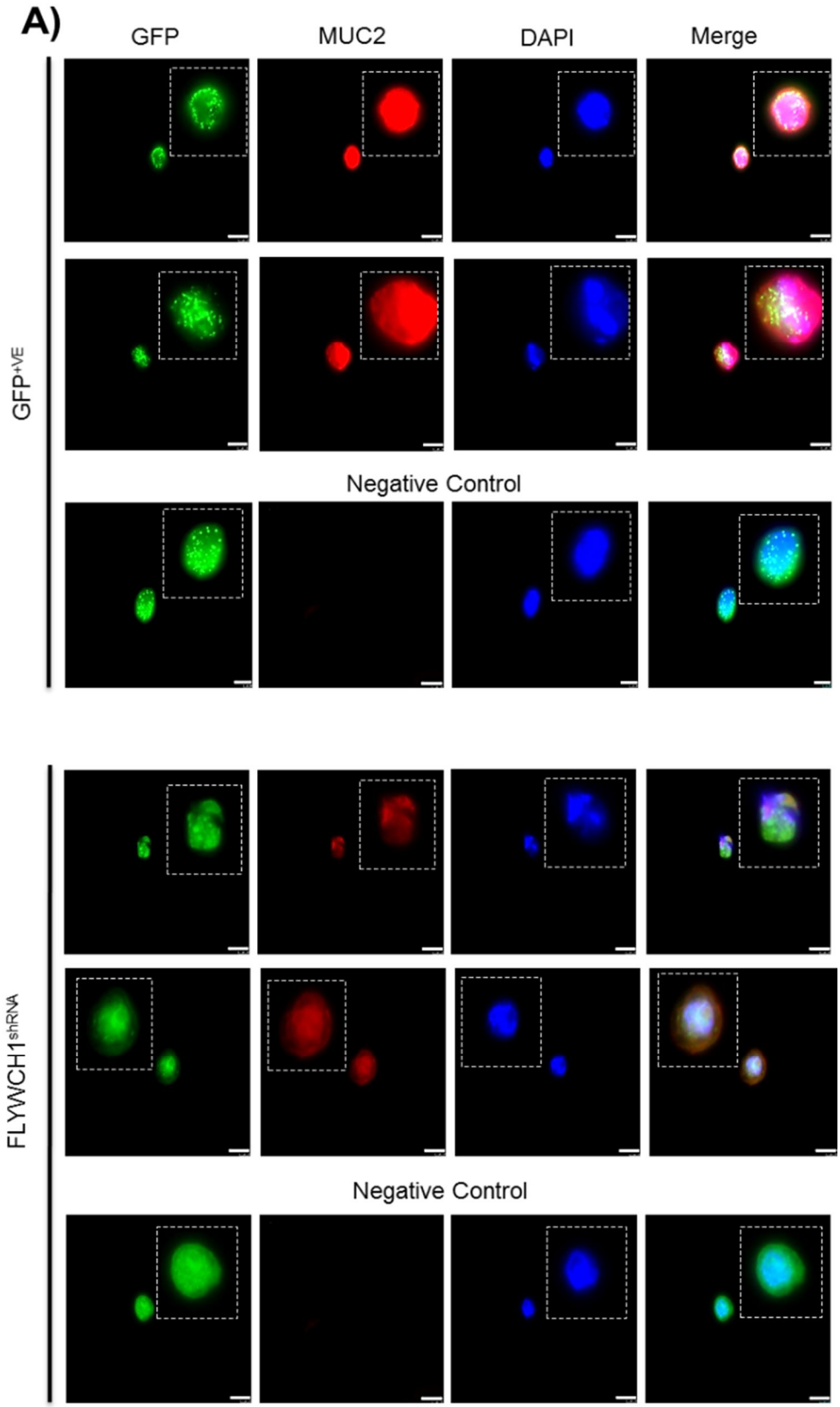


Figure 4-9: Knockdown of FLYWCH1 elevates CD44 expression. Colonospheres where fixed and stained with CD44 antibodies (red). The expression patterns were observed via immunofluorescence microscopy. Negative controls were used in the absence of primary antibody. Dotted lines indicates enlarged cells. Magnification; 100x. Scale Bar, 25 µm. **B)** Fluorescence intensity of CD44 was determined by calculating the Corrected Total Cell Fluorescence [CTCF = Integrated intensity – (area x fluorescence mean)] using ImageJ. Data are represented as mean of 4 individual colonospheres under different conditions. Data are mean ± SD (***, P < 0.001). Experiment was repeated at least on two independent occasions.

The marker MUC2 is an intestinal-type mucin, ordinarily is expressed in normal goblet cells of the small intestine and colon (McIntire et al., 2011) in addition to be associated with epithelial differentiation (Zhou et al., 2015).

In order to evaluate the role of FLYWCH1 in modulating differentiation properties in isolated potential CSCs, the differentiation capabilities of colonospheres derived from SW480 GFP^{+VE} and $FLYWCH1^{shRNA}$ cells were examined with MUC2 differentiation marker under fluorescence microscopy. As shown in (Figure 4-10), the expression levels of MUC2 in $FLYWCH1^{shRNA}$

colonospheres is reduced relative to control counterparts. This result may suggest the involvement of FLYWCH1 in CSCs differentiation processes and a negative regulator of CSC expansion.


A)
GFP
MUC2
DAPI
Merge
GFP+VE
Negative Control
FLYWCH1shRNA
Negative Control

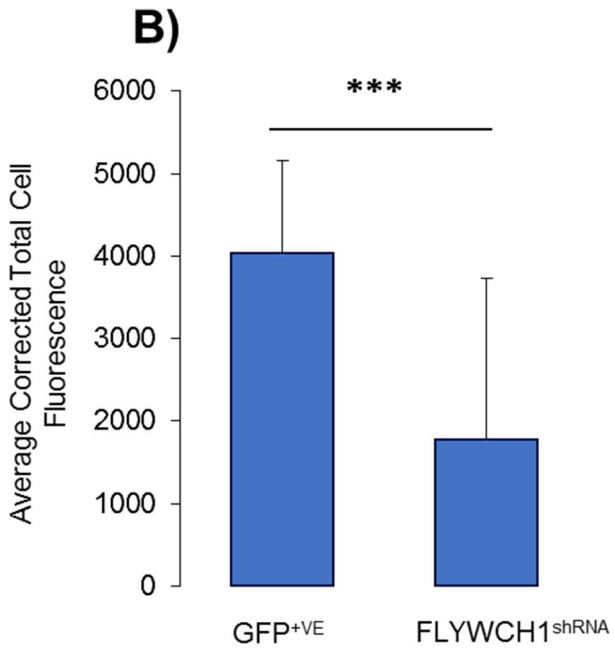


Figure 4-10: Knockdown of FLYWCH1 expression reduces expression of differentiation marker, MUC2. **A)** Following culture and fixation, colonospheres were stained with the expression patterns of MUC2 compared in GFP^{+VE} vs $FLYWCH1^{shRNA}$ were analysed. Dotted lines indicates enlarged cell/s. Dotted lines indicates enlarged cells. Magnification; 100x. Scale Bar, 25 µm. **B)** Fluorescence intensity of MUC2 was determined by calculating the Corrected Total Cell Fluorescence [CTCF = Integrated intensity – (area x fluorescence mean)] using ImageJ. Data are represented as mean of 4 individual colonospheres under different conditions. Data are mean ± SD (***, $P < 0.001$). Experiment was repeated at least on two independent occasions.

4.3 Discussion

The β-catenin nuclear interactors are critical factors that play key roles in gene regulation governed by the Wnt/β-catenin signalling pathway. Following initial characterization of FLYWCH1 in our lab (Muhammed et al., submitted), suggesting the possibility that FLYWCH1 may possess nuclear transcription factor abilities thereby regulating the transcription of other genes, the current work was aimed at establishing the mechanistic role involved in the FLYWCH1-mediated changes in cell morphology. In addition, the mechanism underlying the FLYWCH1-mediated negative regulation of the Wnt/β-catenin signalling pathway was also investigated.

The tumour suppressor role of GSK-3β in Wnt/β-catenin activity is negated due to the presence of mutations in APC or β-catenin, recognised as the most frequently selected mutations in CRC. Hence, the normal effect of GSK-3β activity is suppressed and ON-state activity of Wnt signalling is inappropriately reactivated, stimulating tumour development. As previously described, these mutations result to cytoplasmic and nuclear β-catenin stabilization with subsequent activation of gene transcription, promoting cell proliferation (Wantae et al., 2013). In the current study, the different expression patterns of Wnt/β-catenin signalling components observed in the presence and absence of FLYWCH1 (Figure 4-1 & Figure 4-2) speaks volumes in the sense that it shows that despite FLYWCH1 been a nuclear protein, it may facilitate the degradation of β-catenin. Furthermore, FLYWCH1 may also aid in the prevention of cytoplasmic β-catenin stabilization by increasing levels of E-cadherin as reported in (Chapter 3), which subsequently recruits and associates with β-

catenin to form the E-Cadherin/β-catenin complex, thus preventing its translocation to the nucleus. The E-Cadherin/β-catenin complex plays a critical role in maintaining cell-cell adhesion, cell shape as well as epithelial integrity thereby preventing cell migration (Kim et al., 2002; Nawshad et al., 2007), nevertheless, further studies are required to explore these possibilities.

The role of FLYWCH1 as an antagonist of Wnt signalling was affirmed due to its activation of the GSK3β enzyme (Figure 4-1), thus implicating FLYWCH1 in the regulation of the phosphorylation-dependent destruction of β-catenin. Additionally, pharmacologic inhibition of GSK-3β activity have shown to facilitate β-catenin stabilization and activation of β-catenin and TCF-dependent gene transcription (Jope, 2003; Wu and Pan, 2010) while studies have also shown that phosphorylation of GSK-3β at Ser-9 confers cisplatin resistance to ovarian cancer cells (Cai et al., 2007). Data presented showing that exogenous expression of FLYWCH1 promotes repression of inactive GSK-3β in CRC cell lines provides fascinating insight on the mechanistic role of FLYWCH1 in the Wnt/β-catenin signalling pathway (Figure 4-11). Furthermore, several studies indicate the abundance of nuclear GSK-3β (Caspi et al., 2008; Medina and Wandosell, 2011), thus making it possible for FLYWCH1 to participate in direct interaction with GSK-3β in the nucleus.

Furthermore, the studied effect of FLYWCH1 on GSK-3β activity may be easily unravelled following appreciation of the elusive role of GSK-3β in tumorigenesis, owing to its role in multiple signalling pathways. In contrast to its tumour suppressor role in Wnt/β-catenin signalling, GSK-3β promotes cell proliferation in colon and prostate cancer (Hoesel and Schmid, 2013). Since β-catenin accumulation is a hallmark of CRC, these sets of results (Figure 4-1 &

Figure 4-2) may prove that FLYWCH1 protein can be utilized as a therapeutic agent with GSK-3β (S9) being the target. We also provide more evidence of a FLYWCH1-mediated GSK-3β-activation via the SRB survival assay (Figure 4-3 A - D). The study also indicates a possible competition between FLYWCH1 and TDZD-8 via the SRB survival assay, which showed a delayed response to TDZD-8 in SW480 GFP-FLYWCH1$^{O/E}$ cells (IC_{50} = 91.3 μM) compared to those expressing GFP (IC_{50} = 26.35 μM). The values indicate that a greater concentration of TDZD-8 is needed to inhibit cell survival activity by 50% in SW480 GFP-FLYWCH1$^{O/E}$ cells, confirming the delayed response to TDZD-8. It is likely that the change in response of SW480 cells to TDZD-8 in the presence of FLYWCH1 is due to a possible competition in physical/biochemical interaction between FLYWCH1 and the drug molecule. Whilst TDZD-8 binds to and blocks the tyrosine 216 residue leading to GSK-3β inactivation (Martinez et al., 2002), FLYWCH1 opposingly induces GSK-3β activation. FLYWCH1 may bind to the tyrosine 216 residue, thus competing with TDZD-8 for interaction with GSK-3β. The multifunctional behaviour of the GSK3β enzyme in numerous signalling pathways including Wnt, PI3K/AKT and NF-kB signalling (Maurer et al., 2014), needs further investigation to explore mechanisms of possible FLYWCH1 and GSK-3β interlinking activities. However, since it is evident that FLYWCH1 shares its function as an antagonist of Wnt/β-catenin activity with many other molecules, further investigation of these molecules may aid in understanding FLYWCH1's activity in CRC cells, as they may act in a complex network to modulate Wnt/β-catenin activity.

This study supplements recent findings in our lab suggesting that FLYWCH1 specifically binds to the N-terminal domain of β-catenin to repress transcription

of β-catenin target genes (Muhammad et al., submitted). The N-terminal domain of β-catenin contains the GSK-3β phosphorylation sites, it is also plausible to suggest that FLYWCH1 may specifically facilitate GSK-3β-mediated phosphorylation of Ser-33, Ser-37, and Thr-41. Due to its complex mechanism involved in modulating a plethora of cellular activities ranging from roles played in cell-cell adhesion to regulation of Wnt-driven transcription in normal and abnormal conditions, Wnt/β-catenin signalling pathway is negatively regulated by a variety of proteins. Alternatively, these regulatory proteins, including FLYWCH1, may interact in a complex network to execute negative regulation of Wnt/β-catenin activity (Figure 4-11).

Remarkably, β-catenin-interacting antagonist belonging to the zinc-finger protein family has been identified, displaying remarkable similarities to FLYWCH1. For instance, Glis2 reduces β-catenin/TCF-mediated transcriptional activity in HCT116 CRC cells (Kim et al., 2007). Additionally, Idax, which contains the CXXC-type zinc finger domain has been implicated in the negative regulation of the Wnt/β-catenin signalling pathway (Ko et al., 2013; Kojima et al., 2009). These finding suggests that the zinc-finger binding motif may be essential to FLYWCH1's ability to antagonise Wnt/β-catenin activity. Non-β-catenin-interacting proteins also regulate the Wnt/β-catenin activity. It is well established that the zinc-binding motif allows zinc-finger proteins to bind to DNA, RNA or other proteins (Krishna et al., 2003a). Whilst Glis2, Idax and FLYWCH1 both antagonise Wnt/β-catenin activity, FLYWCH1 does so by direct interaction with β-catenin whilst Idax binds to Dishevelled, another component protein activating Wnt signalling, leading to inhibition of β-catenin/TCF activity in L cells (Hino et al., 2001). However, more screening

methods such as affinity-tagged proteins, mass spectrometry, protein crystallography as wells as computational structure–function predictions approaches amongst others may yield valuable insight into further elucidation of FLYWCH1 and/or β-catenin proteins.

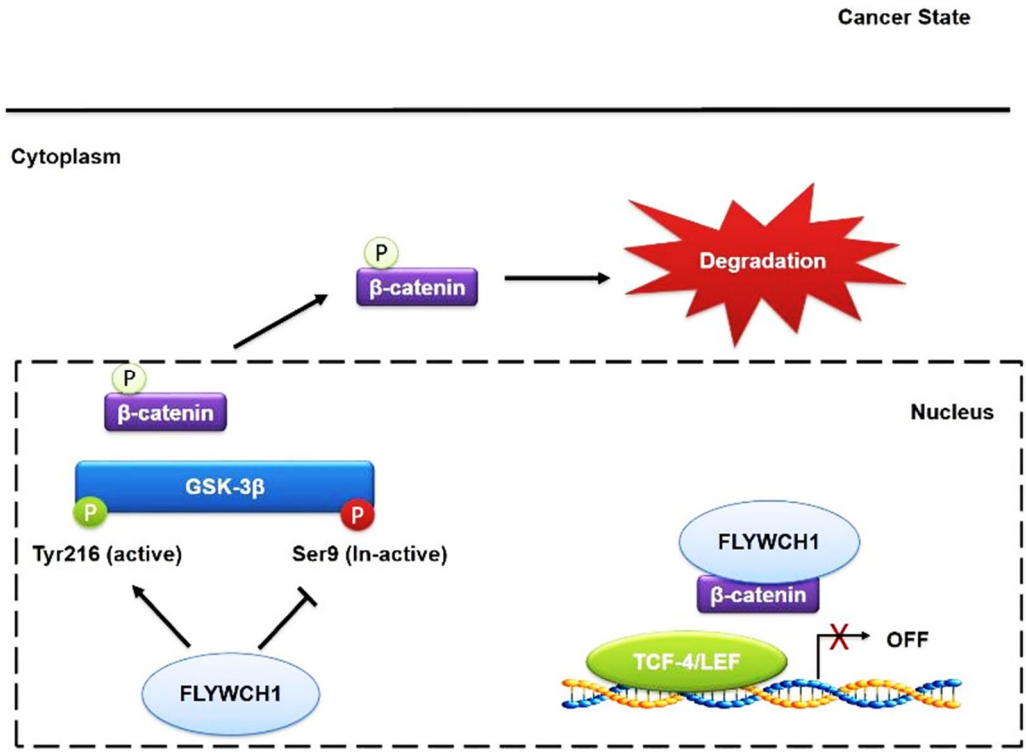


Figure 4-11: Proposed model illustrating the involvement of FLYWCH1 in the regulation of Wnt/β-catenin signalling in cancer state. Activation of nuclear GSK-3β results to phosphorylation of β-catenin, which subsequently translocate to the cytoplasm to undergo proteosomal degradation. In addition, previous studies in our lab suggests a direct interaction between FLYWCH1 and β-catenin could disrupt formation of β-catenin/TCF4 complex thereby preventing the transcription of Wnt target genes that drive cancer and tumour formation (Muhammed et al., submitted).

GSK-3β, a multi-functional serine/threonine kinase that participates in the maintenance of oncogenic transcriptional factors via phosphorylation, with its inactivation been implicated in various tumours (Al-Mulla et al., 2011; Thornton

et al., 2008). Additionally, GSK-3β has also been implicated in EMT processes, either directly or indirectly (Atkins et al., 2012; Kao et al., 2014). The activity of GSK-3β is essential for the preservation of the epithelial architecture as experimental evidence show that pharmacological inhibition of its activity in normal skin and breast epithelial cells results in the manifestation of features associated with EMT (Bachelder et al., 2005). Hence, growth and survival of certain cancer forms such as adenocarcinoma and melanoma is a consequence of deregulated GSK-3β expression and activity as indicated by various *in-vivo* and *in-vitro* studies (Bellei et al., 2008; Chien et al., 2009). Although the exact mechanistic role of GSK-3β in alteration of cell morphology is still poorly understood, the current study was aimed to investigate whether the FLYWCH1-mediated cell morphology changes occur in a GSK-3β dependent manner in SW480 cells. Results however showed that the epithelial-like morphology of SW480 cells ectopically expressing FLYWCH1 remained unchanged following treatment with TDZD-8 (Figure 4-4, bottom panel). However, some morphological changes were observed in SW480 GFP^{+VE} cells treated with 30-60µM of TDZD-8 (Figure 4-4, top panel). This is in agreement with studies implicating GSK-3β in morphological alteration processes in cancer cells (Kubic et al., 2012). These data suggest that FLYWCH1 may modulate alterations in cell morphology in a GSK-3β-independent manner.

The controversial CSC theory is based on the phenomenon that cancer cells may be derived from a rare population of cells also described as cancer stem cell-like cells (CSCLCs) possessing stem cell properties (Beck and Blanpain, 2013; Ibrahim et al., 2012a; Nguyen et al., 2012). CSC have since been identified in squamous skin tumours (Driessens et al., 2012), glioblastomas (Chen et al.,

2012) and intestinal adenomas (Schepers et al., 2012). Experimental evidence from multiple studies suggests that CSCs possess a variety of biological properties similar to normal somatic stem cells such as the self-renewal capability, an integral program for tissue renewal and regeneration. The Wnt pathway, among other pathways, plays crucial roles in the regulation of stem cell/progenitors, cell self-renewal and maintenance in a plethora of systems. Recent studies have established the importance and significant roles played by the canonical Wnt signalling in stem cell self-renewal activities in various tissues and cell types (Yang et al., 2015a). For instance, Wnt3a was shown to contribute to the activation of Wnt signalling and subsequent stimulation of self-renewal properties of mouse embryonic stem cells (ESCs) (Merrill, 2012). Canonical Wnt pathway activation was shown to augment alkaline phosphatase and Cbfa1/Runx2 expression thereby facilitating mesenchymal stem cells (MSCs) osteogenic differentiation (Day et al., 2005; Kim et al., 2013a). Canonical Wnt signalling is also crucial for differentiation and maintenance of the intestine as several scientific evidence have identified the expression of Wnt receptors and ligands such as LRP5, SFRP5, Wnt3/6, Fzd4/6/7 in epithelial cells located at the intestinal crypt base (Gregorieff et al., 2005; Yang et al., 2015a). Hence, perturbation of the pathways controlling stem cell renewal particularly the Wnt signalling pathway contributes significantly to neoplastic transformation.

CSCs that possess self-renewal capacity as well as the potential to differentiate into various cell lineages abundant in cancerous tissues are functionally characterized by a high Wnt pathway activity (Prasetyanti et al., 2013; Vermeulen et al., 2008). As results shown suggests FLYWCH1 as a negative regulator of β-catenin, a central transducer of the canonical Wnt signalling

pathway as well as a positive regulator of let-7 (Chapter 5), the current study was aimed at investigating the role of FLYWCH1 in regulating stem cell properties in CSCs by adopting a colonosphere culture model approach. We reveal, through loss-of-function studies that FLYWCH1 may negatively regulate the growth and proliferation of CSCs (Figure 4-5). Therefore, the role of FLYWCH1 in differentiation and stemness capacities of colonospheres were examined by immunofluorescence assay.

We show that FLYWCH1^{shRNA} derived colonospheres exhibited a high expression of ZEB1 relative to the control (Figure 4-7). Notably, experimental evidence show that the embryonic EMT program can be triggered in cancer cells, resulting to the initiation of metastasis and dissemination, as well as acquisition of stemness properties promoting migration of CSC-phenotype (Lehmann et al., 2016). Metastasis and invasion of carcinomas are frequently activated by induction of aberrant EMT processes mainly driven by the transcription factor ZEB1, enhancing tumour-initiating potential associated with elevated expression of the putative stem cell marker CD44 (Preca et al., 2015). The current study not only reveals the possible role of FLYWCH1 in regulation of stemness properties but it is also in agreement with the possible inverse relationship between FLYWCH1 and ZEB1 reported in (Chapter 3). Furthermore, FLYWCH1^{shRNA} derived colonospheres also showed an elevated expression of β-catenin and a reduced expression of BMP4 differentiation marker (Figure 4-6 & Figure 4-8). Wnt ligands, receptors and inhibitors alike are differentially expressed along the intestinal crypt-villus axis and serve as key stem cell niche factors that govern stem/progenitor cell self-renewal, differentiation, proliferation and migration. For instance, both the canonical and non-canonical Wnt pathway have been

implicated in providing survival and proliferation signals in intestinal epithelium with active Wnt signalling observed in the proliferative compartment while active BMP signalling is observed in the differentiated compartment of the intestinal crypt (Gregorieff and Clevers, 2005; Kosinski et al., 2007). Additionally, the expression patterns of BMP4 observed in FLYWCH1^{shRNA} derived colonospheres vs controls (Figure 4-8) further lays credence to the possible FLYWCH1-mediated regulation of let-7 (reported in Chapter 5). Several studies have identified let-7 miRNA as a regulator of stemness by promoting differentiation and repressing self-renewal in both normal development and cancer state (Yi and Fuchs, 2011). MUC2, another differentiation marker was also downregulated upon knockdown of FLYWCH1 expression (Figure 4-10). This results, therefore uncovers a potential Wnt/β-catenin/BMP/FLYWCH1 crosstalk involved not only in delaying CSC formation but also in the regulation of differentiation.

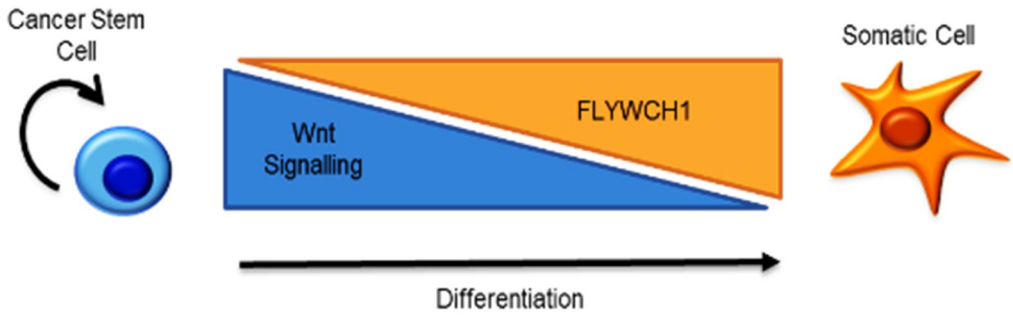


Figure 4-12: Opposing roles of FLYWCH1 on Wnt/β-catenin signalling. Wnt signalling levels identify with stem-like tumour cells that are responsible for promoting tumour growth with tumour suppressor FLYWCH1 having an opposing effect. Chapter 5 discusses FLYWCH1 positive regulation of let-7.

The prevalence of multiple isoforms of CD44 in specific cancer cells has been well documented. Ordinarily, binding of hyaluronic acid (HA) to CD44 receptors regulates stem cells homing (Basakran, 2015). In cancer state, HA (the primary ligand for CD44) is synthesized by CSC to attract tumour-associated macrophages (TAM) in the CSC niches that provide oncogenic growth factors and promote invasiveness (Okuda et al., 2012). Therefore, CD44 has been established as an early diagnostic marker for neoplastic stem cell proliferation in cancers such as, but not restricted to chronic cell leukaemia (Zhang et al., 2013b), colon (Ishimoto et al., 2011), breast (Olsson et al., 2011) and prostate cancers. CD44 also plays a crucial role in cancer development, partly through control of EMT and other pathways (Xu et al., 2015a). The potential FLYWCH1-mediated negative regulation of CD44 expression in colonospheres (Figure 4-9) may indicate a key role in negatively regulating CSCs since multiple evidence suggests an enrichment of CD44 expression in CSCs which are mainly responsible for drug resistance, cancer aggressiveness and tumour relapse (Yan et al., 2015).

Taken together, the data presented in this chapter concludes that FLYWCH1-mediated morphology changes may occur in a GSK-3β independent manner. FLYWCH1 may also negatively regulate β-catenin activity via activation of GSK3β. Based on these data, expression patterns of CD44, ZEB1, β-catenin, MUC2 and BMP4 suggests that FLYWCH1 may also play an important role in the regulation of stemness activity in CSCs by probably restricting self-renewal capacity (Figure 4-12), although analysis of other self-renewal and differentiation marker is highly required to determine the mechanistic role of FLYWCH1 in the regulation of CSC propagation. Additionally, drugs that may

selectively activate FLYWCH1 to stabilize the GSK-3β/β-catenin destruction complex in CRC cells require extensive investigation. Nevertheless, FLYWCH1's role as an antagonist of Wnt/β-catenin activity remains intriguing, as deregulation of Wnt/β-catenin signalling is a prominent feature in colorectal carcinogenesis, making FLYWCH1 a principal target for future colorectal cancer research.

5 CHAPTER 5

Regulation of microRNAs (miRNAs) expression by FLYWCH1

5.1 Brief Introduction

Changes in cell morphology through actin cytoskeleton re-organization and filopodia formation reported in chapter 3, can be mediated by FLYWCH1 and its cofactors. Therefore, we investigated whether alteration of cell morphology caused by FLYWCH1 correlates to mechanism(s) associated in formation of different foci (e.g.; DNA damage foci, chromatin foci, RNA foci and/or nucleolar foci) as distributed by FLYWCH1 protein expression formation foci all over the nucleus (Chapter 3).

In the present chapter, we report via immunofluorescence assay that FLYWCH1 co-localizes with splicing factor 'SC35', although further validation procedures using different luciferase reporter construct suggests no direct involvement of FLYWCH1 in splicing activity. However, more recent reports suggested that these foci besides its role in splicing, are also involved in the RNA and non-coding RNA synthesis such as microRNAs (miRNAs). miRNAs have been identified as not only important regulators of control and developmental processes such as cell proliferation and cell fate determination but also acts as a tumour suppressor and proven to improve overall prognosis in cancer patients (Jansson and Lund, 2012).

Let-7 is one of the most highly conserved miRNAs in animals and is negatively regulated by LIN28 in undifferentiated cells as well as in cancer. Numerous studies have revealed that expression levels of let-7 are generally reduced in cancer state when compared with normal tissues (Osada and Takahashi, 2011). Let-7 and LIN28 establish a double-negative feedback loop that influence a plethora of biological processes ranging from differentiation of stem cell, to

invasion and metastasis, and tumorigenesis (Friedman and Burge, 2014; Piskounova et al., 2008; Zhang et al., 2014b). Let-7 is also generally regarded as a tumour suppressor by either direct/indirect repression of key oncogenes and regulators of the mitogenic pathways (Barh et al., 2010). On one hand, while the regulation of Let-7 miRNAs by LIN28 have been well documented, the action/s of LIN28 proteins on other RNAs still remains unclear (Madison et al., 2013). Experimental studies also reveal that LIN28 proteins are frequently up-regulated in various malignancies originating from three germ layers with let-7 having an opposite effect (Viswanathan et al., 2009; Wang et al., 2015).

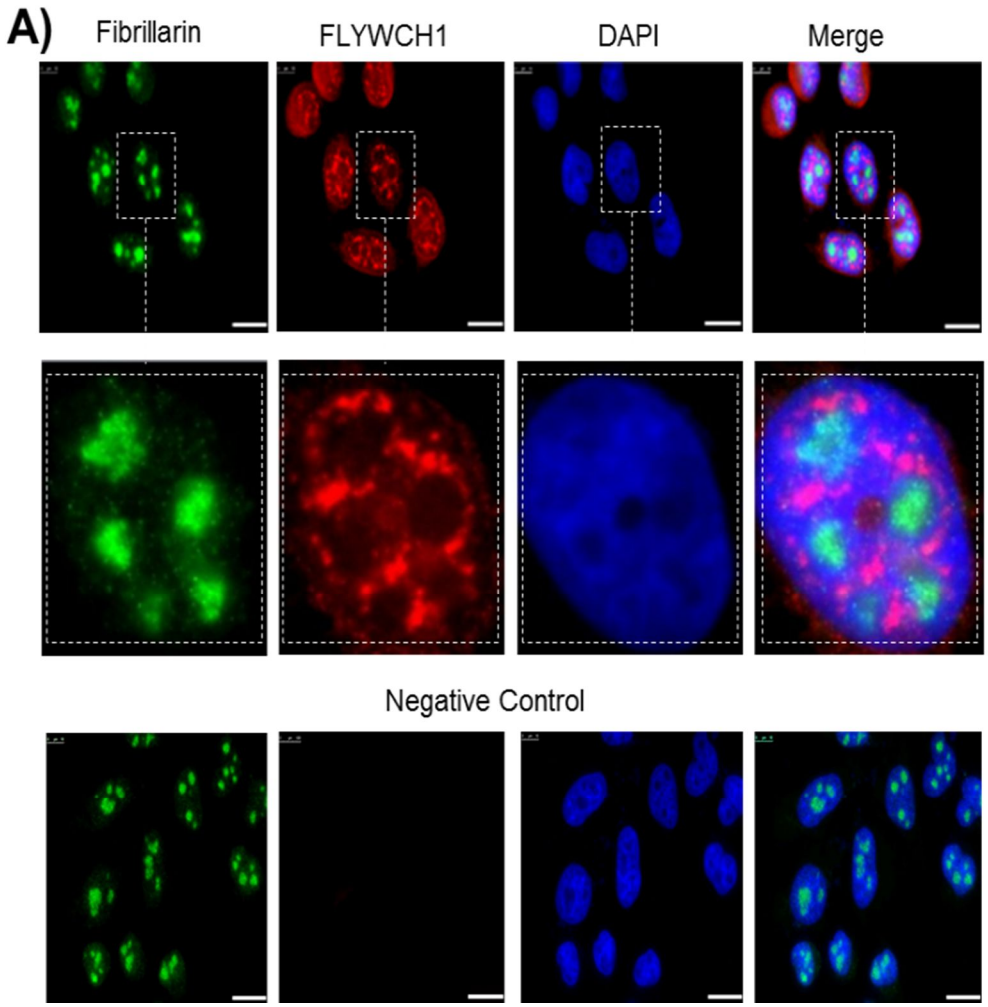
Since studies reveal that enforced expression of let-7 significantly inhibits cancer cell motility by affecting actin dynamics (Hu et al., 2013b), coupled with the FLYWCH1-mediated morphological changes reported in chapter 3, the current data suggest that FLYWCH1 may regulate cancer cells via modulating the let-7 miRNA expression in a LIN28 dependent manner.

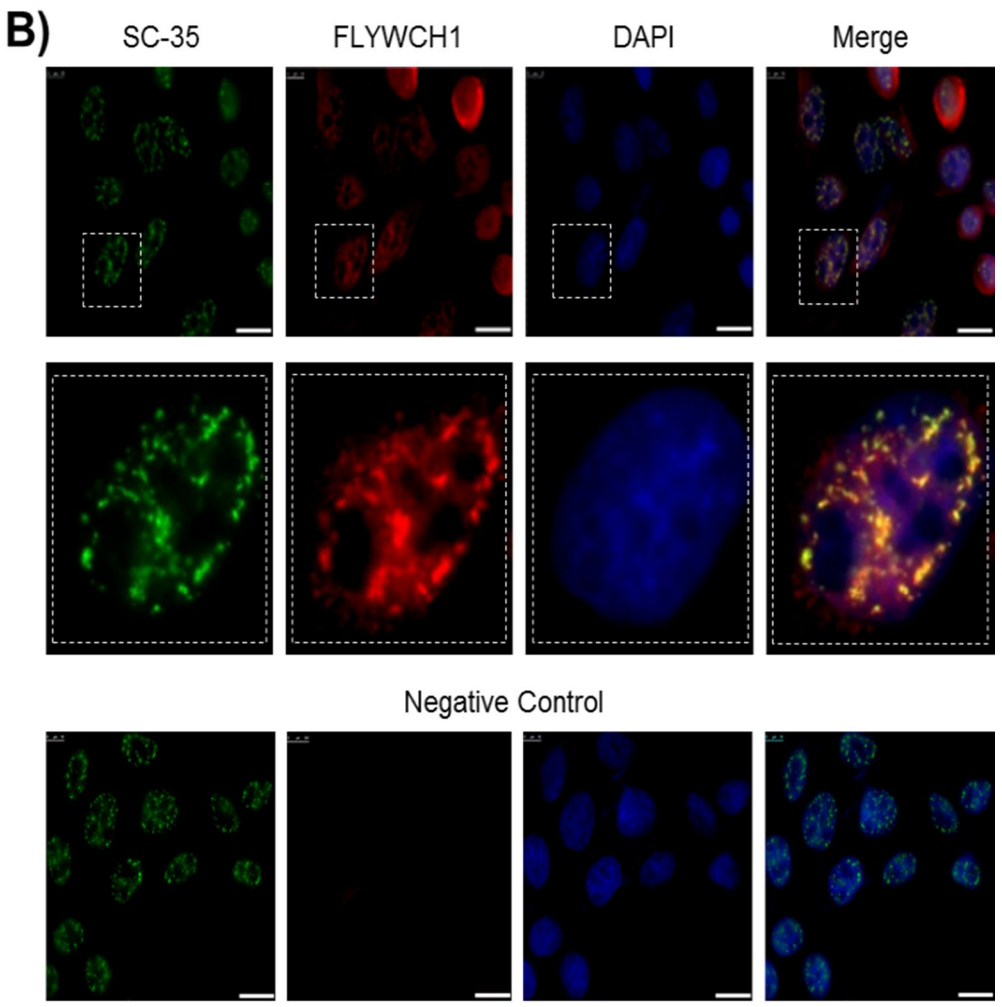
5.2 Results

5.2.1 The FLYWCH1 nuclear speckles co-localizes with nuclear splicing factor “SC35” and partially with heterochromatin marker, HP1α

To determine the cellular localization of FLYWCH1, immunofluorescence assay was initially performed (Chapter 3, Figure 3-1). Confirmation of protein nuclear localization prompted co-localization assays with anti-Fibrillarin antibody (nucleolar marker), a component of a nucleolar small nuclear ribonucleoprotein

(snRNP) particle thought to participate in the first step in processing pre-ribosomal RNA (Amin et al., 2007; Yanagida et al., 2004) however, these two proteins did not show any co-localization (Figure 5-1 A & C). Next, we applied the anti-SC-35 antibody (nuclear speckle), a member of the serine/arginine (SR)-rich family of pre-mRNA splicing factors, which constitute part of the spliceosome (Tripathi et al., 2012). These analysis showed significant co-localization between FLYWCH1 and SC-35 protein (Figure 5-1 B & C).


A)
Fibrillarin
FLYWCH1
DAPI
Merge
Negative Control


B)
SC-35
FLYWCH1
DAPI
Merge
Negative Control

.

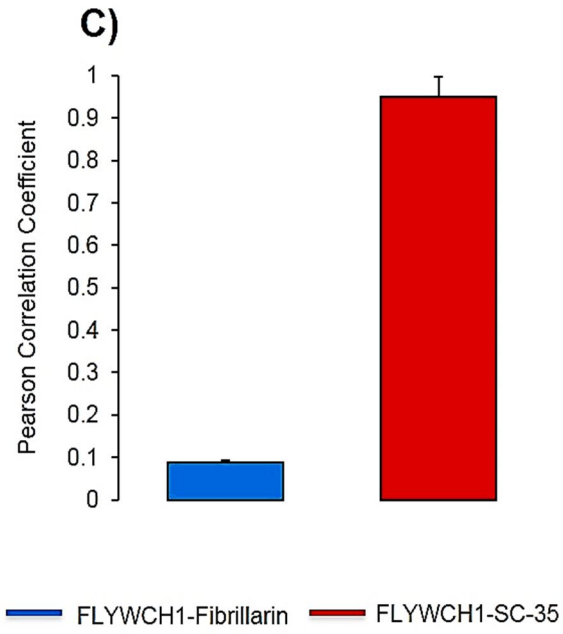
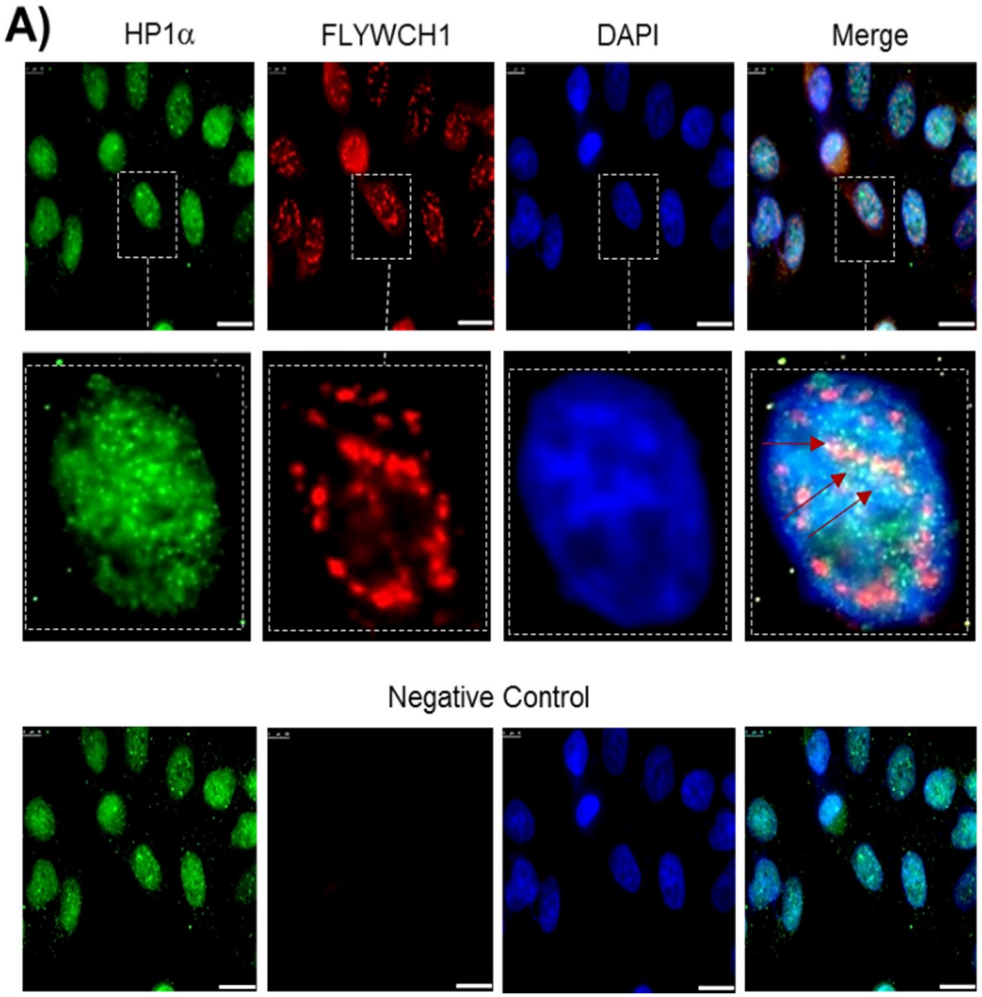


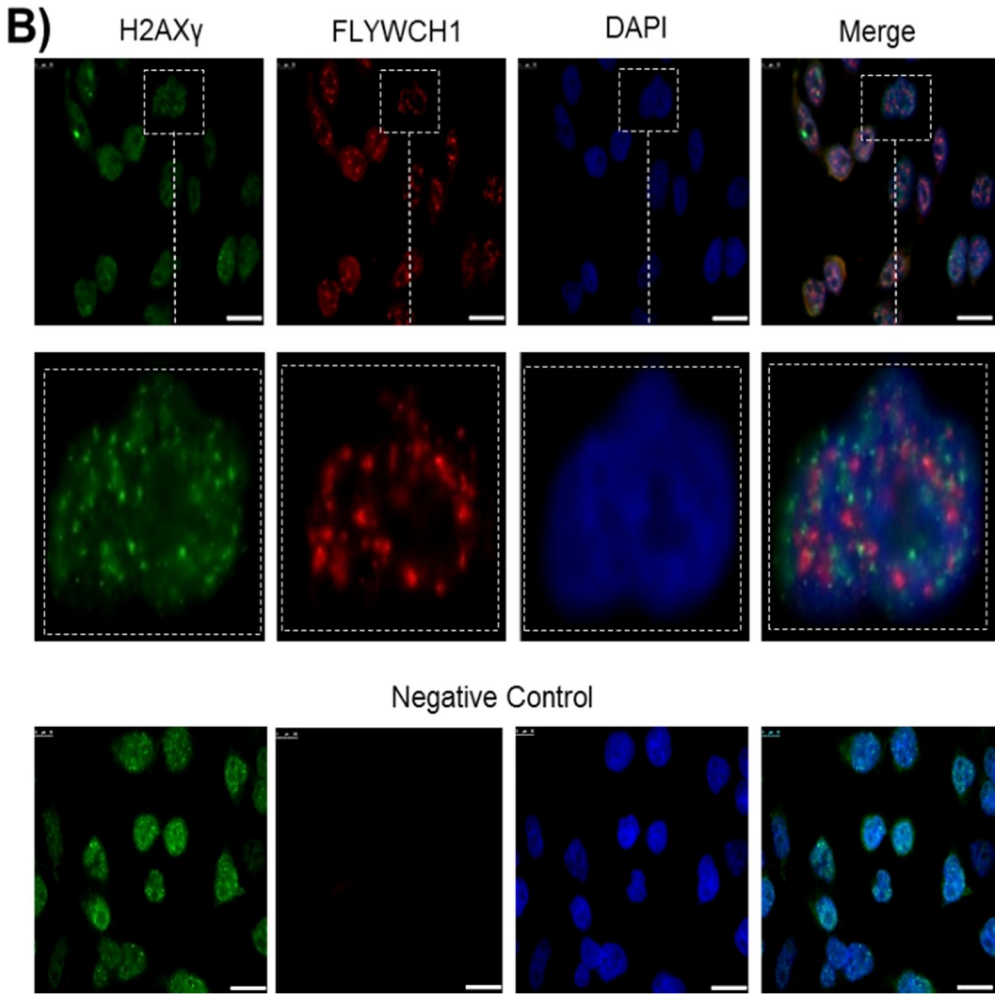
Figure 5-1: FLYWCH1 co-localizes with nuclear splicing factor 'SC35' but not with Fibrillarin. Immunostaining showing endogenous expression of FLYWCH1 (Red) in TIG119 cells does not co-localize with **A)** Fibrillarin. **B)** Co-localization between FLYWCH1 (red) and SC-35 splicing factor (green). Dotted lines indicates enlarged cell/s. Negative controls were used in the absence of primary antibody. Scale bars, 10 µm. Magnification: 100x. **C)** Quantitative analysis of co-localization using Pearson Correlation Coefficient (PCC) with ImageJ. PCC of 30 individual cells were determined. Data are represented as mean of PCC of 30 individual cells +/- SD.

Furthermore, FLYWCH1 co-localization assays were also performed with anti-HP1α antibody (Heterochromatin marker), a member of the heterochromatin protein family which is associated with centromeres (Chu et al., 2014). Strikingly, a fraction of the FLYWCH1 foci co-localizes with HP1α foci (Figure 5-2 A & C). Then, we examined if FLYWCH1 nuclear speckles co-localizes with the phosphorylated H2AX (anti-H2AXγ antibody) which appear specifically at the damaged sites containing DNA double-strand breaks (DSBs) (Sharma et al., 2012). However, we show no co-localisation between

FLYWCH1 and H2AXγ foci (Figure 5-2 B & C). Nevertheless, it's interesting to study FLYWCH1 subcellular localization after the DNA-damage repair signalling pathway is activated by irradiating of cells to DNA damage agents and also whether the partial co-localisation of FLYWCH1/HP1α are significant in modulating the chromatin activity.

These sub-cellular co-localization of FLYWCH1 and SC-35 data led to a hypothesis that FLYWCH1/SC-35 complex protein may regulate the RNA-splicing activity.


A)
HP1α
FLYWCH1
DAPI
Merge
Negative Control


B)
H2AXγ
FLYWCH1
DAPI
Merge
Negative Control

.

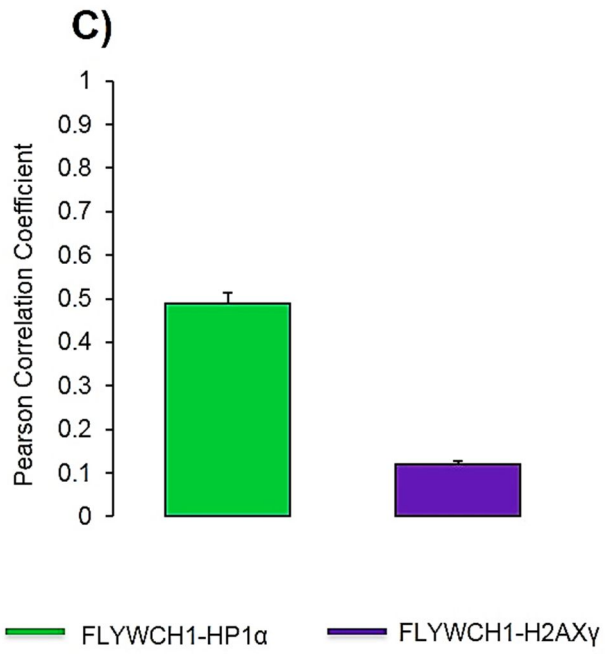


Figure 5-2: FLYWCH1 partially co-localizes with HP1α but not with H2AXγ. Immunostaining showing endogenous expression of FLYWCH1 (Red) in TIG119 cells shows partial co-localization with **A)** HP1α. **B)** No co-locolization was observed with H2AXγ. Red arrows show cluster of HP1α co-localizing with a fraction of FLYWCH1 foci. Dotted lines indicates enlarged cell/s. Negative controls were used in the absence of primary antibody. Magnification: 100x. Scale bars, 10 µm. **C)** Quantitative analysis of co-localization using Pearson Correlation Coefficient (PCC) with ImageJ. PCC of 30 individual cells were determined. Data are represented as mean of PCC of 30 individual cells +/- SD.

5.2.2 Evaluation of FLYWCH1/SC-35 complex in pre-mRNA splicing activity

Several reports suggests that transcription and RNA processing are intimately coupled *in-vivo*, although each process can occur independently *in-vitro*. The identification of factors that facilitate mammalian pre-mRNA splicing *in-vitro*, is generally performed via functional relationship between the transcription and

splicing machineries during gene expression. The most common strategy for the identification of factors that promote splicing efficiency is via analysis of splicing activity *in-vitro*, by utilizing luciferase splicing reporter constructs with splicing donor/acceptor sites.

5.2.2.1 FLYWCH1 with no changes in splicing activity

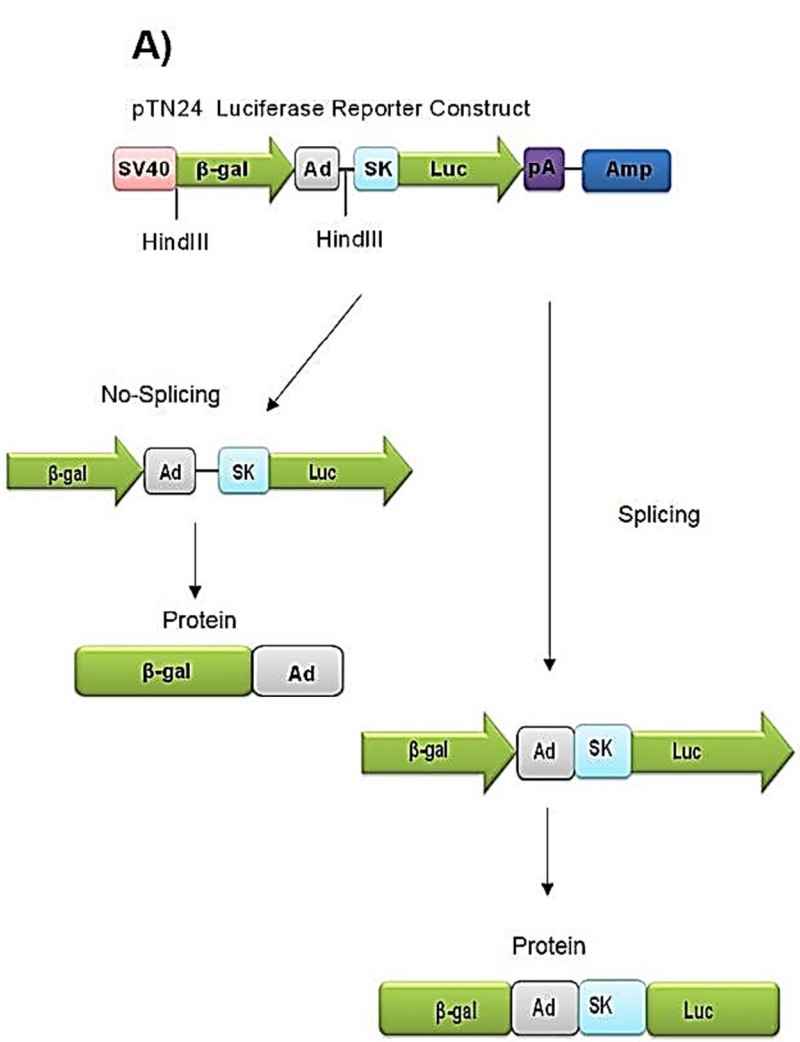
To further elucidate the possible function of punctuated nuclear distribution of FLYWCH1 in RNA-splicing, we have initially used a dual luciferase reporter assay. Herein, two different splicing reporter constructs; pTN24 and the Luc-I reporter plasmids were utilized as outlined below.

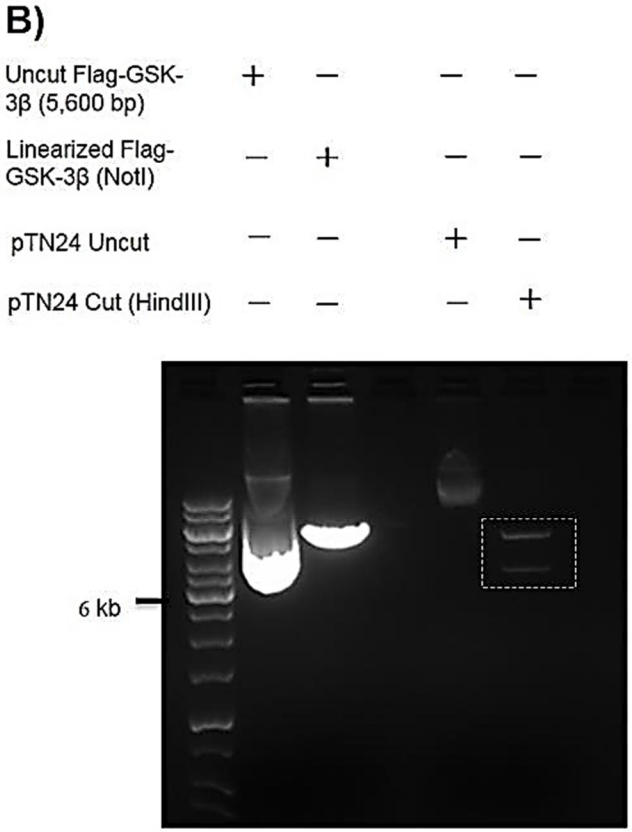
1) The pTN24 plasmid (Figure 5-3 A) contains an upstream reporter (β-galactosidase) and a downstream reporter (luciferase) with an intron with splicing acceptor sides in between the two reporters (Nasim et al., 2002; Nasim and Eperon, 2006) (Figure 5-3 A). Splicing would result to the removal of the intron thus placing the upstream reporter in frame with the downstream reporter, hence only after splicing has occurred would the downstream reporter be expressed while only the upstream reporter is expressed in the absence of splicing. This technique could be utilized to measure the ratio of signals from two different reporters present in a single cistron. For the current experiment, β-galactosidase activity was not required.

Following validation of the pTN24 plasmid via restriction digestion (Figure 5-3 B), expression plasmids encoding FLAG-GSK-3β as well as the pTN24 reporter plasmids were individually transiently transfected into SW480 cells under

different conditions in the presence or absence of MYC-FLYWCH1-WT plasmids along with firefly and *SV40 Renilla* luciferase for normalizing the transfection efficiency. GSK-3β was used in this experiment due to its role in splicing and intranuclear distribution of SC-35 (Hernández et al., 2004) as well as due to the FLYWCH1-mediated phosphorylation regulation of GSK-3β reported in chapter 4. Cells transfected with only the luciferase reporter constructs were used as experimental control, with their luciferase activity via co-transfection and normalization with the *SV40 Renilla* internal control and set arbitrarily to 1. The luciferase activities of other experimental conditions (Figure 5-3 C; lane 2, 3 & 4) were also normalized to *SV40 Renilla* and eventually compared to the control.

The dual luciferase assays revealed that FLYWCH1 overexpression did not instigate any significant changes in luciferase activity relative to the control (Figure 5-3 C, lane 3), while overexpressing GSK-3β was significantly reduced (Figure 5-3 C, lane 2). However, co-transfection with FLYWCH1 resulted in a significant reduction of luciferase activity in GSK-3β overexpressed cells (Figure 5-3 C, lane 4). Following application of these plasmid construct, results obtained suggests that the RNA-splicing activity was un-changed upon enforced FLYWCH1 expression in SW480 cells under different conditions. Therefore, the data suggest that FLYWCH1 may not be involved in splicing.


A)
pTN24 Luciferase Reporter Construct
SV40
β-gal
Ad
SK
Luc
pA
Amp
HindIII
HindIII
No-Splicing
β-gal
Ad
SK
Luc
Protein
β-gal
Ad
Splicing
β-gal
Ad
SK
Luc
Protein
β-gal
Ad
SK
Luc


B)
Uncut Flag-GSK-3β (5,600 bp) + – – –
Linearized Flag-GSK-3β (NotI) – + – –
pTN24 Uncut – – + –
pTN24 Cut (HindIII) – – – +
6 kb

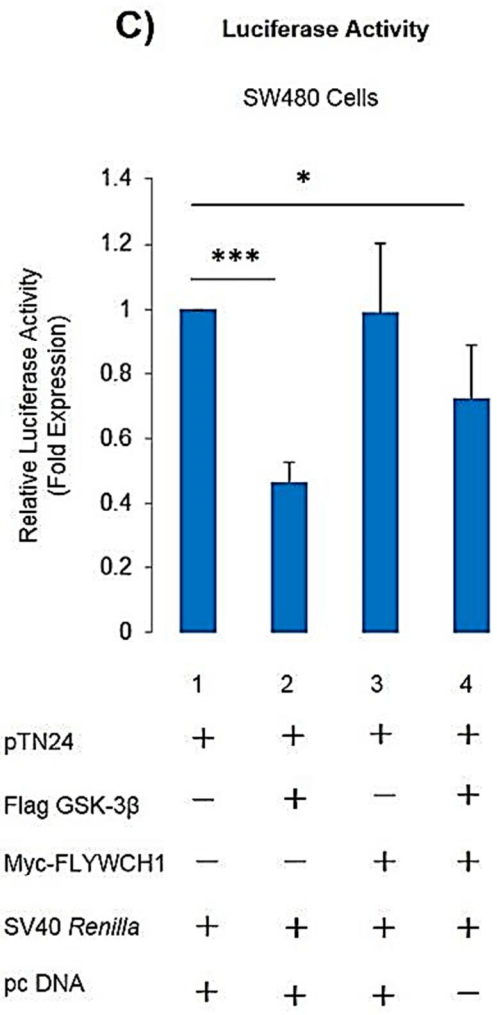
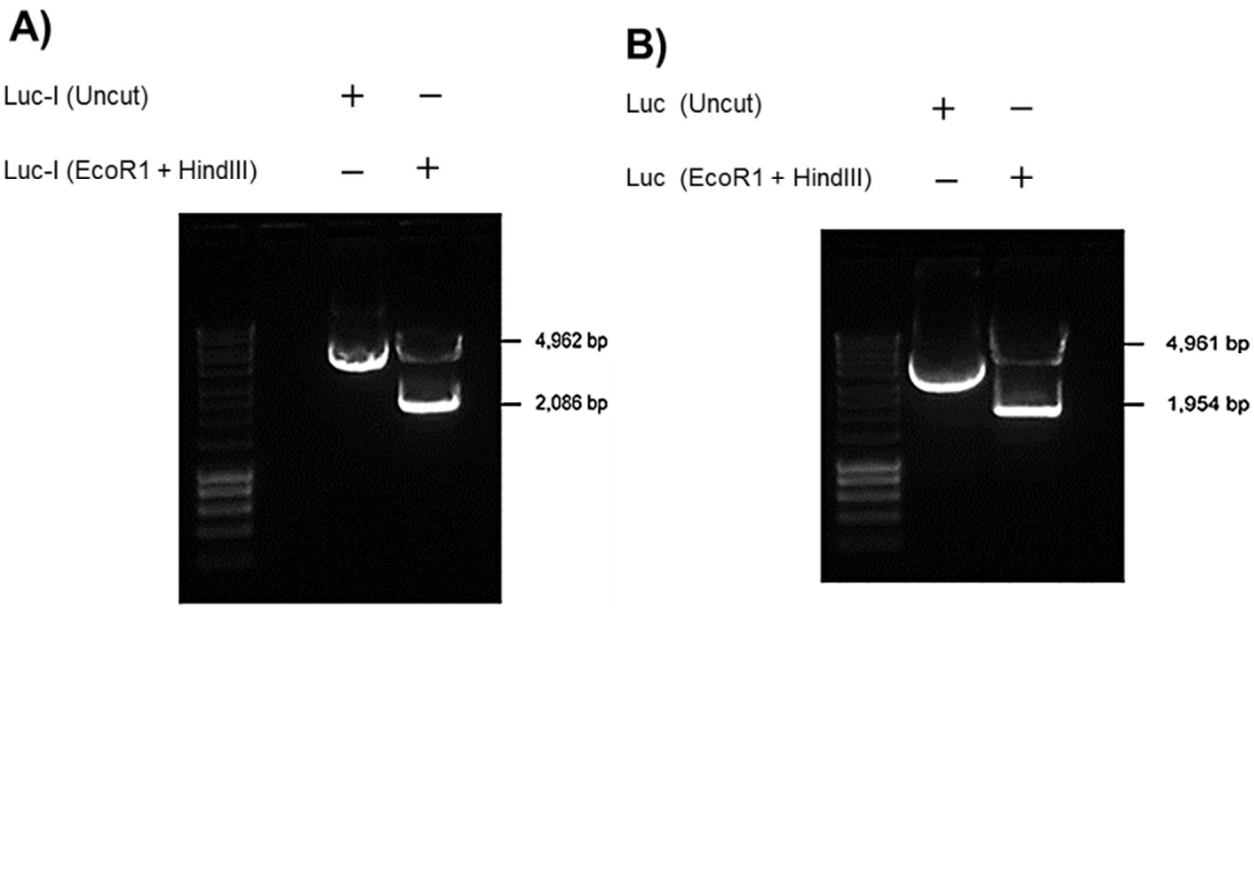

C)
Luciferase Activity
SW480 Cells
Relative Luciferase Activity (Fold Expression)
1.4
1.2
1
0.8
0.6
0.4
0.2
0
*
***
1 2 3 4
pTN24 + + + +
Flag GSK-3β – + – +
Myc-FLYWCH1 – – + +
SV40 Renilla + + + +
pc DNA + + + –

Figure 5-3: FLYWCH1 is not involved in RNA splicing activity. The pTN24 reporter construct was used to analyse the splicing activity of FLYWCH1. **A)** Schematic representation of the pTN24 luciferase reporter construct. **B)** Validation of the pTN24 reporter construct with flag-GSK-3β (Uncut & Linearized). Dotted lines indicates double digestion of pTN24. **C)** Luciferase activity indicating FLYWCH1 is not involved in splicing. Activity of the firefly luciferase reporters relative to *Renilla* luciferase transfection control is indicated as folds of expression (induction/repression). Data are mean ± SD (*, $P < 0.05$; ***, $P < 0.001$). Experiment were carried out in triplicate and repeated on two separate occasions.

2) Another set of plasmids, **Luc-I reporter plasmids** (Younis et al., 2010) was utilized to further assess the splicing activity (Figure 5-4 A, top panel). These reporter systems are composed of two plasmids possessing an open reading frame (ORF) of firefly luciferase with one been interrupted by a chimeric β-globin/immunoglobulin intron (Luc-I) which has been optimized to splice with high efficiency, while the other does not possess an intron (Luc) (Younis et al., 2010) (Figure 5-4 B, top panel). Validation of these plasmids were carried out via restriction enzyme digestion analysis (Figure 5-4 A; bottom panel, Figure 5-4 B; bottom panel).

For this particular experiment, SW480 cells were utilized. SW480 GFP^{+VE} cells (control) and GFP-$FLYWCH1^{O/E}$ cells were individually transfected with the Luc-I reporter. Consistent to the previous pTN24 luciferase data (Figure 5-3), there was no significant change in luciferase activity in GFP-$FLYWCH1^{O/E}$ cells expression relative to GFP control cells (Figure 5-4 C). Taken together, these data suggests that although FLYWCH1 co-localizes with nuclear speckles it is however not involved in splicing activity but may be involved in other mRNA/miRNA–related activity.


A)
Luc-I (Uncut) + –
Luc-I (EcoR1 + HindIII) – +
4,962 bp
2,086 bp
B)
Luc (Uncut) + –
Luc (EcoR1 + HindIII) – +
4,961 bp
1,954 bp

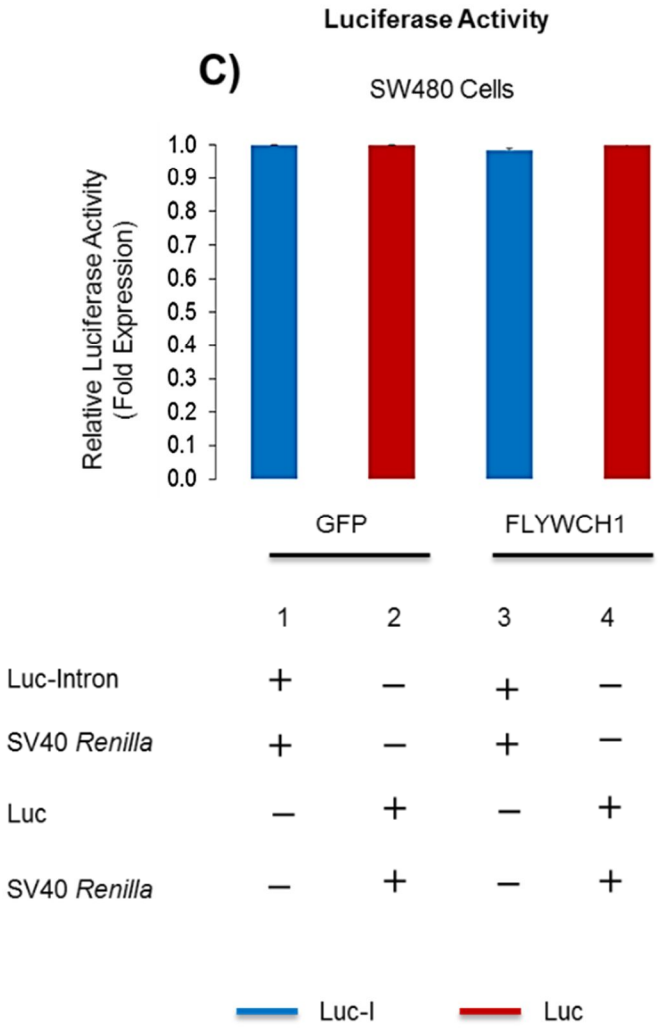

Luciferase Activity
C)
SW480 Cells
Relative Luciferase Activity (Fold Expression)
1.0
0.9
0.8
0.7
0.6
0.5
0.4
0.3
0.2
0.1
0.0
GFP
FLYWCH1
1 2 3 4
Luc-Intron + – + –
SV40 Renilla + – + –
Luc – + – +
SV40 Renilla – + – +
Luc-I
Luc

Figure 5-4: FLYWCH1 is not involved in RNA splicing activity. A second reporter construct, Luc-I (Appendix 9) was used to also analyse the splicing activity of FLYWCH1. **A)** Validation of Luc I construct via restriction digestion. Chimeric intron = 132 nucleotides. **B)** Validation of Luc construct (Appendix 8) via restriction digestion. **C)** SW480 GFP^{+VE} and GFP-$FLYWCH1^{O/E}$ cells were individually transfected with the Luc-Intron (Luc-I). Fold induction/repression of the Luc-I luciferase construct activity relative to *Renilla* are shown as indicated. Experiment carried out in triplicate on two different occasions and data are mean ± SD (no significant changes were detected).

5.2.3 FLYWCH1 modulates the expression of cancer-associated miRNAs in TIG119 and CRC cell lines

Nuclear speckles have been shown to be enriched with pre-miRNA splicing factors (Spector and Lamond, 2011). Since we observed co-localization between FLYWCH1 and SC-35 nuclear speckles marker, we attempted to observe the expression patterns of 84 cancer related miRNAs with FLYWCH1. Therefore, we decided to investigate the miRNA gene expression profile via miRNA microarray technology with the use of Human miFinder miRNA PCR Array (MIHS-001Z, Qiagen) (Figure 5-5 C). RNA immunoprecipitation (RIP) was performed with the aim of mapping out the direct association of FLYWCH1 protein with its associated RNAs from TIG119 GFP-$FLYWCH1^{O/E}$ cells using the anti-GFP antibody (Figure 5-5 A & Figure 5-5 B). For this experiment, we utilized GFP antibodies due to the inability for the FLYWCH1 antibody to detect endogenous expressed FLYWCH1 via western blotting.

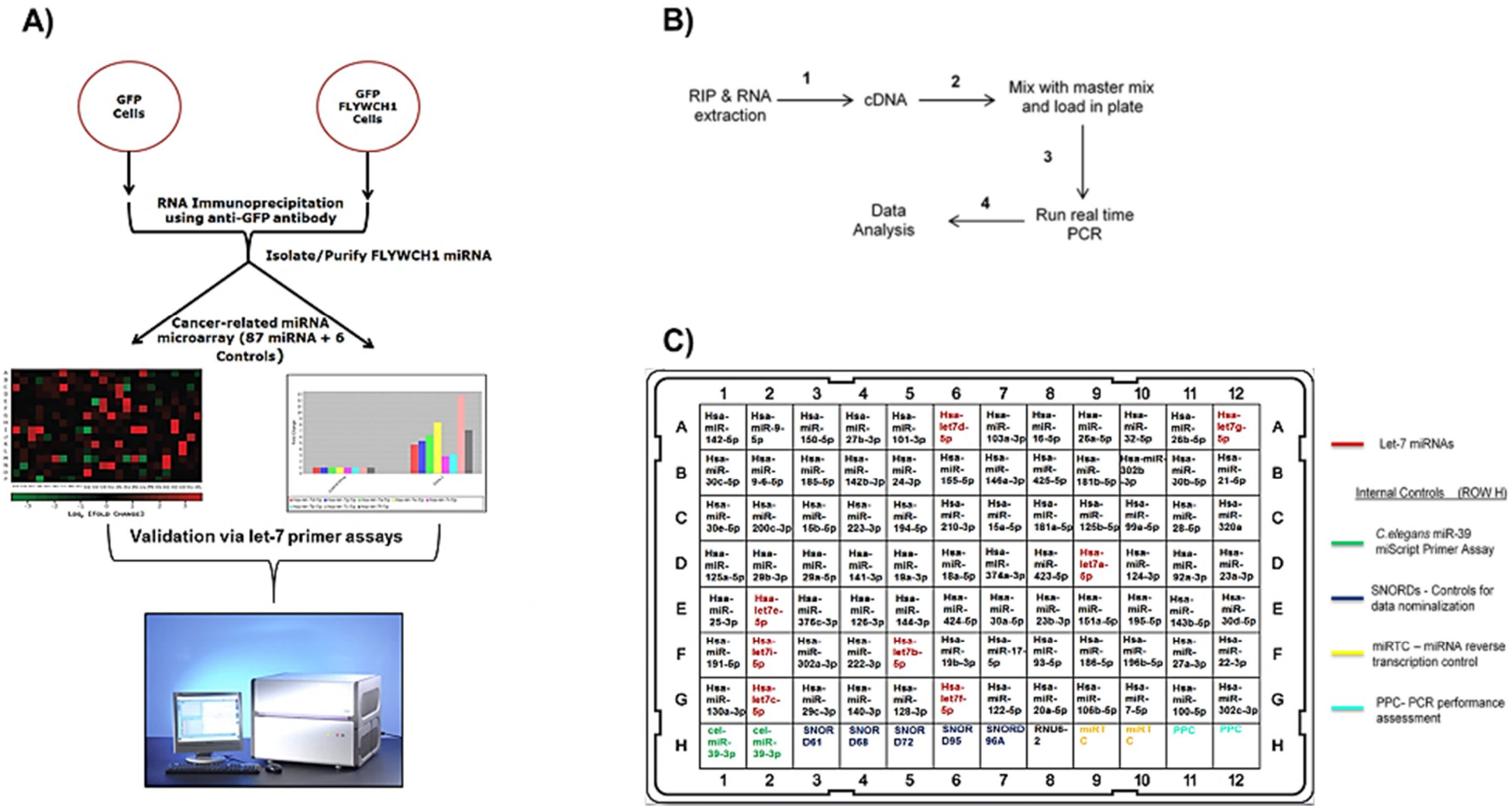
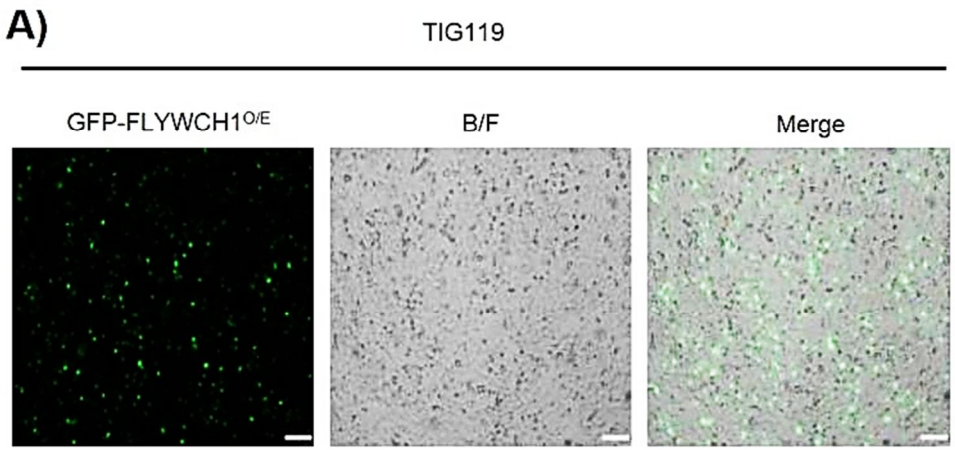


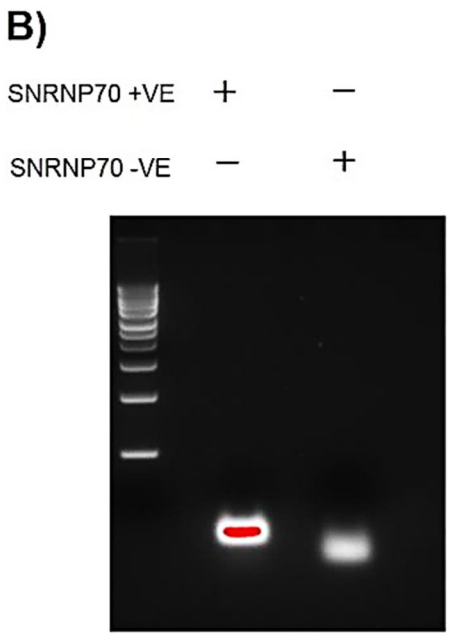
Figure 5-5: Preliminary analysis of FLYWCH1 on miRNA gene expression profile in TIG119 cells. A) Summary of overall methodology used to analyze FLYWCH1-mediated regulation of let-7. Two images gotten from (http://saweb2.sabiosciences.com/mirna_pcr_product/HTML/MAH-102A.html). **B)** Schematic representation of the protocol utilized to carry out the preliminary FLYWCH1 gene expression profiling. **C)** PCR array 96 well plate layout of each miRNA genes and internal controls (MIHS-001Z, Qiagen).

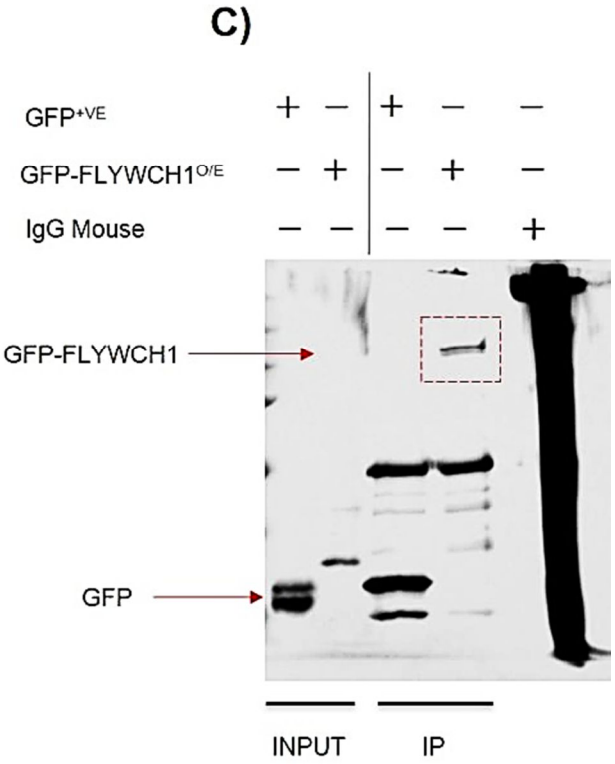
The principle of RIP involves immunoprecipitation of the possible RNA binding protein (RBP) complex with FLYWCH1 together with their relation during gene expression including miRNAs.

Despite successful transfection of GFP-FLYWCH1 (Figure 5-6 A), we were still unable to detect GFP-FLYWCH1 in the input blot by loading of 50µg of protein lysate (Figure 5-6 C, In-put lanes). However, we detected an elevated GFP-FLYWCH1 protein following the immunoprecipitation (IP) (Figure 5-6 C, IP lanes). Following IP, we validated RNAs derived from RIP products, and revealed by examining snRNP70 expression versus the negative control (Figure 5-6 B) according to the manufacturer' guidelines.

Following validation assays we performed quantitative PCR (qPCR) on the representative miRNAs along with miRNAs-housekeeping genes as controls (Figure 5-6 D). A description of the fold expression of all these miRNAs in GFP-FLYWCH1$^{O/E}$ cells compared to the control (Table 5-1) along with the internal controls (Table 5-2). The array results showed that there was an increase in fold expression of most of the tumour suppressor miRNAs including all the let-7 miRNAs genes relative to the control samples (Table 5-1 & Figure 5-6 D).


A)
TIG119
GFP-FLYWCH1O/E
B/F
Merge


B)
SNRNP70 +VE
SNRNP70 -VE


C)
GFP+VE
GFP-FLYWCH1O/E
IgG Mouse
GFP-FLYWCH1
GFP
INPUT
IP

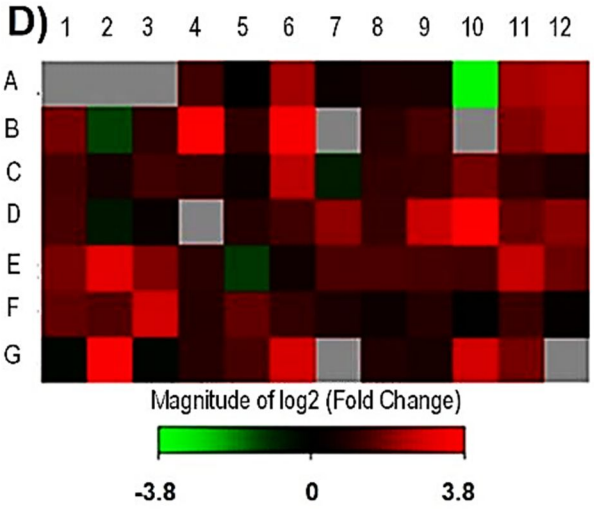

D)
1 2 3 4 5 6 7 8 9 10 11 12
A
B
C
D
E
F
G
Magnitude of log2 (Fold Change)
-3.8
0
3.8

Figure 5-6: Preliminary analysis suggest influence of FLYWCH1 on miRNA gene expression profile. A) Post-transfection of TIG119 GFP-FLYWCH1$^{O/E}$ cells. Magnification, 10x. Scale bar, 10 µm. **B)** PCR analysis of RIP. PCR product of snRNP70 was detected (snRNP70 positive lane) while only primer dimers were detected in the normal rabbit IgG RIP (lane snRNP70 negative). **C)** Protein lysate of TIG119 GFP^{+VE} and GFP-FLYWCH1$^{O/E}$ cells were immunoprecipitated using Protein A/G magnetic beads. Both the input and IP samples were immunoblotted with anti-GFP antibodies. Red arrows indicating the detection of GFP & GFP-FLYWCH1 in the IP blot. **D)** Heat map illustrating the gene expression pattern of 84-known cancer associated miRNAs in GFP-FLYWCH1$^{O/E}$ cells vs GFP^{+VE} control cells. Intense red represents increased fold expression while intense green represents decreased fold expression. All let-7 miRNAs exhibited an increase in fold expression (more than 2-fold increase).

Table 5-1: Full list and fold expression of miRNAs in TIG119 GFP-FLYWCH1$^{O/E}$ relative to control. Colour indicators; **Blue** indicates low expression (LE). **Red** indicates more than 2 fold expression. **Black** indicates less than 2 fold expression. **Green** indicates reduced fold expression. **Purple** indicates let-7 miRNAs. **Yellow** indicates internal controls.

Array Position	miRNA	Fold Expression
A01	hsa-miR-142-5p	LE
A02	hsa-miR-9-5p	LE
A03	hsa-miR-150-5p	LE
A04	hsa-miR-27b-3p	2.5374
A05	hsa-miR-101-3p	1.0023
A06	hsa-let-7d-5p	4.7349
A07	hsa-miR-103a-3p	1.3503
A08	hsa-miR-16-5p	1.674
A09	hsa-miR-26a-5p	1.6625
A10	hsa-miR-32-5p	-12.2666
A11	hsa-miR-26b-5p	4.801
A12	hsa-let-7g-5p	5.3641
B01	hsa-miR-30c-5p	3.539
B02	hsa-miR-96-5p	-2.5257
B03	hsa-miR-185-5p	2.1337
B04	hsa-miR-142-3p	13.7688
B05	hsa-miR-24-3p	2.1785
B06	hsa-miR-155-5p	12.4092
B07	hsa-miR-146a-5p	LE

B08	hsa-miR-425-5p	2.0467
B09	hsa-miR-181b-5p	2.6451
B10	hsa-miR-302b-3p	LE
B11	hsa-miR-30b-5p	3.8194
B12	hsa-miR-21-5p	5.0397
C01	hsa-miR-30e-5p	2.555
C02	hsa-miR-200c-3p	1.6625
C03	hsa-miR-15b-5p	2.5374
C04	hsa-miR-223-3p	2.3349
C05	hsa-miR-194-5p	1.2775
C06	hsa-miR-210-3p	5.5149
C07	hsa-miR-15a-5p	-1.7371
C08	hsa-miR-181a-5p	2.2397
C09	hsa-miR-125b-5p	2.3187
C10	hsa-miR-99a-5p	3.5636
C11	hsa-miR-28-5p	2.1634
C12	hsa-miR-320a	1.7092
D01	hsa-miR-125a-5p	2.682
D02	hsa-miR-29b-3p	-1.5874
D03	hsa-miR-29a-3p	1.2255
D04	hsa-miR-141-3p	LE
D05	hsa-miR-19a-3p	1.9363
D06	hsa-miR-18a-5p	2.5198
D07	hsa-miR-374a-5p	4.1506
D08	hsa-miR-423-5p	2.3027
D09	hsa-let-7a-5p	6.335
D10	hsa-miR-124-3p	14.4534
D11	hsa-miR-92a-3p	3.234
D12	hsa-miR-23a-3p	4.0652
E01	hsa-miR-25-3p	3.6133
E02	hsa-let-7e-5p	8.4172
E03	hsa-miR-376c-3p	3.793
E04	hsa-miR-126-3p	2.0898
E05	hsa-miR-144-3p	-2.308
E06	hsa-miR-424-5p	1.4273
E07	hsa-miR-30a-5p	2.7195
E08	hsa-miR-23b-3p	2.7574
E09	hsa-miR-151a-5p	2.6268
E10	hsa-miR-195-5p	2.5374
E11	hsa-miR-143-3p	6.1192
E12	hsa-miR-30d-5p	3.3481
F01	hsa-miR-191-5p	3.1675
F02	hsa-let-7i-5p	2.8547
F03	hsa-miR-302a-3p	6.9323
F04	hsa-miR-222-3p	1.9498
F05	hsa-let-7b-5p	3.1895
F06	hsa-miR-19b-3p	2.2553
F07	hsa-miR-17-5p	1.7331

F08	hsa-miR-93-5p	1.3597
F09	hsa-miR-186-5p	1.9498
F10	hsa-miR-196b-5p	-1.0187
F11	hsa-miR-27a-3p	2.434
F12	hsa-miR-22-3p	1.1277
G01	hsa-miR-130a-3p	-1.1303
G02	hsa-let-7c-5p	12.8468
G03	hsa-miR-29c-3p	-1.0994
G04	hsa-miR-140-3p	1.9908
G05	hsa-miR-128-3p	2.6451
G06	hsa-let-7f-5p	7.1768
G07	hsa-miR-122-5p	LE
G08	hsa-miR-20a-5p	1.8446
G09	hsa-miR-106b-5p	1.6058
G10	hsa-miR-7-5p	6.9323
G11	hsa-miR-100-5p	3.5884
G12	hsa-miR-302c-3p	LE
H01	cel-miR-39-3p	2.835
H02	cel-miR-39-3p	2.835
H03	SNORD61	-2.0232
H04	SNORD68	1.8067
H05	SNORD72	-2.4228
H06	SNORD95	1.8319
H07	SNORD96A	-1.3256
H08	RNU6-2	1.9634
H09	miRTC	1.651
H10	miRTC	1.7695
H11	PPC	1.7573
H12	PPC	1.1121

Table 5-2: **List of internal controls**

H03	Data norminalization using delta Ct method of relative comparison
H04	Data norminalization using delta Ct method of relative comparison
H05	Data norminalization using delta Ct method of relative comparison
H06	Data norminalization using delta Ct method of relative comparison
H07	Data norminalization using delta Ct method of relative comparison
H08	Data norminalization using delta Ct method of relative comparison
H09	Assessment of reverse transcription performance
H10	Assessment of reverse transcription performance

H11	Assessment of PCR performance
H12	Assessment of PCR performance

Following miRNA gene expression array analysis data, validation of the selected let-7 (a, b, c, d & e) miRNA gene expression level was performed using qRT-PCR technique in fibroblast and CRC cells. Normal and CRC cells under different conditions (GFP^{+VE}, GFP-$FLYWCH1^{O/E}$ and $FLYWCH1^{shRNA}$ cells) were cultured prior to isolation of total RNA including miRNAs and reverse transcription to acquire the cDNA using the miScript PCR system for qRT-PCR analysis.

Firstly, validation of a selected set of miRNAs that were up-regulated upon FLYWCH1 overexpression other than let-7 was performed in TIG119 cells under different conditions. The miRNAs were selected due to their roles in cancer progression. For instance, both miR-143 and miR-124 has been implicated in inhibiting colorectal cancer (Chen et al., 2015; Wu et al., 2013), while miR-142-3p acts as a tumour suppressor by directly repressing HMGB1 in non-small-cell lung carcinoma (Xiao and Liu, 2015). However, miR-96 has been implicated in promoting tumour proliferation and invasion in breast cancer (Zhang et al., 2014a). Following validations via qRT-PCR using specific miRNA primer assays, consistent with our initial miRNA array data (Figure 5-6 D and Table 5-1), we show that the miRNA expressions of the above selected miRNAs were either upregulated or downregulated upon FLYWCH1 ectopic expression (Figure 5-7 A). An opposite effect on these miRNAs were also observed in cells knocked-down with FLYWCH1 expression (Figure 5-7 B).

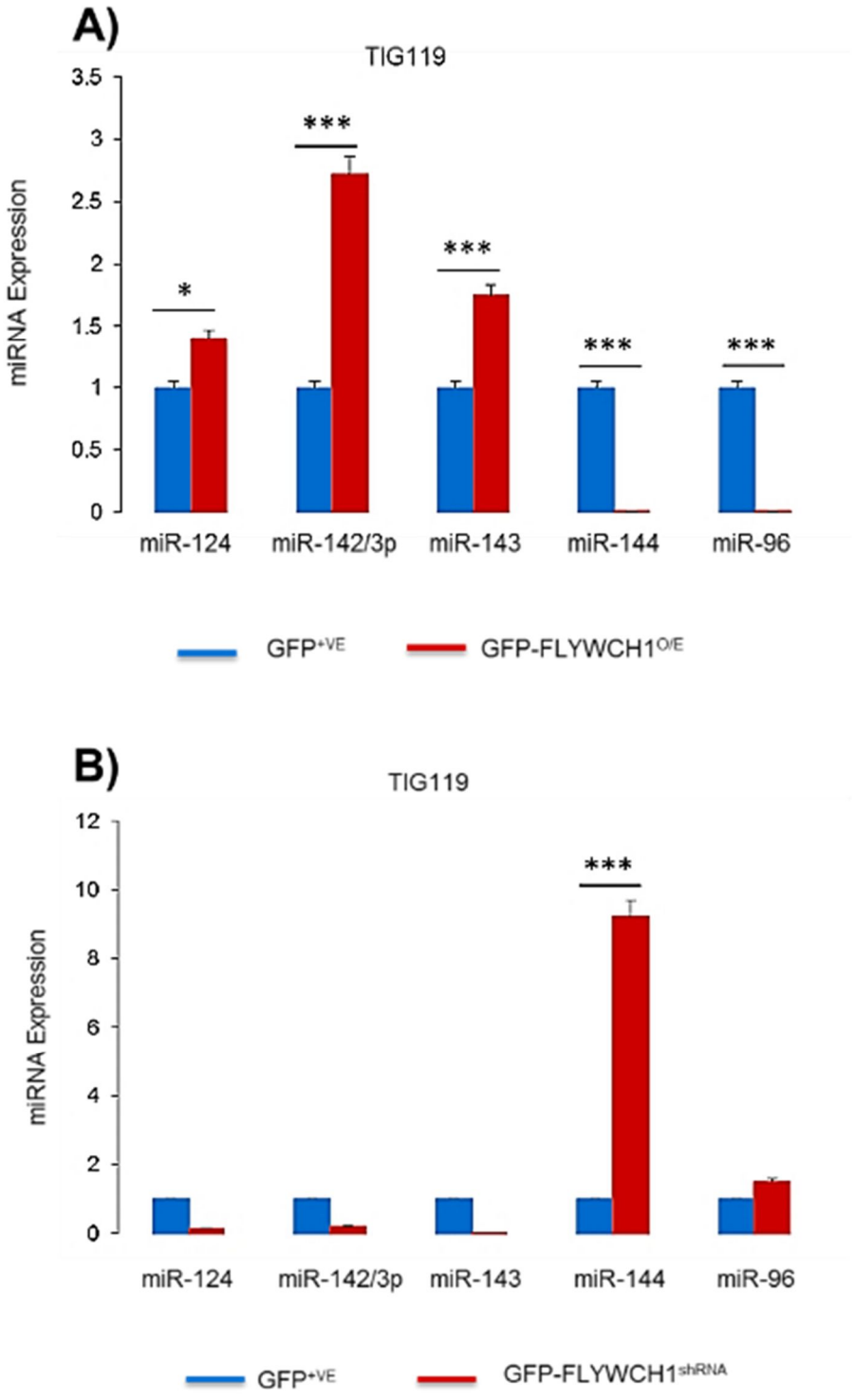


Figure 5-7: FLYWCH1 positively regulates miRNA tumour suppressor expression. Total RNA was extracted from TIG119 cells under different conditions. cDNA was obtained using miScript II RT Kit after which the expression levels of miR-124, miR-142/3p, miR-143, miR-144 and miR-96 were determined as follows; **A)** GFP^{+VE} vs $GFP\text{-}FLYWCH1^{O/E}$ and **B)** GFP^{+VE} vs $FLYWCH1^{shRNA}$. Data are mean ± SD (*, P < 0.05; ***, P < 0.001). Each sets of

experiment are carried out in triplicate and repeated on two independent occasions.

Due to the abundant research findings implicating let-7 as a bonafide tumour suppressor in different forms of cancer (Madison et al., 2015; Thammaiah and Jayaram, 2016), we decided to maintain our focus on let-7 miRNA expression as a tumour suppressor. The relative expression levels of let-7 variants were measured and compared to control cells. Again, consistent with our initial miRNA array data (Figure 5-6 D & Table 5-1), we observed that FLYWCH1 overexpression and knockdown oppositely alters the expression of the let-7 miRNAs in TIG119 and CRC cells (Figure 5-8 A - C & Figure 5-9 A - C). Taken together, these data acquired from different cell lines under different conditions suggests that FLYWCH1 possesses tumour suppressor activity by positively affecting let-7 expression patterns.

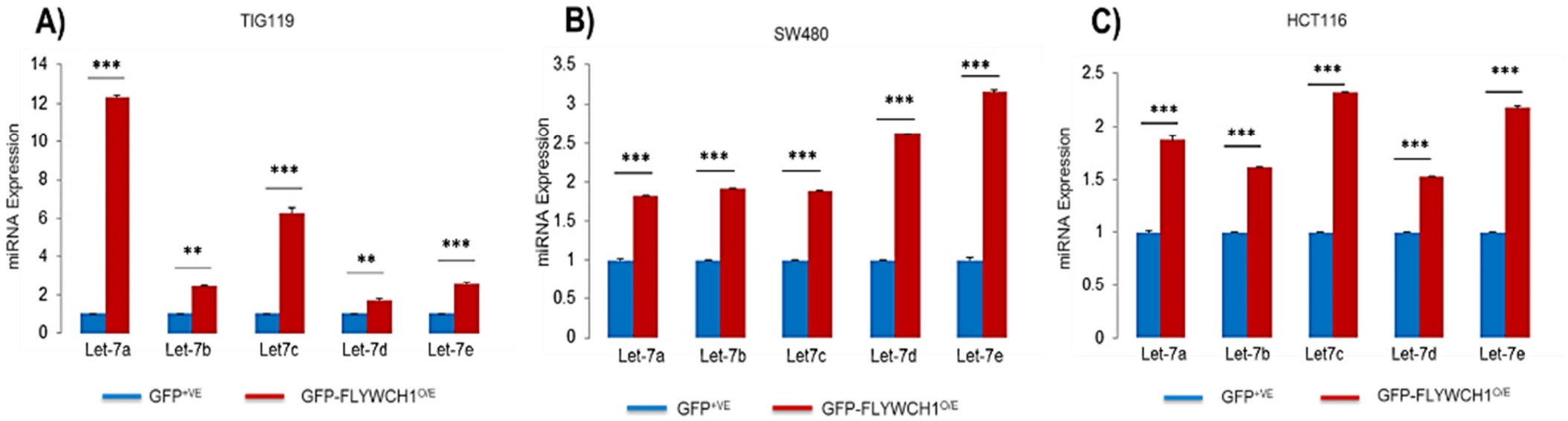


Figure 5-8: Influence of ectopic FLYWCH1 expression on let-7 gene expression profile. Total RNA was extracted from TIG119, SW480 & HCT116 cells under different conditions. cDNA was obtained using miScript II RT Kit after which the let-7 expression of each sets of cell were determined as follows; **A)** TIG119 cells: GFP^{+VE} vs $GFP\text{-}FLYWCH1^{O/E}$, **B)** SW480 cells: GFP^{+VE} vs $GFP\text{-}FLYWCH1^{O/E}$ **C)** HCT116 cells: GFP^{+VE} vs $GFP\text{-}FLYWCH1^{O/E}$. Data are mean ± SD (**, $P < 0.01$; ***, $P < 0.001$). Each sets of experiment are carried out in triplicate and repeated on two independent occasions.

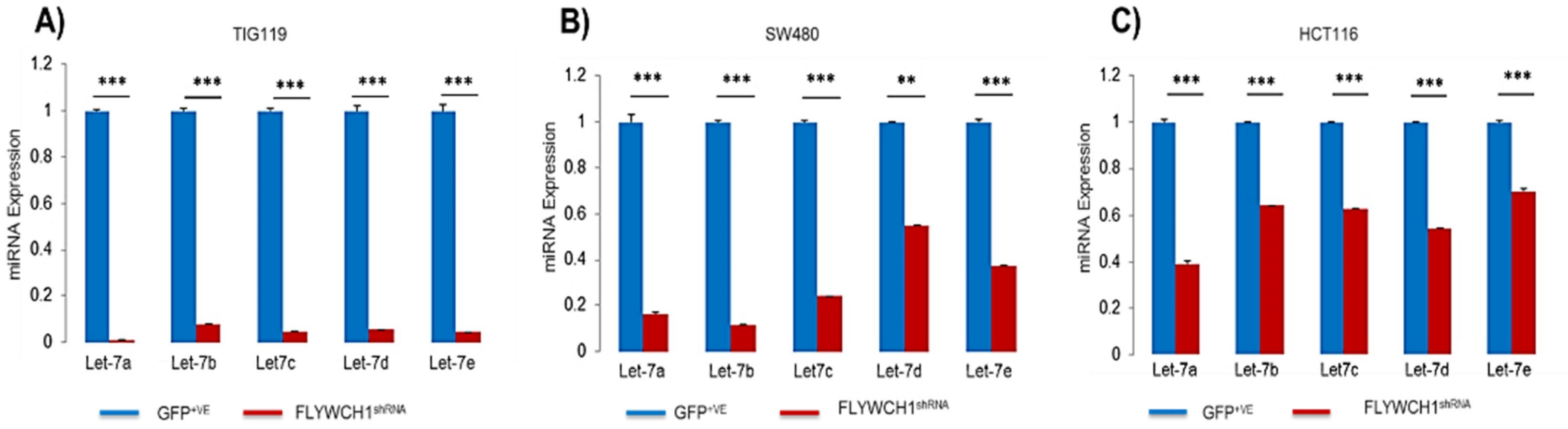


Figure 5-9: Influence of FLYWCH1 knockdown on let-7 gene expression profile. Total RNA was extracted from TIG119, SW480 & HCT116 cells under different conditions. cDNA was obtained using miScript II RT Kit after which the let-7 expression of each set of cells were determined as follows; **A)** TIG119 cells: GFP^{+VE} vs $FLYWCH1^{shRNA}$. **B)** SW480 cells**:** GFP^{+VE} vs $FLYWCH1^{shRNA}$. **C)** HCT116 cells: GFP^{+VE} vs $FLYWCH1^{shRNA}$. Data are mean ± SD (**, $P < 0.01$; ***, $P < 0.001$). Each set of experiments are carried out in triplicate and repeated on two independent occasions.

5.2.4 FLYWCH1-mediated control of let-7 miRNA may reduce cytoplasmic localization of LIN28B in cultured CRC cell lines.

Experimental evidence have repeatedly shown that LIN28A and LIN28B act as post-transcriptional repressors of let-7 biogenesis via direct binding to the loop portion hairpin of pri-let-7 and the stem of pre-let-7, thus inhibiting the binding of Drosha or Dicer respectively (Mayr and Heinemann, 2013; Tsialikas and Romer-Seibert, 2015). Following earlier observations of FLYWCH1-mediated positive regulation of let-7 (Figure 5-6, Table 5-1, Figure 5-8 &Figure 5-9), we decided, also as part of our gain-of-function and loss-of-function properties of FLYWCH1 to investigate whether the FLYWCH1 expression would negatively alter LIN28 expression. Our immunofluorescence data acquired revealed that the levels of cytoplasmic LIN28A were un-altered under these different conditions in TIG119 cells although there appeared to be an increase in LIN28A mostly around the boundary of nuclear membrane in FLYWCH1^{shRNA} cells (Figure 5-10 C). However, there were no changes of LIN28B the cells under different conditions (Figure 5-11 & Figure 5-12).

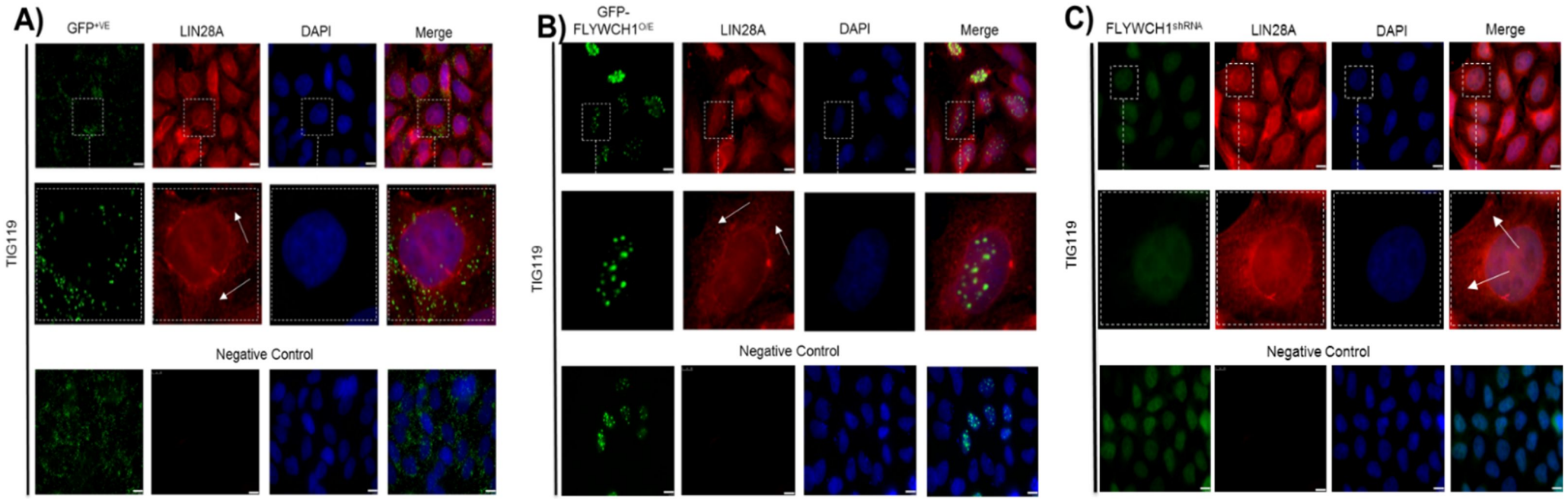


Figure 5-10: FLYWCH1 may alter the expression of LIN28A in TIG119 cells. TIG119 cells under different conditions were stained with LIN28A (red) and DAPI (blue) and visualized under a fluorescent microscope. The expression pattern of LIN28A under different conditions were analyzed as follows; LIN28A: **A)** GFP^{+VE} (control). **B)** GFP-$FLYWCH1^{O/E}$. **C)** $FLYWCH1^{shRNA}$ cells. Arrows indicate the difference in cytoplasmic LIN28A expression. Negative controls were used in the absence of primary antibody. Magnification: 100x. Scale bars, 25 μm.

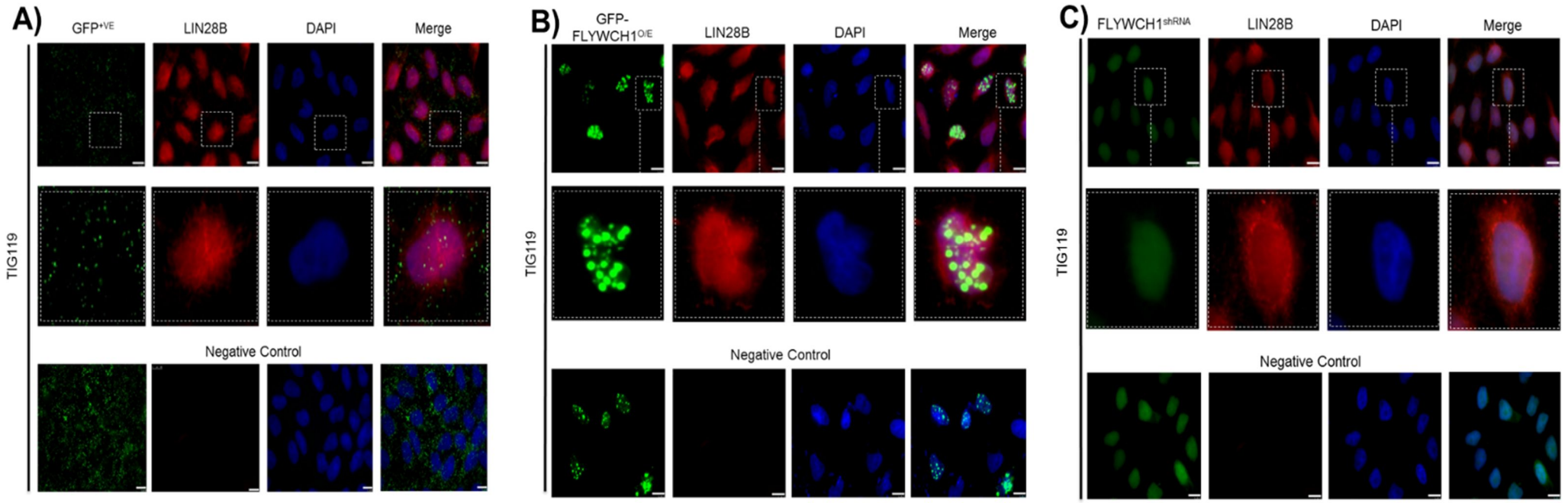


Figure 5-11: FLYWCH1 does not alter the expression of LIN28B in TIG119 cells. TIG119 cells under different conditions were stained with LIN28B (red) and DAPI (blue) and visualized under a fluorescent microscope. The expression pattern of LIN28B under different conditions were analyzed as follows; LIN28B: **A)** GFP^{+VE} (control). **B)** GFP-$FLYWCH1^{O/E}$. **C)** $FLYWCH1^{shRNA}$ cells. Negative controls were used in the absence of primary antibody. Magnification: 100x. Scale bars, 7.5 µm.

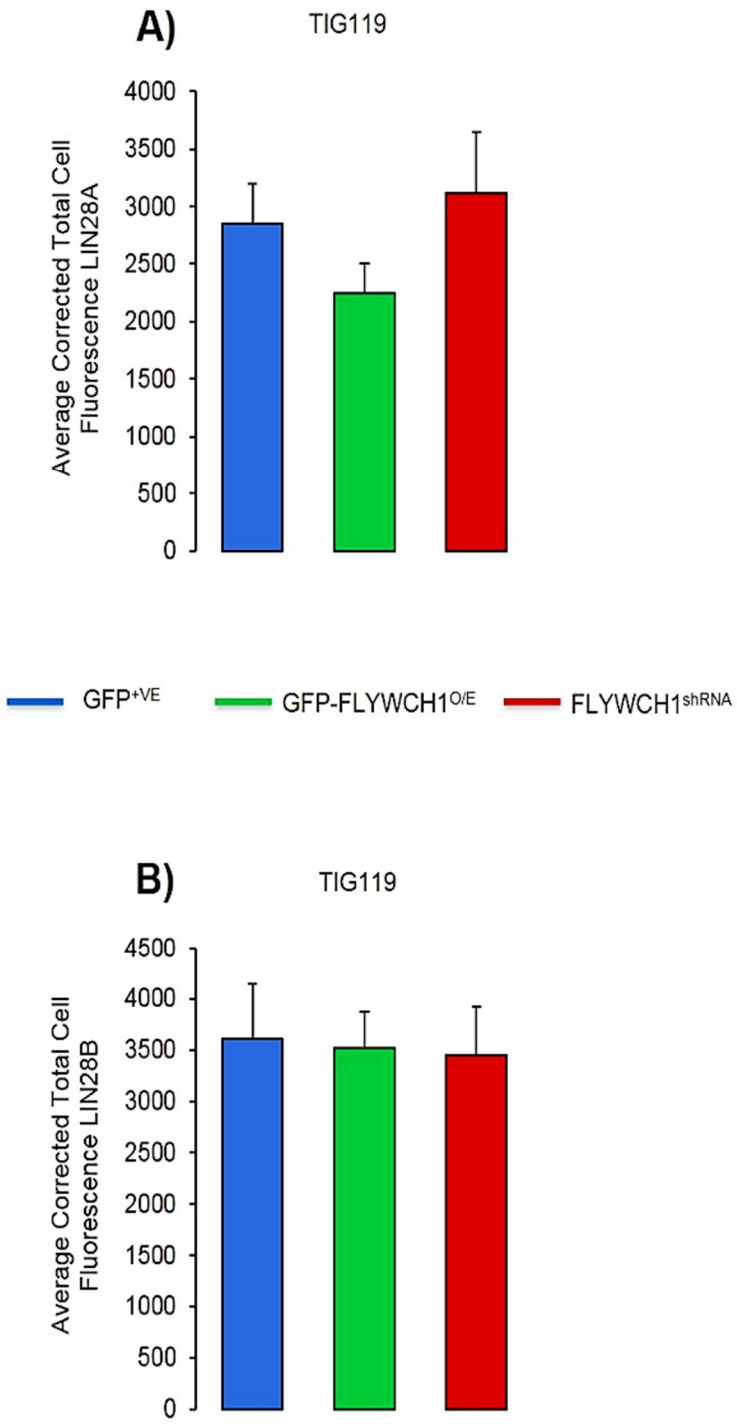


Figure 5-12: **Quantitative analysis of LIN28A and LIN28B in TIG119 cells**. Quantitative analysis of **A)** LIN28A & **B)** LIN28B. Fluorescence intensity was determined by calculating the Corrected Total Cell Fluorescence [CTCF = Integrated intensity – (area x fluorescence mean)] using ImageJ. Data are represented as mean of 30 individual cells under different conditions. Data are mean ± SD (***, P < 0.001). Experiment was repeated at least on two independent occasions.

In SW480 cells, immunofluorescence data showed significant differences in subcellular distribution of LIN28 proteins. Figure 5-13 C, shows an accumulation of LIN28A in the boundaries of the cell membrane of FLYWCH1^{shRNA} cells, while a reduction of LIN28B cytoplasmic localization in SW480 GFP-FLYWCH1$^{O/E}$ cells relative to GFP^{+VE} and FLYWCH1^{shRNA} cells was also observed (Figure 5-14 B). Similar patterns in LIN28B were also observed in HCT116 cells (Appendix 11). Nuclear and cytoplasmic fractionation was also performed to observe the expression patterns of LIN28A and LIN28B upon ectopic FLYWCH1 expression (Data not shown due to technical issues).

.

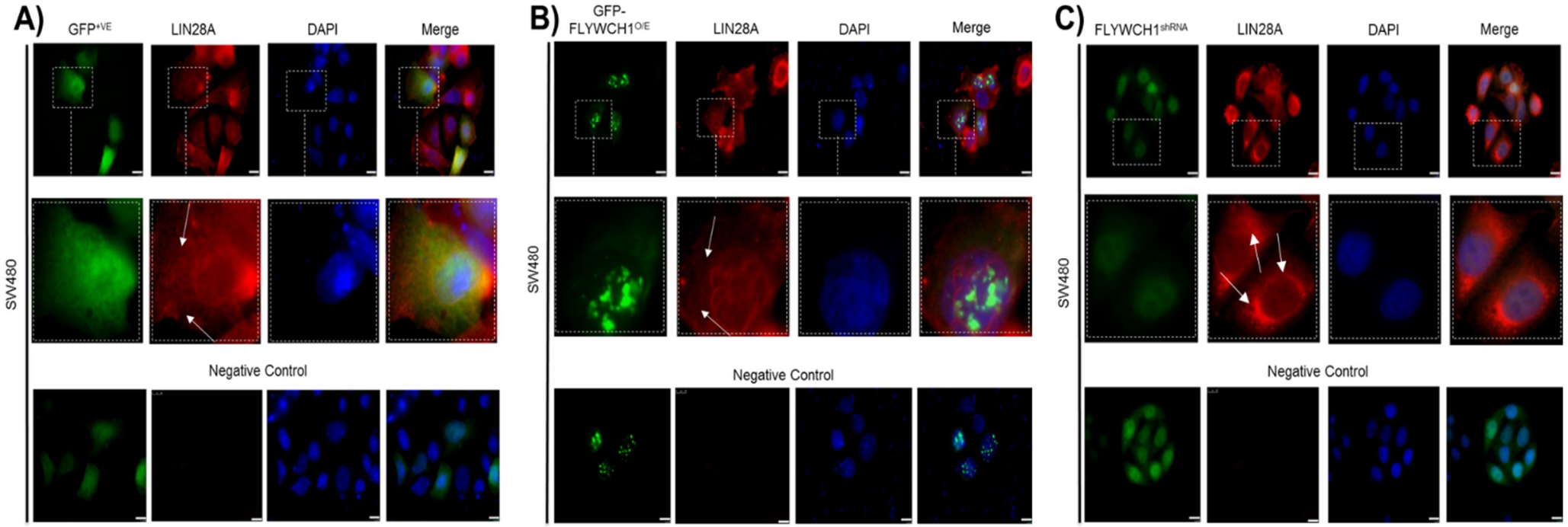


Figure 5-13: FLYWCH1 alters the expression of LIN28A in SW480 cells. SW480 cells under different conditions were stained with LIN28A (red) and DAPI (blue) and visualized under a fluorescent microscope. The expression pattern of LIN28A under different conditions were analyzed as follows; LIN28A: **A)** GFP^{+VE} (control). **B)** GFP-$FLYWCH1^{O/E}$. **C)** $FLYWCH1^{shRNA}$ cells. Arrows indicate the difference in cytoplasmic LIN28A expression. Negative controls were used in the absence of primary antibody. Magnification: 100x. Scale bars, 25 µm.

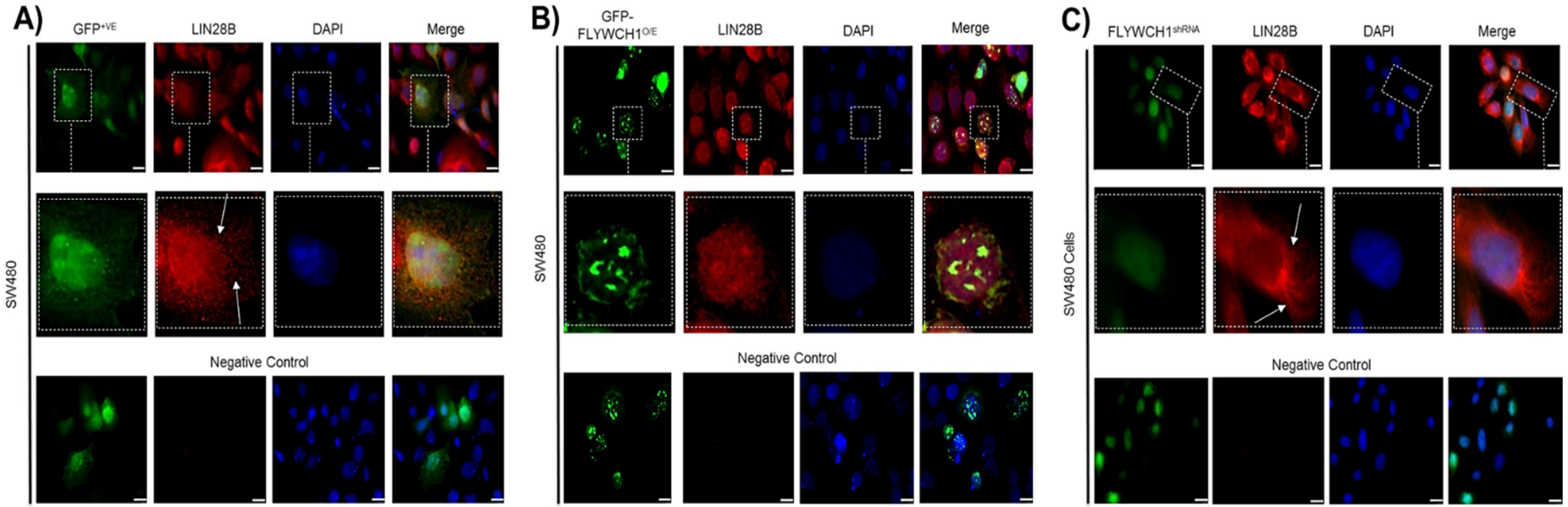


Figure 5-14: FLYWCH1 alters the expression of LIN28B in SW480 cells. SW480 cells under different conditions were stained with LIN28B (red) and DAPI (blue) and visualized under a fluorescent microscope. The expression pattern of LIN28B under different conditions were analyzed as follows; LIN28B: **A)** GFP^{+VE} (control). **B)** GFP-$FLYWCH1^{O/E}$. **C)** GFP-$FLYWCH1^{shRNA}$ cells. Arrows indicate presence of cytoplasmic LIN28B expression. Negative controls were used in the absence of primary antibody. Magnification: 100x. Scale bars, 7.5 µm.

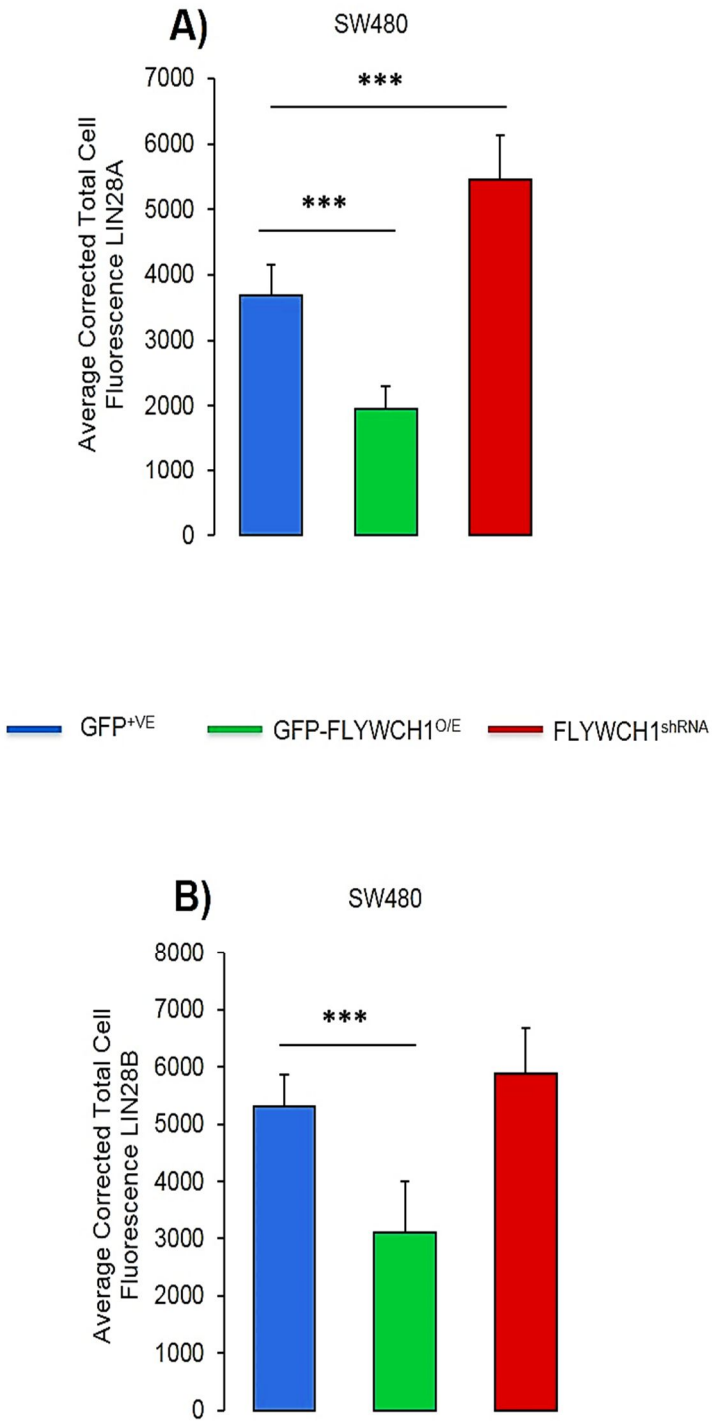


Figure 5-15: Quantitative analysis of LIN28A and LIN28B in SW480 cells. Quantitative analysis of **A)** LIN28A & **B)** LIN28B, fluorescence intensity was determined by calculating the Corrected Total Cell Fluorescence [CTCF = Integrated intensity – (area x fluorescence mean)] using ImageJ. Data are represented as mean of 30 individual cells under different conditions. Data are mean ± SD (***, P < 0.001). Experiment was repeated at least on two independent occasions.

5.2.4.1 FLYWCH1 may regulate the expression of genes targeted by let-7 miRNA

The let-7 family of miRNAs have been identified as crucial regulators of several factors that control cell fate decisions, including oncogenes such as ; Ras, HMGA-2 and c-myc (Büssing et al., 2008; Viswanathan and Daley, 2010) as well as cyclin D1 and D2 cell cycle factors and interleukins, specifically IL6 (Iliopoulos et al., 2009).

Therefore, to investigate whether FLYWCH1 directly binds to let-7 DNA binding elements, luciferase assay was utilized with let-7 reporter construct (Figure 5-16 A). This construct contains a let-7 target site (8x) (**5'**-TCGAGACTATACAAGGATCTACCTCAG) (Iwasaki et al., 2009), and reduction in *Renilla* luciferase activity may suggest a direct potential binding of FLYWCH1 to let-7 DNA-binding sequences present in 3'UTR of let7 target genes. SW480 cells under different conditions (GFP^{+VE}, GFP-$FLYWCH1^{O/E}$ $FLYWCH1^{shRNA}$ cells) were transiently transfected with the let-7 reporter construct (psiCHECK2-Let-7-8x) plasmid. Results indicates that SW480 GFP-$FLYWCH1^{O/E}$ cells significantly activated the let-7 target site relative to control GFP^{+VE} cells (Figure 5-16 B), thus suggesting that FLYWCH1 may directly interact with let-7 DNA binding elements.

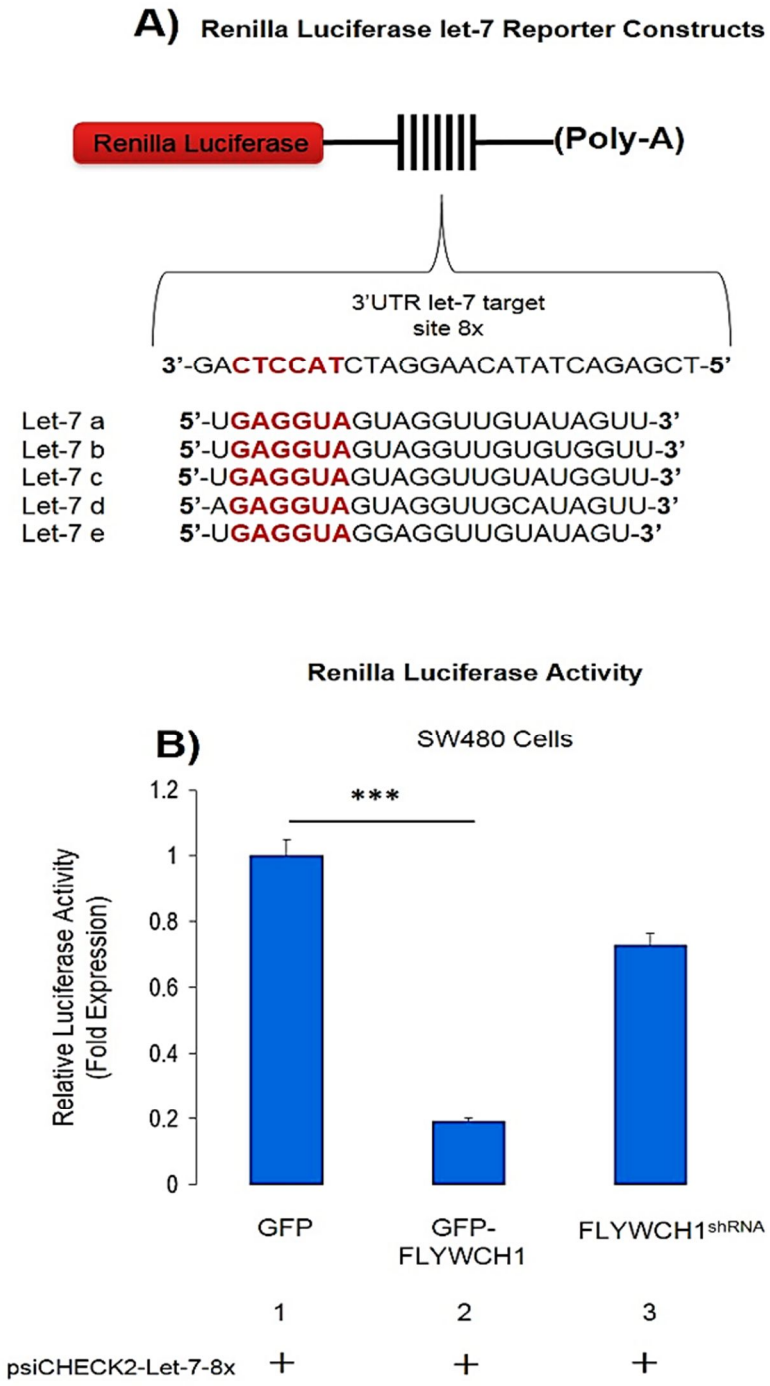


Figure 5-16: FLYWCH1 may bind directly to let-7 3'UTR target. **A)** Schematic representation of Let-7 luciferase reporter construct, psiCHECK2-Let-7-8x showing binding sites with let-7. **B)** SW480 cells under different conditions [GFP^{+VE} (control), $GFP\text{-}FLYWCH1^{O/E}$ & $FLYWCH1^{shRNA}$ cells] were transfected with the Let-7 luciferase reporter construct. Fold expressions of luciferase activity relative to *Renilla* luciferase are indicated. Data are mean ±

SD (***, P < 0.001). Experiment run in triplicate and repeated at least on two independent occasions.

5.2.4.2 FLYWCH1 shows a positive correlation with let-7 in negatively regulating HMGA-2

A major hallmark of most forms of cancers is the heightened expression of High Mobility Group AT-Hook 2 (HMGA-2). Based on the established evidence confirming the natural role of let-7 in the regulation of HMGA-2 by binding to the 7 conserved complementary sites on the 3'UTR of HMGA-2 mRNA (Madison et al., 2015; Wang et al., 2011a), we decided to investigate how enforced expression of FLYWCH1 would influence the regulation of downstream let-7 target HMGA-2 expression via let-7.

Utilizing reporter constructs with the wild type 3'UTR (pmiR-Luc-HMGA2-3'UTR) (Figure 5-17 A) and an empty vector as negative control (Figure 5-17 B) the firefly luciferase activity of each constructs were examined under different conditions. The SV40 *Renilla*-luciferase was utilized as an internal control to normalize variations in the transfection efficiency. Cells co-transfected with the pmiR-Luc-HMGA2-3'UTR reporter constructs, SV40 *Renilla* and pcDNA plasmids were used as experimental controls with their luciferase activity normalized to *Renilla* internal control and then arbitrarily set to 1 (Figure 5-17 C, lane 1). SW480 cells were transiently transfected with either HMGA-2 reporter construct or the control empty vector and co-transfected with let-7b with/without GFP-FLYWCH1 plasmids. Thirty-six hours post-transfection, cells were harvested for firefly luciferase assay analysis. Results revealed a significant repression of firefly luciferase activity upon co-transfection of the

pmiR-Luc-HMGA2-3'UTR construct with let-7b (Figure 5-17, lane 1 vs lane 3) which is due to the direct binding of the let-7 seed sequence to the complementary sequence on the 3'UTR of HMGA2 fragment. Co-transfection of the pmiR-Luc-HMGA2-3'UTR construct with FLYWCH1 also resulted to a repression of 3'UTR activity relative to the control (Figure 5-17, lane 1 vs lane 5). Co-transfection of the pmiR-Luc-HMGA2-3'UTR construct with both FLYWCH1 & let-7b resulted to the lowest luciferase activity relative to the control and the rest of the conditions (Figure 5-17; lane 1 vs lane 7). This data confirms a positive correlation between FLYWCH1 and let-7 in negatively regulating HMGA-2.

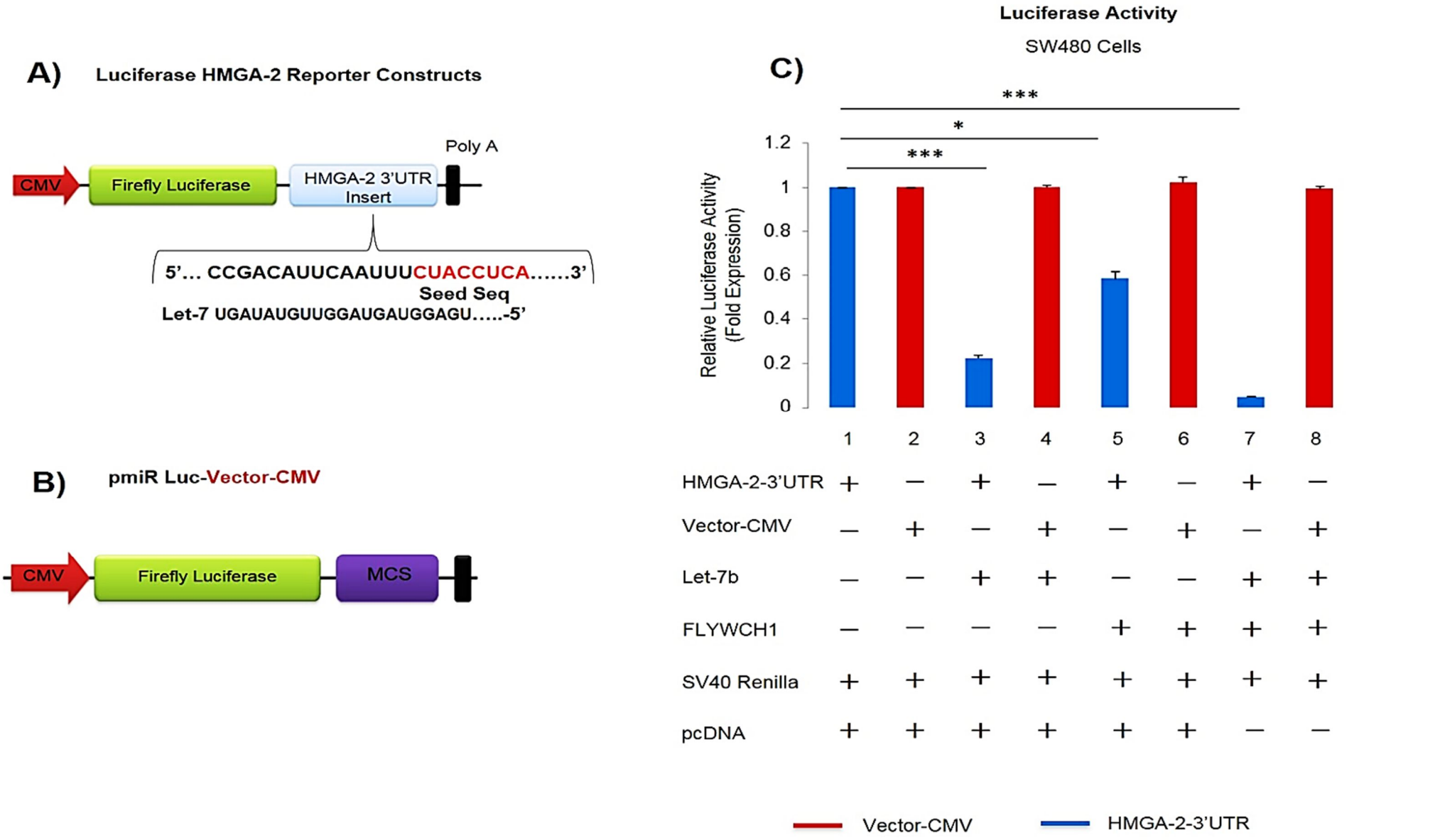

A)
Luciferase HMGA-2 Reporter Constructs
Poly A
CMV
Firefly Luciferase
HMGA-2 3'UTR Insert
5'… CCGACAUUCAAUUUCUACCUCA……3'
Seed Seq
Let-7 UGAUAUGUUGGAUGAUGGAGU…..-5'
B)
pmiR Luc-Vector-CMV
CMV
Firefly Luciferase
MCS
C)
Luciferase Activity
SW480 Cells
***
*
***
Relative Luciferase Activity (Fold Expression)
1.2
1
0.8
0.6
0.4
0.2
0
1 2 3 4 5 6 7 8
HMGA-2-3'UTR + – + – + – + –
Vector-CMV – + – + – + – +
Let-7b – – + + – – + +
FLYWCH1 – – – – + + + +
SV40 Renilla + + + + + + + +
pcDNA + + + + + + – –
Vector-CMV
HMGA-2-3'UTR

Figure 5-17: FLYWCH1 shows positive correlation with let-7 in repressing HMGA-2. **A)** Luciferase HMGA-2 Reporter Construct & **B)** Control vector. **C)** SW480 cells were transiently transfected with either the HMGA-2 Reporter Construct or pmiR Luc-Vector-CMV as well as with/without let-7b and GFP-FLYWCH1 plasmids in the presence of *Renilla*. Fold expression of luciferase activity relative to *Renilla* luciferase are shown. Data are mean ± SD (*, $P < 0.05$; ***, $P < 0.001$). Each set of experiments are carried out in triplicate and repeated on two independent occasions.

It has been reported that the Wnt-β-catenin pathway represses let-7 miRNA expression via activation of LIN28 (Cai et al., 2013b; Madison et al., 2015), however the mechanism driving this phenomenon remains un-clear pertaining to whether a direct interaction between let-7 and β-catenin occurs to facilitate this process. As a result, the possible direct interaction between let-7 and β-catenin was investigated. The let-7 reporter construct (Figure 5-16 A) was utilized and transfected in SW480 cells. Also, co-transfection with both β-catenin and GFP-FLYWCH1 or individually were performed. However, the data showed there was no alteration of let-7 target site upon enforced β-catenin expression (Figure 5-18). Based on this data, we conclude that the physical interaction between let-7 and β-catenin may not be involved in the regulation of the Wnt-β-catenin pathway.

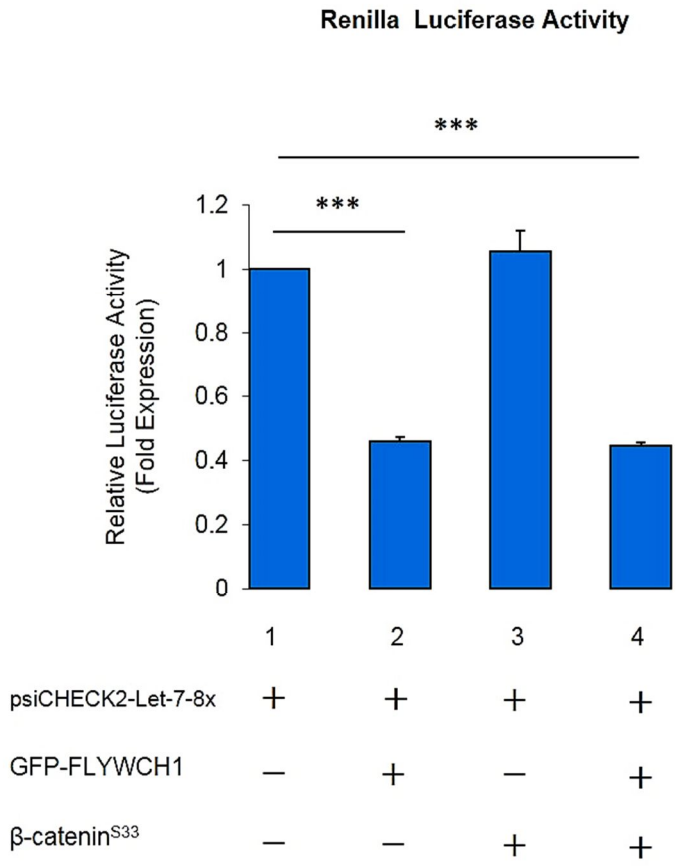


Figure 5-18: Ectopic expression of β-catenin have no effect on let-7/luciferase reporter activity. SW480 cells were all transiently transfected with Let-7 luciferase reporter construct. Conditions included individual or co-transfection of GFP-FLYWCH1 and β-catenin. Folds expression of *Renilla* luciferase activity are shown. Data are mean ± SD (**, P < 0.01; ***, P < 0.001).

5.2.5 Gene Expression Profiling for FLYWCH1 in Correlation with Let-7 in Colon cancer tissues

To further investigate the potential disease relevance of our above observations, we decided to measure/correlate the expression patterns of FLYWCH1 and let-7 in human tissue samples under different conditions. Previously, *in-vitro* studies showed that enforced expression of FLYWCH1 in normal (TIG119) and CRCs

resulted to an increased expression of let-7 a, b c d & e. Therefore, a cohort of nine; normal, primary and metastasis tissue samples derived from colorectal cancer patients was performed to analyse FLYWCH1 expression under different conditions as well as correlate the expression patterns with let-7.

Following tissue homogenization (Section 2.11), we observed that the expression of FLYWCH1 and let-7a were significantly reduced in primary and metastasis samples relative to normal samples (with the metastasis samples having the lowest expression) (Figure 5-19). This is consistent with our initial analysis on TIG119 and CRC cell lines showing enforced expression of FLYWCH1 increased the expression levels of let-7 miRNAs. These data reveal a direct correlation between FLYWCH1 and let-7 in colorectal cancer patient samples.

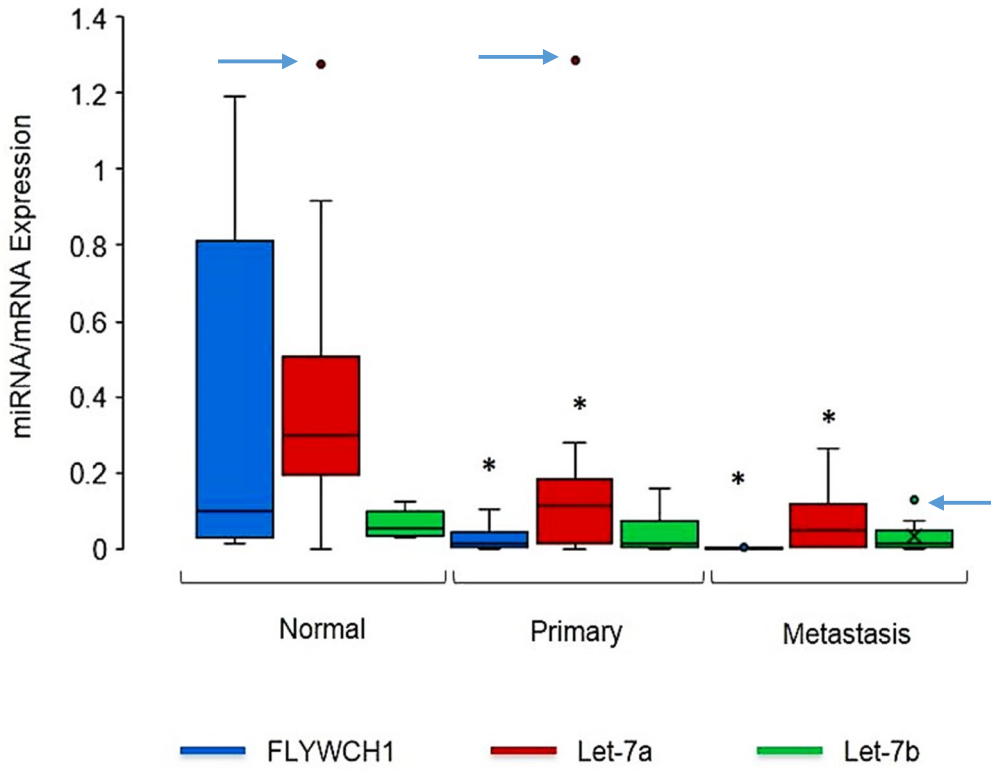


Figure 5-19: Influence of FLYWCH1 on let-7 gene expression profile in normal vs primary tumour vs metastasis samples. MiRNA/mRNA expression profiles of FLYWCH1, let-7a and let-7b in a range of normal, primary and metastatic tissue samples obtained from a colorectal cancer patient. Data are mean ± SD (*, $P < 0.05$). Blue arrows point to outliers. Each set of experiments were carried out in triplicate and repeated on two independent occasions.

5.3 Discussion

Herein, we provide preliminary evidence suggesting that FLYWCH1 may be involved in the positive regulation of the let-7 group of miRNAs via direct interaction, thus possessing tumour suppressor activity. The FLYWCH motif among different proteins has been identified in *Drosophila* (Dai et al., 2004b; Dorn and Krauss, 2003) and *C. elegans* (Beaster-Jones and Okkema, 2004a), while more recently FLYWCH1 has been briefly studied in coronary heart disease (Asl et al., 2015). Therefore, there is limited scientific information regarding the biological activity of this protein especially in humans. However, one major function of proteins with FLYWCH domain, established in *C. elegans* is the DNA binding ability, as well as the regulation of embryonic miRNAs (Ow et al., 2008a).

Notwithstanding, the expression pattern exhibited by FLYWCH1 in the nucleus encouraged us to carry out co-localization assay with SC-35 nuclear speckle marker (Figure 5-1 B). In mammalian cells the pre-mRNA splicing machinery, comprised of spliceosome subunits, small nuclear ribonucleoprotein particles (snRNPs), and other non-snRNP protein splicing factors, exhibits a punctate nuclear localization pattern termed “a speckled pattern” and also referred to as “SC-35 domains” (Lamond and Spector, 2003; Wu et al., 2010a). Most importantly, the nuclear speckles are sites of eukaryotic gene regulation via pre-mRNA splicing, involving regulated alternative splicing. In general, the removal of introns is facilitated by the spliceosome, a complex of various snRNAs and associated proteins including SR proteins (Bradley et al., 2015). SR proteins are key splicing factors crucial in alternative and constitutive

splicing, transcription elongation and miRNA transport. Here, we reveal co-localization between FLYWCH1 and nuclear speckles 'SC35' (Figure 5-1 B), thus leading to the possibility that FLYWCH1 is involved in either pre-mRNA splicing, including regulated alternative splicing necessary for gene regulation and post-transcriptional gene modification (Wu et al., 2010a) or mRNA and miRNA biosynthesis. However, experimental assays of the possible splicing activity of FLYWCH1 utilizing 2 different luciferase reporter splicing constructs showed that FLYWCH1 may not be involved in splicing (Figure 5-3 & Figure 5-4).

Although our reporter assays suggests that FLYWCH1 speckles may not be involved in splicing activity, other studies have shown that nascent RNA and non-coding pre-miRNA co-localise and are often found at the nuclear speckles (Lamond and Spector, 2003; Morimoto and Boerkoel, 2013). It is also important to note that one of the components of the nuclear speckle is non-coding RNAs such as microRNAs (miRNA). Apart from the polycistronic and intergenic biogenesis of miRNAs, miRNAs are also generated via intronic sequences of protein-coding or non-coding transcription units made available through mRNA splicing (Lin et al., 2006; Ramalingam et al., 2014). In *C. elegans,* FLH-1, FLH-2 and FLH-3 set of transcription factors also possess the conserved FLYWCH domain in the N-termini (Ow et al., 2008a).

Interestingly, according to Ow el al. (2008), experiments performed in yeast one-hybrid (Y1H) screens revealed that during embryogenesis, the transcription factors repress the transcription of a group of miRNAs, in particular lin-4 that are normally expressed post-embryonically. More interestingly, LIN28 has been identified as a downstream target of lin-4 (Tsialikas and Romer-Seibert, 2015).

Also, FLYWCH motif containing protein, PEB-1, was observed to bind to promoters of several miRNAs in *C. elegans* (Martinez et al., 2008). These observations highlight the possible role of FLYWCH-motif containing proteins in biogenesis and regulation of certain miRNAs in *C. elegans.* This lead to the possibility that FLYWCH1 may modulate transcriptional product of miRNAs in humans or alternatively be involved in the shuttling of miRNAs from the interchromatin granule clusters to other regions of the nucleus and cytoplasm. Therefore, human FLYWCH1 may be able to execute similar effect on miRNAs in normal & CRC cells.

Aberrant expression of certain miRNAs has been proven to be associated with cancer initiation, progression and metastasis in a plethora of human malignancies (Iorio and Croce, 2012; Lin and Gregory, 2015). One of these sets of miRNAs is the lethal-7 (let-7) miRNA family. In normal human physiology, let-7 is primarily involved in embryonic development, cell adhesion, muscle formation and gene regulation. First identified in *C. elegans* it has been shown to be involved in the coordination of developmental timing in *C. elegans* (Reinhart et al., 2000; Vella et al., 2004) as well as mid-gestation developmental program *in-vitro* (Gurtan et al., 2013) and other developmental processes (Großhans et al., 2005). The let-7 family of miRNAs exists in multiple copies in the genome. To differentiate between multiple isoforms, a letter is normally inserted after let-7 to denote a let-7 possessing a slightly different sequence (Roush and Slack, 2008). In addition, a number is also included at the end to indicate that the same sequence exists in multiple genomic locations. For instance, three different precursors generate the mature let-7a sequence (let-7a-1, let-7a-2 and let-7a-3).

Interestingly, our studies indicate that FLYWCH1 may possess miRNA-related activities following preliminary miRNA expression profiling (Figure 5-6 D &Table 5-1). We then decided to focus on the let-7 group of miRNAs due to its highly-documented tumour suppressor activity (Akao et al., 2006; Chien et al., 2015; Zhang et al., 2007). For instance, ras, c-Myc, Janus protein tyrosine kinase (JAK), high-mobility group A (HMGA), and signal transducer and activator of transcription 3 (STAT3) are key oncogenes that promote tumorigenesis, proliferation, metastasis and invasion are targeted and negatively regulated by let-7 (Wang et al., 2012). We demonstrate that let-7 was up-regulated in TIG119 and CRC cells relative to controls (Figure 5-8), while conversely, let-7 miRNA expression was strongly down-regulated in cells knocked down for endogenous FLYWCH1 expression (Figure 5-9). Also, analysis of samples derived from colorectal cancer patients showed that FLYWCH1 and let-7a expression levels were elevated in normal tissue samples but showed a steady significant decline of expression in primary tumour and metastatic samples respectively (Figure 5-19). These results were further consolidated by the possibility of direct interaction between FLYWCH1 and let-7 (Figure 5-16). Furthermore, our studies not only show a positive correlation between FLYWCH1 and let-7 in participating in the post-transcriptional regulation of HMGA2, we also reveal that FLYWCH1 independently facilitates the post-transcriptional regulation of HMGA2 (Figure 5-17). However, more extensive target validation analysis are required to be performed. These results suggest that FLYWCH1 possesses tumour suppressor activity by most likely modulating let-7 expression *in-vitro.*

Two highly conserved LIN28 paralogs, LIN28A and LIN28B have been identified in mammals. Cytoplasmic LIN28A facilitates degradation of the let-

7 pre-miRNA by adding an oligouridine tail to the 3′ end by recruiting the terminal uridyl transferase (TUTase) Zcchc11 (TUTase4/TUT4), thereby blocking Dicer cleavage (Zhou et al., 2013). However, nuclear LIN28B, on the other hand, hinders pri-pre-miRNA processing through a TUTase-independent mechanism (Piskounova et al., 2011; Thornton et al., 2012). Ordinarily, the post-transcriptional regulation of let-7 by LIN28 is highly essential for normal development and contributes to the pluripotent state by inhibiting let-7 mediated differentiation of embryonic stem cells (ESCs) (Lozoya et al., 2014; Shyh-Chang and Daley, 2013; Thornton and Gregory, 2012). However, in cancer state, activation of LIN28A and LIN28B occurs in several different primary human tumours displaying low levels of let-7 expression while this effect is abrogated upon enforced let-7 expression in these cells (Iliopoulos et al., 2009; Viswanathan et al., 2009; Wang et al., 2015).

Herein, we also demonstrated that FLYWCH1-mediated regulation of let-7 expression via LIN28 may occur in a cell specific-dependent manner by observing, *in-vitro*, the protein expression pattern of LIN28 under different cellular conditions. Since earlier results showed a positive correlating expression pattern between human FLYWCH1 and let-7, we expected to observe an inverse expression pattern of LIN28 upon overexpression of GFP-FLYWCH1. We show that FLYWCH1 may be involved in trans-localization of both LIN28A and LIN28B from their respective sites as revealed mainly by immunofluorescence analysis. Knock-down of FLYWCH1 seemed to cause an increase in LIN28A in the nuclear membrane in both TIG119 and SW480 cells (Figure 5-10 C, Figure 5-13 C) while a reduced LIN28B expression in the

cytoplasm in SW480 and HCT116 GFP-FLYWCH1$^{O/E}$ cells was observed (Figure 5-14 B, Appendix 11).

Here, we demonstrate that localization of LIN28B and LIN28A may not entirely be restricted in the nucleus and cytoplasm respectively with its presence also observed in the cytoplasm and nucleus respectively. This is in agreement with other studies suggesting LIN28B may also be localized in the cytoplasm but shuttled into the nucleus in a cell-cycle dependent manner (Guo et al., 2006; Molenaar et al., 2012; Zhou et al., 2013). Additionally, LIN28A can also shuttle between the cytoplasm and nucleus (Tsialikas and Romer-Seibert, 2015), however this is surprising since LIN28A lacks the nuclear localization signal (NLS) motif. Hence, it may be plausible to suggest that FLYWCH1 regulates the shuttling of both LIN28A and LIN28B between the nucleus and cytoplasm. Additionally, both LIN28 A/B possesses a highly conserved regions comprising of a cold-shock domain (CSD) and two Cys-Cys-His-Cys (CCHC) zinc finger domains, which promotes an RNA-binding function (Piskounova et al., 2011; Zhou et al., 2013). However, as opposed to LIN28A, LIN28B is comprised of a nucleolar localization signal (NoLS) between the CSD and first zinc finger domain as well as a nuclear localization signal (NLS) at the C-terminal end (Zhou et al., 2013). As FLYWCH1 is also localized in the nucleus, it may therefore directly bind to LIN28B to hinder its translocation to the cytoplasm thus preventing the blockade of let-7 biogenesis and maturation in the cytoplasm. However, the possibility of a direct interaction between FLYWCH1 and LIN28B is yet to be determined. Furthermore, the cluster of LIN28A observed on the nuclear membrane boundary (Figure 5-10 C & Figure 5-13 C) could be mRNA granules called stress granules. Stress granules are usually

formed in response to oxidative stress and heat (Balzer and Moss, 2007). Studies have also indicated a link between oxidative stress and cancer (Reuter et al., 2010). Therefore, a more robust analysis is required to assess the FLYWCH1-mediated trans-localization of LIN28A/B and its effect on other cancer related cellular conditions.

The relationship between miRNAs and Wnt-β-catenin pathway has been identified in a variety of cellular contexts, although it remains un-clear in stem cells, particularly cancer stem cells. Few downstream miRNA targets of the Wnt-β-catenin pathway such as miR302 (Bräutigam et al., 2013) and miR181 (Ji et al., 2011) have been identified. In contrast, many upstream modulated miRNAs of the Wnt-β-catenin pathway have been identified, of which miR-315 (Silver et al., 2007) and miR-135a/b (Nagel et al., 2008) upregulate, while miR-200a (Korpal et al., 2008; Saydam et al., 2009), and miR-8 (Kennell et al., 2008) all interact with Wnt-β-catenin pathway components to downregulate β-catenin transcriptional activity. Although recent advances demonstrate an inverse relationship between the Wnt/β-catenin pathway and let-7 miRNA expression (Cai et al., 2013b; Madison et al., 2015), the exact mechanism that drives this event remains poorly understood. FLYWCH1 acts as a negative regulator of the Wnt/β-catenin pathway by directly interacting with un-phosphorylated β-catenin (Muhammed et al., submitted), therefore we attempted to understand the mechanism involving FLYWCH1, let-7 and β-catenin. However, results obtained suggests that let-7 remains unchanged upon ectopic expression of nuclear β-catenin (Figure 5-18). Nevertheless, the reported negative regulation of the canonical Wnt pathway by let-7 miRNA may be due to direct or indirect

cross-talk and interaction with other components of the Wnt/β-catenin signalling pathway.

In summary, we reveal a possible novel regulation pathway of let-7 miRNA in a LIN28 dependent manner controlled by FLYWCH1 (Figure 5-20), thus may possess a tumour suppressor activity. However, future extensive studies such as *in-vivo* transgenic and xenograft studies are highly warranted to understand the role of FLYWCH1-mediated regulation of let-7 in normal physiology and cancer.

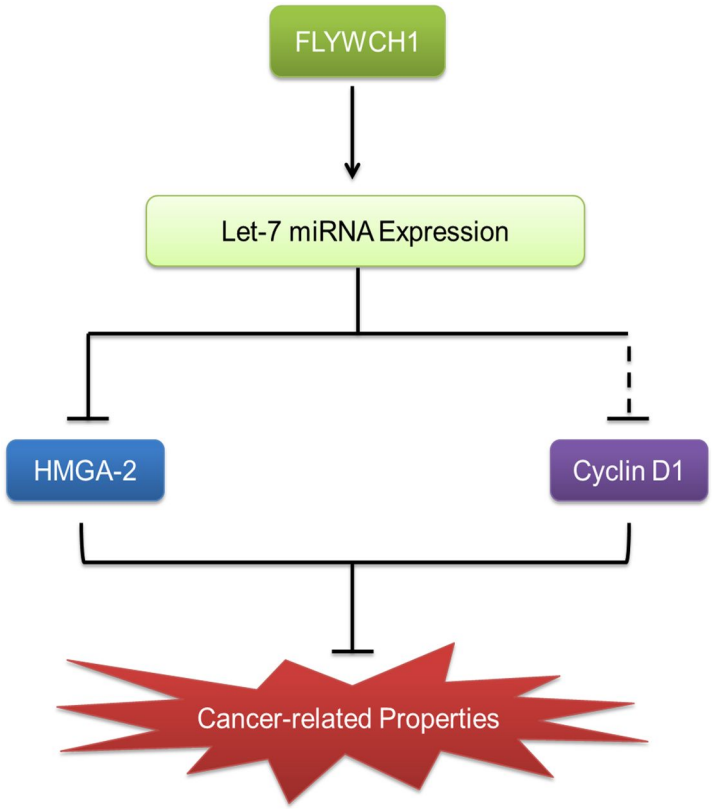


Figure 5-20: Proposed FLYWCH1-mediated regulation of let-7. A simplified diagram showing the possible mechanism by which FLYWCH1 exerts its tumour suppressor activity in a let-7 dependent manner. FLYWCH1 negatively regulates the Wnt/β-catenin pathway while augmenting let-7 expression which would in turn transcriptionally repress oncogenic targets such as HMGA-2, and cyclin-D1. Dashed lines indicates indirect interaction.

6 CHAPTER 6

General Discussion

6.1 Overview

Colorectal cancer (CRC) is a common form of cancer that mostly occurs due to the formation of adenomatous polyps (adenomas). Oncogenes and mutations of tumour suppressor genes are primarily responsible for the progression and maintenance of this form of cancer.

The Wnt pathway is tightly regulated at both transcriptional and post-translational regulators; therefore aberrant Wnt activity often results in developmental disorders and diseases including but not limited to cancer (Novellasdemunt et al., 2015). For instance, during metastatic processes, epithelial cancer cells require certain characteristics such as elevated expression of mesenchymal markers as well as other alterations in their microenvironment to enable invasion of adjacent tissues and progression to metastatic high-grade tumours. Furthermore, inappropriate Wnt signals coupled with a loss of E-cadherin also contributes to cytoplasmic β-catenin accumulation and facilitates EMT activity (Lamouille et al., 2014; Yang et al., 2015b).

Although Wnt signalling via the β-catenin/TCF complex is well documented as a prerequisite for activation of Wnt-target genes, this pathway cannot always lead to gene activation. Accumulated evidence over the past decade have identified several proteins that interact with nuclear β-catenin to antagonize its transcriptional activity leading to transcriptional repression of Wnt-target genes. Accordingly, maintaining the balance between activation and repression of Wnt signalling pathway is an essential task during normal development. In this vein and in certain circumstances, Wnt-signals need to be quenched in order to allow healthy organogenesis during embryonic development.

More recently, we have identified a novel transcription regulator with a FLYWCH/Zn-finger DNA-binding domain called "FLYWCH1" that is bound to β-catenin. Despite the limited information on FLYWCH1, our preliminary data suggest that the FLYWCH1 protein acts as a negative regulator of Wnt/β-catenin signalling pathway by competing with TCF4 and interacting with β-catenin thereby preventing transcription of Wnt target genes (Muhammad et al, submitted).

Due to the increase of knowledge about protein and gene changes in cells that sustain cancer progression, the FLYWCH1 protein possesses the potential to uncover novel mechanisms and pathways that may be involved in early cancer development governed by aberrant Wnt/β-catenin signalling. These knowledge would provide an avenue for the discovery of better diagnostic tools for disease and potential anti-cancer drug targets. This would be particularly beneficial to CRC patients because over 80% of CRC tumours cases exhibits hyper-activated β-catenin signals. Additionally, patients suffering from other forms of cancer such as breast cancer, lung cancer and melanoma could also benefit from this research due to the aberrant signalling of the Wnt pathway in these forms of cancer.

Therefore, in this thesis, my study was focussed on further characterization on the biological activity of FLYWCH1 within normal and CRC cell lines by utilizing mainly extensive *in-vitro* model systems and at the end analysis of potential mechanism and clinical relevance using samples from colorectal cancer patients. Overall, this study revealed that:

i. FLYWCH1 overexpression caused changes cell morphology in cultured CRC cells from an irregular to a more circular and epithelial phenotype via possible cytoskeletal re-organization. Cell morphology, could cause changes on cell motility and cell migration.

ii. Our data also show from the immunostaining assay of colonosphere that FLYWCH1 may play a role on dynamics of CRC-CSCs division between self-renewal and differentiation of cancer cells.

iii. Anti-FLYWCH1 antibody labels FLYWCH1 as a speckled pattern in the nucleus, and co-localizes with splicing factor SC-35.

iv. FLYWCH1 antagonizes the canonical β-catenin pathway by promoting the GSK-3β activation.

v. FLYWCH1 may be associated with the biogenesis of miRNAs, while positively regulating the expression of tumour-suppressor let-7 miRNAs.

vi. FLYWCH1 regulates cell morphology by regulating the EMT-transcription factor ZEB1 via E-cadherin induction.

6.2 FLYWCH1 mediates the anti-migratory effects of CRC cells via alterations in cell-cell adhesion

Key features of cancer aggressiveness and progression are metastasis, tumorigenic capacity and resistance to conventional chemo/radiotherapy. Metastasis, the dissemination of cancer cells to distant organs causing secondary cancer is predominantly driven by EMT, which has been identified as a critical process associated with the transformation of epithelial cells toward a motile

mesenchymal state. These hallmarks contribute to the prevention of cancer treatments. Metastasis is an intricate process involving the remodelling of the cell cytoskeleton to enable motility. The various components of the cytoskeleton including microtubules, actin microfilaments, microtubules and intermediate filaments act together in synergy and their functions are well organized in normal cells (Fife et al., 2014). In order for metastasis to occur, tumour cells must undergo the following steps: primary tumour detachment and anoikis (cell detachment-induced cell death) evasion → cell invasion and metastasis → intravasation → blood vessel transportation → extravasation → proliferation of secondary tumour (Fife et al., 2014; Steeg, 2006). However, despite recent breakthroughs in medical advances, cancer metastases remain a significant clinical complication that emphasizes the importance of understanding the metastatic process that drives carcinoma development. As a result, development of novel therapeutic agents depends on uncovering the underlying molecular mechanism that elicits metastatic cancer progression.

Herein our data suggested that FLYWCH1 overexpression promotes morphological changes from a fibroblastic-like to a more epithelial phenotype in CRC cells (Figure 3-6), possibly through cytoskeleton re-arrangement. It was also observed that FLYWCH1 might regulate filopodial formation, which is necessary for cell motility (Figure 3-8). Furthermore, in CRC cells, FLYWCH1 overexpression appeared to positively regulate E-Cadherin (Figure 3-12 &Figure 3-13) while having a negative effect on ZEB1-EMT transcription factor (Figure 3-13 &Figure 3-14). These observations may signify a role of FLYWCH1 in regulating EMT, however, this was not the case as no changes were observed in vimentin and ZEB2 expression levels (Figure 3-13). The actin cytoskeleton

plays key roles in cell events such as, but not restricted to differentiation, membrane organization, motility, cell division, all of which depend on actin filament remodelling. Moreover, scientific studies also highlight the importance of filopodia or actin-rich filopodia-like structures during cellular migration in 3D (Jacquemet et al., 2015). Additionally, we reveal that FLYWCH1 also appears to regulate the formation of stress fibre-like formation in TIG119 cells, although without having an effect on the cell morphology (Figure 3-5 C).

Various studies have indicated a direct relationship between actin dynamics and morphological changes demonstrating a crucial role of the actin cytoskeleton in the cancer development (Sun et al., 2015). Therefore, alterations in physical properties and phenotypic profiles of cells are deterministic descriptors of metastatic properties (Hanahan and Weinberg, 2011). Obstruction in actin cytoskeleton rearrangement and cell migration could also be associated with mesenchymal epithelial transition (MET) (Nelson et al., 2008), a process contrary to EMT. In contrast to EMT, MET is characterized by an abundance of epithelial-specific proteins, such as E-cadherin, and down-regulation of mesenchymal-specific molecules, such as N-cadherin and vimentin. Equally, accumulating evidence indicates a key role played by β-catenin in promoting metastasis while the E-Cadherin/β-catenin complex plays a critical role in maintaining cell-cell adhesion, cell shape as well as epithelial integrity thereby preventing cell migration (Kidani et al., 2014).

Furthermore, studies have continued to provide evidence of a link between adhesion and Wnt signalling through β-catenin as cadherin enrichment have been shown to regulate β-catenin signalling pool (Daugherty and Gottardi, 2007). Therefore, cell migration and morphological changes mediated by

FLYWCH1 might trigger the modulation of the genetic program downstream to β-catenin/TCF4 signalling. Thus, the positive and negative regulation of E-cadherin and β-catenin respectively by FLYWCH1 could suggest a crosstalk between Wnt signalling and adhesion mediated via FLYWCH1.

We also show a quantitative analysis of FLYWCH1 adhesion properties (Figure 3-9) as well as the inhibitory effect on wound healing in CRCs (Figure 3-10). Following the discovery of the β-catenin interacting property of FLYWCH1, we can also alternatively suggest that the inhibitory effect of FLYWCH1 on cell migration may be associated to cell shape alterations through modulation of the genetic program downstream to β-catenin/TCF4 signalling. For instance, signalling through the Wnt/β-catenin pathway controls the expression of various genes that control filopodia formation and consequently, cell morphology and migration/invasion; such as CDH1, c-Jun, Fascin1 and Eph/ephrin molecules (Alt-Holland et al., 2008; Cortina et al., 2007; Jiao et al., 2010). However, it is also important to note that the involvement of MET/EMT processes through other signalling events is not ruled out.

During EMT, expressions of epithelial proteins involved in cell junction processes are generally down regulated. These changes in gene expression hinder the de-novo epithelial cell–cell junctions formation thereby resulting to the depletion of the epithelial barrier function (Lamouille et al., 2014; Peinado et al., 2007). For instance, studies demonstrate the involvement of ZEB1 in driving pro-metastatic actin cytoskeletal remodelling by downregulating the expression of certain tumour suppressor miRNAs, particularly miR-34a (Ahn et al., 2012). Following the FLYWCH1-mediated down-regulation of ZEB1 expression and the consequent increase of E-cadherin expression in CRCs and

colonospheres (Figure 4-7) as well as the opposing expression of FLYWCH1 and ZEB1 in colorectal cancer patient samples (Figure 3-14), we can suggest that FLYWCH1 prevents the ZEB1-mediated transcriptional repression of E-cadherin. Alternatively, coupled with the presence of DNA binding zinc finger domain, FLYWCH1 may acts as a nuclear transcription factor by regulating the transcription of other genes that control cytoskeletal re-modelling. Therefore, considering the FLYWCH1-mediated changes on ZEB1, E-cadherin and the cytoskeletal/morphological changes observed in normal and CRCs we can speculate that FLYWCH1 may contribute to the depletion of protein components of the actin-rich pseudopodia of metastatic cancer cells altering actin cytoskeleton dynamics, thereby resulting to morphological changes facilitated by induction of E-cadherin expression and MET-like alterations. Moreover, emerging evidence implicating miRNAs, including let-7 as key regulatory molecules in a diverse range of biological and pathologic processes including EMT are abundant (Li et al., 2009; Wu et al., 2015). Therefore, the revelation of the FLYWCH1-mediated regulation of let-7 (reported in Chapter 5) further highlights the significance of FLYWCH1 in inhibiting cell motility and enhancing cytoskeletal dynamics.

Taken together, we provide a notion that the FLYWCH1-mediated changes in cell morphology involves a crosstalk with the Wnt/β-catenin signalling pathways and a possible transcriptional regulation might be associated to morphological alterations via ZEB1 by FLYWCH1. However, the mechanism underlying the possible FLYWCH1-mediated regulation of cytoskeleton remodelling still requires further investigation with special focus on the Rho family GTPase signalling pathway.

6.3 Molecular mechanism underlying role of FLYWCH1 in Wnt/β-catenin signalling pathway

Numerous *in-vitro* and *in-vivo* studies have demonstrated the necessity of the Wnt/β-catenin signalling pathway in a diverse range of developmental and physiological processes; hence, dysregulation of the pathway is linked to several human diseases including cancers. Apart from the crosstalk with other pathways, the complexity of the pathway is compounded by the abundance of several key components that regulate β-catenin stability. Previous studies acquired from Dr. Nateri's lab utilizing site directed mutagenesis and Co-IP aided in the identification of the last three FLYWCH motifs of human FLYWCH1 necessary for the interaction with the N-terminal domain of β-catenin (Muhammed et al., submitted). Further transcriptional analysis also revealed FLYWCH1-mediated repression of β-catenin trans-activational activity. Therefore, the current study was aimed to further investigate the mechanistic role played by FLYWCH1 in negatively regulating the Wnt/β-catenin signalling pathway.

Intriguingly, we revealed an inverse effect of FLYWCH1 on GSK-3β activity as FLYWCH1 over-expression in CRC resulted to an up-regulation of activated GSK-3β, down-regulation of inactive GSK-3β and subsequent increase in total β-catenin (Figure 4-1 &Figure 4-2). Thus, the data suggest that FLYWCH1 regulates GSK-3β-mediated β-catenin phosphorylation. Multiple components of the Wnt/β-catenin pathway, including frizzled receptor, Wnt co-receptor LRP6, members of the β-catenin destruction complex (CK1, GSK-3β, APC, Axin, β-catenin) and dishevelled (Dvl), are all regulated by phosphorylation.

Phosphorylation represents a crucial mechanism responsible for the systematic control of β-catenin levels within normal and abnormal cells as well as Wnt/β-catenin pathway activation (Gao et al., 2014a). Indeed, several models have been suggested to explain the Wnt-mediated inhibition of β-catenin phosphorylation by GSK-3β via various mechanisms. For instance, studies show that during Wnt signal transduction, sequestration of GSK-3β from the cytoplasm into multi-vesicular bodies hinders GSK-3β activity (Taelman et al., 2010). Also, plausible evidence suggests that Wnt-activated LRP6 directly inhibits GSK-3β function (Cselenyi et al., 2008), while upon Wnt stimulation, GSK-3β-mediated phosphorylation of Axin at Ser-497/500 declines (Aaltonen et al., 2009; Kim et al., 2013b). A comprehensive description of the models that govern GSK-3β-mediated control of β-catenin are provided in (Gao et al., 2014a).

Herein, we proposed a different mechanism describing the FLYWCH1-mediated inhibition of the Wnt/β-catenin signalling pathway in cancer state. FLYWCH1 may facilitate the phosphorylation and subsequent activation of nuclear GSK-3β at Tyr-216 and the blockade of phosphorylation at Ser-9 resulting to the eventual ubiquitination and proteasomal degradation of β-catenin (Figure 4-1). Phosphorylation of GSK-3β at the Ser-9 position prevents β-catenin degradation while phosphorylation at the Tyr-216 position tends to mediate β-catenin degradation (Huang et al., 2010). Mutation of the β-catenin gene is also one of the major factors that contribute to aberrant Wnt/β-catenin signalling observed in CRCs (Clevers and Nusse, 2012).

Transcriptional repressors have been found to antagonize nuclear β-catenin activity through different mechanisms such as retardation of β-catenin/TCF complex (Ito et al., 2008; Tago et al., 2000; Wu et al., 2010b). Additionally,

following initial discovery of the direct interaction between FLYWCH1 and β-catenin, FLYWCH1 may undergo interaction with nuclear β-catenin to disrupt the transcriptional activity of β-catenin/TCF4 complex resulting to impaired β-catenin signalling (Muhammed et al., submitted). However, the experimental evidence here, suggests that FLYWCH1 may have a direct influence as a negative regulator of the β-catenin signalling pathway by influencing GSK-3β activity via a possible feedback-loop regulation mechanism of the β-catenin downstream target(s). The relationship between FLYWCH1 and GSK-3β was further validated following the discovery of changes in the IC_{50} values of GSK-3β inhibitor, TDZD-8 thus indicating that a greater concentration of TDZD-8 is needed to inhibit cell survival activity by 50% in SW480 cells over-expressing FLYWCH1, confirming the FLYWCH1-mediated reduced response to TDZD-8 (Figure 4-3). This is suggestive of a possible competition between FLYWCH1 and TDZD-8 for interacting with β-catenin via GSK-3β. However, additional bio-chemical methods may be required to identify if FLYWCH1 directly interacts with GSK-3β protein.

The FLYWCH1-mediated regulation of the Wnt/β-catenin signalling pathway has profound implications in stem cell proliferation as studies show that the Wnt/β-catenin signalling pathway contributes to the self-renewal of CSCs (Mao et al., 2014). Interestingly, results showed an elevated β-catenin expression in colonospheres derived from SW480 FLYWCH1^{shRNA} cells (Figure 4-6). Since *in-situ* hybridization analysis of *Flywch*1 was shown to be highly expressed at the crypts base of mouse intestine (Muhammed et al., submitted) where the *Lgr*5^{+ve} stem cells are enriched (Barker et al., 2007), and that its expression is also restricted to sporadic population of cells in both human and *Apc*$^{Min/+}$ mouse

intestinal tumours, coupled with the negative regulation of the Wnt/β-catenin signalling pathway, it is therefore, credible to hypothesize that FLYWCH1 may govern intestinal stem cells homeostasis in normal conditions and regulate cancer stem cells activity during cancer development via negative regulation of the Wnt/β-catenin pathway.

In summary, these data attempts to explain the mechanism/s underlying the FLYWCH-mediated regulation of Wnt/β-catenin signalling pathway in colorectal cancer state (Figure 6-1).

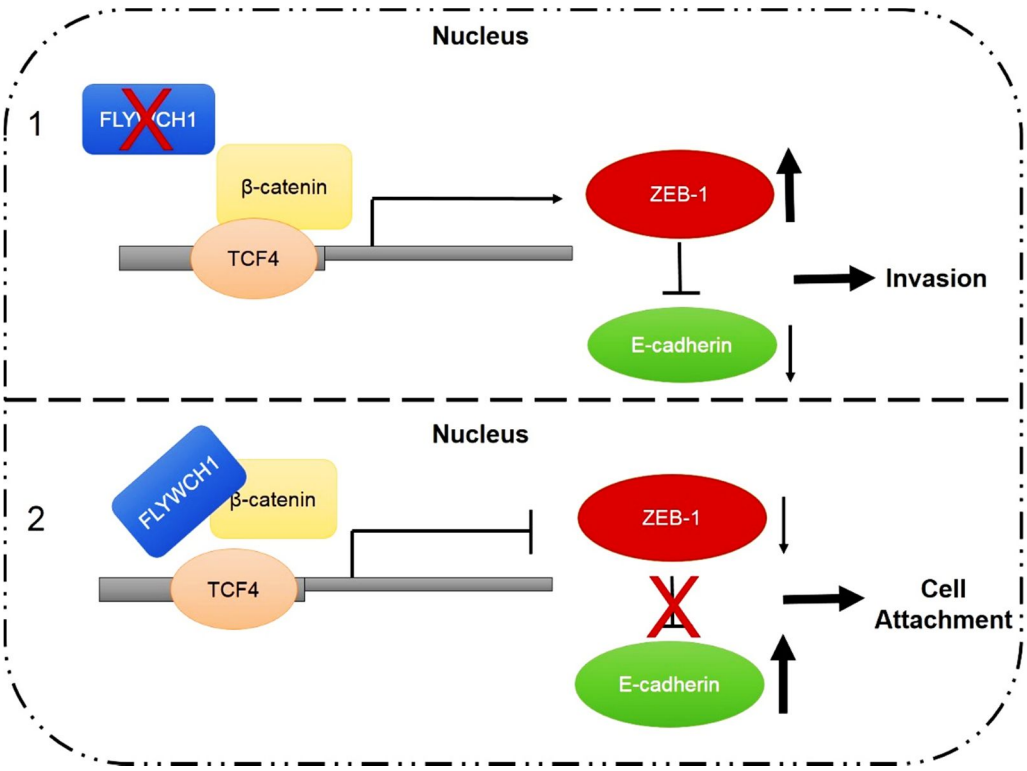


Figure 6-1: FLYWCH1 modulates transcriptional activity of canonical Wnt pathway (TCF4/β-catenin) to regulate ZEB1 expression. 1) In the absence of FLYWCH1, β-catenin/TCF4 binds directly to the ZEB1 promoter to facilitate its transcription and consequent transcriptional repression of E-cadherin. **2)** FLYWCH1 hinders interaction between β-catenin and TCF4 (Muhammed et al., submitted) thereby contributing to the downregulation of endogenous ZEB1 and up-regulation of E-cadherin (Chapter 3).

6.4 FLYWCH1 and let7 miRNA expression in CRCs

Over the past few years, miRNAs have not only emerged as integral regulators of gene expression at post-transcriptional level but also respond to signalling molecules to affect cell function(s). Recent technological advances have produced multiple high-throughput bioinformatics methods designed for profiling miRNA expression and identifying miRNA targets involved in a plethora of pathways that regulate normal physiology and various diseases. Despite this, less attention has been devoted towards understanding the underlying mechanisms that drives alterations in miRNA expression, especially in cancer cells. Recent evidence indicates that some miRNAs can either function as oncogenes or as tumour suppressors and expression profiling analyses have revealed characteristic miRNA signatures in certain human cancers. Although, individual interactions between components of the canonical Wnt pathway and miRNAs in normal and cancer state have already been established (Kang and Hata, 2015), we have simply just began to comprehend the role of miRNAs, not only in normal human development but also in tumour progression mediated by the canonical Wnt-signalling and vice-versa especially due to the fact that multiple components are involved in this complex network. MiRNAs crosstalk with a variety of key cellular signalling networks such as Wnt, transforming growth factor-β and Notch, control stem cell activity in maintaining tissue homeostasis, while if dysregulated contributes to the initiation and progression of cancer. Furthermore, the Wnt pathway in cooperation with LIN28 has being shown to negatively regulate let-7 miRNA (Tu et al., 2015), a bonafide tumour suppressor.

Here, we provide evidence of the FLYWCH1-mediated regulation of let-7 miRNA expression in CRCs (Figure 5-8 & Figure 5-9), possibly via direct interaction (Figure 5-16). This is also coupled with the discovery that the FLYWCH1-mediated regulation of let-7 may occur in a LIN28 dependent manner (Figure 5-10, Figure 5-13, Figure 5-14 & Appendix 10 & 11). Furthermore, since experimental evidence suggest the localization of noncoding RNA to nuclear bodies known as nuclear speckles (Leucci et al., 2013; Nakagawa et al., 2012), the involvement of FLYWCH1 in miRNA regulation was further substantiated by the co-localization of FLYWCH1 with nuclear speckle marker 'SC35' (Figure 5-1 B). The let-7 miRNA has been shown to govern differentiation and cell proliferation. Importantly, several recent studies have attributed the reduction of let-7 expression to increased tumorigenesis and poor patient prognosis. Moreover, let-7 have also been found to regulate "stemness" by hindering self-renewal and facilitating differentiation in both normal development and cancer state (Büssing et al., 2008). Therefore, these results implicate FLYWCH1 as possessing tumour suppressor properties. MiRNA expression profiling can be an important tool for diagnostics and treatment of a plethora of diseases. Since tumours are composed of heterogeneous population of cells, therefore estimated expression profile of the pure cancer verses normal cell type could be inferred by differential expression of miRNAs from one cancer cell to another.

Contemporary research suggest that proteins with the classical Cys_2His_2 zinc finger motif can exhibit very different functional tendencies; acting as transcription factors that function by recognition of specific DNA and RNA sequences (Font and Mackay, 2010; Laity et al., 2001). Our data strongly

suggests that the FLYWCH1 protein positively regulates let-7 miRNAs expression in both normal cells and CRCs (Table 5-1, Figure 5-6 D, Figure 5-8 & Figure 5-9). The mere fact that alterations of miRNA expressions was observed in the current study lays credence to the RNA-binding property of the zinc finger motif conserved in FLYWCH1. Several members of the let-7 miRNA family are downregulated in various forms of cancers, including colorectal cancer. They are also thought to possess tumour suppressor activity by lowering anti-apoptotic and growth-promoting proteins. Nevertheless, the expression of certain member/s of the let-7 family may vary based on the form of cancer, for instance let-7a have been shown to be downregulated in breast, melanoma and pancreatic cancers but is up-regulated in ovarian and lung cancer (Boyerinas et al., 2010). However, medical and research advancement has made it possible to identify the mechanism(s) that govern the correlation between cancer and let-7 levels (Powers et al., 2016). Therefore, the identification of FLYWCH1 as a potential regulator of let-7 levels could further improve the understanding of let-7 miRNA control in cancer state. Moreover, a direct relationship between let-7 and FLYWCH1 mRNA expression in CRC patient samples (Figure 5-19) was observed thereby suggesting a FLYWCH1-mediated regulation of let-7 during colorectal cancer development.

Due to the FLYWCH1-mediated regulation of let-7, we attempted to investigate whether FLYWCH1 have an opposite effect of LIN28. The different expression patterns of both LIN28A and LIN28B in the presence and absence of FLYWCH1 prompts the possibility of a FLYWCH1-mediated control of let-7 by regulating the translocation of LIN28 between the nucleus and cytoplasm (Figure 5-10, Figure 5-13, Figure 5-14, Appendix 10 & 11). FLYWCH1 may also be involved

in preventing the translocation of LIN28B to the cytoplasm. A restriction of LIN28B shuttling to the cytoplasm further enhance let-7 miRNA maturation and binding to RISC complex in the cytoplasm.

The fact that both let-7 and LIN28 are not only involved in cancer and tumour development but also other developmental processes also shows the importance of FLYWCH1. Additionally, the current studies shows that the effect of FLYWCH1 on key cellular processes correlates with let-7. Recent experimental evidence continue to suggest provocatively that Let-7 depletion coupled with β-catenin accumulation may contribute to a cancer stem cell phenotype in the intestine, thereby promoting CRC development (Borah et al., 2015; Madison et al., 2015). The controversial cancer stem-like cell (CSC) theory is based on the phenomenon that cancer cells may be derived from a rare population of cells possessing stem cell properties (Beck and Blanpain, 2013; Ibrahim et al., 2012a; Nguyen et al., 2012). Recent studies have established the importance and significant roles played by the canonical Wnt-signalling in stemness activities in various tissues and cell types (Yang et al., 2015a). For instance, Wnt3a was shown to foster the formation of embryonic stem cell (ESC)-like colonies (Sato et al., 2004). Canonical Wnt pathway activation was shown to augment alkaline phosphatase and Cbfa1/Runx2 expression thereby facilitating mesenchymal stem cells (MSCs) osteogenic differentiation (Day et al., 2005; Kim et al., 2013a). Additionally, the let-7 family, also a negative regulator of β-catenin, is another crucial modulator of ESC differentiation (Viswanathan et al., 2008). Therefore, it was interesting to observe that colonospheres derived from SW480 FLYWCH1^{shRNA} exhibited high expression of β-catenin (Figure 4-6), ZEB1 (Figure 4-7), CD44 (Figure 4-9) and low expression of differentiation marker

BMP4 (Figure 4-8) and MUC2 (Figure 4-10). These results are suggestive of a possible FLYWCH1-let-7 network that could suppress CSCs tumour activity by hindering stemness and metastasis (Figure 6-2).

To sum up, the biochemical data presented in this work shows FLYWCH1 controls let-7 expression and may have important implications for colon cancer progression and stemness activities.

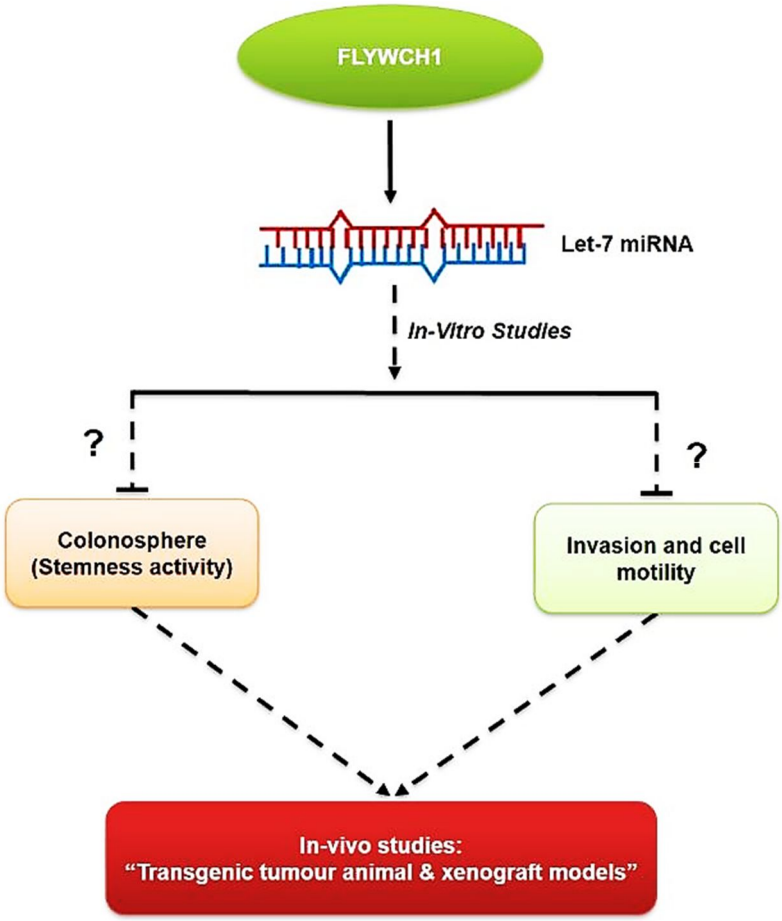


Figure 6-2: **FLYWCH1-mediated regulation of let-7.** Biological processes that drive cancer progression could be regulated by the FLYWCH1-mediated regulation of let-7 *in-vitro*. This is consistent with various studies identifying let-7 as a tumour suppressor miRNA. Further *in-vivo* studies are required to validate FLYWCH1-mediated role in let-7 biogenesis.

6.5 Experimental Limitations

1) Evidence of FLYWCH1's influence on GSK3β activity and hence tumour suppressor activity in colorectal tumorigenesis was limited to HCT116 and SW480 cells. Repeating the experiments in other CRC cell lines other than HCT116 and SW480 cell lines would have improved the reliability of the results and allowed wider application of the study. Also, time limitations did not allow comparison to other GSK3β inhibitors, for example lithium chloride, which would have provided further insight into FLYWCH1's effect on GSK3β activity and determined whether the possible competition between FLYWCH1 and the GSK3β inhibitor is limited to TDZD-8.
2) Endogenous expression of FLYWCH1 could not be detected using western blotting technique although endogenous expression of FLYWCH1 was detectable via fluorescent immunostaining using the same anti-FLYWCH1 antibody. As a result, validation of the knockdown of FLYWCH1 at protein level was assessed solely via immuno-fluorescence while expression at gene level was also analyzed via the qRT-PCR and the standard RT-PCR assays.
3) Although we were able to assess the gain-of-function and loss-of-function properties of FLYWCH1 by transient transfection and application of a lentiviral-based gene delivery system to acquire stable expression of eGFP reporter and GFP-FLYWCH1 knockdown in normal and CRC cell lines (TIG119, HCT116 & SW480) we were unable to generate stable expression of full-length eGFP-FLYWCH1 gene.

Following the application of different approaches such as western blotting, microscopic observations, genomic PCR analysis, luciferase and migration assays to extensively characterize the exogenous FLYWCH1, preliminary analyses revealed a spontaneous mutation on the integrated eGFP-FLYWCH1 in both HCT116 and HEK293T stable cell lines resulting in a modified, un-functional FLYWCH1 protein unable to interact with β-catenin (Muhammed et al., submitted). Additional attempts to generate cells stably expressing FLYWCH1 also resulted to the gradual loss of eGFP-FLYWCH1 followed by the abnormal death of GFP-FLYWCH1^{+VE} cells. Therefore, applying an inducible promoter (e.g.; a tetracycline-inducible gene expression cassette) for FLYWCH1 protein expression will be suitable for future studies.

4) The absence of subcutaneous, xenografts or metastatic mouse models was another limitation in this study. Such approaches are beneficial in validating and exploring possible FLYWCH1-mediated anti-tumorigenic properties, which can be accomplished, via either loss-of-function or gain-of-function *in-vivo* approaches. However, generation of cells stably expressing FLYWCH1 was required.
5) We were unable to perform gene expression profiling analysis of miRNAs via intestinal crypt isolation utilizing intestinal organoid cultures. This organoid system already established in our lab (Lorenzi et al., 2016), is an effective tissue stem cell derived three dimensional (3D) model and a useful tool predominantly for functional study (Onyido et al., 2016). This technique mimics the microenvironment of the adult

intestine, as dividing LGR5+ stem cells are intercalated with Paneth cells and located at the crypt base of the intestine. These organoids therefore provides a highly physiologically relevant phenotype and would have being an ideal tool to assess the role of FLYWCH1 in the maintenance of stem cell compartment.

6) Analysis of FLYWCH1 expressions as well as correlation of the expression patterns with let-7 were carried out with nine samples each of normal, primary and metastasis tissue samples. This experiment could be repeated with a larger number of samples of each condition (normal, primary & metastatic) using immunohistochemistry (IHC). However, current anti-FLYWCH1 antibodies examined in our lab are not suitable for IHC.

6.6 Concluding Remarks & future directions

The research findings of this thesis highlights the biological significance of FLYWCH1 in antagonizing the canonical Wnt signalling pathway, positively regulating let-7 miRNA expression and control of cell motility and morphological alterations that may reverse EMT-like characteristics. Consistent with current research outcomes in Dr. Nateri's laboratory, FLYWCH1's tumour suppressor activity highlights its importance as a potential gene therapy agent or for the possible production of anti-tumour drugs. Drugs that may selectively activate FLYWCH1 to stabilize the GSK3β/β-catenin destruction complex in CRC cells require extensive investigation. The role of FLYWCH1 as an antagonist of Wnt/β-catenin activity remains intriguing, as deregulation of

Wnt/β-catenin signalling is a prominent feature in colorectal carcinogenesis, making FLYWCH1 a principal target for future colorectal cancer research. Therefore, given the regulatory importance of nuclear cofactors (both coactivators and co-repressors) on Wnt signalling pathway, it is, therefore, predictable that our newly described FLYWCH1 protein-protein interaction with the nuclear β-catenin as well as the possible FLYWCH1-mediated phosphorylation and inactivation of GSK-3β could have crucial involvement in normal versus tumour development. Nevertheless, the contributions of FLYWCH1 in the therapeutic field is currently far from realization therefore, the findings of this study warrant a larger follow-up investigation of this newly identified human protein.

Although credible data regarding functional analysis of FLYWCH1 was provided in the current work, a series of complementary research and further analyses are required to establish the cellular implications of FLYWCH1 in the biological processes in normal and pathological state in more detail. Areas that require further attention are briefly described below:

1) Identification of a specific and effective antibody that detect the endogenous level of FLYWCH1 and investigate possible post-translationally modification/s via western blotting.
2) Utilization of the intestinal organoid-culture system as a platform for Lentiviral-based-overexpression for β-cateninS33A (pLVX-FLAG-β-cateninS33A) and Lentiviral-shRNA-based-knockdown for FLYWCH1 as well as examining the miRNAs expression levels (specifically let-7) in correlation with FLYWCH1 in intestinal crypts and 3D-organoids cultures.

3) Investigate the clinical significance of defined miRNAs (let-7) in CRC tissues using a CRC tissue microarray (TMA) using *in-situ* hybridization (ISH) for let-7 miRNA and its correlation with FLYWCH1 expression using IHC (immunohistochemistry).
4) Observe the effect of exogenous expression of FLYWCH1 on morphological changes and cytoskeletal remodelling on a larger range of cancer cell lines such as HT29 and DLD-1. This will provide valuable insight on the role of FLYWCH1 in modulating cytoskeletal alterations in normal vs cancer cells.
5) Identification of the possible post-transcriptional and/or post-translational modification mechanism(s) that govern the expression and/or activity of FLYWCH1.
6) Following preliminary observation of expression patterns of stem cell and differentiation markers in colonospheres derived from SW480 GFP^{+VE} and $FLYWCH1^{shRNA}$ cells (Chapter 4), additional studies are required to investigate the possible regulatory mechanistic role of FLYWCH1 in the regulation of self-renewal and differentiation in normal vs cancer cell lines via organoid platforms by the use of BrdU pulse-chase labelling approach.
7) Investigate the global downstream targets by RNA-seq, RNA Immunoprecipitation (RIP)-seq and Chromatin Immunoprecipitation (ChIP)-seq.
8) *In-vivo* animal studies such as knockout mice or xenograft could **i)** be useful tools in further investigating the tissue homeostasis and/or tumorigenic properties of FLYWCH1, **ii)** can also provide an avenue for

the validation of FLYWCH1-mediated control of let-7 miRNAs as well as the FLYWCH1 negative regulation of Wnt-signalling pathway.

REFERENCES

Aaltonen, K., Amini, R.-M., Heikkilä, P., Aittomäki, K., Tamminen, A., Nevanlinna, H., and Blomqvist, C. (2009). High cyclin B1 expression is associated with poor survival in breast cancer. British journal of cancer *100*, 1055-1060.

Abashidze, A., Gold, V., Anavi, Y., Greenspan, H., and Weil, M. (2014). Involvement of IKAP in peripheral target innervation and in specific JNK and NGF signaling in developing PNS neurons. PloS one *9*, e113428.

Abdelmaksoud-Damak, R., Miladi-Abdennadher, I., Triki, M., Khabir, A., Charfi, S., Ayadi, L., Frikha, M., Sellami-Boudawara, T., and Mokdad-Gargouri, R. (2015). Expression and Mutation Pattern of β-Catenin and Adenomatous Polyposis Coli in Colorectal Cancer Patients. Archives of medical research *46*, 54-62.

Ahn, Y.-H., Gibbons, D.L., Chakravarti, D., Creighton, C.J., Rizvi, Z.H., Adams, H.P., Pertsemlidis, A., Gregory, P.A., Wright, J.A., and Goodall, G.J. (2012). ZEB1 drives prometastatic actin cytoskeletal remodeling by downregulating miR-34a expression. The Journal of clinical investigation *122*, 3170-3183.

Akao, Y., Nakagawa, Y., and Naoe, T. (2006). let-7 microRNA functions as a potential growth suppressor in human colon cancer cells. Biological and Pharmaceutical Bulletin *29*, 903-906.

Al-Mulla, F., Bitar, M.S., Al-Maghrebi, M., Behbehani, A.I., Al-Ali, W., Rath, O., Doyle, B., Tan, K.Y., Pitt, A., and Kolch, W. (2011). Raf kinase inhibitor protein RKIP enhances signaling by glycogen synthase kinase-3β. Cancer research *71*, 1334-1343.

Alt-Holland, A., Shamis, Y., Riley, K.N., DesRochers, T.M., Fusenig, N.E., Herman, I.M., and Garlick, J.A. (2008). E-cadherin suppression directs cytoskeletal rearrangement and intraepithelial tumor cell migration in 3D human skin equivalents. Journal of Investigative Dermatology *128*, 2498-2507.

Aman, A., and Piotrowski, T. (2008). Wnt/beta-catenin and Fgf signaling control collective cell migration by restricting chemokine receptor expression. Dev Cell *15*, 749-761.

Ameres, S.L., and Zamore, P.D. (2013). Diversifying microRNA sequence and function. Nature reviews Molecular cell biology *14*, 475-488.

Amin, M.A., Matsunaga, S., Ma, N., Takata, H., Yokoyama, M., Uchiyama, S., and Fukui, K. (2007). Fibrillarin, a nucleolar protein, is required for normal nuclear morphology and cellular growth in HeLa cells. Biochemical and biophysical research communications *360*, 320-326.

Anastas, J.N., and Moon, R.T. (2013). WNT signalling pathways as therapeutic targets in cancer. Nature Reviews Cancer *13*, 11-26.

Angers, S., and Moon, R.T. (2009). Proximal events in Wnt signal transduction. Nature reviews Molecular cell biology *10*, 468-477.

Aoki, K., and Taketo, M.M. (2007). Adenomatous polyposis coli (APC): a multi-functional tumor suppressor gene. Journal of cell science *120*, 3327-3335.

Asl, H.F., Talukdar, H.A., Kindt, A.S., Jain, R.K., Ermel, R., Ruusalepp, A., Nguyen, K.-D.H., Dobrin, R., Reilly, D.F., and Schunkert, H. (2015). Expression quantitative trait Loci acting across multiple tissues are enriched in inherited risk for coronary artery disease. Circulation: Cardiovascular Genetics, CIRCGENETICS. 114.000640.

Atkins, R.J., Dimou, J., Paradiso, L., Morokoff, A.P., Kaye, A.H., Drummond, K.J., and Hovens, C.M. (2012). Regulation of glycogen synthase kinase-3 beta (GSK-3β) by the Akt pathway in gliomas. Journal of Clinical Neuroscience *19*, 1558-1563.

Augsten, M. (2014). Cancer-associated fibroblasts as another polarized cell type of the tumor microenvironment. Frontiers in oncology *4*.

Babaei-Jadidi, R., Li, N., Saadeddin, A., Spencer-Dene, B., Jandke, A., Muhammad, B., Ibrahim, E.E., Muraleedharan, R., Abuzinadah, M., and Davis, H. (2011). FBXW7 influences murine intestinal homeostasis and cancer, targeting Notch, Jun, and DEK for degradation. The Journal of experimental medicine *208*, 295-312.

Bachelder, R.E., Yoon, S.-O., Franci, C., de Herreros, A.G., and Mercurio, A.M. (2005). Glycogen synthase kinase-3 is an endogenous inhibitor of Snail transcription implications for the epithelial–mesenchymal transition. The Journal of cell biology *168*, 29-33.

Balzer, E., and Moss, E.G. (2007). Localization of the developmental timing regulator Lin28 to mRNP complexes, P-bodies and stress granules. RNA biology *4*, 16-25.

Barh, D., Malhotra, R., Ravi, B., and Sindhurani, P. (2010). MicroRNA let-7: an emerging next-generation cancer therapeutic. Current oncology *17*, 70.

Barker, N., and Clevers, H. (2006). Mining the Wnt pathway for cancer therapeutics. Nature reviews Drug discovery *5*, 997-1014.

Barker, N., Hurlstone, A., Musisi, H., Miles, A., Bienz, M., and Clevers, H. (2001). The chromatin remodelling factor Brg-1 interacts with beta-catenin to promote target gene activation. EMBO J *20*, 4935-4943.

Barker, N., van Es, J.H., Kuipers, J., Kujala, P., van den Born, M., Cozijnsen, M., Haegebarth, A., Korving, J., Begthel, H., Peters, P.J., *et al.* (2007). Identification of stem cells in small intestine and colon by marker gene Lgr5. Nature *449*, 1003-1007.

Basakran, N.S. (2015). CD44 as a potential diagnostic tumor marker. Saudi medical journal *36*, 273-279.

Beaster-Jones, L., and Okkema, P.G. (2004a). DNA binding and in vivo function of C. elegans PEB-1 require a conserved FLYWCH motif. Journal of molecular biology *339*, 695-706.

Beaster-Jones, L., and Okkema, P.G. (2004b). DNA binding and in vivo function of C.elegans PEB-1 require a conserved FLYWCH motif. J Mol Biol *339*, 695-706.

Beck, B., and Blanpain, C. (2013). Unravelling cancer stem cell potential. Nature Reviews Cancer *13*, 727-738.

Bellei, B., Flori, E., Izzo, E., Maresca, V., and Picardo, M. (2008). GSK3β inhibition promotes melanogenesis in mouse B16 melanoma cells and normal human melanocytes. Cellular signalling *20*, 1750-1761.

Benson, K., Cramer, S., and Galla, H.-J. (2013). Impedance-based cell monitoring: barrier properties and beyond. Fluids Barriers CNS *10*, 5.

Bilić, J., Huang, Y.-L., Davidson, G., Zimmermann, T., Cruciat, C.-M., Bienz, M., and Niehrs, C. (2007). Wnt induces LRP6 signalosomes and promotes dishevelled-dependent LRP6 phosphorylation. Science *316*, 1619-1622.

Bitarte, N., Bandres, E., Boni, V., Zarate, R., Rodriguez, J., Gonzalez-Huarriz, M., Lopez, I., Javier Sola, J., Alonso, M.M., and Fortes, P. (2011). MicroRNA-451 Is Involved in the Self-renewal, Tumorigenicity, and Chemoresistance of Colorectal Cancer Stem Cells. Stem cells *29*, 1661-1671.

Boehm, M., and Nabel, E.G. (2001). Cell Cycle and Cell Migration New Pieces to the Puzzle. Circulation *103*, 2879-2881.

Borah, A., Raveendran, S., Rochani, A., Maekawa, T., and Kumar, D. (2015). Targeting self-renewal pathways in cancer stem cells: clinical implications for cancer therapy. Oncogenesis *4*, e177.

Bordonaro, M., Tewari, S., Cicco, C.E., Atamna, W., and Lazarova, D.L. (2011). A switch from canonical to noncanonical Wnt signaling mediates drug resistance in colon cancer cells. PLoS One *6*, e27308.

Boyerinas, B., Park, S.-M., Hau, A., Murmann, A.E., and Peter, M.E. (2010). The role of let-7 in cell differentiation and cancer. Endocrine-related cancer *17*, F19-F36.

Boyle, P., and Langman, J. (2000). ABC of colorectal cancer: Epidemiology. BMJ: British Medical Journal *321*, 805.

Bradley, T., Cook, M.E., and Blanchette, M. (2015). SR proteins control a complex network of RNA-processing events. Rna *21*, 75-92.

Brandhagen, B.N., Tieszen, C.R., Ulmer, T.M., Tracy, M.S., Goyeneche, A.A., and Telleria, C.M. (2013). Cytostasis and morphological changes induced by mifepristone in human metastatic cancer cells involve cytoskeletal filamentous actin reorganization and impairment of cell adhesion dynamics. BMC cancer *13*, 35.

Bräutigam, C., Raggioli, A., and Winter, J. (2013). The Wnt/β-catenin pathway regulates the expression of the miR-302 cluster in mouse ESCs and P19 cells. PloS one *8*, e75315.

Brayer, K.J., and Segal, D.J. (2008a). Keep your fingers off my DNA: protein-protein interactions mediated by C2H2 zinc finger domains. Cell Biochem Biophys *50*, 111-131.

Brayer, K.J., and Segal, D.J. (2008b). Keep your fingers off my DNA: protein–protein interactions mediated by C2H2 zinc finger domains. Cell biochemistry and biophysics *50*, 111-131.

Büchner, K., Roth, P., Schotta, G., Krauss, V., Saumweber, H., Reuter, G., and Dorn, R. (2000). Genetic and molecular complexity of the position effect variegation modifier mod (mdg4) in Drosophila. Genetics *155*, 141-157.

Burridge, K., and Wittchen, E.S. (2013). The tension mounts: stress fibers as force-generating mechanotransducers. J Cell Biol *200*, 9-19.

Büssing, I., Slack, F.J., and Großhans, H. (2008). let-7 microRNAs in development, stem cells and cancer. Trends in molecular medicine *14*, 400-409.

Cai, G., Wang, J., Xin, X., Ke, Z., and Luo, J. (2007). Phosphorylation of glycogen synthase kinase-3 ss at serine 9 confers cisplatin resistance in ovarian cancer cells. International journal of oncology *31*, 657.

Cai, W.-Y., Wei, T.-Z., Luo, Q.-C., Wu, Q.-W., Liu, Q.-F., Yang, M., Ye, G.-D., Wu, J.-F., Chen, Y.-Y., and Sun, G.-B. (2013a). The Wnt–β-catenin pathway represses let-7 microRNA expression through transactivation of Lin28 to augment breast cancer stem cell expansion. Journal of cell science *126*, 2877-2889.

Cai, W.-Y., Wei, T.-Z., Luo, Q.-C., Wu, Q.-W., Liu, Q.-F., Yang, M., Ye, G.-D., Wu, J.-F., Chen, Y.-Y., and Sun, G.-B. (2013b). The Wnt–β-catenin pathway represses let-7 microRNA expression through transactivation of Lin28 to augment breast cancer stem cell expansion. J Cell Sci *126*, 2877-2889.

Cai, X., Hagedorn, C.H., and Cullen, B.R. (2004). Human microRNAs are processed from capped, polyadenylated transcripts that can also function as mRNAs. Rna *10*, 1957-1966.

Cai, Z., Tang, X., Gao, H., Tang, C., Nandakumar, V., Jones, L., Ye, H., Lou, F., Zhang, D., and Sun, H. (2014). APC, FBXW7, KRAS, PIK3CA, and TP53 Gene Mutations in Human Colorectal Cancer Tumors Frequently Detected by Next-Generation DNA Sequencing. Journal of Molecular and Genetic Medicine *2014*.

Caspi, M., Zilberberg, A., Eldar-Finkelman, H., and Rosin-Arbesfeld, R. (2008). Nuclear GSK-3β inhibits the canonical Wnt signalling pathway in a β-catenin phosphorylation-independent manner. Oncogene *27*, 3546-3555.

Chaffer, C.L., Marjanovic, N.D., Lee, T., Bell, G., Kleer, C.G., Reinhardt, F., D'Alessio, A.C., Young, R.A., and Weinberg, R.A. (2013). Poised chromatin at the ZEB1 promoter enables breast cancer cell plasticity and enhances tumorigenicity. Cell *154*, 61-74.

Chen, C., Peng, Y., Peng, Y., Peng, J., and Jiang, S. (2014). miR-135a-5p inhibits 3T3-L1 adipogenesis through activation of canonical Wnt/β-catenin signaling. Journal of molecular endocrinology *52*, 311-320.

Chen, J., Li, Y., Yu, T.-S., McKay, R.M., Burns, D.K., Kernie, S.G., and Parada, L.F. (2012). A restricted cell population propagates glioblastoma growth after chemotherapy. Nature *488*, 522-526.

Chen, Z., Liu, S., Tian, L., Wu, M., Ai, F., Tang, W., Zhao, L., Ding, J., Zhang, L., and Tang, A. (2015). miR-124 and miR-506 inhibit colorectal cancer progression by targeting DNMT3B and DNMT1. Oncotarget *6*, 38139.

Chien, A.J., Moore, E.C., Lonsdorf, A.S., Kulikauskas, R.M., Rothberg, B.G., Berger, A.J., Major, M.B., Hwang, S.T., Rimm, D.L., and Moon, R.T. (2009). Activated Wnt/ß-catenin signaling in melanoma is associated with decreased proliferation in patient tumors and a murine melanoma model. Proceedings of the National Academy of Sciences *106*, 1193-1198.

Chien, C.-S., Wang, M.-L., Chu, P.-Y., Chang, Y.-L., Liu, W.-H., Yu, C.-C., Lan, Y.-T., Huang, P.-I., Lee, Y.-Y., and Chen, Y.-W. (2015). Lin28B/Let-7 Regulates Expression of Oct4 and Sox2 and Reprograms Oral Squamous Cell Carcinoma Cells to a Stem-like State. Cancer research.

Chu, L., Huo, Y., Liu, X., Yao, P., Thomas, K., Jiang, H., Zhu, T., Zhang, G., Chaudhry, M., and Adams, G. (2014). The Spatiotemporal Dynamics of Chromatin Protein HP1α Is Essential for Accurate Chromosome Segregation during Cell Division. Journal of Biological Chemistry *289*, 26249-26262.

Chu, P.-Y., Hu, F.-W., Yu, C.-C., Tsai, L.-L., Yu, C.-H., Wu, B.-C., Chen, Y.-W., Huang, P.-I., and Lo, W.-L. (2013). Epithelial–mesenchymal transition transcription factor ZEB1/ZEB2 co-expression predicts poor prognosis and maintains tumor-initiating properties in head and neck cancer. Oral oncology *49*, 34-41.

Church, V.L., and Francis-West, P. (2002). Wnt signalling during limb development. International Journal of Developmental Biology *46*, 927-936.

Clarke, A.R. (2006). Wnt signalling in the mouse intestine. Oncogene *25*, 7512-7521.

Clevers, H. (2006). Wnt/beta-catenin signaling in development and disease. Cell *127*, 469-480.

Clevers, H., Loh, K.M., and Nusse, R. (2014). An integral program for tissue renewal and regeneration: Wnt signaling and stem cell control. Science *346*, 1248012.

Clevers, H., and Nusse, R. (2012). Wnt/β-catenin signaling and disease. Cell *149*, 1192-1205.

Comijn, J., Berx, G., Vermassen, P., Verschueren, K., van Grunsven, L., Bruyneel, E., Mareel, M., Huylebroeck, D., and Van Roy, F. (2001). The two-handed E box binding zinc finger protein SIP1 downregulates E-cadherin and induces invasion. Molecular cell *7*, 1267-1278.

Coombs, G.S., Yu, J., Canning, C.A., Veltri, C.A., Covey, T.M., Cheong, J.K., Utomo, V., Banerjee, N., Zhang, Z.H., and Jadulco, R.C. (2010). WLS-dependent secretion of WNT3A requires Ser209 acylation and vacuolar acidification. Journal of cell science *123*, 3357-3367.

Cordes, K.R., Sheehy, N.T., White, M.P., Berry, E.C., Morton, S.U., Muth, A.N., Lee, T.-H., Miano, J.M., Ivey, K.N., and Srivastava, D. (2009). miR-145 and miR-143 regulate smooth muscle cell fate and plasticity. Nature *460*, 705-710.

Cortina, C., Palomo-Ponce, S., Iglesias, M., Fernández-Masip, J.L., Vivancos, A., Whissell, G., Huma, M., Peiró, N., Gallego, L., and Jonkheer, S. (2007). EphB–ephrin-B interactions suppress colorectal cancer progression by compartmentalizing tumor cells. Nature genetics *39*, 1376-1383.

Cselenyi, C.S., Jernigan, K.K., Tahinci, E., Thorne, C.A., Lee, L.A., and Lee, E. (2008). LRP6 transduces a canonical Wnt signal independently of Axin degradation by inhibiting GSK3's phosphorylation of β-catenin. Proceedings of the National Academy of Sciences *105*, 8032-8037.

Dai, J., Li, Y., Ji, C., Jin, F., Zheng, Z., Wang, X., Sun, X., Xu, X., Gu, S., and Xie, Y. (2004a). Characterization of two novel KRAB-domain-containing zinc finger genes, ZNF460 and ZNF461, on human chromosome 19q13. 1→ q13. 4. Cytogenetic and genome research *103*, 74-78.

Dai, M.-S., Sun, X.-X., Qin, J., Smolik, S.M., and Lu, H. (2004b). Identification and characterization of a novel Drosophila melanogaster glutathione S-transferase-containing FLYWCH zinc finger protein. Gene *342*, 49-56.

Dal Col, J., and Dolcetti, R. (2008). GSK-3b inhibition: at the crossroad between Akt and mTOR constitutive activation to enhance cyclin D1 protein stability in mantle cell lymphoma. Cell Cycle *7*, 2813-2816.

Daniels, D.L., and Weis, W.I. (2005). Beta-catenin directly displaces Groucho/TLE repressors from Tcf/Lef in Wnt-mediated transcription activation. Nat Struct Mol Biol *12*, 364-371.

Daugherty, R.L., and Gottardi, C.J. (2007). Phospho-regulation of β-catenin adhesion and signaling functions. Physiology *22*, 303-309.

Davidson, K.C., Adams, A.M., Goodson, J.M., McDonald, C.E., Potter, J.C., Berndt, J.D., Biechele, T.L., Taylor, R.J., and Moon, R.T. (2012). Wnt/β-catenin signaling promotes differentiation, not self-renewal, of human embryonic stem cells and is repressed by Oct4. Proceedings of the National Academy of Sciences *109*, 4485-4490.

Day, T.F., Guo, X., Garrett-Beal, L., and Yang, Y. (2005). Wnt/β-catenin signaling in mesenchymal progenitors controls osteoblast and chondrocyte differentiation during vertebrate skeletogenesis. Developmental cell *8*, 739-750.

de Marcondes, P.G., Bastos, L.G., de-Freitas-Junior, J.C., Rocha, M.R., and Morgado-Diaz, J.A. (2016a). EphA4-mediated signaling regulates the aggressive phenotype of irradiation survivor colorectal cancer cells. Tumour biology : the journal of the International Society for Oncodevelopmental Biology and Medicine.

de Marcondes, P.G., Bastos, L.G., de-Freitas-Junior, J.C.M., Rocha, M.R., and Morgado-Díaz, J.A. (2016b). EphA4-mediated signaling regulates the aggressive phenotype of irradiation survivor colorectal cancer cells. Tumor Biology *37*, 12411-12422.

de Sousa, E.M.F., Vermeulen, L., Richel, D., and Medema, J.P. (2011). Targeting Wnt signaling in colon cancer stem cells. Clinical Cancer Research *17*, 647-653.

Deng, H., Lv, L., Li, Y., Zhang, C., Meng, F., Pu, Y., Xiao, J., Qian, L., Zhao, W., and Liu, Q. (2014). miR-193a-3p regulates the multi-drug resistance of bladder cancer by targeting the LOXL4 gene and the Oxidative Stress pathway. Molecular cancer *13*, 234-234.

Deng, X., Wu, B., Xiao, K., Kang, J., Xie, J., Zhang, X., and Fan, Y. (2015). MiR-146b-5p promotes metastasis and induces epithelial-mesenchymal transition in thyroid cancer by targeting ZNRF3. Cellular Physiology and Biochemistry *35*, 71-82.

Dey, N., Barwick, B.G., Moreno, C.S., Ordanic-Kodani, M., Chen, Z., Oprea-Ilies, G., Tang, W., Catzavelos, C., Kerstann, K.F., and Sledge, G.W. (2013). Wnt signaling in triple negative breast cancer is associated with metastasis. BMC cancer *13*, 537.

Dorn, R., and Krauss, V. (2003). The modifier of mdg4 locus in Drosophila: functional complexity is resolved by trans splicing. Genetica *117*, 165-177.

Dorn, R., Reuter, G., and Loewendorf, A. (2001). Transgene analysis proves mRNA trans-splicing at the complex mod (mdg4) locus in Drosophila. Proceedings of the National Academy of Sciences *98*, 9724-9729.

Dovat, S., Ronni, T., Russell, D., Ferrini, R., Cobb, B.S., and Smale, S.T. (2002). A common mechanism for mitotic inactivation of C2H2 zinc finger DNA-binding domains. Genes & development *16*, 2985-2990.

Driessens, G., Beck, B., Caauwe, A., Simons, B.D., and Blanpain, C. (2012). Defining the mode of tumour growth by clonal analysis. Nature *488*, 527-530.

Dunn, K.W., Kamocka, M.M., and McDonald, J.H. (2011). A practical guide to evaluating colocalization in biological microscopy. American Journal of Physiology-Cell Physiology *300*, C723-C742.

Elrod-Erickson, M., Rould, M.A., Nekludova, L., and Pabo, C.O. (1996). Zif268 protein–DNA complex refined at 1.6 Å: a model system for understanding zinc finger–DNA interactions. Structure *4*, 1171-1180.

Fearon, E.R. (2011). Molecular genetics of colorectal cancer. Annual Review of Pathology: Mechanisms of Disease *6*, 479-507.

Fevr, T., Robine, S., Louvard, D., and Huelsken, J. (2007). Wnt/β-catenin is essential for intestinal homeostasis and maintenance of intestinal stem cells. Molecular and cellular biology *27*, 7551-7559.

Fife, C., McCarroll, J., and Kavallaris, M. (2014). Movers and shakers: cell cytoskeleton in cancer metastasis. British journal of pharmacology *171*, 5507-5523.

Finn, R.D., Mistry, J., Tate, J., Coggill, P., Heger, A., Pollington, J.E., Gavin, O.L., Gunasekaran, P., Ceric, G., Forslund, K., *et al.* (2010). The Pfam protein families database. Nucleic Acids Research *38*, D211-D222.

Flynt, A.S., Greimann, J.C., Chung, W.-J., Lima, C.D., and Lai, E.C. (2010). MicroRNA biogenesis via splicing and exosome-mediated trimming in Drosophila. Molecular cell *38*, 900-907.

Fodde, R. (2002). The APC gene in colorectal cancer. European journal of cancer *38*, 867-871.

Font, J., and Mackay, J.P. (2010). Beyond DNA: zinc finger domains as RNA-binding modules. Engineered Zinc Finger Proteins: Methods and Protocols, 479-491.

Förstemann, K., Tomari, Y., Du, T., Vagin, V.V., Denli, A.M., Bratu, D.P., Klattenhoff, C., Theurkauf, W.E., and Zamore, P.D. (2005). Normal microRNA maturation and germ-line stem cell maintenance requires Loquacious, a double-stranded RNA-binding domain protein. PLoS biology *3*, e236.

Friedman, R.C., and Burge, C.B. (2014). MicroRNA Target Finding by Comparative Genomics. In RNA Sequence, Structure, and Function: Computational and Bioinformatic Methods (Springer), pp. 457-476.

Gaj, T., Gersbach, C.A., and Barbas, C.F. (2013). ZFN, TALEN, and CRISPR/Cas-based methods for genome engineering. Trends in biotechnology *31*, 397-405.

Ganss, B., and Jheon, A. (2004). Zinc finger transcription factors in skeletal development. Critical Reviews in Oral Biology & Medicine *15*, 282-297.

Gao, C., Xiao, G., and Hu, J. (2014a). Regulation of Wnt/β-catenin signaling by posttranslational modifications. Cell & bioscience *4*, 1.

Gao, C., Xiao, G., and Hu, J. (2014b). Regulation of Wnt/β-catenin signaling by posttranslational modifications. Cell & bioscience *4*, 13.

Geetha-Loganathan, P., Nimmagadda, S., and Scaal, M. (2008). Wnt signaling in limb organogenesis. Organogenesis *4*, 109-115.

Ghahhari, N.M., and Babashah, S. (2015). Interplay between microRNAs and WNT/β-catenin signalling pathway regulates epithelial–mesenchymal transition in cancer. European journal of cancer *51*, 1638-1649.

Glinka, A., Dolde, C., Kirsch, N., Huang, Y.L., Kazanskaya, O., Ingelfinger, D., Boutros, M., Cruciat, C.M., and Niehrs, C. (2011). LGR4 and LGR5 are R-spondin receptors mediating Wnt/β-catenin and Wnt/PCP signalling. EMBO reports *12*, 1055-1061.

Grady, W.M., and Carethers, J.M. (2008). Genomic and epigenetic instability in colorectal cancer pathogenesis. Gastroenterology *135*, 1079-1099.

Graham, F.L., Smiley, J., Russell, W.C., and Nairn, R. (1977). Characteristics of a human cell line transformed by DNA from human adenovirus type 5. J Gen Virol *36*, 59-74.

Gregorieff, A., and Clevers, H. (2005). Wnt signaling in the intestinal epithelium: from endoderm to cancer. Genes & development *19*, 877-890.

Gregorieff, A., Pinto, D., Begthel, H., Destrée, O., Kielman, M., and Clevers, H. (2005). Expression pattern of Wnt signaling components in the adult intestine. Gastroenterology *129*, 626-638.

Großhans, H., Johnson, T., Reinert, K.L., Gerstein, M., and Slack, F.J. (2005). The temporal patterning microRNA let-7 regulates several transcription factors at the larval to adult transition in C. elegans. Developmental cell *8*, 321-330.

Gu, W., Li, X., and Wang, J. (2014). miR-139 regulates the proliferation and invasion of hepatocellular carcinoma through the WNT/TCF-4 pathway. Oncology reports *31*, 397-404.

Guo, W.-h., and Wang, Y.-l. (2012). A three-component mechanism for fibroblast migration with a contractile cell body that couples a myosin II–independent propulsive anterior to a myosin II–dependent resistive tail. Molecular biology of the cell *23*, 1657-1663.

Guo, Y., Chen, Y., Ito, H., Watanabe, A., Ge, X., Kodama, T., and Aburatani, H. (2006). Identification and characterization of lin-28 homolog B (LIN28B) in human hepatocellular carcinoma. Gene *384*, 51-61.

Gurtan, A.M., Ravi, A., Rahl, P.B., Bosson, A.D., JnBaptiste, C.K., Bhutkar, A., Whittaker, C.A., Young, R.A., and Sharp, P.A. (2013). Let-7 represses Nr6a1 and a mid-gestation developmental program in adult fibroblasts. Genes & development *27*, 941-954.

Ha, M., and Kim, V.N. (2014). Regulation of microRNA biogenesis. Nature reviews Molecular cell biology *15*, 509-524.

Hanahan, D., and Weinberg, R.A. (2011). Hallmarks of cancer: the next generation. Cell *144*, 646-674.

Hanas, J., Hazuda, D., Bogenhagen, D., Wu, F., and Wu, C. (1983). Xenopus transcription factor A requires zinc for binding to the 5 S RNA gene. Journal of Biological Chemistry *258*, 14120-14125.

Hayes, J., Peruzzi, P.P., and Lawler, S. (2014). MicroRNAs in cancer: biomarkers, functions and therapy. Trends in molecular medicine *20*, 460-469.

Haynes, J., Srivastava, J., Madson, N., Wittmann, T., and Barber, D.L. (2011). Dynamic actin remodeling during epithelial–mesenchymal transition depends on increased moesin expression. Molecular biology of the cell *22*, 4750-4764.

He, L., He, X., Lim, L.P., De Stanchina, E., Xuan, Z., Liang, Y., Xue, W., Zender, L., Magnus, J., and Ridzon, D. (2007). A microRNA component of the p53 tumour suppressor network. Nature *447*, 1130-1134.

He, L., Thomson, J.M., Hemann, M.T., Hernando-Monge, E., Mu, D., Goodson, S., Powers, S., Cordon-Cardo, C., Lowe, S.W., and Hannon, G.J. (2005). A microRNA polycistron as a potential human oncogene. nature *435*, 828-833.

He, X.C., Zhang, J., Tong, W.-G., Tawfik, O., Ross, J., Scoville, D.H., Tian, Q., Zeng, X., He, X., and Wiedemann, L.M. (2004). BMP signaling inhibits intestinal stem cell self-renewal through suppression of Wnt–β-catenin signaling. Nature genetics *36*, 1117-1121.

Hecht, A., Vleminckx, K., Stemmler, M.P., van Roy, F., and Kemler, R. (2000). The p300/CBP acetyltransferases function as transcriptional coactivators of beta-catenin in vertebrates. EMBO J *19*, 1839-1850.

Herbst, A., Jurinovic, V., Krebs, S., Thieme, S.E., Blum, H., Göke, B., and Kolligs, F.T. (2014). Comprehensive analysis of β-catenin target genes in colorectal carcinoma cell lines with deregulated Wnt/β-catenin signaling. BMC genomics *15*, 1.

Hernández, F., Pérez, M., Lucas, J.J., Mata, A.M., Bhat, R., and Avila, J. (2004). Glycogen synthase kinase-3 plays a crucial role in tau exon 10 splicing and intranuclear distribution of SC35 Implications for Alzheimer's disease. Journal of Biological Chemistry *279*, 3801-3806.

Hino, S.-i., Kishida, S., Michiue, T., Fukui, A., Sakamoto, I., Takada, S., Asashima, M., and Kikuchi, A. (2001). Inhibition of the Wnt signaling pathway by Idax, a novel Dvl-binding protein. Molecular and cellular biology *21*, 330-342.

Hodel, M.R., Corbett, A.H., and Hodel, A.E. (2001). Dissection of a nuclear localization signal. Journal of Biological Chemistry *276*, 1317-1325.

Hoesel, B., and Schmid, J.A. (2013). The complexity of NF-κB signaling in inflammation and cancer. Molecular cancer *12*, 86.

Holland, J.D., Klaus, A., Garratt, A.N., and Birchmeier, W. (2013). Wnt signaling in stem and cancer stem cells. Current opinion in cell biology *25*, 254-264.

Hsieh, I.-S., Chang, K.-C., Tsai, Y.-T., Ke, J.-Y., Lu, P.-J., Lee, K.-H., Yeh, S.-D., Hong, T.-M., and Chen, Y.-L. (2012). MicroRNA-320 suppresses the stem cell-like characteristics of prostate cancer cells by down-regulating the Wnt/beta-catenin signaling pathway. Carcinogenesis, bgs371.

Hu, W., Ye, Y., Zhang, W., Wang, J., Chen, A., and Guo, F. (2013a). miR‐142‐3p promotes osteoblast differentiation by modulating Wnt signaling. Molecular medicine reports *7*, 689-693.

Hu, X., Guo, J., Zheng, L., Li, C., Zheng, T.M., Tanyi, J.L., Liang, S., Benedetto, C., Mitidieri, M., and Katsaros, D. (2013b). The heterochronic microRNA let-7 inhibits cell motility by regulating the genes in the actin cytoskeleton pathway in breast cancer. Molecular Cancer Research *11*, 240-250.

Huang, J., Hamasaki, H., Nakamoto, T., Honda, H., Hirai, H., Saito, M., Takato, T., and Sakai, R. (2002). Differential regulation of cell migration, actin stress fiber organization, and cell transformation by functional domains of Crk-associated substrate. Journal of Biological Chemistry *277*, 27265-27272.

Huang, K., Zhang, J.-X., Han, L., You, Y.-P., Jiang, T., Pu, P.-Y., and Kang, C.-S. (2010). MicroRNA roles in beta-catenin pathway. Molecular cancer *9*, 252.

Humtsoe, J.O., Liu, M., Malik, A.B., and Wary, K.K. (2010). Lipid phosphate phosphatase 3 stabilization of beta-catenin induces endothelial cell migration and formation of branching point structures. Mol Cell Biol *30*, 1593-1606.

Ibrahim, E.E., Babaei-Jadidi, R., Saadeddin, A., Spencer-Dene, B., Hossaini, S., Abuzinadah, M., Li, N., Fadhil, W., Ilyas, M., Bonnet, D., *et al.* (2012a). Embryonic NANOG activity defines colorectal cancer stem cells and modulates through AP1- and TCF-dependent mechanisms. Stem cells (Dayton, Ohio) *30*, 2076-2087.

Ibrahim, E.E., Babaei-Jadidi, R., Saadeddin, A., Spencer-Dene, B., Hossaini, S., Abuzinadah, M., Li, N., Fadhil, W., Ilyas, M., and Bonnet, D. (2012b). Embryonic NANOG Activity Defines Colorectal Cancer Stem Cells and Modulates through AP1-and TCF-dependent Mechanisms. Stem Cells *30*, 2076-2087.

Iliopoulos, D., Hirsch, H.A., and Struhl, K. (2009). An epigenetic switch involving NF-κB, Lin28, Let-7 MicroRNA, and IL6 links inflammation to cell transformation. Cell *139*, 693-706.

Iorio, M.V., and Croce, C.M. (2012). microRNA involvement in human cancer. Carcinogenesis *33*, 1126-1133.

Ireland, H., Kemp, R., Houghton, C., Howard, L., Clarke, A.R., Sansom, O.J., and Winton, D.J. (2004). Inducible Cre-mediated control of gene expression in the murine gastrointestinal tract: effect of loss of β-catenin. Gastroenterology *126*, 1236-1246.

Ishimoto, T., Nagano, O., Yae, T., Tamada, M., Motohara, T., Oshima, H., Oshima, M., Ikeda, T., Asaba, R., and Yagi, H. (2011). CD44 variant regulates redox status in cancer cells by stabilizing the xCT subunit of system xc− and thereby promotes tumor growth. Cancer cell *19*, 387-400.

Ishitani, T., Kishida, S., Hyodo-Miura, J., Ueno, N., Yasuda, J., Waterman, M., Shibuya, H., Moon, R.T., Ninomiya-Tsuji, J., and Matsumoto, K. (2003). The TAK1-NLK mitogen-activated protein kinase cascade functions in the Wnt-5a/Ca2+ pathway to antagonize Wnt/β-catenin signaling. Molecular and cellular biology *23*, 131-139.

Isobe, T., Hisamori, S., Hogan, D.J., Zabala, M., Hendrickson, D.G., Dalerba, P., Cai, S., Scheeren, F., Kuo, A.H., and Sikandar, S.S. (2014). miR-142 regulates the tumorigenicity of human breast cancer stem cells through the canonical WNT signaling pathway. Elife *3*, e01977.

Ito, K., Lim, A.C., Salto-Tellez, M., Motoda, L., Osato, M., Chuang, L.S., Lee, C.W., Voon, D.C., Koo, J.K., Wang, H., *et al.* (2008). RUNX3 attenuates beta-catenin/T cell factors in intestinal tumorigenesis. Cancer Cell *14*, 226-237.

Iwasaki, S., Kawamata, T., and Tomari, Y. (2009). Drosophila argonaute1 and argonaute2 employ distinct mechanisms for translational repression. Molecular cell *34*, 58-67.

Jacquemet, G., Hamidi, H., and Ivaska, J. (2015). Filopodia in cell adhesion, 3D migration and cancer cell invasion. Current opinion in cell biology *36*, 23-31.

James, V., Zhang, Y., Foxler, D.E., de Moor, C.H., Kong, Y.W., Webb, T.M., Self, T.J., Feng, Y., Lagos, D., and Chu, C.-Y. (2010). LIM-domain proteins, LIMD1, Ajuba, and WTIP are required for microRNA-mediated gene silencing. Proceedings of the National Academy of Sciences *107*, 12499-12504.

Jang, G.-B., Kim, J.-Y., Cho, S.-D., Park, K.-S., Jung, J.-Y., Lee, H.-Y., Hong, I.-S., and Nam, J.-S. (2015). Blockade of Wnt/β-catenin signaling suppresses breast cancer metastasis by inhibiting CSC-like phenotype. Scientific reports *5*.

Jansson, M.D., and Lund, A.H. (2012). MicroRNA and cancer. Molecular oncology *6*, 590-610.

Ji, J., Yamashita, T., and Wang, X.W. (2011). Wnt/beta-catenin signaling activates microRNA-181 expression in hepatocellular carcinoma. Cell & bioscience *1*, 1.

Ji, S., Ye, G., Zhang, J., Wang, L., Wang, T., Wang, Z., Zhang, T., Wang, G., Guo, Z., and Luo, Y. (2012). miR-574-5p negatively regulates Qki6/7 to impact

β-catenin/Wnt signalling and the development of colorectal cancer. Gut, gutjnl-2011-301083.

Jia, Y., Yang, Y., Zhan, Q., Brock, M.V., Zheng, X., Yu, Y., Herman, J.G., and Guo, M. (2012). Inhibition of SOX17 by microRNA 141 and methylation activates the WNT signaling pathway in esophageal cancer. The Journal of Molecular Diagnostics *14*, 577-585.

Jiao, X., Katiyar, S., Willmarth, N.E., Liu, M., Ma, X., Flomenberg, N., Lisanti, M.P., and Pestell, R.G. (2010). c-Jun induces mammary epithelial cellular invasion and breast cancer stem cell expansion. Journal of Biological Chemistry *285*, 8218-8226.

Johnston, S., Gallaher, Z., and Czaja, K. (2012). Exogenous reference gene normalization for real-time reverse transcription-polymerase chain reaction analysis under dynamic endogenous transcription. Neural regeneration research *7*, 1064.

Jope, R.S. (2003). Lithium and GSK-3: one inhibitor, two inhibitory actions, multiple outcomes. Trends in pharmacological sciences *24*, 441-443.

Kajiyama, H., Kikkawa, F., Khin, E., Shibata, K., Ino, K., and Mizutani, S. (2003). Dipeptidyl peptidase IV overexpression induces up-regulation of E-cadherin and tissue inhibitors of matrix metalloproteinases, resulting in decreased invasive potential in ovarian carcinoma cells. Cancer Res *63*, 2278-2283.

Kalin, T.V., Wang, I.-C., Ackerson, T.J., Major, M.L., Detrisac, C.J., Kalinichenko, V.V., Lyubimov, A., and Costa, R.H. (2006). Increased levels of the FoxM1 transcription factor accelerate development and progression of prostate carcinomas in both TRAMP and LADY transgenic mice. Cancer research *66*, 1712-1720.

Kamiyama, H., Noda, H., Konishi, F., and Rikiyama, T. (2014). Molecular biomarkers for the detection of metastatic colorectal cancer cells. World journal of gastroenterology: WJG *20*, 8928.

Kang, H., and Hata, A. (2015). The role of microRNAs in cell fate determination of mesenchymal stem cells: balancing adipogenesis and osteogenesis. BMB reports *48*, 319.

Kanwar, S.S., Yu, Y., Nautiyal, J., Patel, B.B., and Majumdar, A.P. (2010). The Wnt/β-catenin pathway regulates growth and maintenance of colonospheres. Molecular cancer *9*, 1.

Kao, S.-H., Wang, W.-L., Chen, C.-Y., Chang, Y.-L., Wu, Y.-Y., Wang, Y.-T., Wang, S.-P., Nesvizhskii, A.I., Chen, Y.-J., and Hong, T.-M. (2014). GSK3β controls epithelial–mesenchymal transition and tumor metastasis by CHIP-mediated degradation of Slug. Oncogene *33*, 3172-3182.

Katoh, M. (2007). Networking of WNT, FGF, Notch, BMP, and Hedgehog signaling pathways during carcinogenesis. Stem cell reviews *3*, 30-38.

Kellis, M., Wold, B., Snyder, M.P., Bernstein, B.E., Kundaje, A., Marinov, G.K., Ward, L.D., Birney, E., Crawford, G.E., and Dekker, J. (2014). Defining

functional DNA elements in the human genome. Proceedings of the National Academy of Sciences *111*, 6131-6138.
Kennell, J.A., Gerin, I., MacDougald, O.A., and Cadigan, K.M. (2008). The microRNA miR-8 is a conserved negative regulator of Wnt signaling. Proceedings of the National Academy of Sciences *105*, 15417-15422.
Kidani, T., Nakamura, A., Kamei, S., Norimatsu, Y., Miura, H., and Masuno, H. (2014). Overexpression of cytoplasmic β-catenin inhibits the metastasis of the murine osteosarcoma cell line LM8. Cancer cell international *14*, 1.
Kikuchi, A., Yamamoto, H., Sato, A., and Matsumoto, S. (2011). New insights into the mechanism of Wnt signaling pathway activation. Int Rev Cell Mol Biol *291*, e71.
Kim, J.H., Liu, X., Wang, J., Chen, X., Zhang, H., Kim, S.H., Cui, J., Li, R., Zhang, W., and Kong, Y. (2013a). Wnt signaling in bone formation and its therapeutic potential for bone diseases. Therapeutic advances in musculoskeletal disease *5*, 13-31.
Kim, K.-A., Kakitani, M., Zhao, J., Oshima, T., Tang, T., Binnerts, M., Liu, Y., Boyle, B., Park, E., and Emtage, P. (2005). Mitogenic influence of human R-spondin1 on the intestinal epithelium. Science *309*, 1256-1259.
Kim, K., Lu, Z., and Hay, E.D. (2002). DIRECT EVIDENCE FOR A ROLE OF β-CATENIN/LEF-1 SIGNALING PATHWAY IN INDUCTION OF EMT. Cell biology international *26*, 463-476.
Kim, N.H., Kim, H.S., Kim, N.-G., Lee, I., Choi, H.-S., Li, X.-Y., Kang, S.E., Cha, S.Y., Ryu, J.K., and Na, J.M. (2011a). p53 and miRNA-34 are Suppressors of Canonical Wnt Signaling. Science signaling *4*, ra71.
Kim, S.-E., Huang, H., Zhao, M., Zhang, X., Zhang, A., Semonov, M.V., MacDonald, B.T., Zhang, X., Abreu, J.G., and Peng, L. (2013b). Wnt stabilization of β-catenin reveals principles for morphogen receptor-scaffold assemblies. Science *340*, 867-870.
Kim, S.-J., Oh, J.-S., Shin, J.-Y., Lee, K.-D., Sung, K.W., Nam, S.J., and Chun, K.-H. (2011b). Development of microRNA-145 for therapeutic application in breast cancer. Journal of controlled release *155*, 427-434.
Kim, Y.S., Kang, H.S., and Jetten, A.M. (2007). The Kruppel-like zinc finger protein Glis2 functions as a negative modulator of the Wnt/beta-catenin signaling pathway. FEBS Lett *581*, 858-864.
Ko, M., An, J., Bandukwala, H.S., Chavez, L., Äijö, T., Pastor, W.A., Segal, M.F., Li, H., Koh, K.P., and Lähdesmäki, H. (2013). Modulation of TET2 expression and 5-methylcytosine oxidation by the CXXC domain protein IDAX. Nature *497*, 122-126.
Kojima, T., Shimazui, T., Hinotsu, S., Joraku, A., Oikawa, T., Kawai, K., Horie, R., Suzuki, H., Nagashima, R., and Yoshikawa, K. (2009). Decreased expression of CXXC4 promotes a malignant phenotype in renal cell carcinoma by activating Wnt signaling. Oncogene *28*, 297-305.
Komiya, Y., and Habas, R. (2008). Wnt signal transduction pathways. Organogenesis *4*, 68-75.

Koo, B.-K., Spit, M., Jordens, I., Low, T.Y., Stange, D.E., van de Wetering, M., van Es, J.H., Mohammed, S., Heck, A.J., and Maurice, M.M. (2012). Tumour suppressor RNF43 is a stem-cell E3 ligase that induces endocytosis of Wnt receptors. Nature *488*, 665-669.

Korpal, M., Lee, E.S., Hu, G., and Kang, Y. (2008). The miR-200 family inhibits epithelial-mesenchymal transition and cancer cell migration by direct targeting of E-cadherin transcriptional repressors ZEB1 and ZEB2. Journal of Biological Chemistry *283*, 14910-14914.

Kosinski, C., Li, V.S., Chan, A.S., Zhang, J., Ho, C., Tsui, W.Y., Chan, T.L., Mifflin, R.C., Powell, D.W., and Yuen, S.T. (2007). Gene expression patterns of human colon tops and basal crypts and BMP antagonists as intestinal stem cell niche factors. Proceedings of the National Academy of Sciences *104*, 15418-15423.

Krausova, M., and Korinek, V. (2014). Wnt signaling in adult intestinal stem cells and cancer. Cellular signalling *26*, 570-579.

Krauss, V., and Dorn, R. (2004). Evolution of the trans-splicing Drosophila locus mod (mdg4) in several species of Diptera and Lepidoptera. Gene *331*, 165-176.

Krishna, S.S., Majumdar, I., and Grishin, N.V. (2003a). Structural classification of zinc fingers SURVEY AND SUMMARY. Nucleic acids research *31*, 532-550.

Krishna, S.S., Majumdar, I., and Grishin, N.V. (2003b). Structural classification of zinc fingers: survey and summary. Nucleic Acids Res *31*, 532-550.

Krzywinski, M., and Altman, N. (2014). Points of significance: visualizing samples with box plots. Nature methods *11*, 119-120.

Kubic, J.D., Mascarenhas, J.B., Iizuka, T., Wolfgeher, D., and Lang, D. (2012). GSK-3 promotes cell survival, growth, and PAX3 levels in human melanoma cells. Molecular Cancer Research *10*, 1065-1076.

Kuhnert, F., Davis, C.R., Wang, H.-T., Chu, P., Lee, M., Yuan, J., Nusse, R., and Kuo, C.J. (2004). Essential requirement for Wnt signaling in proliferation of adult small intestine and colon revealed by adenoviral expression of Dickkopf-1. Proceedings of the National Academy of Sciences *101*, 266-271.

Kumar, M.S., Erkeland, S.J., Pester, R.E., Chen, C.Y., Ebert, M.S., Sharp, P.A., and Jacks, T. (2008). Suppression of non-small cell lung tumor development by the let-7 microRNA family. Proceedings of the National Academy of Sciences *105*, 3903-3908.

Laity, J.H., Dyson, H.J., and Wright, P.E. (2000). DNA-induced α-helix capping in conserved linker sequences is a determinant of binding affinity in Cys 2-His 2 zinc fingers. Journal of molecular biology *295*, 719-727.

Laity, J.H., Lee, B.M., and Wright, P.E. (2001). Zinc finger proteins: new insights into structural and functional diversity. Current opinion in structural biology *11*, 39-46.

Lamond, A.I., and Spector, D.L. (2003). Nuclear speckles: a model for nuclear organelles. Nature reviews Molecular cell biology *4*, 605-612.

Lamouille, S., Xu, J., and Derynck, R. (2014). Molecular mechanisms of epithelial–mesenchymal transition. Nature reviews Molecular cell biology *15*, 178.

Langan, T.J., and Chou, R.C. (2011). Synchronization of mammalian cell cultures by serum deprivation. Cell Cycle Synchronization: Methods and Protocols, 75-83.

Lao, V.V., and Grady, W.M. (2011). Epigenetics and colorectal cancer. Nature Reviews Gastroenterology and Hepatology *8*, 686-700.

Larman, B.W., Karolak, M.J., Adams, D.C., and Oxburgh, L. (2009). Chordin-like 1 and twisted gastrulation 1 regulate BMP signaling following kidney injury. Journal of the American Society of Nephrology *20*, 1020-1031.

Larue, L., and Bellacosa, A. (2005). Epithelial–mesenchymal transition in development and cancer: role of phosphatidylinositol 3′ kinase/AKT pathways. Oncogene *24*, 7443-7454.

Lawson, D.A., Bhakta, N.R., Kessenbrock, K., Prummel, K.D., Yu, Y., Takai, K., Zhou, A., Eyob, H., Balakrishnan, S., and Wang, C.-Y. (2015). Single-cell analysis reveals a stem-cell program in human metastatic breast cancer cells. Nature.

Lee, J.-S., Galvin, K.M., and Shi, Y. (1993). Evidence for physical interaction between the zinc-finger transcription factors YY1 and Sp1. Proceedings of the National Academy of Sciences *90*, 6145-6149.

Lee, S.-Y., Saito, T., Mitomi, H., Hidaka, Y., Murakami, T., Nomura, R., Watanabe, S., and Yao, T. (2015). Mutation spectrum in the Wnt/β-catenin signaling pathway in gastric fundic gland-associated neoplasms/polyps. Virchows Archiv *467*, 27-38.

Lehmann, W., Mossmann, D., Kleemann, J., Mock, K., Meisinger, C., Brummer, T., Herr, R., Brabletz, S., Stemmler, M.P., and Brabletz, T. (2016). ZEB1 turns into a transcriptional activator by interacting with YAP1 in aggressive cancer types. Nature communications *7*.

Leon, O., and Roth, M. (2000). Zinc fingers: DNA binding and protein-protein interactions. Biol Res *33*, 21-30.

Leucci, E., Patella, F., Waage, J., Holmstrøm, K., Lindow, M., Porse, B., Kauppinen, S., and Lund, A.H. (2013). microRNA-9 targets the long non-coding RNA MALAT1 for degradation in the nucleus. Scientific reports *3*, 2535.

Li, F.Q., Mofunanya, A., Fischer, V., Hall, J., and Takemaru, K. (2010). Nuclear-cytoplasmic shuttling of Chibby controls beta-catenin signaling. Mol Biol Cell *21*, 311-322.

Li, M., Hu, X., Zhu, J., Zhu, C., Zhu, S., Liu, X., Xu, J., Han, S., and Yu, Z. (2014). Overexpression of miR-19b impairs cardiac development in zebrafish by targeting ctnnb1. Cellular Physiology and Biochemistry *33*, 1988-2002.

Li, N., Lorenzi, F., Kalakouti, E., Normatova, M., Babaei-Jadidi, R., Tomlinson, I., and Nateri, A.S. (2015). FBXW7-mutated colorectal cancer cells exhibit aberrant expression of phosphorylated-p53 at serine-15. Oncotarget *6*, 9240.

Li, Y., VandenBoom, T.G., Kong, D., Wang, Z., Ali, S., Philip, P.A., and Sarkar, F.H. (2009). Up-regulation of miR-200 and let-7 by natural agents leads to the reversal of epithelial-to-mesenchymal transition in gemcitabine-resistant pancreatic cancer cells. Cancer research *69*, 6704-6712.

Li, Y., Wang, L., Pappan, L., Galliher-Beckley, A., and Shi, J. (2012). IL-1β promotes stemness and invasiveness of colon cancer cells through Zeb1 activation. Molecular cancer *11*, 87.

Lien, W.-H., and Fuchs, E. (2014). Wnt some lose some: transcriptional governance of stem cells by Wnt/β-catenin signaling. Genes & development *28*, 1517-1532.

Lim, J., and Thiery, J.P. (2012). Epithelial-mesenchymal transitions: insights from development. Development *139*, 3471-3486.

Lin, G.L., and Hankenson, K.D. (2011). Integration of BMP, Wnt, and notch signaling pathways in osteoblast differentiation. Journal of cellular biochemistry *112*, 3491-3501.

Lin, S.-L., Miller, J.D., and Ying, S.-Y. (2006). Intronic microRNA (miRNA). BioMed Research International *2006*.

Lin, S., and Gregory, R.I. (2015). MicroRNA biogenesis pathways in cancer. Nature Reviews Cancer *15*, 321-333.

Liu, Y., Huang, T., Zhao, X., and Cheng, L. (2011). MicroRNAs modulate the Wnt signaling pathway through targeting its inhibitors. Biochemical and biophysical research communications *408*, 259-264.

Liu, Y.P., Schopman, N.C., and Berkhout, B. (2013). Dicer-independent processing of short hairpin RNAs. Nucleic acids research, gkt036.

Liu, Z., Long, J., Du, R., Ge, C., Guo, K., and Xu, Y. (2016). miR-204 regulates the EMT by targeting snai1 to suppress the invasion and migration of gastric cancer. Tumor Biology, 1-9.

López-Knowles, E., Zardawi, S.J., McNeil, C.M., Millar, E.K., Crea, P., Musgrove, E.A., Sutherland, R.L., and O'Toole, S.A. (2010). Cytoplasmic localization of β-catenin is a marker of poor outcome in breast cancer patients. Cancer Epidemiology Biomarkers & Prevention *19*, 301-309.

Lorenzi, F., Babaei-Jadidi, R., Sheard, J., Spencer-Dene, B., and Nateri, A.S. (2016). Fbxw7-associated drug resistance is reversed by induction of terminal differentiation in murine intestinal organoid culture. Molecular Therapy-Methods & Clinical Development *3*, 16024.

Lozoya, T., Domínguez, F., Romero-Ruiz, A., Steffani, L., Martínez, S., Monterde, M., Ferri, B., Núñez, M.J., Zamora, O., and Gurrea, M. (2014). The lin28/let-7 system in early human embryonic tissue and ectopic pregnancy.

Lu, D., Searles, M.A., and Klug, A. (2003). Crystal structure of a zinc-finger–RNA complex reveals two modes of molecular recognition. Nature *426*, 96-100.

Lüchtenborg, M., Weijenberg, M.P., Wark, P.A., Saritas, A.M., Roemen, G.M., Muijen, G.N., Bruïne, A.P., Brandt, P.A., and Goeij, A.F. (2005). Mutations in APC, CTNNB1 and K-ras genes and expression of hMLH1 in sporadic colorectal carcinomas from the Netherlands Cohort Study. BMC cancer *5*, 1.

Luo, J. (2009). Glycogen synthase kinase 3β (GSK3β) in tumorigenesis and cancer chemotherapy. Cancer letters *273*, 194-200.

Lupo, A., Cesaro, E., Montano, G., Zurlo, D., Izzo, P., and Costanzo, P. (2013). KRAB-zinc finger proteins: a repressor family displaying multiple biological functions. Current genomics *14*, 268-278.

Lustig, B., Jerchow, B., Sachs, M., Weiler, S., Pietsch, T., Karsten, U., van de Wetering, M., Clevers, H., Schlag, P.M., and Birchmeier, W. (2002). Negative feedback loop of Wnt signaling through upregulation of conductin/axin2 in colorectal and liver tumors. Molecular and cellular biology *22*, 1184-1193.

MacDonald, B.T., Tamai, K., and He, X. (2009). Wnt/β-catenin signaling: components, mechanisms, and diseases. Developmental cell *17*, 9-26.

Madison, B.B., Jeganathan, A.N., Mizuno, R., Winslow, M.M., Castells, A., Cuatrecasas, M., and Rustgi, A.K. (2015). Let-7 represses carcinogenesis and a stem cell phenotype in the intestine via regulation of Hmga2. PLoS Genet *11*, e1005408.

Madison, B.B., Liu, Q., Zhong, X., Hahn, C.M., Lin, N., Emmett, M.J., Stanger, B.Z., Lee, J.-S., and Rustgi, A.K. (2013). LIN28B promotes growth and tumorigenesis of the intestinal epithelium via Let-7. Genes & development *27*, 2233-2245.

Mani, S.A., Guo, W., Liao, M.J., Eaton, E.N., Ayyanan, A., Zhou, A.Y., Brooks, M., Reinhard, F., Zhang, C.C., Shipitsin, M., *et al.* (2008). The epithelial-mesenchymal transition generates cells with properties of stem cells. Cell *133*, 704-715.

Mao, J., Fan, S., Ma, W., Fan, P., Wang, B., Zhang, J., Wang, H., Tang, B., Zhang, Q., and Yu, X. (2014). Roles of Wnt/β-catenin signaling in the gastric cancer stem cells proliferation and salinomycin treatment. Cell death & disease *5*, e1039.

Mao, Q., Li, Y., Zheng, X., Yang, K., Shen, H., Qin, J., Bai, Y., Kong, D., Jia, X., and Xie, L. (2008). Up-regulation of E-cadherin by small activating RNA inhibits cell invasion and migration in 5637 human bladder cancer cells. Biochemical and biophysical research communications *375*, 566-570.

Mao, Y.S., Zhang, B., and Spector, D.L. (2011). Biogenesis and function of nuclear bodies. Trends in Genetics *27*, 295-306.

Martinez, A., Alonso, M., Castro, A., Pérez, C., and Moreno, F.J. (2002). First non-ATP competitive glycogen synthase kinase 3 β (GSK-3β) inhibitors: thiadiazolidinones (TDZD) as potential drugs for the treatment of Alzheimer's disease. Journal of medicinal chemistry *45*, 1292-1299.

Martinez, N.J., Ow, M.C., Barrasa, M.I., Hammell, M., Sequerra, R., Doucette-Stamm, L., Roth, F.P., Ambros, V.R., and Walhout, A.J. (2008). A C. elegans genome-scale microRNA network contains composite feedback motifs with high flux capacity. Genes & development *22*, 2535-2549.

Matsuda, Y., Schlange, T., Oakeley, E.J., Boulay, A., and Hynes, N.E. (2009). WNT signaling enhances breast cancer cell motility and blockade of the WNT

pathway by sFRP1 suppresses MDA-MB-231 xenograft growth. Breast Cancer Res *11*, R32.

Maurer, U., Preiss, F., Brauns-Schubert, P., Schlicher, L., and Charvet, C. (2014). GSK-3–at the crossroads of cell death and survival. J Cell Sci *127*, 1369-1378.

Mayor, R., and Theveneau, E. (2014). The role of the non-canonical Wnt–planar cell polarity pathway in neural crest migration. Biochemical Journal *457*, 19-26.

Mayr, F., and Heinemann, U. (2013). Mechanisms of Lin28-mediated miRNA and mRNA regulation—a structural and functional perspective. International journal of molecular sciences *14*, 16532-16553.

McCubrey, J.A., Steelman, L.S., Bertrand, F.E., Davis, N.M., Sokolosky, M., Abrams, S.L., Montalto, G., D'Assoro, A.B., Libra, M., and Nicoletti, F. (2014). GSK-3 as potential target for therapeutic intervention in cancer.

McIntire, M.G., Soucy, G., Vaughan, T.L., Shahsafaei, A., and Odze, R.D. (2011). MUC2 is a highly specific marker of goblet cell metaplasia in the distal esophagus and gastroesophageal junction. The American journal of surgical pathology *35*, 1007-1013.

Medema, J.P. (2013). Cancer stem cells: the challenges ahead. Nature cell biology *15*, 338-344.

Medina, M., and Wandosell, F. (2011). Deconstructing GSK-3: the fine regulation of its activity. International Journal of Alzheimer's Disease *2011*.

Meister, G. (2013). Argonaute proteins: functional insights and emerging roles. Nature Reviews Genetics.

Meister, G., and Tuschl, T. (2004). Mechanisms of gene silencing by double-stranded RNA. Nature *431*, 343-349.

Mendez, M.G., Kojima, S., and Goldman, R.D. (2010). Vimentin induces changes in cell shape, motility, and adhesion during the epithelial to mesenchymal transition. FASEB J *24*, 1838-1851.

Merrill, B.J. (2012). Wnt pathway regulation of embryonic stem cell self-renewal. Cold Spring Harbor perspectives in biology *4*, a007971.

Metcalfe, C., and Bienz, M. (2011). Inhibition of GSK3 by Wnt signalling–two contrasting models. J Cell Sci *124*, 3537-3544.

Mikels, A., and Nusse, R. (2006). Wnts as ligands: processing, secretion and reception. Oncogene *25*, 7461-7468.

Miller, J., McLachlan, A., and Klug, A. (1985). Repetitive zinc-binding domains in the protein transcription factor IIIA from Xenopus oocytes. The EMBO journal *4*, 1609.

Miller, J.R., Hocking, A.M., Brown, J.D., and Moon, R.T. (1999). Mechanism and function of signal transduction by the Wnt/beta-catenin and Wnt/Ca2+ pathways. Oncogene *18*, 7860-7872.

Molenaar, J.J., Domingo-Fernández, R., Ebus, M.E., Lindner, S., Koster, J., Drabek, K., Mestdagh, P., van Sluis, P., Valentijn, L.J., and van Nes, J. (2012). LIN28B induces neuroblastoma and enhances MYCN levels via let-7 suppression. Nature genetics *44*, 1199-1206.

Mongelard, F., Labrador, M., Baxter, E.M., Gerasimova, T.I., and Corces, V.G. (2002). Trans-splicing as a novel mechanism to explain interallelic complementation in Drosophila. Genetics *160*, 1481-1487.

Morikawa, T., Kuchiba, A., Yamauchi, M., Meyerhardt, J.A., Shima, K., Nosho, K., Chan, A.T., Giovannucci, E., Fuchs, C.S., and Ogino, S. (2011). Association of CTNNB1 (β-catenin) alterations, body mass index, and physical activity with survival in patients with colorectal cancer. Jama *305*, 1685-1694.

Morimoto, M., and Boerkoel, C.F. (2013). The role of nuclear bodies in gene expression and disease. Biology *2*, 976-1033.

Moser, B., Hochreiter, B., Herbst, R., and Schmid, J.A. (2016). Fluorescence colocalization microscopy analysis can be improved by combining object-recognition with pixel-intensity-correlation. Biotechnology Journal.

Nagel, R., le Sage, C., Diosdado, B., van der Waal, M., Vrielink, J.A.O., Bolijn, A., Meijer, G.A., and Agami, R. (2008). Regulation of the adenomatous polyposis coli gene by the miR-135 family in colorectal cancer. Cancer research *68*, 5795-5802.

Najafabadi, H.S., Mnaimneh, S., Schmitges, F.W., Garton, M., Lam, K.N., Yang, A., Albu, M., Weirauch, M.T., Radovani, E., and Kim, P.M. (2015). C2H2 zinc finger proteins greatly expand the human regulatory lexicon. Nature biotechnology *33*, 555-562.

Nakagawa, S., Ip, J.Y., Shioi, G., Tripathi, V., Zong, X., Hirose, T., and Prasanth, K.V. (2012). Malat1 is not an essential component of nuclear speckles in mice. Rna *18*, 1487-1499.

Nasim, M.T., Chowdhury, H., and Eperon, I. (2002). A double reporter assay for detecting changes in the ratio of spliced and unspliced mRNA in mammalian cells. Nucleic acids research *30*, e109-e109.

Nasim, M.T., and Eperon, I.C. (2006). A double-reporter splicing assay for determining splicing efficiency in mammalian cells. Nature protocols *1*, 1022-1028.

Nateri, A.S., Riera-Sans, L., Da Costa, C., and Behrens, A. (2004). The ubiquitin ligase SCFFbw7 antagonizes apoptotic JNK signaling. Science *303*, 1374-1378.

Nateri, A.S., Spencer-Dene, B., and Behrens, A. (2005). Interaction of phosphorylated c-Jun with TCF4 regulates intestinal cancer development. Nature *437*, 281-285.

Nawshad, A., Medici, D., Liu, C.-C., and Hay, E.D. (2007). TGFβ3 inhibits E-cadherin gene expression in palate medial-edge epithelial cells through a Smad2-Smad4-LEF1 transcription complex. Journal of cell science *120*, 1646-1653.

Nelson, C.M., Khauv, D., Bissell, M.J., and Radisky, D.C. (2008). Change in cell shape is required for matrix metalloproteinase-induced epithelial-mesenchymal transition of mammary epithelial cells. J Cell Biochem *105*, 25-33.

Network, C.G.A. (2012). Comprehensive molecular characterization of human colon and rectal cancer. Nature *487*, 330-337.

Nguyen, L.V., Vanner, R., Dirks, P., and Eaves, C.J. (2012). Cancer stem cells: an evolving concept. Nature Reviews Cancer *12*, 133-143.
Nishino, J., Kim, I., Chada, K., and Morrison, S.J. (2008). Hmga2 promotes neural stem cell self-renewal in young but not old mice by reducing p16 Ink4a and p19 Arf expression. Cell *135*, 227-239.
Novellasdemunt, L., Antas, P., and Li, V.S. (2015). Targeting Wnt signaling in colorectal cancer. A Review in the Theme: Cell Signaling: Proteins, Pathways and Mechanisms. American Journal of Physiology-Cell Physiology *309*, C511-C521.
Nusse, R. (2012). Wnt signaling. Cold Spring Harbor perspectives in biology *4*, a011163.
Nusse, R., Fuerer, C., Ching, W., Harnish, K., Logan, C., Zeng, A., Ten Berge, D., and Kalani, Y. (2008). Wnt signaling and stem cell control. Paper presented at: Cold Spring Harbor symposia on quantitative biology (Cold Spring Harbor Laboratory Press).
O'Connor, K., and Chen, M. (2013). Dynamic functions of RhoA in tumor cell migration and invasion. Small GTPases *4*, 141-147.
Okuda, H., Kobayashi, A., Xia, B., Watabe, M., Pai, S.K., Hirota, S., Xing, F., Liu, W., Pandey, P.R., and Fukuda, K. (2012). Hyaluronan Synthase HAS2 Promotes Tumor Progression in Bone by Stimulating the Interaction of Breast Cancer Stem–Like Cells with Macrophages and Stromal Cells. Cancer research *72*, 537-547.
Olson, E.N. (2006). Gene regulatory networks in the evolution and development of the heart. Science *313*, 1922-1927.
Olsson, E., Honeth, G., Bendahl, P.-O., Saal, L.H., Gruvberger-Saal, S., Ringnér, M., Vallon-Christersson, J., Jönsson, G., Holm, K., and Lövgren, K. (2011). CD44 isoforms are heterogeneously expressed in breast cancer and correlate with tumor subtypes and cancer stem cell markers. BMC cancer *11*, 1.
Onyido, E.K., Sweeney, E., and Nateri, A.S. (2016). Wnt-signalling pathways and microRNAs network in carcinogenesis: experimental and bioinformatics approaches. Molecular Cancer *15*, 56.
Osada, H., and Takahashi, T. (2011). let-7 and miR-17-92: Small-sized major players in lung cancer development. Cancer science *102*, 9-17.
Ow, M.C., Martinez, N.J., Olsen, P.H., Silverman, H.S., Barrasa, M.I., Conradt, B., Walhout, A.J., and Ambros, V. (2008a). The FLYWCH transcription factors FLH-1, FLH-2, and FLH-3 repress embryonic expression of microRNA genes in C. elegans. Genes & development *22*, 2520-2534.
Ow, M.C., Martinez, N.J., Olsen, P.H., Silverman, H.S., Barrasa, M.I., Conradt, B., Walhout, A.J., and Ambros, V. (2008b). The FLYWCH transcription factors FLH-1, FLH-2, and FLH-3 repress embryonic expression of microRNA genes in C. elegans. Genes Dev *22*, 2520-2534.
Pancione, M., Remo, A., and Colantuoni, V. (2012). Genetic and epigenetic events generate multiple pathways in colorectal cancer progression. Pathology research international *2012*.

Papworth, M., Kolasinska, P., and Minczuk, M. (2006). Designer zinc-finger proteins and their applications. Gene *366*, 27-38.
Parikh, A., Lee, C., Joseph, P., Marchini, S., Baccarini, A., Kolev, V., Romualdi, C., Fruscio, R., Shah, H., and Wang, F. (2014). microRNA-181a has a critical role in ovarian cancer progression through the regulation of the epithelial–mesenchymal transition. Nature communications *5*.
Pavletich, N.P., and Pabo, C.O. (1991). Zinc finger-DNA recognition: crystal structure of a Zif268-DNA complex at 2.1 A. Science *252*, 809-817.
Pavletich, N.P., and Pabo, C.O. (1993). Crystal structure of a five-finger GLI-DNA complex: new perspectives on zinc fingers. Science *261*, 1701-1707.
Peinado, H., Olmeda, D., and Cano, A. (2007). Snail, Zeb and bHLH factors in tumour progression: an alliance against the epithelial phenotype? Nature Reviews Cancer *7*, 415-428.
Pellegrin, S., and Mellor, H. (2007). Actin stress fibres. Journal of cell science *120*, 3491-3499.
Peng, Y., and Croce, C.M. (2016). The role of MicroRNAs in human cancer. Signal Transduction and Targeted Therapy *1*, 15004.
Perez, K., Walsh, R., Brilliant, K., Noble, L., Yakirevich, E., Breese, V., Jackson, C., Chatterjee, D., Pricolo, V., and Roth, L. (2013). Heterogeneity of colorectal cancer (CRC) in reference to KRAS proto-oncogene utilizing WAVE technology. Experimental and molecular pathology *95*, 74-82.
Persikov, A.V., Osada, R., and Singh, M. (2009). Predicting DNA recognition by Cys2His2 zinc finger proteins. Bioinformatics *25*, 22-29.
Persikov, A.V., and Singh, M. (2013). De novo prediction of DNA-binding specificities for Cys2His2 zinc finger proteins. Nucleic acids research, gkt890.
Peterson, T.A., Adadey, A., Santana-Cruz, I., Sun, Y., Winder, A., and Kann, M.G. (2010). DMDM: domain mapping of disease mutations. Bioinformatics *26*, 2458-2459.
Pillai, R.S. (2005). MicroRNA function: multiple mechanisms for a tiny RNA? Rna *11*, 1753-1761.
Piskounova, E., Polytarchou, C., Thornton, J.E., LaPierre, R.J., Pothoulakis, C., Hagan, J.P., Iliopoulos, D., and Gregory, R.I. (2011). Lin28A and Lin28B inhibit let-7 microRNA biogenesis by distinct mechanisms. Cell *147*, 1066-1079.
Piskounova, E., Viswanathan, S.R., Janas, M., LaPierre, R.J., Daley, G.Q., Sliz, P., and Gregory, R.I. (2008). Determinants of microRNA processing inhibition by the developmentally regulated RNA-binding protein Lin28. Journal of Biological Chemistry *283*, 21310-21314.
Powers, J.T., Tsanov, K.M., Pearson, D.S., Roels, F., Spina, C.S., Ebright, R., Seligson, M., de Soysa, Y., Cahan, P., and Theißen, J. (2016). Multiple mechanisms disrupt the let-7 microRNA family in neuroblastoma. Nature.
Prasetyanti, P.R., Zimberlin, C.D., Bots, M., Vermeulen, L., Felipe De Sousa, E.M., and Medema, J.P. (2013). Regulation of stem cell self-renewal and

differentiation by Wnt and Notch are conserved throughout the adenoma-carcinoma sequence in the colon. Molecular cancer *12*, 1.

Preca, B.T., Bajdak, K., Mock, K., Sundararajan, V., Pfannstiel, J., Maurer, J., Wellner, U., Hopt, U.T., Brummer, T., and Brabletz, S. (2015). A self-enforcing CD44s/ZEB1 feedback loop maintains EMT and stemness properties in cancer cells. International Journal of Cancer *137*, 2566-2577.

Provost, E., Hersperger, G., Timmons, L., Ho, W.Q., Hersperger, E., Alcazar, R., and Shearn, A. (2006). Loss-of-function mutations in a glutathione S-transferase suppress the prune-Killer of prune lethal interaction. Genetics *172*, 207-219.

Radisky, D.C. (2005). Epithelial-mesenchymal transition. Journal of cell science *118*, 4325-4326.

Radulescu, S., Ridgway, R., Cordero, J., Athineos, D., Salgueiro, P., Poulsom, R., Neumann, J., Jung, A., Patel, S., and Woodgett, J. (2013). Acute WNT signalling activation perturbs differentiation within the adult stomach and rapidly leads to tumour formation. Oncogene *32*, 2048-2057.

Ramalingam, P., Palanichamy, J.K., Singh, A., Das, P., Bhagat, M., Kassab, M.A., Sinha, S., and Chattopadhyay, P. (2014). Biogenesis of intronic miRNAs located in clusters by independent transcription and alternative splicing. Rna *20*, 76-87.

Rao, T.P., and Kühl, M. (2010). An Updated Overview on Wnt Signaling Pathways A Prelude for More. Circulation research *106*, 1798-1806.

Razin, S., Borunova, V., Maksimenko, O., and Kantidze, O. (2012). Cys2His2 zinc finger protein family: classification, functions, and major members. Biochemistry (Moscow) *77*, 217-226.

Reinhart, B.J., Slack, F.J., Basson, M., Pasquinelli, A.E., Bettinger, J.C., Rougvie, A.E., Horvitz, H.R., and Ruvkun, G. (2000). The 21-nucleotide let-7 RNA regulates developmental timing in Caenorhabditis elegans. nature *403*, 901-906.

Reuter, S., Gupta, S.C., Chaturvedi, M.M., and Aggarwal, B.B. (2010). Oxidative stress, inflammation, and cancer: how are they linked? Free Radical Biology and Medicine *49*, 1603-1616.

Reya, T., and Clevers, H. (2005). Wnt signalling in stem cells and cancer. Nature *434*, 843-850.

Ridenour, D.A., McLennan, R., Teddy, J.M., Semerad, C.L., Haug, J.S., and Kulesa, P.M. (2014). The neural crest cell cycle is related to phases of migration in the head. Development *141*, 1095-1103.

Ridley, A.J., Schwartz, M.A., Burridge, K., Firtel, R.A., Ginsberg, M.H., Borisy, G., Parsons, J.T., and Horwitz, A.R. (2003). Cell migration: integrating signals from front to back. Science *302*, 1704-1709.

Rolle, K., Piwecka, M., Belter, A., Wawrzyniak, D., Jeleniewicz, J., Barciszewska, M.Z., and Barciszewski, J. (2016). The Sequence and Structure Determine the Function of Mature Human miRNAs. PloS one *11*, e0151246.

Romero-Pérez, L., López-García, M.Á., Díaz-Martín, J., Biscuola, M., Castilla, M.Á., Tafe, L.J., Garg, K., Oliva, E., Matias-Guiu, X., and Soslow, R.A. (2013). ZEB1 overexpression associated with E-cadherin and microRNA-200 downregulation is characteristic of undifferentiated endometrial carcinoma. Modern Pathology *26*, 1514-1524.

Roulois, D., Yau, H.L., Singhania, R., Wang, Y., Danesh, A., Shen, S.Y., Han, H., Liang, G., Jones, P.A., and Pugh, T.J. (2015). DNA-demethylating agents target colorectal cancer cells by inducing viral mimicry by endogenous transcripts. Cell *162*, 961-973.

Roush, S., and Slack, F.J. (2008). The let-7 family of microRNAs. Trends in cell biology *18*, 505-516.

Rouya, C., Siddiqui, N., Morita, M., Duchaine, T.F., Fabian, M.R., and Sonenberg, N. (2014). Human DDX6 effects miRNA-mediated gene silencing via direct binding to CNOT1. Rna *20*, 1398-1409.

Salazar, K.D., Lankford, S.M., and Brody, A.R. (2009). Mesenchymal stem cells produce Wnt isoforms and TGF-β1 that mediate proliferation and procollagen expression by lung fibroblasts. American Journal of Physiology-Lung Cellular and Molecular Physiology *297*, L1002-L1011.

Samowitz, W.S., Slattery, M.L., Sweeney, C., Herrick, J., Wolff, R.K., and Albertsen, H. (2007). APC mutations and other genetic and epigenetic changes in colon cancer. Molecular cancer research *5*, 165-170.

Sanchez-Tillo, E., de Barrios, O., Siles, L., Cuatrecasas, M., Castells, A., and Postigo, A. (2011). beta-catenin/TCF4 complex induces the epithelial-to-mesenchymal transition (EMT)-activator ZEB1 to regulate tumor invasiveness. Proc Natl Acad Sci U S A *108*, 19204-19209.

Sánchez-Tilló, E., de Barrios, O., Siles, L., Cuatrecasas, M., Castells, A., and Postigo, A. (2011). β-catenin/TCF4 complex induces the epithelial-to-mesenchymal transition (EMT)-activator ZEB1 to regulate tumor invasiveness. Proceedings of the National Academy of Sciences *108*, 19204-19209.

Saneyoshi, T., Kume, S., Amasaki, Y., and Mikoshiba, K. (2002). The Wnt/calcium pathway activates NF-AT and promotes ventral cell fate in Xenopus embryos. Nature *417*, 295-299.

Sato, A., Yamamoto, H., Sakane, H., Koyama, H., and Kikuchi, A. (2010). Wnt5a regulates distinct signalling pathways by binding to Frizzled2. The EMBO journal *29*, 41-54.

Sato, N., Meijer, L., Skaltsounis, L., Greengard, P., and Brivanlou, A.H. (2004). Maintenance of pluripotency in human and mouse embryonic stem cells through activation of Wnt signaling by a pharmacological GSK-3-specific inhibitor. Nature medicine *10*, 55-63.

Satoh, S., Daigo, Y., Furukawa, Y., Kato, T., Miwa, N., Nishiwaki, T., Kawasoe, T., Ishiguro, H., Fujita, M., and Tokino, T. (2000). AXIN1 mutations in hepatocellular carcinomas, and growth suppression in cancer cells by virus-mediated transfer of AXIN1. Nature genetics *24*, 245-250.

Saydam, O., Shen, Y., Würdinger, T., Senol, O., Boke, E., James, M.F., Tannous, B.A., Stemmer-Rachamimov, A.O., Yi, M., and Stephens, R.M. (2009). Downregulated microRNA-200a in meningiomas promotes tumor growth by reducing E-cadherin and activating the Wnt/β-catenin signaling pathway. Molecular and cellular biology *29*, 5923-5940.

Schepers, A.G., Snippert, H.J., Stange, D.E., van den Born, M., van Es, J.H., van de Wetering, M., and Clevers, H. (2012). Lineage tracing reveals Lgr5+ stem cell activity in mouse intestinal adenomas. Science *337*, 730-735.

Schmalhofer, O., Brabletz, S., and Brabletz, T. (2009). E-cadherin, beta-catenin, and ZEB1 in malignant progression of cancer. Cancer metastasis reviews *28*, 151-166.

Schuijers, J., and Clevers, H. (2012). Adult mammalian stem cells: the role of Wnt, Lgr5 and R-spondins. The EMBO journal *31*, 2685-2696.

Sero, J.E., Sailem, H.Z., Ardy, R.C., Almuttaqi, H., Zhang, T., and Bakal, C. (2015). Cell shape and the microenvironment regulate nuclear translocation of NF-κB in breast epithelial and tumor cells. Molecular systems biology *11*, 790.

Shaheen, S., Ahmed, M., Lorenzi, F., and Nateri, A.S. (2016). Spheroid-Formation (Colonosphere) Assay for in Vitro Assessment and Expansion of Stem Cells in Colon Cancer. Stem Cell Reviews and Reports, 1-8.

Sharma, A., Singh, K., and Almasan, A. (2012). Histone H2AX phosphorylation: a marker for DNA damage. DNA repair protocols, 613-626.

Sheikh, A., Niazi, A.K., Ahmed, M.Z., Iqbal, B., Anwer, S.M.S., and Khan, H.H. (2014). The role of Wnt signaling pathway in carcinogenesis and implications for anticancer.

Shen, G., Jia, H., Tai, Q., Li, Y., and Chen, D. (2013). miR-106b downregulates adenomatous polyposis coli and promotes cell proliferation in human hepatocellular carcinoma. Carcinogenesis *34*, 211-219.

Shyh-Chang, N., and Daley, G.Q. (2013). Lin28: primal regulator of growth and metabolism in stem cells. Cell Stem Cell *12*, 395-406.

Silva, R.d., Marie, S.K., Uno, M., Matushita, H., Wakamatsu, A., Rosemberg, S., and Oba-Shinjo, S.M. (2013). CTNNB1, AXIN1 and APC expression analysis of different medulloblastoma variants. Clinics *68*, 167-172.

Silver, S.J., Hagen, J.W., Okamura, K., Perrimon, N., and Lai, E.C. (2007). Functional screening identifies miR-315 as a potent activator of Wingless signaling. Proceedings of the National Academy of Sciences *104*, 18151-18156.

Singh, A.B., Sharma, A., Smith, J.J., Krishnan, M., Chen, X., Eschrich, S., Washington, M.K., Yeatman, T.J., Beauchamp, R.D., and Dhawan, P. (2011). Claudin-1 up-regulates the repressor ZEB-1 to inhibit E-cadherin expression in colon cancer cells. Gastroenterology *141*, 2140-2153.

Smith, B.N., and Bhowmick, N.A. (2016). Role of EMT in Metastasis and Therapy Resistance. Journal of clinical medicine *5*, 17.

Smith, G., Carey, F.A., Beattie, J., Wilkie, M.J., Lightfoot, T.J., Coxhead, J., Garner, R.C., Steele, R.J., and Wolf, C.R. (2002). Mutations in APC, Kirsten-

ras, and p53—alternative genetic pathways to colorectal cancer. Proceedings of the National Academy of Sciences *99*, 9433-9438.
Sobel, K., Tham, M., Stark, H.J., Stammer, H., Prätzel-Wunder, S., Bickenbach, J.R., and Boukamp, P. (2015). Wnt-3a-activated human fibroblasts promote human keratinocyte proliferation and matrix destruction. International Journal of Cancer *136*, 2786-2798.
Song, J.L., Nigam, P., Tektas, S.S., and Selva, E. (2015). MicroRNA regulation of Wnt signaling pathways in development and disease. Cellular signalling *27*, 1380-1391.
Soni, M., and Lai, F. (2011). Cell-based co-transfection microarrays for use with HEK293T cells on a poly D-lysine-coated polystyrene microplate. Methods Mol Biol *706*, 13-25.
Spector, D.L., and Lamond, A.I. (2011). Nuclear speckles. Cold Spring Harbor perspectives in biology *3*, a000646.
Spencer, A., and Baker, A.B. (2016). High Throughput Label Free Measurement of Cancer Cell Adhesion Kinetics Under Hemodynamic Flow. Scientific reports *6*.
Stadler, C., Rexhepaj, E., Singan, V.R., Murphy, R.F., Pepperkok, R., Uhlén, M., Simpson, J.C., and Lundberg, E. (2013). Immunofluorescence and fluorescent-protein tagging show high correlation for protein localization in mammalian cells. Nature methods *10*, 315-323.
Steeg, P.S. (2006). Tumor metastasis: mechanistic insights and clinical challenges. Nature medicine *12*, 895-904.
Stewart, B.W., and Wild, C. (2014). World Cancer Report 2014. International Agency for Research on Cancer. World Health Organization *505*.
Stewart, D.J. (2014). Wnt signaling pathway in non–small cell lung cancer. Journal of the National Cancer Institute *106*, djt356.
Su, W.-L., Kleinhanz, R.R., and Schadt, E.E. (2011). Characterizing the role of miRNAs within gene regulatory networks using integrative genomics techniques. Molecular systems biology *7*.
Subramaniam, R., Mizoguchi, A., and Mizoguchi, E. (2016). Mechanistic roles of epithelial and immune cell signaling during the development of colitis-associated cancer. Cancer research frontiers *2*, 1.
Subramanian, M., Rao, S.R., Thacker, P., Chatterjee, S., and Karunagaran, D. (2014). MiR-29b Downregulates Canonical Wnt Signaling by Suppressing Coactivators of β-Catenin in Human Colorectal Cancer Cells. Journal of cellular biochemistry *115*, 1974-1984.
Sugimura, R., and Li, L. (2010). Noncanonical Wnt signaling in vertebrate development, stem cells, and diseases. Birth Defects Research Part C: Embryo Today: Reviews *90*, 243-256.
Sun, B., Fang, Y., Li, Z., Chen, Z., and Xiang, J. (2015). Role of cellular cytoskeleton in epithelial-mesenchymal transition process during cancer progression (Review). Biomedical reports *3*, 603-610.

Szulcek, R., Bogaard, H.J., and van Nieuw Amerongen, G.P. (2014). Electric cell-substrate impedance sensing for the quantification of endothelial proliferation, barrier function, and motility. JoVE (Journal of Visualized Experiments), e51300-e51300.

Taelman, V.F., Dobrowolski, R., Plouhinec, J.-L., Fuentealba, L.C., Vorwald, P.P., Gumper, I., Sabatini, D.D., and De Robertis, E.M. (2010). Wnt signaling requires sequestration of glycogen synthase kinase 3 inside multivesicular endosomes. Cell *143*, 1136-1148.

Tago, K., Nakamura, T., Nishita, M., Hyodo, J., Nagai, S., Murata, Y., Adachi, S., Ohwada, S., Morishita, Y., Shibuya, H., *et al.* (2000). Inhibition of Wnt signaling by ICAT, a novel beta-catenin-interacting protein. Genes Dev *14*, 1741-1749.

Takahashi, R.-u., Miyazaki, H., and Ochiya, T. (2014). The role of microRNAs in the regulation of cancer stem cells. Alterations of Epigenetics and MicroRNAs in Cancer and Cancer Stem Cell, 55.

Takahashi, Y., Chen, Y., Moiseyev, G., and Ma, J.-x. (2006). Two point mutations of RPE65 from patients with retinal dystrophies decrease the stability of RPE65 protein and abolish its isomerohydrolase activity. Journal of Biological Chemistry *281*, 21820-21826.

Takemaru, K., Yamaguchi, S., Lee, Y.S., Zhang, Y., Carthew, R.W., and Moon, R.T. (2003). Chibby, a nuclear beta-catenin-associated antagonist of the Wnt/Wingless pathway. Nature *422*, 905-909.

Ten Berge, D., Kurek, D., Blauwkamp, T., Koole, W., Maas, A., Eroglu, E., Siu, R.K., and Nusse, R. (2011). Embryonic stem cells require Wnt proteins to prevent differentiation to epiblast stem cells. Nature cell biology *13*, 1070-1075.

Thammaiah, C.K., and Jayaram, S. (2016). Role of let-7 family microRNA in breast cancer. Non-coding RNA Research.

Thiery, J.P. (2002). Epithelial–mesenchymal transitions in tumour progression. Nature Reviews Cancer *2*, 442-454.

Thomas, J., Ohtsuka, M., Pichler, M., and Ling, H. (2015). MicroRNAs: clinical relevance in colorectal cancer. International journal of molecular sciences *16*, 28063-28076.

Thornton, J.E., Chang, H.-M., Piskounova, E., and Gregory, R.I. (2012). Lin28-mediated control of let-7 microRNA expression by alternative TUTases Zcchc11 (TUT4) and Zcchc6 (TUT7). Rna *18*, 1875-1885.

Thornton, J.E., and Gregory, R.I. (2012). How does Lin28 let-7 control development and disease? Trends in cell biology *22*, 474-482.

Thornton, T.M., Pedraza-Alva, G., Deng, B., Wood, C.D., Aronshtam, A., Clements, J.L., Sabio, G., Davis, R.J., Matthews, D.E., and Doble, B. (2008). Phosphorylation by p38 MAPK as an alternative pathway for GSK3β inactivation. Science *320*, 667-670.

Tojkander, S., Gateva, G., and Lappalainen, P. (2012). Actin stress fibers–assembly, dynamics and biological roles. J Cell Sci *125*, 1855-1864.

Topol, L., Chen, W., Song, H., Day, T.F., and Yang, Y. (2009). Sox9 inhibits Wnt signaling by promoting β-catenin phosphorylation in the nucleus. Journal of Biological Chemistry *284*, 3323-3333.

Townsend, D.M., Manevich, Y., He, L., Hutchens, S., Pazoles, C.J., and Tew, K.D. (2009). Novel role for glutathione S-transferase π regulator of protein S-glutathionylation following oxidative and nitrosative stress. Journal of Biological Chemistry *284*, 436-445.

Townsley, F.M., Cliffe, A., and Bienz, M. (2004). Pygopus and Legless target Armadillo/beta-catenin to the nucleus to enable its transcriptional co-activator function. Nat Cell Biol *6*, 626-633.

Tripathi, V., Song, D.Y., Zong, X., Shevtsov, S.P., Hearn, S., Fu, X.-D., Dundr, M., and Prasanth, K.V. (2012). SRSF1 regulates the assembly of pre-mRNA processing factors in nuclear speckles. Molecular biology of the cell *23*, 3694-3706.

Tsialikas, J., and Romer-Seibert, J. (2015). LIN28: roles and regulation in development and beyond. Development *142*, 2397-2404.

Tu, H.-C., Schwitalla, S., Qian, Z., LaPier, G.S., Yermalovich, A., Ku, Y.-C., Chen, S.-C., Viswanathan, S.R., Zhu, H., and Nishihara, R. (2015). LIN28 cooperates with WNT signaling to drive invasive intestinal and colorectal adenocarcinoma in mice and humans. Genes & development *29*, 1074-1086.

Ueno, K., Hiura, M., Suehiro, Y., Hazama, S., Hirata, H., Oka, M., Imai, K., Dahiya, R., and Hinoda, Y. (2008). Frizzled-7 as a potential therapeutic target in colorectal cancer. Neoplasia *10*, 697-705.

Urrutia, R. (2003). KRAB-containing zinc-finger repressor proteins. Genome Biol *4*, 231.

Valastyan, S., and Weinberg, R.A. (2010). miR-31: a crucial overseer of tumor metastasis and other emerging roles. Cell Cycle *9*, 2124-2129.

Valinezhad Orang, A., Safaralizadeh, R., and Kazemzadeh-Bavili, M. (2014). Mechanisms of miRNA-mediated gene regulation from common downregulation to mRNA-specific upregulation. International journal of genomics *2014*.

Vallenius, T. (2013). Actin stress fibre subtypes in mesenchymal-migrating cells. Open biology *3*, 130001.

Valvezan, A.J., and Klein, P.S. (2012). GSK-3 and Wnt signaling in neurogenesis and bipolar disorder. Front Mol Neurosci *5*.

van de Wetering, M., Sancho, E., Verweij, C., de Lau, W., Oving, I., Hurlstone, A., van der Horn, K., Batlle, E., Coudreuse, D., and Haramis, A.-P. (2002). The β-catenin/TCF-4 complex imposes a crypt progenitor phenotype on colorectal cancer cells. Cell *111*, 241-250.

Van der Flier, L.G., Sabates–Bellver, J., Oving, I., Haegebarth, A., De Palo, M., Anti, M., Van Gijn, M.E., Suijkerbuijk, S., Van de Wetering, M., and Marra, G. (2007). The intestinal Wnt/TCF signature. Gastroenterology *132*, 628-632.

van Es, J.H., Haegebarth, A., Kujala, P., Itzkovitz, S., Koo, B.-K., Boj, S.F., Korving, J., van den Born, M., van Oudenaarden, A., and Robine, S. (2012). A

critical role for the Wnt effector Tcf4 in adult intestinal homeostatic self-renewal. Molecular and cellular biology *32*, 1918-1927.
van Zijp, J.v.d.V., Hoekstra, H.J., and Basson, M.D. (2008). Evolving management of colorectal cancer. World J Gastroenterol *14*, 3956-3967.
Vella, M.C., Choi, E.-Y., Lin, S.-Y., Reinert, K., and Slack, F.J. (2004). The C. elegans microRNA let-7 binds to imperfect let-7 complementary sites from the lin-41 3′ UTR. Genes & development *18*, 132-137.
Vermeulen, L., Todaro, M., de Sousa Mello, F., Sprick, M.R., Kemper, K., Alea, M.P., Richel, D.J., Stassi, G., and Medema, J.P. (2008). Single-cell cloning of colon cancer stem cells reveals a multi-lineage differentiation capacity. Proceedings of the National Academy of Sciences *105*, 13427-13432.
Vichai, V., and Kirtikara, K. (2006). Sulforhodamine B colorimetric assay for cytotoxicity screening. Nature protocols *1*, 1112-1116.
Viswanathan, S.R., and Daley, G.Q. (2010). Lin28: A microRNA regulator with a macro role. Cell *140*, 445-449.
Viswanathan, S.R., Daley, G.Q., and Gregory, R.I. (2008). Selective blockade of microRNA processing by Lin28. Science *320*, 97-100.
Viswanathan, S.R., Powers, J.T., Einhorn, W., Hoshida, Y., Ng, T., Toffanin, S., O'Sullivan, M., Lu, J., Philips, L.A., and Lockhart, V.L. (2009). Lin28 enhances tumorigenesis and is associated with advanced human malignancies. Nature genetics *41*, 843.
Wang, A.-M., Huang, T.-T., Hsu, K.-W., Huang, K.-H., and Fang, W.-L. (2014). Yin Yang 1 is a target of microRNA-34 family and contributes to gastric carcinogenesis. Oncotarget *5*, 5002-5016.
Wang, D., Qiu, C., Zhang, H., Wang, J., Cui, Q., and Yin, Y. (2010). Human microRNA oncogenes and tumor suppressors show significantly different biological patterns: from functions to targets. PLoS One *5*, e13067.
Wang, T., Wang, G., Hao, D., Liu, X., Wang, D., Ning, N., and Li, X. (2015). Aberrant regulation of the LIN28A/LIN28B and let-7 loop in human malignant tumors and its effects on the hallmarks of cancer. Molecular cancer *14*, 1.
Wang, T., and Xu, Z. (2010). miR-27 promotes osteoblast differentiation by modulating Wnt signaling. Biochemical and biophysical research communications *402*, 186-189.
Wang, X., Cao, L., Wang, Y., Wang, X., Liu, N., and You, Y. (2012). Regulation of let-7 and its target oncogenes (Review). Oncology letters *3*, 955-960.
Wang, X., Liu, X., Li, A.Y.-J., Chen, L., Lai, L., Lin, H.H., Hu, S., Yao, L., Peng, J., and Loera, S. (2011a). Overexpression of HMGA2 promotes metastasis and impacts survival of colorectal cancers. Clinical Cancer Research *17*, 2570-2580.
Wang, Z., Lin, S., Li, J.J., Xu, Z., Yao, H., Zhu, X., Xie, D., Shen, Z., Sze, J., and Li, K. (2011b). MYC protein inhibits transcription of the microRNA cluster MC-let-7a-1~ let-7d via noncanonical E-box. Journal of Biological Chemistry *286*, 39703-39714.

Wantae, K., Minseong, K., and Eek-hoon, J. (2013). Wnt/beta-catenin signalling: from plasma membrane to nucleus. Biochemical Journal *450*, 9-21.
Wegener, J., Keese, C.R., and Giaever, I. (2000). Electric cell–substrate impedance sensing (ECIS) as a noninvasive means to monitor the kinetics of cell spreading to artificial surfaces. Experimental cell research *259*, 158-166.
Wolfe, S.A., Grant, R.A., Elrod-Erickson, M., and Pabo, C.O. (2001). Beyond the "recognition code": structures of two Cys2His2 zinc finger/TATA box complexes. Structure *9*, 717-723.
Wong, T.-S., Gao, W., and Chan, J.Y.-W. (2014). Transcription regulation of E-cadherin by zinc finger E-box binding homeobox proteins in solid tumors. BioMed research international *2014*.
Wong, T.S., Chan, W.S., Li, C.H., Liu, R.W., Tang, W.W., Tsao, S.W., Tsang, R.K., Ho, W.K., Wei, W.I., and Chan, J.Y. (2010). Curcumin alters the migratory phenotype of nasopharyngeal carcinoma cells through up-regulation of E-cadherin. Anticancer research *30*, 2851-2856.
Wu, A., Wu, K., Li, J., Mo, Y., Lin, Y., Wang, Y., Shen, X., Li, S., Li, L., and Yang, Z. (2015). Let-7a inhibits migration, invasion and epithelial-mesenchymal transition by targeting HMGA2 in nasopharyngeal carcinoma. Journal of translational medicine *13*, 1.
Wu, D., and Murashov, A. (2012). MicroRNA-431 regulates axon regeneration in mature sensory neurons by targeting the Wnt antagonist Kremen1. Frontiers in molecular neuroscience *6*, 35-35.
Wu, D., and Pan, W. (2010). GSK3: a multifaceted kinase in Wnt signaling. Trends in biochemical sciences *35*, 161-168.
Wu, H., Sun, S., Tu, K., Gao, Y., Xie, B., Krainer, A.R., and Zhu, J. (2010a). A splicing-independent function of SF2/ASF in microRNA processing. Molecular cell *38*, 67-77.
Wu, X.-L., Cheng, B., Li, P.-Y., Huang, H.-J., Zhao, Q., Dan, Z.-L., Tian, D.-A., and Zhang, P. (2013). MicroRNA-143 suppresses gastric cancer cell growth and induces apoptosis by targeting COX-2. World J Gastroenterol *19*, 7758-7765.
Wu, Y., Zhang, Y., Zhang, H., Yang, X., Wang, Y., Ren, F., Liu, H., Zhai, Y., Jia, B., Yu, J., *et al.* (2010b). p15RS attenuates Wnt/{beta}-catenin signaling by disrupting {beta}-catenin.TCF4 Interaction. J Biol Chem *285*, 34621-34631.
Xia, X., Li, Y., Wang, W., Tang, F., Tan, J., Sun, L., Li, Q., Sun, L., Tang, B., and He, S. (2015). MicroRNA-1908 functions as a glioblastoma oncogene by suppressing PTEN tumor suppressor pathway. Molecular cancer *14*, 1.
Xiao, P., and Liu, W.-L. (2015). MiR-142-3p functions as a potential tumor suppressor directly targeting HMGB1 in non-small-cell lung carcinoma. International journal of clinical and experimental pathology *8*, 10800.
Xie, M., and Steitz, J.A. (2014). Versatile microRNA biogenesis in animals and their viruses. RNA biology *11*, 673-681.

Xu, H., Tian, Y., Yuan, X., Wu, H., Liu, Q., Pestell, R.G., and Wu, K. (2015a). The role of CD44 in epithelial–mesenchymal transition and cancer development. OncoTargets and therapy *8*, 3783.

Xu, J., Zhu, X., Wu, L., Yang, R., Yang, Z., Wang, Q., and Wu, F. (2012). MicroRNA-122 suppresses cell proliferation and induces cell apoptosis in hepatocellular carcinoma by directly targeting Wnt/β-catenin pathway. Liver International *32*, 752-760.

Xu, W., Ji, J., Xu, Y., Liu, Y., Shi, L., Liu, Y., Lu, X., Zhao, Y., Luo, F., and Wang, B. (2015b). MicroRNA-191, by promoting the EMT and increasing CSC-like properties, is involved in neoplastic and metastatic properties of transformed human bronchial epithelial cells. Molecular carcinogenesis *54*.

Xue, J., Chen, Y., Wu, Y., Wang, Z., Zhou, A., Zhang, S., Lin, K., Aldape, K., Majumder, S., and Lu, Z. (2015). Tumour suppressor TRIM33 targets nuclear β-catenin degradation. Nature communications *6*.

Yamanaka, H., Moriguchi, T., Masuyama, N., Kusakabe, M., Hanafusa, H., Takada, R., Takada, S., and Nishida, E. (2002). JNK functions in the non-canonical Wnt pathway to regulate convergent extension movements in vertebrates. EMBO reports *3*, 69-75.

Yan, Y., Zuo, X., and Wei, D. (2015). Concise review: emerging role of CD44 in cancer stem cells: a promising biomarker and therapeutic target. Stem Cells Transl Med *4*, 1033-1043.

Yanagida, M., Hayano, T., Yamauchi, Y., Shinkawa, T., Natsume, T., Isobe, T., and Takahashi, N. (2004). Human fibrillarin forms a sub-complex with splicing factor 2-associated p32, protein arginine methyltransferases, and tubulins α3 and β1 that is independent of its association with preribosomal ribonucleoprotein complexes. Journal of Biological Chemistry *279*, 1607-1614.

Yang, J.-S., and Lai, E.C. (2011). Alternative miRNA biogenesis pathways and the interpretation of core miRNA pathway mutants. Molecular cell *43*, 892-903.

Yang, K., Wang, X., Zhang, H., Wang, Z., Nan, G., Li, Y., Zhang, F., Mohammed, M.K., Haydon, R.C., and Luu, H.H. (2015a). The evolving roles of canonical WNT signaling in stem cells and tumorigenesis: implications in targeted cancer therapies. Laboratory Investigation.

Yang, K., Wang, X., Zhang, H., Wang, Z., Nan, G., Li, Y., Zhang, F., Mohammed, M.K., Haydon, R.C., and Luu, H.H. (2016). The evolving roles of canonical WNT signaling in stem cells and tumorigenesis: implications in targeted cancer therapies. Laboratory Investigation *96*, 116-136.

Yang, X., Li, L., Huang, Q., Xu, W., Cai, X., Zhang, J., Yan, W., Song, D., Liu, T., and Zhou, W. (2015b). Wnt signaling through Snail1 and Zeb1 regulates bone metastasis in lung cancer. American journal of cancer research *5*, 748.

Yeung, T.M., Chia, L.A., Kosinski, C.M., and Kuo, C.J. (2011). Regulation of self-renewal and differentiation by the intestinal stem cell niche. Cellular and Molecular Life Sciences *68*, 2513-2523.

Yi, R., and Fuchs, E. (2011). MicroRNAs and their roles in mammalian stem cells. J Cell Sci *124*, 1775-1783.
Yilmaz, M., and Christofori, G. (2010). Mechanisms of motility in metastasizing cells. Molecular Cancer Research *8*, 629-642.
You, X.J., Bryant, P.J., Jurnak, F., and Holcombe, R.F. (2007). Expression of Wnt pathway components frizzled and disheveled in colon cancer arising in patients with inflammatory bowel disease. Oncology reports *18*, 691-694.
Younis, I., Berg, M., Kaida, D., Dittmar, K., Wang, C., and Dreyfuss, G. (2010). Rapid-response splicing reporter screens identify differential regulators of constitutive and alternative splicing. Molecular and cellular biology *30*, 1718-1728.
Yu, J.-M., Sun, W., Hua, F., Xie, J., Lin, H., Zhou, D.-D., and Hu, Z.-W. (2015). BCL6 induces EMT by promoting the ZEB1-mediated transcription repression of E-cadherin in breast cancer cells. Cancer letters *365*, 190-200.
Zeng, X., Huang, H., Tamai, K., Zhang, X., Harada, Y., Yokota, C., Almeida, K., Wang, J., Doble, B., and Woodgett, J. (2008). Initiation of Wnt signaling: control of Wnt coreceptor Lrp6 phosphorylation/activation via frizzled, dishevelled and axin functions. Development *135*, 367-375.
Zhang, B., Pan, X., Cobb, G.P., and Anderson, T.A. (2007). microRNAs as oncogenes and tumor suppressors. Developmental biology *302*, 1-12.
Zhang, J.-g., Shi, Y., Hong, D.-f., Song, M., Huang, D., Wang, C.-y., and Zhao, G. (2015a). MiR-148b suppresses cell proliferation and invasion in hepatocellular carcinoma by targeting WNT1/β-catenin pathway. Scientific reports *5*.
Zhang, J., Kong, X., Li, J., Luo, Q., Li, X., Shen, L., Chen, L., and Fang, L. (2014a). miR-96 promotes tumor proliferation and invasion by targeting RECK in breast cancer. Oncology reports *31*, 1357-1363.
Zhang, L., Sun, H., Zhao, F., Lu, P., Ge, C., Li, H., Hou, H., Yan, M., Chen, T., and Jiang, G. (2012a). BMP4 administration induces differentiation of CD133+ hepatic cancer stem cells, blocking their contributions to hepatocellular carcinoma. Cancer research *72*, 4276-4285.
Zhang, N., Li, X., Wu, C., Dong, Y., Cai, M., Mok, M., Wang, H., Chen, J., Ng, S., and Chen, M. (2013a). microRNA-7 is a novel inhibitor of YY1 contributing to colorectal tumorigenesis. Oncogene *32*, 5078-5088.
Zhang, S., Wu, C.C., Fecteau, J.-F., Cui, B., Chen, L., Zhang, L., Wu, R., Rassenti, L., Lao, F., and Weigand, S. (2013b). Targeting chronic lymphocytic leukemia cells with a humanized monoclonal antibody specific for CD44. Proceedings of the National Academy of Sciences *110*, 6127-6132.
Zhang, Y., Wang, R., Miao, L., Jiang, H., Yuan, H., Ma, H., and Chen, N. (2014b). Genetic variants in let-7/Lin28 modulate the risk of oral cavity cancer in a Chinese Han population. Scientific reports *4*.
Zhang, Y., Wei, W., Cheng, N., Wang, K., Li, B., Jiang, X., and Sun, S. (2012b). Hepatitis C virus-induced up-regulation of microRNA-155 promotes hepatocarcinogenesis by activating Wnt signaling. Hepatology *56*, 1631-1640.

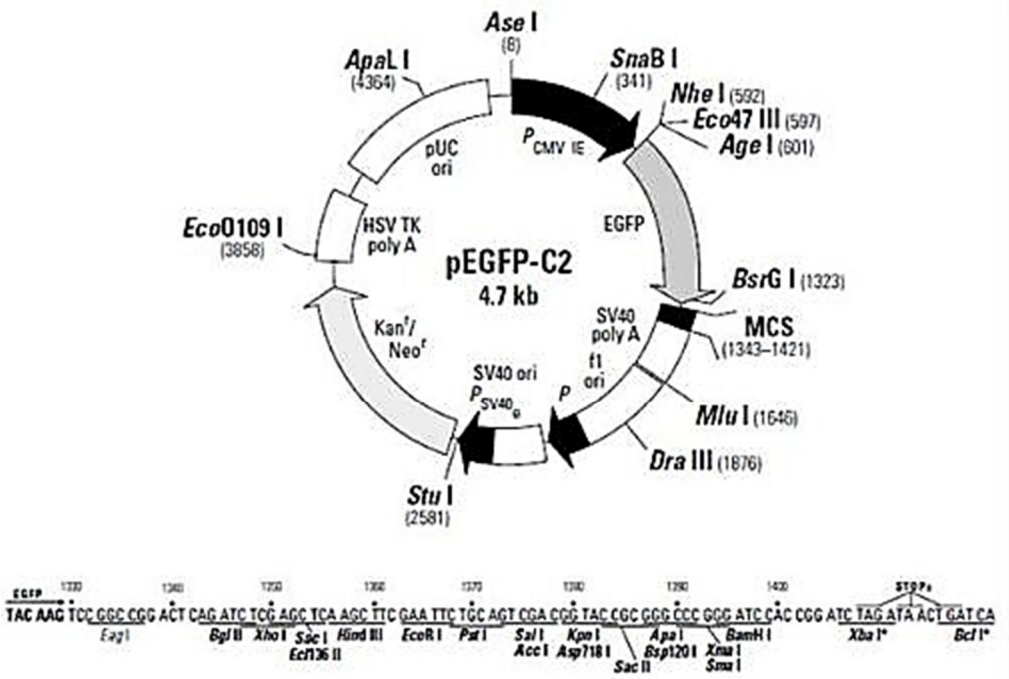
Zhang, Y., Yeh, L.-K., Zhang, S., Call, M., Yuan, Y., Yasunaga, M., Kao, W.W.-Y., and Liu, C.-Y. (2015b). Wnt/β-catenin signaling modulates corneal epithelium stratification via inhibition of Bmp4 during mouse development. Development *142*, 3383-3393.

Zhou, J., Ng, S.-B., and Chng, W.-J. (2013). LIN28/LIN28B: an emerging oncogenic driver in cancer stem cells. The international journal of biochemistry & cell biology *45*, 973-978.

Zhou, Y., Rychahou, P., Wang, Q., Weiss, H.L., and Evers, B.M. (2015). TSC2/mTORC1 signaling controls Paneth and goblet cell differentiation in the intestinal epithelium. Cell death & disease *6*, e1631.

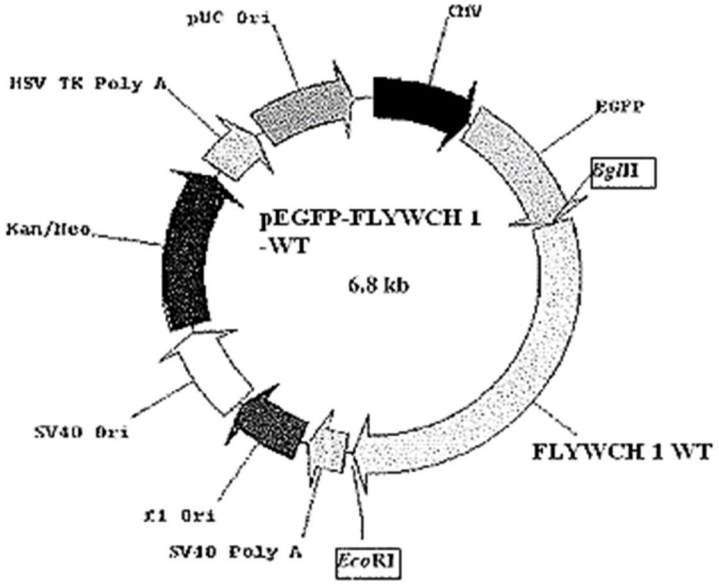
APPENDIX

Appendix 1: pEGFP-C2 plasmid vector

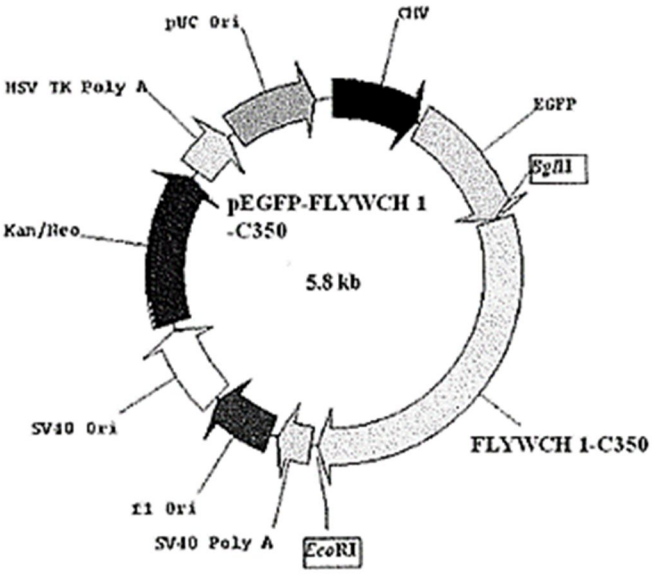


Restriction Map and Multiple Cloning Site (MCS) of pEGFP-C2. (Unique restriction sites are in bold). The *Eag* I site is not unique. The *Xba* I site cannot be used for fusions since it contains an in-frame stop codon. The *Xba* I and *Bcl* I sites (*) are methylated in the DNA provided by BD Biosciences Clontech. If you wish to digest the vector with these enzymes, you will need to transform the vector into a *dam*+ host and make fresh DNA.

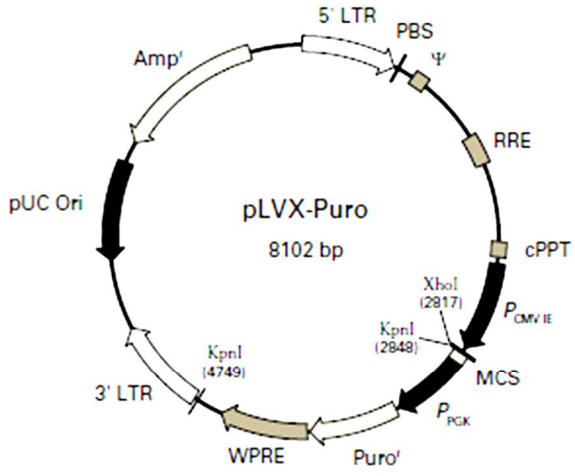
Appendix 2: pEGFP-FLYWCH1 WT plasmid vector

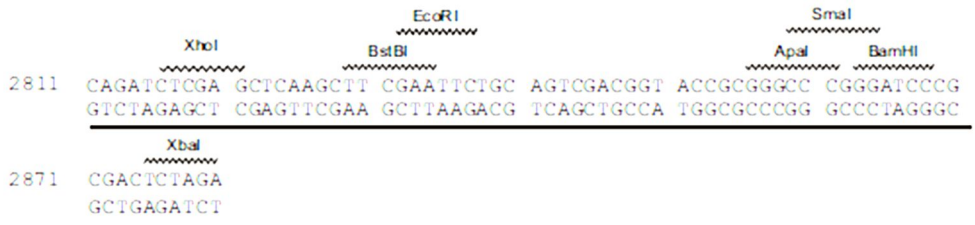


Appendix 3: pEGFP-FLYWCH1-ΔC350 plasmid vector.



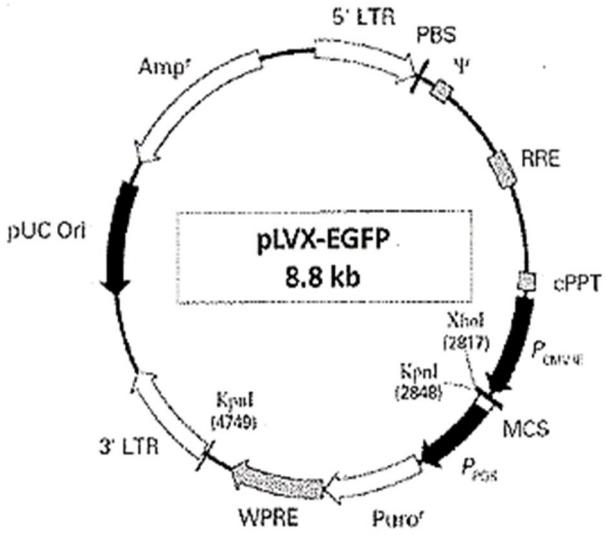
Appendix 4: pLVX-Puro plasmid vector



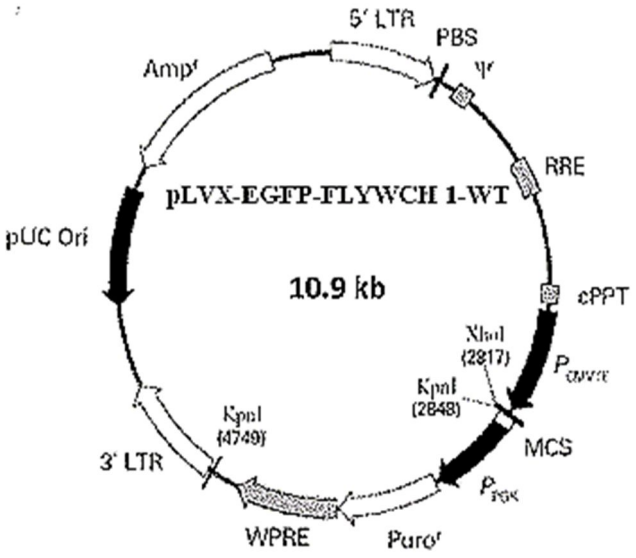


pLVX-Puro Vector Map and Multiple Cloning Site (MCS).

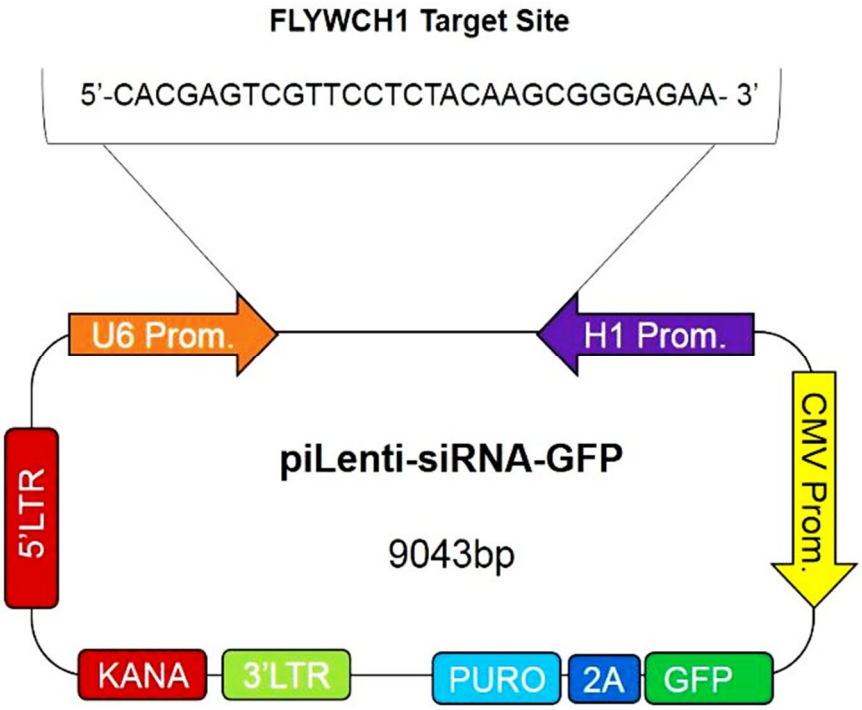
Appendix 5: pLVX-EGFP plasmid vector.



Appendix 6: pLVX-EGFP-FLYWCH1 WT plasmid vector

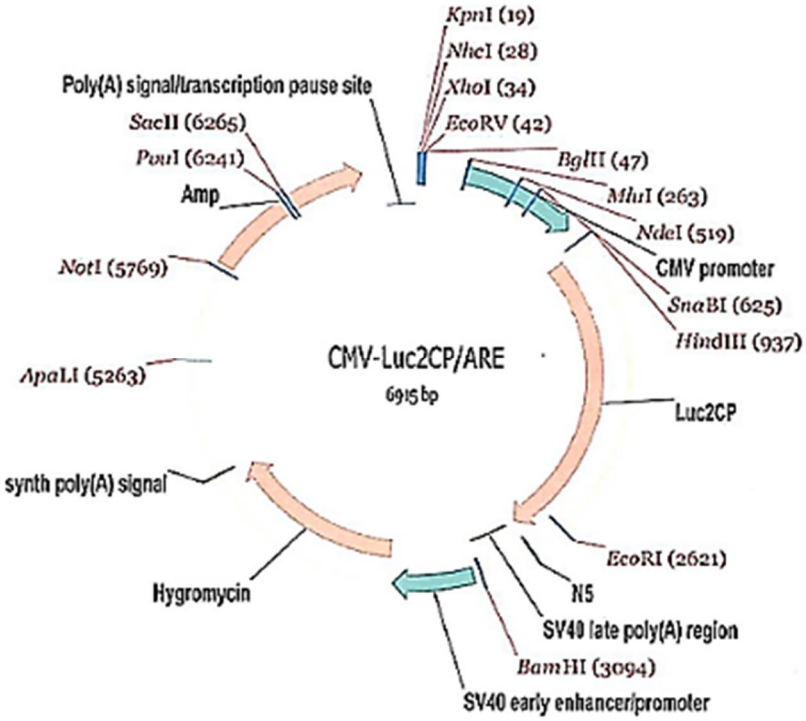


Appendix 7: piLenti-shRNA-FLYWCH1-GFP plasmid map

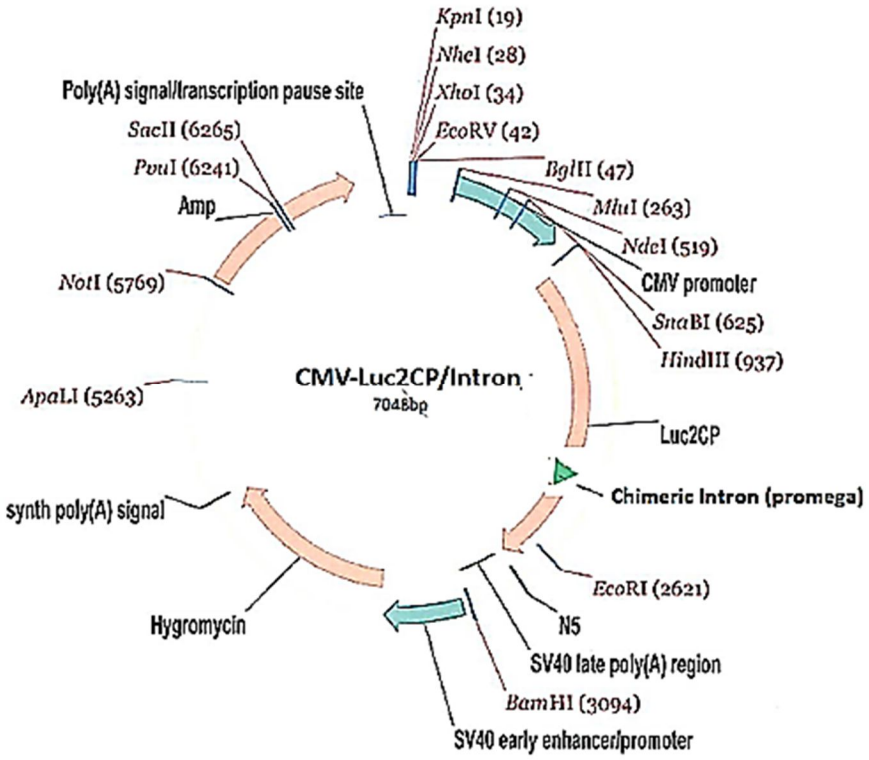


Adapted from https://www.abmgood.com/FLYWCH1-shRNA-Lentivectors-i008000.html#5

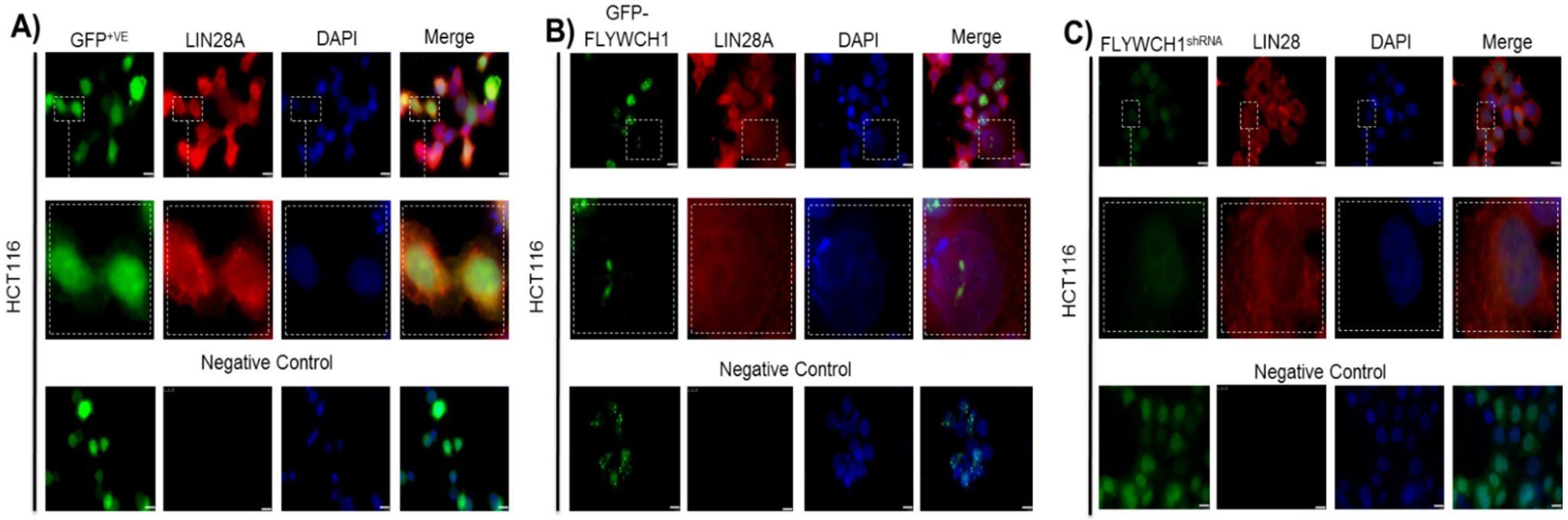
Appendix 8: Intron-less (Luc) plasmid construct



Appendix 9: Intron (Luc-I) plasmid construct

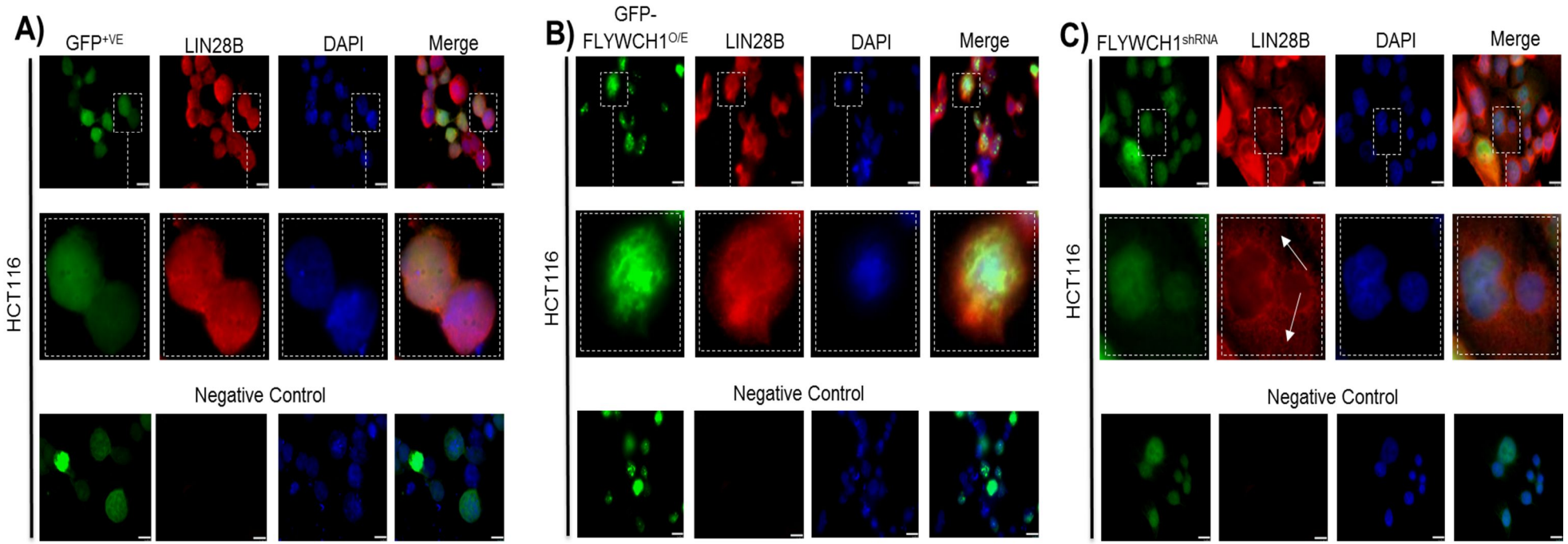


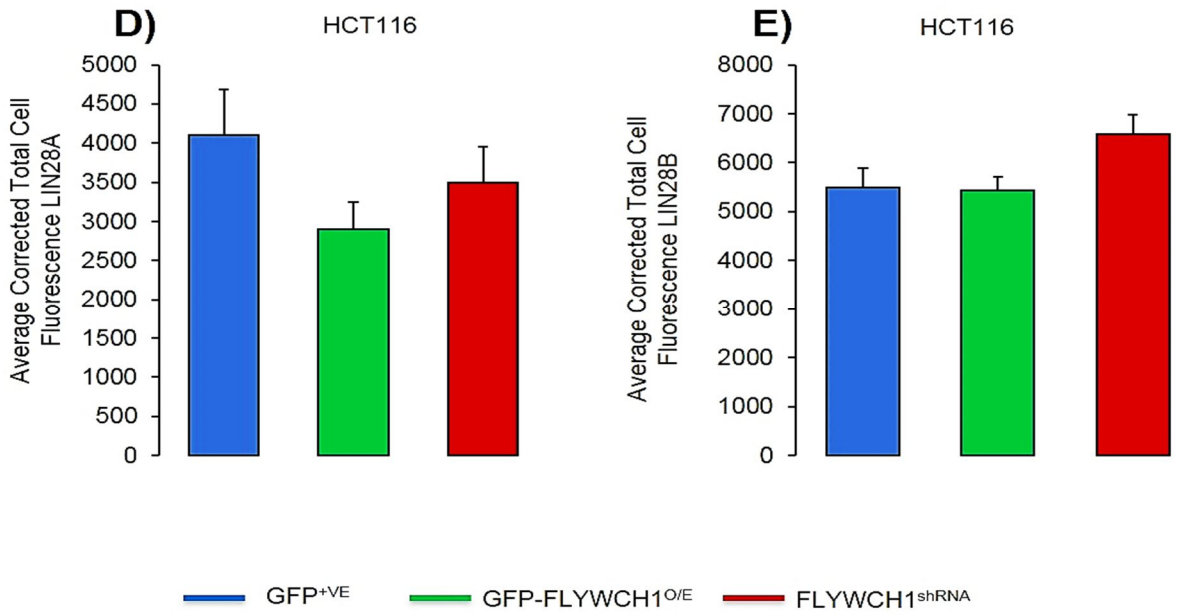
Appendix 10: LIN28A expression pattern in HCT116 cell lines



FLYWCH1 alters the expression of LIN28A in HCT116 cells. HCT116 cells under different conditions were stained with LIN28A (red) and DAPI (blue) and visualized under a fluorescent microscope. The expression pattern of LIN28A under different conditions were analyzed as follows; LIN28A: **A)** GFP^{+VE} (control). **B)** GFP-$FLYWCH1^{O/E}$. **C)** $FLYWCH1^{shRNA}$ cells. Negative controls were used in the absence of primary antibody. Magnification: 100x. Scale bars, 250 µm.

Appendix 11: LIN28B expression pattern in HCT116 cell lines





FLYWCH1 alters the expression of LIN28B in HCT116 cells. HCT116 cells under different conditions were stained with LIN28B (red) and DAPI (blue) and visualized under a fluorescent microscope. The expression pattern of LIN28B under different conditions were analyzed as follows; LIN28B: **A)** GFP^{+VE} (control). **B)** GFP-$FLYWCH1^{O/E}$. **C)** GFP-$FLYWCH1^{shRNA}$ cells. Negative controls were used in the absence of primary antibody. Magnification: 100x. Scale bars, 7.5 µm. Quantitative analysis of **D)** LIN28 A & **E)** LIN28 B, fluorescence intensity was determined by calculating the Corrected Total Cell Fluorescence [CTCF = Integrated intensity – (area x fluorescence mean)] using ImageJ. Data are represented as mean of 30 individual cells under different conditions. Data are mean ± SD. Experiment was repeated at least on two independent occasions.